TRANSPORTATION RESEARCH
RECORD

No. 1514

Bridges, Other Structures, and Hydraulics and Hydrology; Soils, Geology, and Foundations

---

Design and Performance of Underground Pipe

A peer-reviewed publication of the Transportation Research Board

TRANSPORTATION RESEARCH BOARD
NATIONAL RESEARCH COUNCIL

NATIONAL ACADEMY PRESS
WASHINGTON, D.C. 1995

Transportation Research Record 1514
ISSN 0361-1981
ISBN 0-309-06202-0
Price: $26.00

Subscriber Category
IIC bridges, other structures, and hydraulics and hydrology
IIIA soils, geology, and foundations

Printed in the United States of America

Sponsorship of Transportation Research Record 1514

GROUP 2—DESIGN AND CONSTRUCTION OF TRANSPORTATION FACILITIES
Chairman: Michael G. Katona, U.S. Air Force Armstrong Laboratory

Structures Section
Chairman: David B. Beal, New York State Department of Transportation

Committee on Culverts and Hydraulic Structures
Chairman: A. P. Moser, Utah State University
Kenneth J. Boedecker, Jr., Frieda R. Brinskelle, Gongkang Fu, James B. Goddard, James J. Hill, John Owen Hurd, Paige E. Johnson, Iraj I. Kaspar, Michael G. Katona, Carl E. Kurt, Bryan E. Little, Norman W. Loeffler, Timothy J. McGrath, John J. Meyer, John D. O'Fallon, John C. Potter, James C. Schluter, Gerald O. Soderlind, Robert P. Walker, Jr.

Soil Mechanics Section
Chairman: Verne C. McGuffey

Committee on Subsurface Soil-Structure Interaction
Chairman: Thomas C. Sandford, University of Maine
Arnold Aronowitz, Timothy J. Beach, Jeffrey Enyart, Lester H. Gabriel, James B. Goddard, William A. Grottkau, John Owen Hurd, D. Tom Iseley, Jey K. Jeyapalan, Michael G. Katona, Salah Y. Khayyat, Kenneth K. Kienow, Steven R. Kramer, John M. Kurdziel, Michael C. McVay, Samuel C. Musser, Priscilla P. Nelson, Thomas D. O'Rourke, Shad M. Sargand, James C. Schluter, Allen L. Sehn, Ernest T. Selig, Sunil Sharma, Mehdi S. Zarghamee

Transportation Research Board Staff
Robert E. Spicher, Director, Technical Activities
D. W. Dearasaugh, Jr., Engineer of Design
G. P. Jayaprakash, Engineer of Soils, Geology, and Foundations
Nancy A. Ackerman, Director, Reports and Editorial Services

Sponsorship is indicated by a footnote at the end of each paper. The organizational units, officers, and members are as of December 31, 1994.

Transportation Research Record 1514

Contents

Foreword

This volume contains 10 peer-reviewed papers, most of which were presented at two sessions during the 1995 Annual Meeting of the Transportation Research Board.

Havens et al. describe initial efforts toward the development of a design procedure to determine the necessity and magnitude of restraining force to prevent uplift failures of corrugated metal pipe culverts. Bowers and Swaminathan present information on the performance of a large, buried conduit obtained from instrumentation of a 4.4 m diameter corrugated steel, multiplate keyhole-slotted conduit under 20m of earth fill. Hill and Laumann describe the first known precast concrete box culverts, installed in Minnesota in 1974, their advantages, and performance. Moore and Hu examine performance limits for profiled HDPE pipe under large hoop compression using three-dimensional finite element analysis. Rogers and Chapman describe tests that simulate various trenchless pipe installation techniques to determine the patterns and magnitudes of displacements in the surrounding soil. Moore uses a three-dimensional finite element stress analysis program to examine the response of profiled polyethylene pipe under various burial conditions. Sargand et al. describe a part of a major field testing program of plastic pipes in which two polyvinyl chloride pipes were fully instrumented and loaded to failure. Lohnes et al. present the results of a survey on uplift failures of corrugated metal pipes along with an analysis of two specific failures. Kjartanson et al. describe a multiphase research project involving full-scale field testing to develop a rational design methodology for corrugated metal pipe inlet tiedowns. Rogers et al. present the development of stiffness requirements for profile-wall flexible pipes as well as an assessment of their limitations.

Longitudinal Strength and Stiffness of Corrugated Steel Pipe

BRIAN T. HAVENS, F. WAYNE KLAIBER, ROBERT A. LOHNES, AND LOREN W. ZACHARY

Iowa, as well as other states, has experienced several failures of corrugated metal (CMP) culverts, apparently because of inlet flotation. In Iowa, most of these failures have occurred on secondary roads. In a survey of Iowa county engineers, 31 CMP culvert failures occurred within a 5-year period (1983 to 1988). A survey of state departments of transportation revealed nine CMP failures within the 5 years preceding 1992. Design standards from various states for tiedowns to resist uplift showed resisting forces ranging from 44.5 kN (10 kips) to 293.7 kN (66 kips) for pipes 2.03 m (80 in.) in diameter. Data from the survey of states verified an earlier conclusion based on responses from Iowa county engineers that when end restraint is not provided, there is a potential for uplift failures. Further, standards for existing restraint systems have an unclear theoretical or experimental basis, or both. Discussed here is the initial phase of a research program at Iowa State University, where a design procedure is being developed to determine the necessity and magnitude of restraining force to prevent CMP uplift failures. Theoretical relationships were developed for predicting the longitudinal stiffness, yield moment capacity, and ultimate moment capacity of CMP. Full-scale tests of steel CMPs 1.22 m (4 ft) and 1.83 m (6 ft) in diameter experimentally determined EI factors of 2.49 MN-m^2 (869 $\times$ 10^6 in^2-lb) and 2.61 $\times$ 10^6 N-m^2 (911 $\times$ 10^6 in^2-lb), respectively (3 $\times$ 1 corrugation style). The agreement of theoretical and experimental results verifies the accuracy of the theoretical relationships which will be used in the development of rational design standards.

Corrugated metal pipes (CMP) often serve as an inexpensive means for crossing small streams and thus are important components in the transportation system. Iowa, as well as other states in recent years, has experienced several CMP failures because of inlet flotation. Analytical design procedures in use today frequently overlook or underestimate the possibility of longitudinal flexural failures which may result from uneven settlement beneath the CMP or inlet uplift because of pore water pressure. Pressure beneath the inlet may be caused by a hydraulic head differential between the CMP inlet and outlet, by high storm flows, or by partial or full blockage of the inlet (*1*). The uplift can be aggravated by a small amount of water in the CMP, by minimum soil cover on the CMP, or by ineffective seepage cut-off below the inlet. Pore pressures can cause the inlet end of the CMP to deflect upward, which will result in longitudinal bending; longitudinal bends up to 90 degrees will often lead to erosion of the soil and roadway above the CMP (*2*). In some situations, the entire CMP may be dislodged from its existing location (*3*).

A multiphase research project funded by the Iowa Department of Transportation (Iowa DOT) was undertaken at Iowa State University to develop CMP design methods to prevent uplift failures. This paper presents the results of the second phase in this investigation.

B. T. Havens, Woodward-Clyde Consultants, 101 South 108 Ave., Omaha, Nebr. 68154. W. Klaiber and R. A. Lohnes, Department of Civil and Constr. Engr., Iowa State University, Ames, Iowa 50011. L. W. Zachary, Aeronautic Engineering and Engineering Mechanics, Iowa State University, Ames, Iowa 50011.

In this phase, theoretical relationships were developed for predicting the longitudinal stiffness, yield moment capacity, and ultimate moment capacity of CMP with any corrugation style, strength, and stiffness characteristics. Laboratory tests were conducted on steel pipes (3 $\times$ 1 corrugation style) to experimentally evaluate the accuracy of the theoretical relationships when applied to these specific pipes. Results from the first and third phases of this research project are detailed in the papers by Lohnes et al. and Kjartanson et al. elsewhere in this volume.

EXPERIMENTAL WORK

Test Specimens

To address the lack of relevant flexural test information available in the literature, a program of flexural tests of large diameter CMP specimens was initiated. Two test specimens (1.22-m (4-ft) diameter and 1.83-m (6-ft) diameter) were selected for testing. Descriptions of the two test specimens are shown in Table 1. The two specimens in Table 1 will be denoted throughout this document as ISU1 (1.22-m (4-ft) diameter) and ISU2 (1.83-m (6-ft) diameter).

Load Frame

The CMP specimens were simply supported and a uniformly distributed load was applied in increments along the length of the pipe.

Figure 1 is a photograph of ISU1 being tested in the load frame. More details on the load frame are presented in the work of Klaiber et al. (*4*).

As observed in Figure 1, wire rope suspended between upright columns provided end support for the specimens. This type of support facilitated testing various diameters of CMP with minimal adjustments and permitted end rotation. To prevent horizontal movement of the test specimens, brackets that allowed end rotation and vertical deflection were attached to one end of the CMP. Reinforced concrete diaphragms were cast in both ends of the CMP test specimens to add strength and prevent local failure.

Test Procedure

The testing program included a service load test and a failure load test for each specimen. In the service load tests, it was planned to limit applied loading to the elastic range; however, both specimens experienced some plastic deformation in the service load tests. During the failure load tests, each specimen was loaded into the range of plastic deformation until a corrugation collapsed on the compression side of the CMP.

TABLE 1 Flexural Test Specimens

Parameter	ISU1	ISU2
Diameter, m	1.21	1.83
Corrugation style	3 x 1	3 x 1
Fabrication style	Helical Welded Seam	Helical Welded Seam
Nominal length, m	6.10	7.62
Effective length, m	6.01	7.45
Gage	12	14
Nominal uncoated thickness, cm	0.2657	0.1897
Weight, N/m	730	1095

Note: 1 m = 3.28 ft
1 cm = 0.394 in.
1 N/m = 0.0685 lbf/ft

Load was applied to the CMP specimens in predetermined increments with sandbags on top of the pipe and water inside the pipes. Initial increments of loading were applied with uniformly distributed sandbags of known weight. In the failure tests, when additional weight was required, load was applied by adding water inside the specimens. The end concrete diaphragms contained the water in the pipes. By monitoring the depth of water in the specimens, the nonuniform loading (i.e., varying depth of water) was taken into account.

Instrumentation

Each test specimen was instrumented with electrical-resistance strain gauges, direct current displacement transducers (DCDTs), dial gauges, deflection gauges, and manometers. Electrical instrumentation was monitored and recorded after each load increment with a computer-controlled data acquisition system. All other instrumentation was recorded manually after each load increment.

Strain gauges were installed at the centerline of the specimen and at the quarter point sections. At the centerline of the specimens, strain gauges were attached on the top and bottom surface of the CMP as shown in Figure 2. Thus, it was possible to measure longitudinal and hoop strain at the three locations. At the quarter points, strain gauges were positioned on the top and bottom of the specimens so that longitudinal strains could be measured.

DCDTs were positioned longitudinally around the circumference of the CMP, as shown in Figure 3, at the centerline of the specimens to measure movements between corrugation peaks. The DCDTs were attached so that at each location there was a nominal gauge length of 15.24 cm (6 in.). DCDTs were also used to measure changes in the horizontal CMP diameter at the centerline of the specimens as loading was applied.

Vertical deflections of the specimens were determined by reading with surveying levels engineering scales attached to the specimens. This system was used because the expected deflections would exceed the range of the DCDTs available. Vertical deflections were measured at the top and bottom of the specimens at the centerline, and at the bottom of the specimens at quarter point locations. Deflection data at the centerline of the specimens were used to determine changes in the vertical diameter of the specimens.

Dial gauges were used at the ends of the specimens to determine vertical deflections at these locations because of elongation of the wire rope with applied loading. Deflections at quarter points and centerline were adjusted to account for the wire rope elongation.

Manometers were attached to the bottom of the test specimens (quarter points and centerline) to determine the depth of water in the

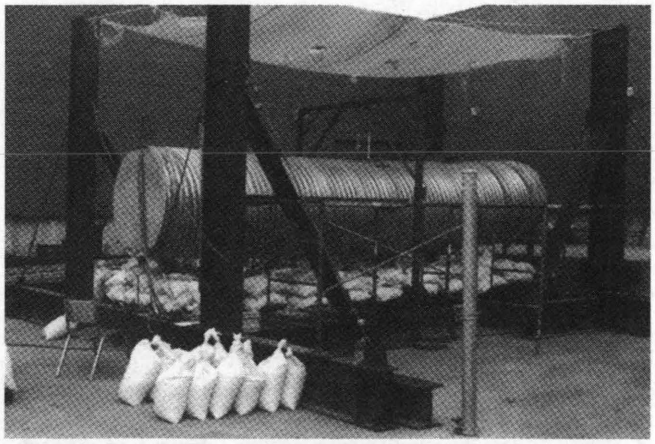

FIGURE 1 Load frame with ISU1 being tested.

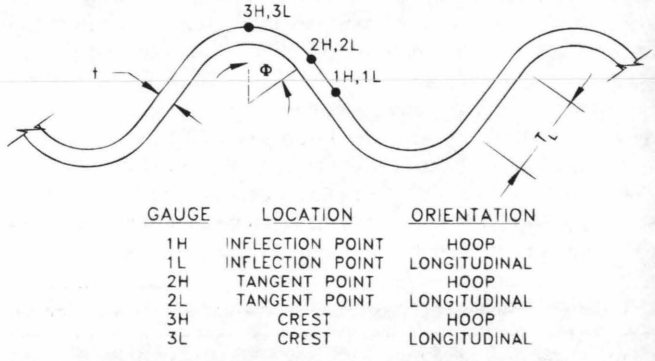

GAUGE	LOCATION	ORIENTATION
1H	INFLECTION POINT	HOOP
1L	INFLECTION POINT	LONGITUDINAL
2H	TANGENT POINT	HOOP
2L	TANGENT POINT	LONGITUDINAL
3H	CREST	HOOP
3L	CREST	LONGITUDINAL

FIGURE 2 Location of centerline strain gauges on top and bottom of CMP.

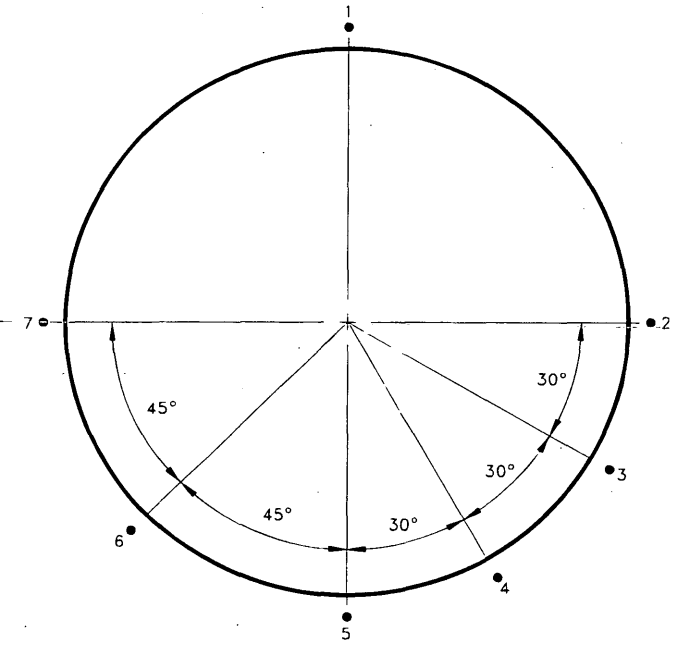

FIGURE 3 Location of DCDTs around circumference of CMP at centerline of span.

CMP specimens at any load increment. With these data, the variation in applied load with deflection of the specimens could be determined.

Experimental Results

The following general observations apply to both specimens; more details can be found in the thesis by Havens (*5*). Strains on the tension side of the specimens were generally smaller than strains measured at the corresponding corrugation positions on the compression side. These strains indicate higher stresses are associated with the collapse of corrugations (top of specimen) than the elongation of corrugations (bottom of specimens). Strain data from the quarter point locations of the specimens indicated symmetrical behavior.

In general, horizontal corrugation crest displacements were proportional to the vertical distance from the CMP neutral axis. Horizontal crest displacements at the top and bottom of the specimens were not always similar values, indicating the possibility of unsymmetrical behavior with respect to the neutral axis of the specimens. Significant changes in the diameters of the specimens occurred depending on the method of load placement.

The relationships between the midspan deflections and the moment for specimens ISU1 and ISU2, respectively, are shown in Figures 4 and 5. In each of these figures, service loading (dashed lines) as well as failure loading (solid lines) are illustrated. The moments at zero deflection are because of the weight of the CMP. The vertical lines at the end of each curve represent the sudden deflections that occur when the specimens reach their ultimate capacity.

The service load data in Figure 4 shows a linear load-deflection curve between Point A and Point B because of sand loading. The curve becomes nonlinear between Point B and Point C because of the non-uniform water loading and an increase in the vertical diameter of the CMP, which causes the measured vertical deflections to increase. Thus, the vertical deflection results from both flexure and localized cross-section deformations. The load-deflection response in the failure test shows a linear curve from Point D to Point C where the loading is all sand. The loading between Point C and Point E is water. At Point E, a load shift occurred when a portion of the sand load fell from the CMP. Although the midspan moment on the CMP decreased, the CMP deflection increased, suggesting that significant plastic deformations of the CMP occurred at or before the instant the load decreased. Points F and G represent the midspan moments because of load remaining on the CMP immediately after the load shift and because of load reapplied to the CMP. Point H is the projected deflection at which the ultimate CMP moment was reached,

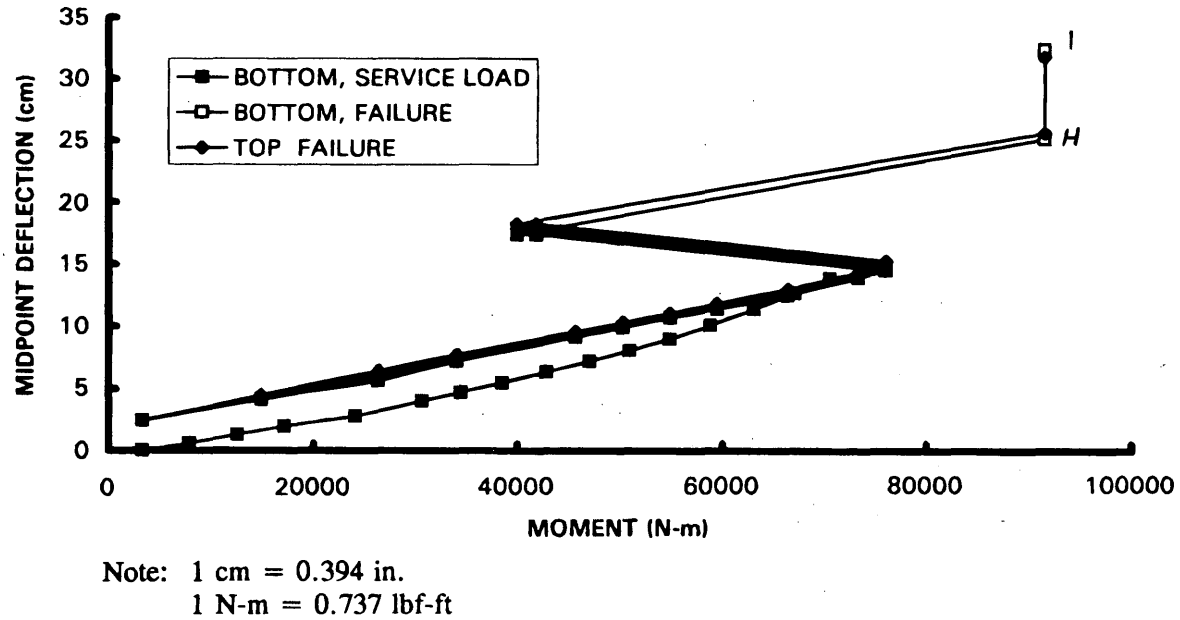

FIGURE 4 Moment versus midspan deflection (ISU1).

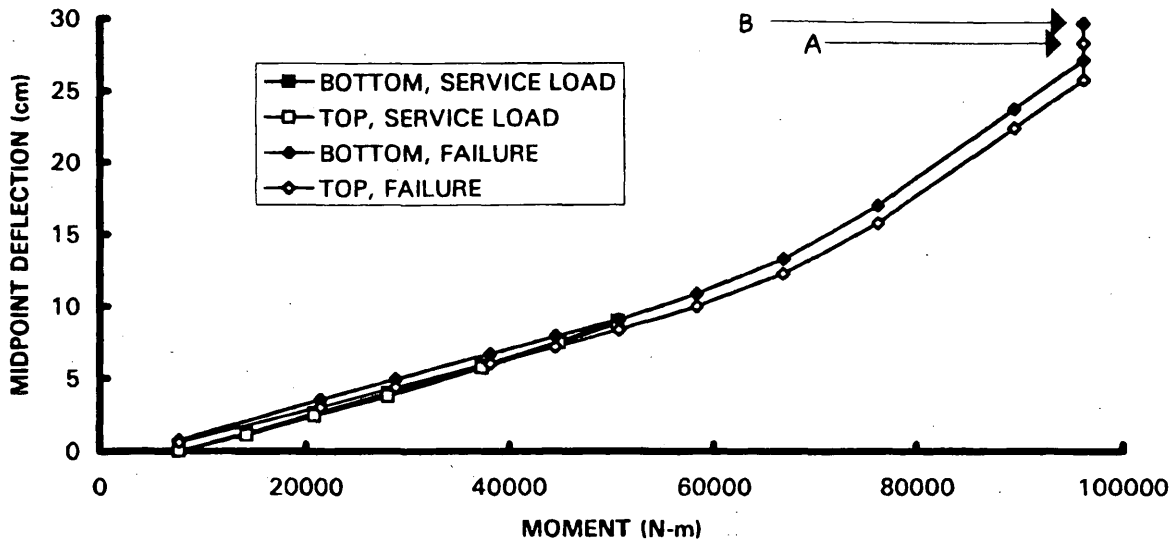

Note: 1 cm = 0.394 in.
1 N-m = 0.737 lbf-ft

FIGURE 5 Moment versus midspan deflection (ISU2).

and Point I is the measured deflection that occurred after the specimen collapsed.

Figure 5 indicates fairly uniform behavior throughout service load and failure tests for ISU2. The primary difference between the deflection curves for service load and failure may be because of the minor plastic deformations that occurred during the service load tests. Points A and B are projected midspan post-collapse deflections. Actual values for those points were not obtained because of failure of the deflection measurement system.

Corrugations in ISU1 collapsed at a distance of 10.16 to 12.70 cm (4 to 5 in.) from the centerline. Corrugations collapsed in ISU2 at two locations. One collapse occurred at a welded seam approximately 33.02 cm (13 in.) from the centerline and the other collapse occurred approximately 1.12 m (44 in.) from the midspan on the opposite half of the span. The second collapse followed the first by approximately 20 to 30 sec.

Longitudinal moment capacities, stiffness values, and midspan deflections from test data are summarized in Table 2. In this table, yield moments are taken as those moments occurring when the relationship between the longitudinal strain at the corrugation crest and the applied moment becomes nonlinear. A range is given for the yield moment for ISU2 as it was difficult to identify the actual point. Midspan yield deflections for ISU2 are also presented as a range. Ultimate moments were reached when the corrugation under the greatest strain collapsed. At this magnitude, the specimen could not carry additional load without excessive, unpredictable deflection.

TABLE 2 Experimental Test Results

	Specimen	
Parameter	ISU1	ISU2
Yield Moment, kN-m	30.7	28.1-37.3
Ultimate Moment, kN-m	91.5	96.3
EI, MN-m^2	2.49	2.61
Mid-span Defl., cm @ yield moment	3.81	3.81-5.84[b]
Mid-span Defl., cm @ ult. moment	<13.7[c]	>27.2[c]

[a] difficult to interpret a single value for location of non-linear behavior; range is used
[b] deflections in the range of interpreted yield moment
[c] unable to measure deflection at instant of incipient collapse

Note: 1 kN-m = 737 lbf-ft
1 MN-m^2 = 2.42 x 10^6 lbf-ft^2
1 cm = 0.394 in.

Maximum deflection values are reported just before the large deflection associated with corrugation collapse. For both specimens, the ultimate moment was reached between load increments, so the deflection under ultimate moment was not measured and is indicated as a value greater than the measured deflection at the previous load increment.

Values of stiffness (EI) in Table 2 were calculated from the service load test assuming that each simple-span CMP specimen was subjected to uniform distributed loading. This was an appropriate assumption for ISU1 in which only sandbag loading was used in the service load test. For ISU2 in which water loading was used in the service load test, corrections were required for non-uniform loading. Basic load deformation relationships were used to determine the EI values from the experimental data.

The modulus of elasticity of the steel was assumed to be the commonly accepted value of 200 MPa (29×10^6 psi). Poisson's ratio, ν, for steel was taken as 0.3.

The ratios of hoop strains, ϵ_H, to longitudinal strains, ϵ_L, were calculated for each test at two locations on the top of the CMP specimens. Strain ratios were used to calculate the stress ratio, K_σ, which is the ratio of hoop stress to longitudinal stress. From test data, the average strain ratio was found to be 0.38. The stress ratio, K_σ, can be written as indicated below:

$$K_\sigma = \frac{\sigma_H}{\sigma_L} = \frac{\left(\frac{\epsilon_H}{\epsilon_L}\right) + \upsilon}{\left[\left(\frac{\epsilon_H}{\epsilon_L}\right)\upsilon\right] + 1} \tag{1}$$

where

ϵ_L is the longitudinal strain,
ϵ_H is the hoop strain, and
ν is Poisson's ratio.

Using the strain ratio of 0.38 and Equation 1, the stress ratio, K_σ, is found to be 0.64 for 3×1 pipe.

THEORETICAL DEVELOPMENT

Theoretical Longitudinal Moment Capacity

Based on the principles of mechanics, observations, and data from the flexural tests, relationships were developed for calculating the longitudinal moment capacity of CMP.

A free body diagram of the quarter cycle indicated in Figure 6 is at the critically stressed location in the transverse section. In Figure 6(*b*), dP and $dP + d\,(dp/dx)$ are the compressive forces acting on the ends of the corrugation. The moment, M_c, is the local moment on the corrugation. Forces F_{H1} and F_{H2} are the forces acting on the sides of this longitudinal section resulting from hoop stresses that are resisted by the force, V.

In the development of a relationship for the CMP moment, M_E, the following assumptions are made:

- Hoop strains at the inflection point that are typically small are assumed to be zero;
- Hoop and longitudinal strains are assumed to vary linearly with the distance from the corrugation neutral axis (CNA) indicated in Figure 6(*b*); and
- Force, dP, is assumed to vary from a maximum at the top of the CMP to zero at the CMP neutral axis.

The stresses on this element are related to the applied forces and moments on the element by using the principles of mechanics. For details on this development, the reader is referred to the work of Klaiber et al. (*6*). The CMP moment, M_E, because of a specified limiting stress, may be expressed as:

$$M_E = \frac{2\pi r\, t\sigma_L}{d_c}\left[\frac{rt}{6} + K\sigma\left(\frac{L_T^2 \cos\phi}{12} R_{TP} + K_\lambda R\right)\right] \tag{2}$$

where

σ_L signifies a limiting longitudinal stress within the elastic range;
K_σ is the ratio of hoop stress to longitudinal stress for any CMP element;
d_c is the corrugation depth indicated in Figure 6(*a*);
r is the CMP radius;
t is the CMP wall thickness;
L_T is the length of the tangent section in each corrugation cycle as indicated in Figure 6(*a*);
ϕ is the tangent angle indicated in Figure 6(*a*);
R_{TP} is ratio of the distance from the CNA to the tangent point to the distance from the CNA to the crest of the corrugation;
K_λ is a constant that depends on the corrugation geometry; the average value for all pipe gauges may be taken as 0.3828 in. for 3×1 CMP, 0.2174 in. for $2\frac{2}{3} \times \frac{1}{2}$ CMP, and 0.2124 in. for $2 \times \frac{1}{2}$ CMP; values for specific gauges may be calculated using relationships presented in the work of Havens (*5*); and
R is the corrugation radius.

Theoretical Longitudinal Ultimate Moment Capacity

Flexural failure of CMP has been defined at a limiting biaxial yield stress on the critical compression-side corrugation. However, considerable moment capacity may exist before the onset of corrugation collapse and severe vertical deflection of the CMP. A formula was developed to calculate this ultimate moment capacity based in part on the previously developed relationship for M_E.

To estimate the ultimate moment capacity from the test data (strains), it was determined that the critically stressed element on the compression side of the CMP had yielded and a plastic hinge formed as more load was applied. This plastic hinge begins at the crest and extends down to the tangent point at incipient collapse. Although a portion of the CMP section yields, other regions of the CMP cross-section behave elastically. An angle designated as θ_{EP}, as indicated in Figure 7, divides the two assumed regions of elastic behavior and plastic behavior. The resisting moment capacity of the elastic region is a modification of the formula developed for determining the limiting stress moment capacity. The resisting moment capacity of the elastic regions and that of the plastic regions is as follows:

$$M_{E(\theta EP)} = \frac{8r\, t\sigma_L}{d_c \cos\theta_{EP}}\left[\frac{rt}{6} + K_\sigma\left(\frac{L_T^2 \cos\phi}{12} R_{TP} + K_\lambda R\right)\right] \times \left[\frac{\pi}{4} - \frac{\theta_{EP}}{2} - \frac{\sin 2\theta_{EP}}{4}\right] \tag{3}$$

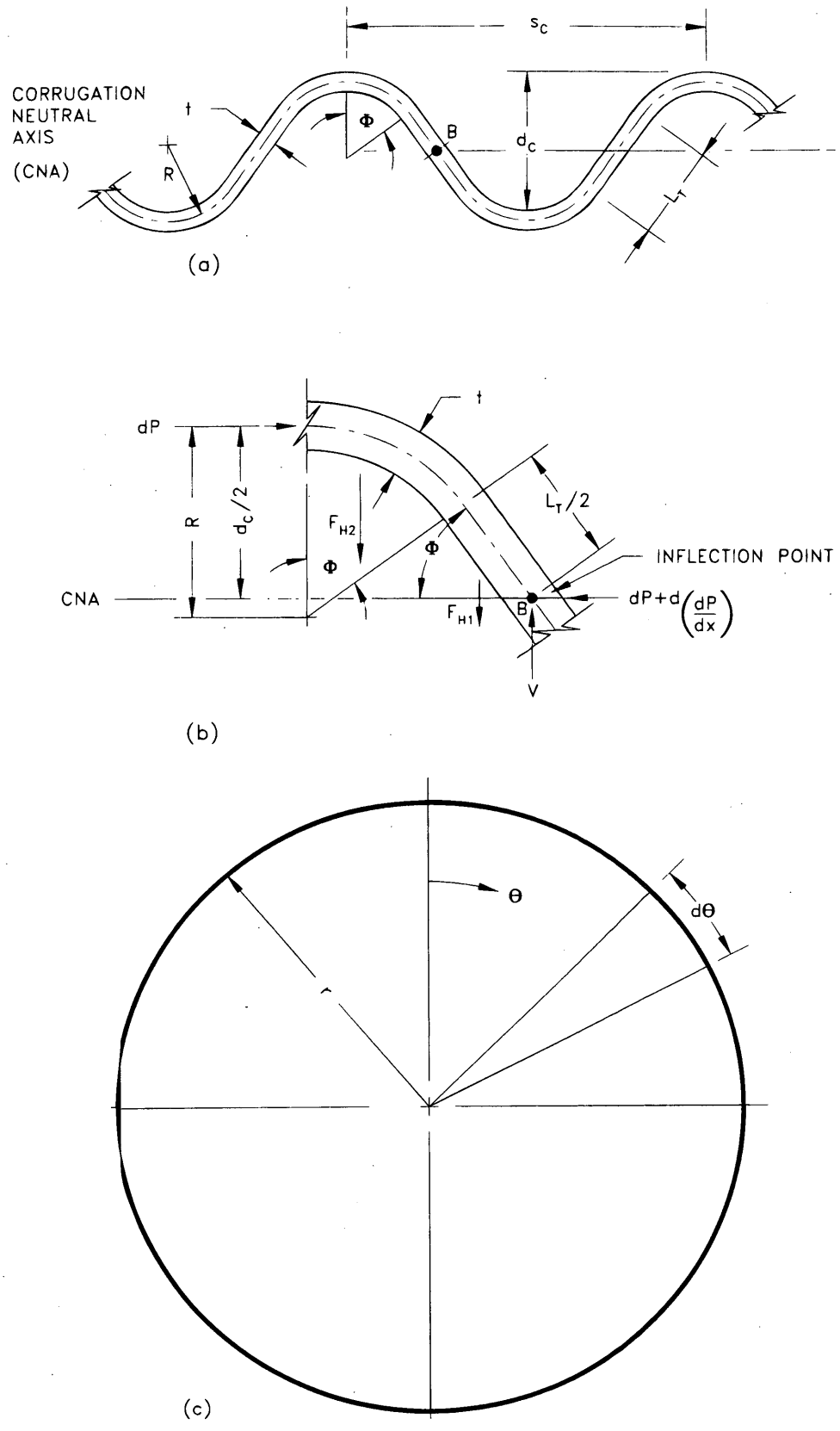

FIGURE 6 Description of CMP: (a) corrugation details; (b) free body diagram of one-quarter corrugation cycle; (c) transverse cross section.

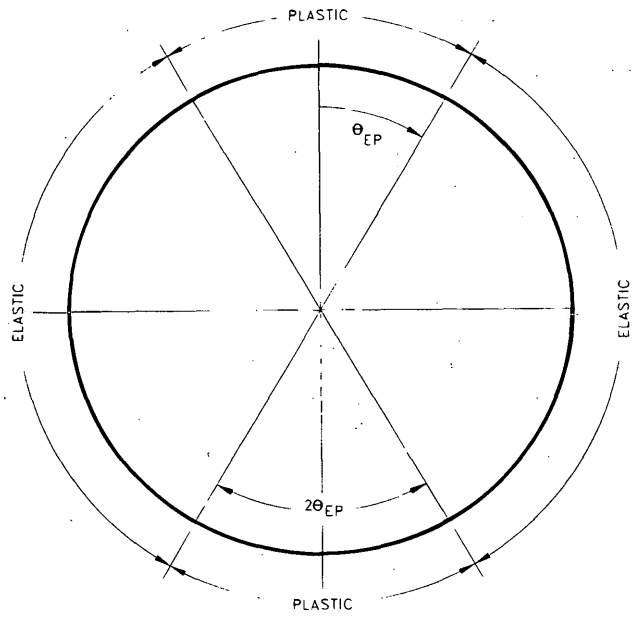

FIGURE 7 Assumed elastic and plastic regions of CMP at ultimate flexural strength.

where $M_{E(\theta EP)}$ is the elastic region moment contribution to the ultimate moment.

$$M_{P(\theta EP)} = \frac{4\sigma_{YL} rt}{\sin\phi}\left[K_\sigma\left(R\phi\frac{L_T}{6}\right)\cos\phi + \frac{rt}{2L_T}\right]\sin\theta_{EP} \quad (4)$$

where $M_{P(\theta EP)}$ is the ultimate moment contribution from the plastic region. The ultimate moment based on θ_{EP} is the sum of the resisting moments from the two previous relationships:

$$M_{U(\theta EP)} = M_{P(\theta EP)} + M_{E(\theta EP)} \quad (5)$$

Using the ultimate moments obtained from the tests and the previously determined value of 0.64 for K_σ, a value for θ_{EP} was calculated to be 73.4 degrees. The contribution to the moment capacity from the elastic part of the cross-section is small, however, in comparison to the contribution from the plastic part of the cross-section. With the assumption that the entire cross-section is subjected to plastic deformation (θ_{EP} = 90 degrees), the ultimate moment capacity simplifies to the following relationship:

$$M_u = \frac{4\sigma_{YL} rt}{\sin\phi}\left[K_\sigma\left(R\phi + \frac{L_T}{6}\right)\cos\phi + \frac{rt}{2L_T}\right] \quad (6)$$

Theoretical EI Factor

In order to calculate CMP vertical deflections, an EI term is required. Moment of inertia, I, is a function of the CMP geometry; however, the calculation of I for CMP is complex because the CMP transverse cross-section is not constant in the longitudinal direction. The moment of inertia for CMP is considerably smaller than the I of a smooth-wall pipe ($I = \pi r^3 t$), because the smooth wall has a constant transverse cross-section which is much stiffer.

To develop an expression for I, an energy approach was used to determine a relationship between the applied load and the CMP midspan vertical deflection. Several assumptions were made about the distribution of stresses throughout the CMP. Loading is assumed to produce a moment on the CMP such that the critically stressed element on the compression side of the CMP is at a specified limiting stress within the elastic range. All other elements in the CMP are assumed to be at stress levels lower than the limiting stress. Stresses at these other locations are quantified to account for variables such as position of element in span, relationship of element to CNA, and relationship of element to CMP neutral axis. Strain energy imparted to the CMP specimen by the applied loads is related to the elemental stresses as follows:

$$U = 2\sum_{n=1}^{N_R}\int\left(\frac{\sigma_{P1}^2}{2E} + \frac{\sigma_{P2}^2}{2E}\right)dV \quad (7)$$

where $ds = rd\theta$, $dV = rd\theta dtdx$, N_R is the number of quarter-cycle segments in one-half of the CMP length, n is the quarter-cycle segment count number used in the summation, and σ_{P1} and σ_{P2} are the principal stresses on each element. The strain energy is then related to deflection of the CMP specimen as follows:

$$\frac{\partial U}{\partial P} = \Delta_V = \left[\frac{4\sigma_{MAX}^2 rK_G\pi t}{EM_{MAX}^2 d_c^2}\right]\left(\frac{1}{3} + K_\sigma^2\right)\sum_{n=1}^{N_R} 2M_x \quad (8)$$

where M_x is the moment at a distance x from the end. From beam theory, the EI factor is then related to the applied moment and limiting stress as follows:

$$EI = \frac{s_c}{4}\left[\frac{M_{MAX}^2 Ed_c^2}{4\sigma_{MAX}^2 rK_G\pi t}\right]\left[\frac{3}{1+3K_\sigma^2}\right] \quad (9)$$

Incorporating Equation 2, the following relationship for EI is determined:

$$EI = \frac{E\pi s_c rt}{4K_G}\left[\frac{3}{1+3K_\sigma^2}\right]\left[\frac{rt}{6} + K_\sigma\left(\frac{L_T^3\sin\phi\cos\phi}{12d_c} + K_\lambda R\right)\right]^2 \quad (10)$$

where, except for K_G and s_c, all terms have been previously defined. K_G is a geometric parameter which may be taken as 0.09215 in.^{3} for 3 × 1 CMP, 0.01928 in.^{3} for 2⅔ × ½ CMP, and 0.01388 in.^{3} for 2 × ½ CMP; note that these values are averages for all common pipe gauges. Values for specific gauges may be calculated using relationships presented in the work of Havens (*5*). The corrugation crest spacing (length of one cycle) is denoted as s_c.

Application of Theoretical Relationships

The theoretical relationships were developed for use with CMP of any metal type and any corrugation style consisting of circular arcs connected by tangents. Most of the parameters needed for application of the relationships can be determined theoretically. However, the stress ratio (K_σ) must be determined experimentally for specific corrugation styles. The relationships in this paper are validated only with test data from 3 × 1 CMP.

Helix Angle Effects on Strength and Stiffness

The helix angle of CMP varies from approximately 33 degrees for small diameter pipes to 6 degrees for large diameter pipes, with

variations resulting from corrugation style and manufacturer. It was postulated by Lane (*6*) that CMP with helix angles less than 8 degrees will act similar to CMP with annular corrugations. The relationships developed for longitudinal moment capacity and stiffness assume circumferential corrugations. This assumption is expected to be reasonable for the larger diameter pipes tested as part of the ISU study, but may not be valid when the theoretical formulas are applied to smaller diameter pipes, where the helix angle may be related to substantial increases in stiffness. Neglecting the helix angle effects should be conservative, as the beam strength of helical pipe of equal size and gauge is greater than that of annular CMP because of the diagonal direction of the corrugations (*7*).

Comparison of Experimental and Theoretical Results

Experimental results and theoretical values calculated from Equations 2, 6, and 10 are shown in Table 3. Equation 2 predicts nonconservative yield moments which are 11.5 percent high for ISU1 and 3.6 to 37.7 percent high for ISU2. The main reasons for this difference are that it is very difficult to determine the yield moment experimentally and the variation in yield stress from specimen to specimen. Values calculated for the ultimate moments from Equation 6 are in excellent agreement with the experimental values being 1.5 percent low for ISU1 and 4.2 percent high for ISU2. Recall, however, that the theoretical values are based on an assumption that the entire cross section is yielding.

Values for *EI* determined by using Equation 10 are in reasonable agreement with the experimental values. The theoretical values of EI are 4.3 percent low and 8.1 percent high for ISU1 and ISU2, respectively.

SUMMARY AND CONCLUSIONS

Presented in this paper are the results of one phase of an ongoing investigation whose overall objective is to determine when restraint is required to prevent uplift failures in CMP. In this phase of the study, three CMPs were loaded to failure to determine experimental values for yield moments, ultimate moments, and "stiffness" *EI*.

Theoretical relationships were derived for determining the yield moment, ultimate moment, and the "stiffness" *EI* for CMPs of various diameters, gauges, and corrugation geometry. The theoretical relationship for yield moments from Equation 2 provides slightly unconservative values. Variation in the yield strength of steel is believed to be the main reason for the difference. Theoretical ultimate moment capacities obtained using Equation 6 are in good agreement with the values that were obtained experimentally. The relationship for "stiffness" *EI*, Equation 10, provides values that are in good agreement with the experimental values determined.

ACKNOWLEDGMENTS

The research presented in this paper was conducted by the Engineering Research Institute of Iowa State University, and was funded by the Highway Research Board and the Highway Division, Iowa DOT, Ames, Iowa. The authors wish to thank various engineers from the Iowa DOT, especially D.D. Coy for his support, encouragement, and counseling. Appreciation is also extended to R.L. Meinzer of Contech Construction Products, Inc., Topeka, Kansas, for donating the numerous sections of CMP used in the tests. Special thanks are also accorded the numerous undergraduate students who assisted with the various phases of the project.

TABLE 3 Comparison of Experimental and Theoretical Values

	ISU1	ISU2
Experimental Yield Moment, kN-m	30.7	28.1 to 37.3
Theoretical Yield Moment, kN-m	34.2	38.7
Difference from experimental value (%)	+11.5	+3.6 to +37.7
Experimental Ultimate Moment, kN-m	91.5	96.3
Theoretical Yield Moment, kN-m	90.2	100
Difference from experimental value (%)	-1.5	+4.2
Experimental EI Factor, MN-m^2	2.49	2.61
Theoretical EI Factor, MN-m^2	2.39	2.83
Difference from experimental value (%)	-4.3	+8.1

Note: 1 kN-m = 737 lbf-ft
1 MN-m^2 = 2.42 x 10^6 lbf-ft^2

REFERENCES

1. *Pipe Culvert Inlet and Outlet Protection.* Notice N 5040.3. FHWA, U.S. Department of Transportation, April 26, 1974.
2. Edgerton, R. C. Culvert Inlet Failures-A Case History. *Highway Research Board Bulletin 286*, 1960, pp. 13–21.
3. Pestotnik, C. *Report on Flexible Culvert Inlet Flotation Failures Survey.* Letter to County Engineers, Iowa DOT Ref. No. 521.1, Feb. 20, 1976.
4. Klaiber, F. W., R. A. Lohnes, L. W. Zachary, T. A. Austin, B. T. Havens, and B. T. McCurnin. *Design Methodology for Corrugated Metal Pipe Tiedowns: Phase I.* Final Report ISU-ERI-Ames-93409, Engineering Research Institute, Iowa State University, Ames, Iowa, 1993, 181 pp.
5. Havens, B. T. *Determination of the Longitudinal Strength and Stiffness of Corrugated Metal Pipe.* M.S. thesis, Iowa State University, Ames, Iowa, 1993.
6. Lane, W. W. *Comparative Studies on Corrugated Metal Culvert Pipes.* Report No. EES-236, Engineering Experiment Station, Ohio State University, Feb. 1965.
7. Armco Drainage and Metal Products. *Handbook of Drainage and Construction Products.* Armco, Middletown, Ohio, 1955.

The opinions, findings, and conclusions expressed herein are those of the authors and not necessarily those of the Iowa DOT or the Highway Research Board.

Publication of this paper sponsored by Committee on Culverts and Hydraulic Structures.

Measured Performance of 4.4-Meter Diameter Multiplate Keyhole-Slotted Conduit Under 20-Meter Earthfill

MARK T. BOWERS AND SRINIVASAN SWAMINATHAN

The need for information on the performance of large buried conduits was the catalyst for an instrumentation program for the Ohio Department of Transportation. A corrugated steel, multiplate keyhole-slotted conduit 4.4 m in diameter, 249 m long, under 20 m of earthfill was instrumented to obtain readings of earth pressures and measurements of changes in diameter as well as slip between the conduit plates. Eight pneumatic total pressure cells were installed at the springline with three more placed just above the crown. Near-field stresses have deviated by 15 to 40 percent from stresses calculated free of arching effects. Stresses in most cells have been decreasing slowly, indicating stress relief in the long-term behavior of the conduit. Diametral deformation stations were established at 7.62-m intervals throughout the length of the conduit. Four readings of diameter were made at each station (vertical, horizontal, and the two 45-degree diagonals). Excellent agreement with expected behavior of conduit geometry has been observed. A significant amount of plate slip occurred during the first few days following construction of the fill, but slippage has slowed with time. Measurement of earth pressures near the conduit wall has shown that slotted joints do permit greater burial depths than would conventional bolted joints.

A corrugated steel conduit 4.4 m in diameter and 249 m in length was constructed in June 1991 at the site of Ramp R of the Ronald Reagan Cross County Highway, Hamilton County, Ohio for the Ohio Department of Transportation (ODOT). ODOT engineers wished to validate the design concepts, numerical modeling, and construction procedures for such large, flexible structures. Of special interest was the action of slotted joints. Katona and Akl (*1*) indicated that

> . . . bolt holes slotted in the circumferential direction . . . permit relative circumferential contraction of the plates. As the culvert circumferentially contracts from joint slippage, the surrounding soil envelope is forced into a compression arch, which in turn carries a greater portion of additional loading. When all joint slippage is complete, the culvert again acts as a continuous unit so that further loading will be carried by both the structure and the soil arch. Ultimate failure in thrust typically occurs by seam failure, but at a burial depth significantly greater than that of a standard culvert without slotted joints. (*1*)

This case appeared to be an ideal beginning for the necessary data base. The authors referred to Selig et al. (*2*) for concepts related to measuring the performance of the conduit. Whereas Selig et al. (*2*) established instrumentation at one location, these authors gathered data over the entire length of the conduit and under more than double the fill height of the system tested by Selig et al. (*2*).

M. T. Bowers, Department of Civil and Environmental Engineering, 741 Baldwin Hall, P.O. Box 210071, University of Cincinnati, Cincinnati, Ohio 45221-0071. S. Swaminathan, The H. C. Nutting Company, P.O. Box C, 4120 Airport Road, Cincinnati, Ohio 45226.

INSTRUMENTATION AND MEASUREMENT

Instrumentation Plan

The first author established an instrumentation plan that was accepted by ODOT engineers. The plan involved frequent reading of earth pressure cells, measurement of the deformed conduit geometry with backfill loading and time, measurements of the slip of the keyhole-slotted joints, records of the soil backfill characteristics and compaction data, and surveyed elevations as the fill depth increased. The elevation view of the conduit and the profile of the overlying fill at Ramp R are shown in Figure 1. The instrumentation layout in elevation view is depicted in Figure 2, while the layout in plan view is shown in Figure 3.

The pressure cells chosen were Slope Indicator Company Pneumatic Total Pressure Cell Model 51482. These cells are an extremely sensitive and economical means for determining static total pressure on a plane surface. Eight earth pressure cells were installed (June 19) at the springline of the conduit, and the final three cells were placed (June 24) just above the crown. An excavation 4.6 × 2.4 × 1.22 m deep was made to accommodate the cluster of springline cells. The base of the excavation was then backfilled with layers of clean sand and compacted to at least the same degree of compaction as the surrounding earthfill and leveled. The cells were individually installed in small excavated pockets, each approximately twice the size of the cell. Each cell was positioned in its pocket and checked for correct functioning, alignment, and level. The pocket was then backfilled using clean sand to a density similar to that of the surrounding soil, taking care that no particles large enough to damage the tubing or cell performance were present. Tubing was run from the cells through 50-mm diameter holes cut in the conduit wall at the springline. The tubing was then connected to a terminal pipe mounted on the inside wall of the conduit at its midlength and approximately 3 m above the invert. Slack was provided in the tubing to avoid stressing or shearing of the polyethylene at the soil-conduit wall as the backfill soil consolidated.

Deformation points were established at 7.62-m intervals along the 249-m length of the conduit. Each point was marked with white fluorescent paint so that the locations could be seen easily when working in the conduit with flashlights. A total of 33 stations were marked. Four readings of diameter were taken at each observation point: vertical, horizontal, and two diagonals at 45 degrees from vertical. Permanent marks were established to ensure that the readings were taken at consistent positions with successive monitoring. Measurements were made using an aluminum rod that could be dismantled for easy transport. The three-piece rod had a section that moved against a scale. The outer two sections were of known

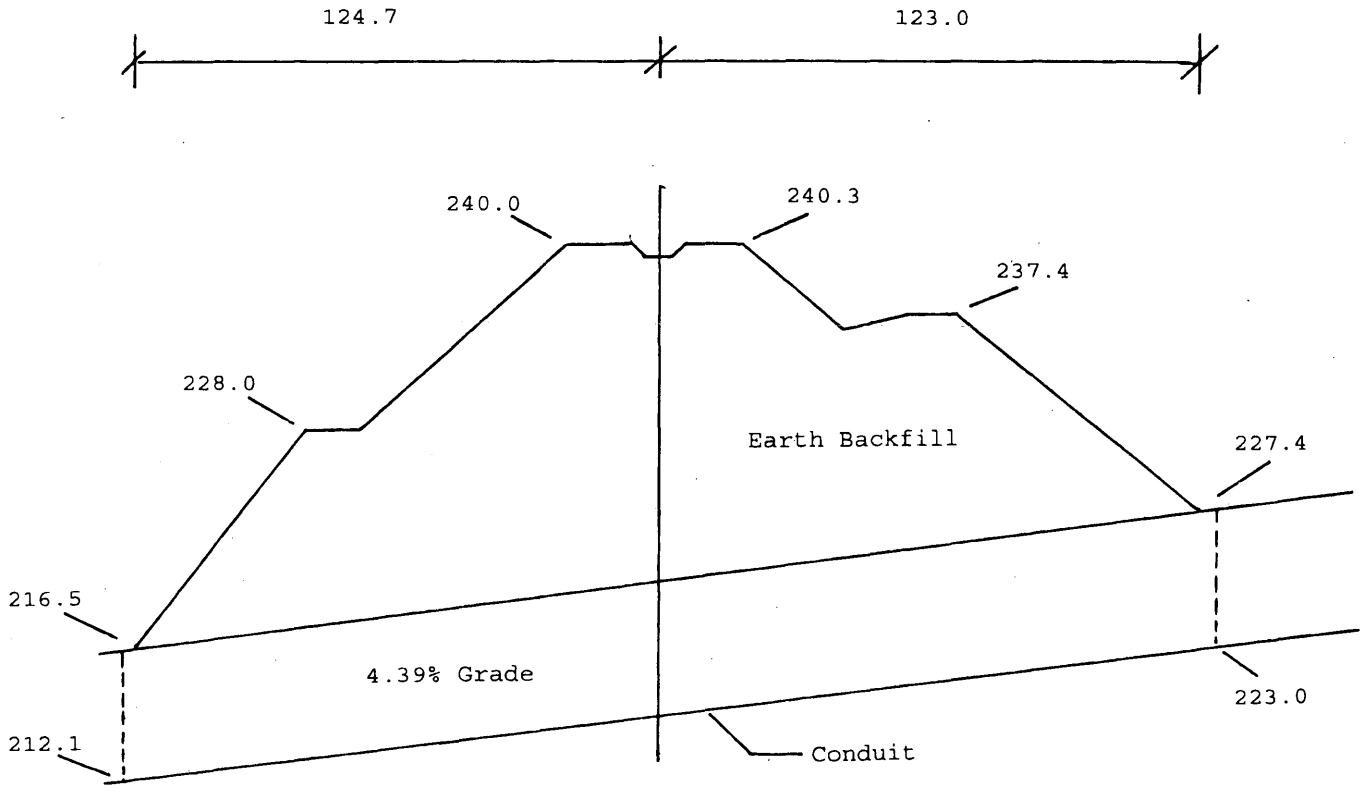

FIGURE 1 Elevation view of conduit with overlying fill (numbers represent elevations and lengths in meters).

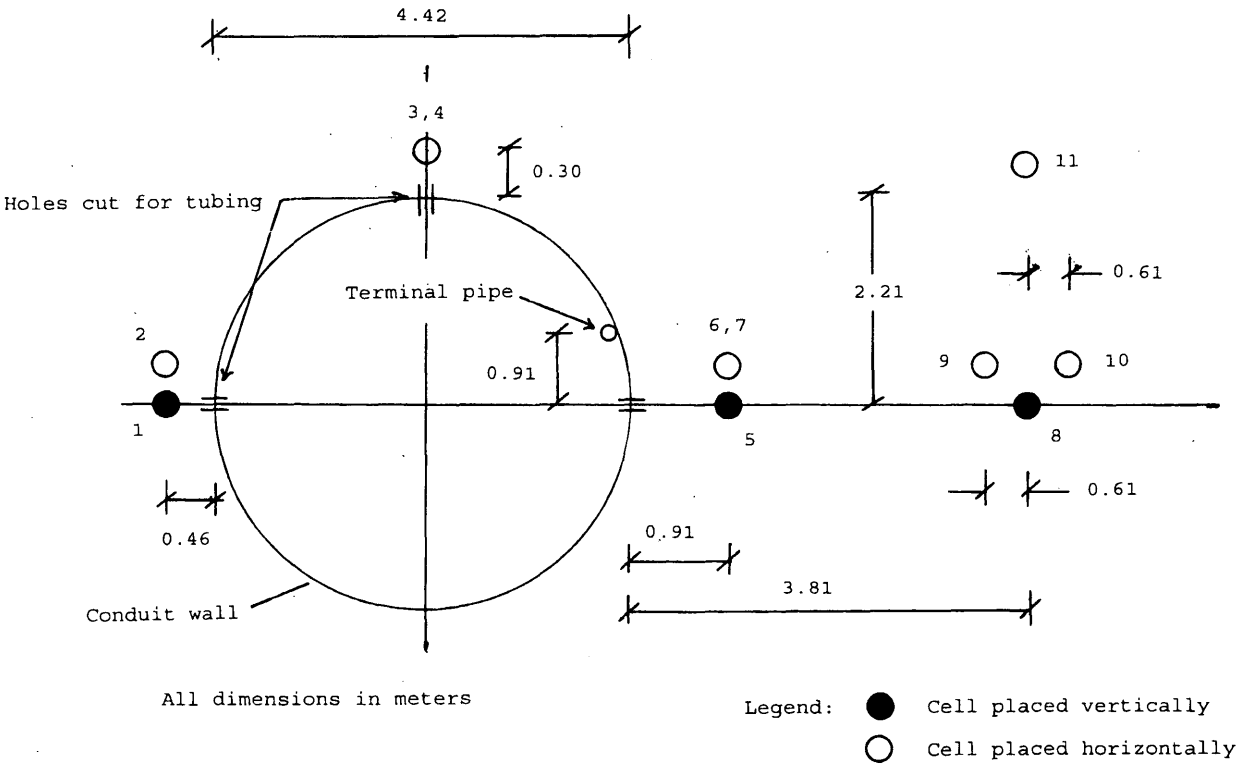

FIGURE 2 Elevation view of instrumentation layout for conduit (looking upstream).

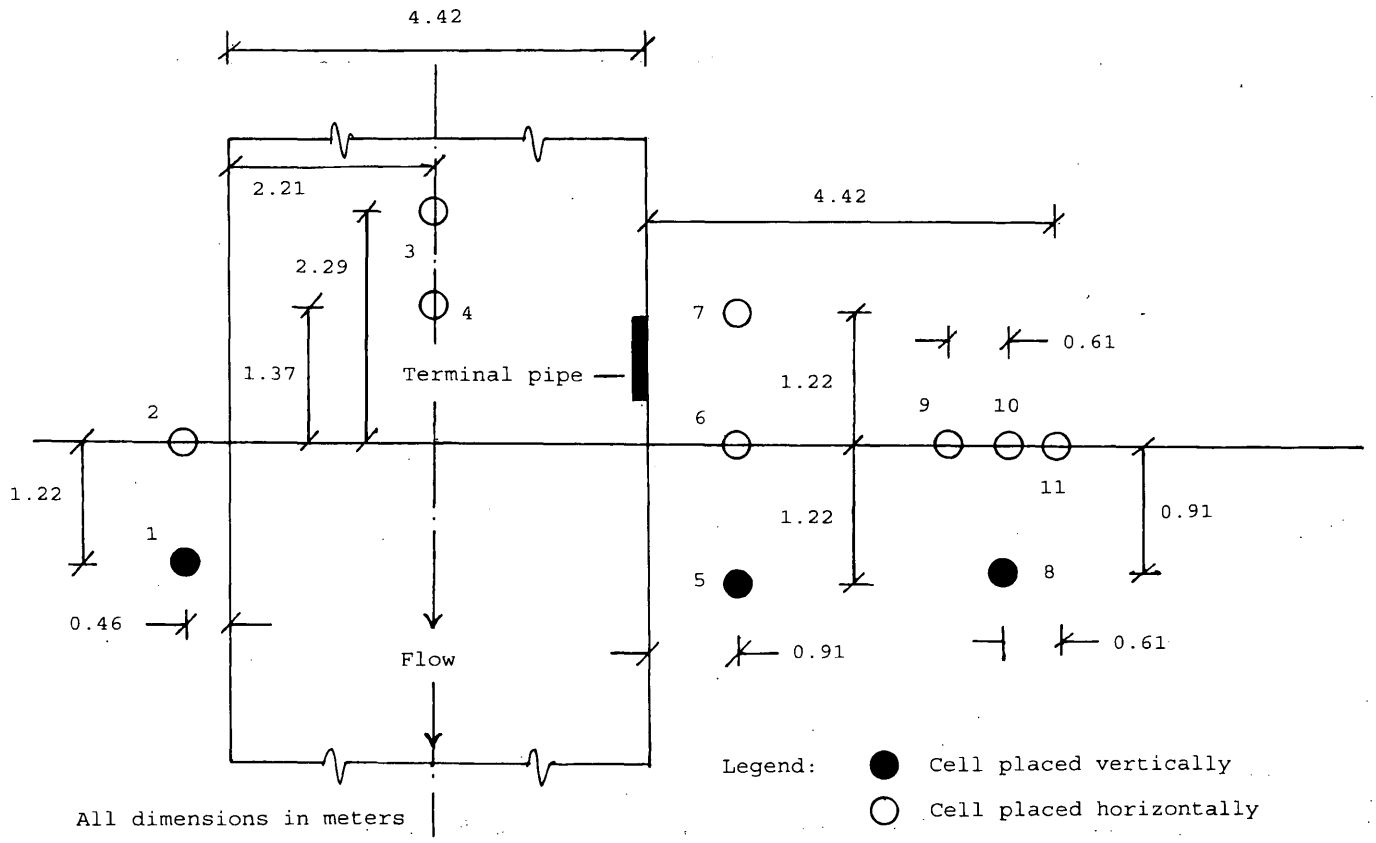

FIGURE 3 Plan view of instrumentation layout for conduit.

length. Hence, the field team merely had to place the needled ends of the rod against the permanent marks on the conduit walls and read the scale to obtain the diameter at a particular station. Care was taken to ensure that minimum flexure was present in the rod. The change in the rod length caused by temperature changes was insignificant. Repeatability to within 1 mm was obtained. All the data gathered in the field was transferred to computer data files for processing.

Regular monitoring of the keyhole-slotted joint slippage was undertaken. A simple procedure was adopted for this purpose. Using a steel punch, two distinctly visible sharp punch marks were made on either side of the multiplate bolt connection in the conduit wall. As the maximum amount of earthfill was near the midlength of the conduit, the keyhole connections in that area were monitored. A total of 16 observation points (eight points upstream and eight downstream of the centerline) 7.62 m apart were established. Slippage along the springline connections to the right and left of the conduit were monitored. The 10th and 20th bolt connections downstream and upstream of the centerline were also monitored. For the latter locations, the springline and invert bolt connections to the right and left of the conduit were measured, using time and fill placement as variables.

Earth Pressure Cell Measurements

Backfilling operations commenced on June 24, 1991; construction activity was temporarily suspended (contractor choice) from June 27 to August 29, 1991 just after the crown was covered. The earthfill was completed by October 17, 1991. All 11 earth pressure cells have functioned properly through early 1994.

A comparison between measured and calculated earth pressures has been made. The calculated earth pressures are the product of the unit weight of the compacted backfill material and the depth of fill at a particular cell location. Reports of compaction tests using the nuclear method were obtained from ODOT at regular intervals. The wet unit weight of the compacted fill varied from 19.8 to 21.7 kN/cu.m. The calculated earth pressures do not consider any effect of arching or other soil-structure phenomenon. Horizontal earth pressures were calculated by multiplying the vertical earth pressure by an average earth pressure coefficient of 0.37 (given the soil backfill type and compaction characteristics). The variation of the measured and calculated earth pressures with increasing fill height at the location of Cell 9 (free field, measuring vertical stress) is shown in Figure 4. The Cell 9 pressure readings compare quite well with the calculated pressures. The pressure is seen to steadily increase as fill placement continued. The measured pressures are about 34.5 kPa (5 psi) lower than the calculated pressures during most of the fill placement. The final recorded pressure was 412.3 kPa (59.8 psi) which is about 24.1 kPa (3.5 psi) lower than the calculated pressure for that fill height. This difference is reasonable given the average data from the compaction of the backfill.

The variation in the measured and calculated earth pressures with increasing fill height near the conduit wall at Cell 5 (near field, measuring horizontal stress) are depicted in Figure 5. While the recorded stresses increase in a near linear manner, the measured

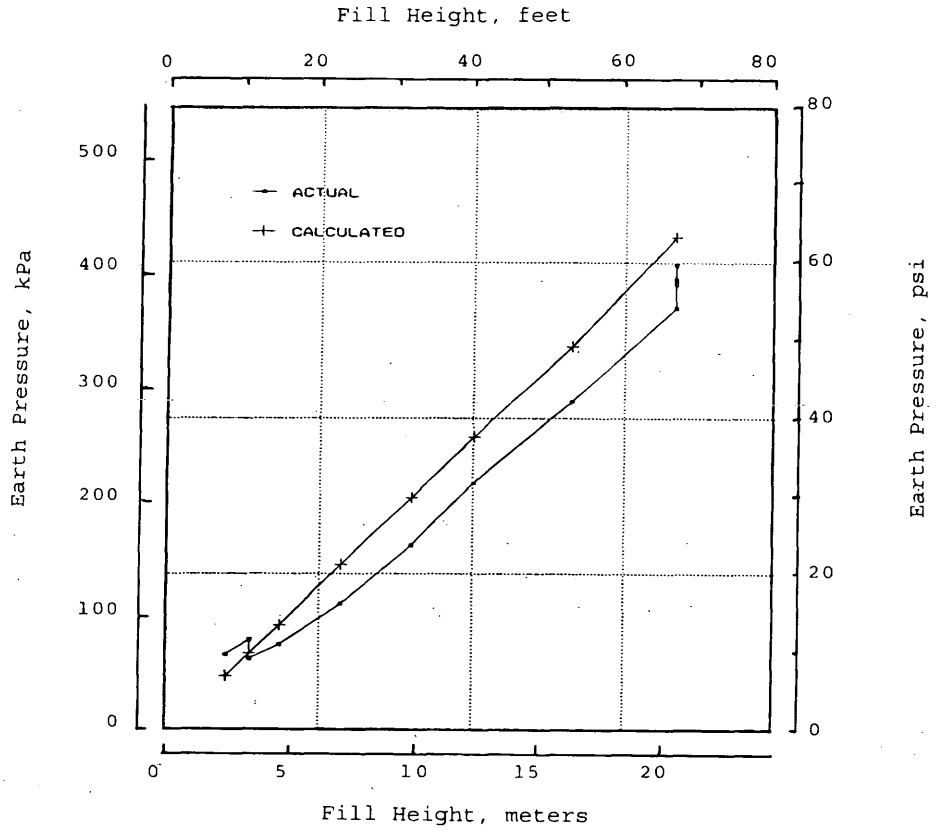

FIGURE 4 Variation of Cell 9 measured and calculated earth pressures with increasing fill height.

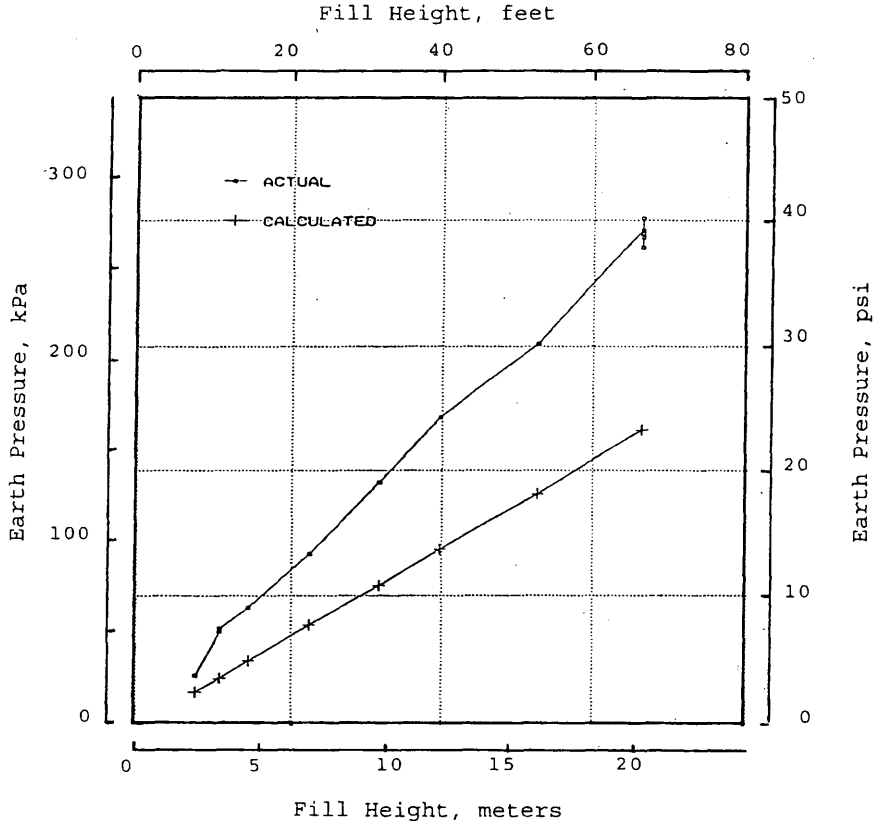

FIGURE 5 Variation of Cell 5 measured and calculated earth pressures with increasing fill height.

stress was found to always exceed the calculated stress. This makes sense given the lateral bulging of the conduit and the induced horizontal thrust against the soil backfill.

The measured and calculated vertical stresses at the crown of the conduit are shown in Figures 6 and 7. Replicate pressure Cells 3 and 4 were placed 1 m apart and 0.3 m above the conduit within the sand backfill. In each case the measured vertical pressure is less than the calculated pressure after the first 3 m of fill had been placed. The difference in this case is caused by arching within the soil backfill.

Excellent agreement between vertical free field measured and calculated stresses is indicated in Figure 8. The difference between the two is less than 13.8 kPa (2 psi).

Conduit Deformation Measurements

Thirty-three observation points at 7.62-m intervals were established along the entire length of the conduit. Horizontal, vertical, and two quarter-point measurements were made. The following designations apply to subsequent figures.

- 1-1 = Vertical Measurement Line
- 2-2 = Horizontal Measurement Line
- 3-3 = Quarter Point (right side) Measurement Line
- 4-4 = Quarter Point (left side) Measurement Line

The orientation scheme for the diameter deformations is depicted in Figure 9. Deformations along the length of the conduit as measured 20 January 1992 (3 months after the fill was completed) are shown in Figure 10. In the figure, positive deformation indicates elongation, while negative deformation represents shortening relative to the baseline measurements. Deformations have been plotted on a magnified scale to provide better understanding of the behavior of the conduit. The maximum vertical flattening is 96.5 mm (3.8 in.) at a point 137 m (450 ft) into the conduit. Horizontal elongation at the same location is 40.1 mm (1.58 in.), while the maximum elongation of 44.5 mm (1.75 in.) occurs 7.6 m (25 ft) further into the conduit length. The maximum shortening along quarter point (3-3) is 50.0 mm (1.97 in.) at a point 160 m (525 ft) into the conduit, and 49.0 mm (1.93 in.) along quarter point (4-4) at a point 122 m (400 ft) into the conduit. Maximum deformations occur between 61 to 183 m from the upstream mouth of the conduit where the fill height is greatest. Deformations increase from the upstream end towards the midlength of the conduit then gradually decrease as one approaches the downstream end.

Vertical Deformation Along the Conduit

The variation of the vertical shortening (squash) along the length of the conduit at various stages of fill placement is illustrated in Fig-

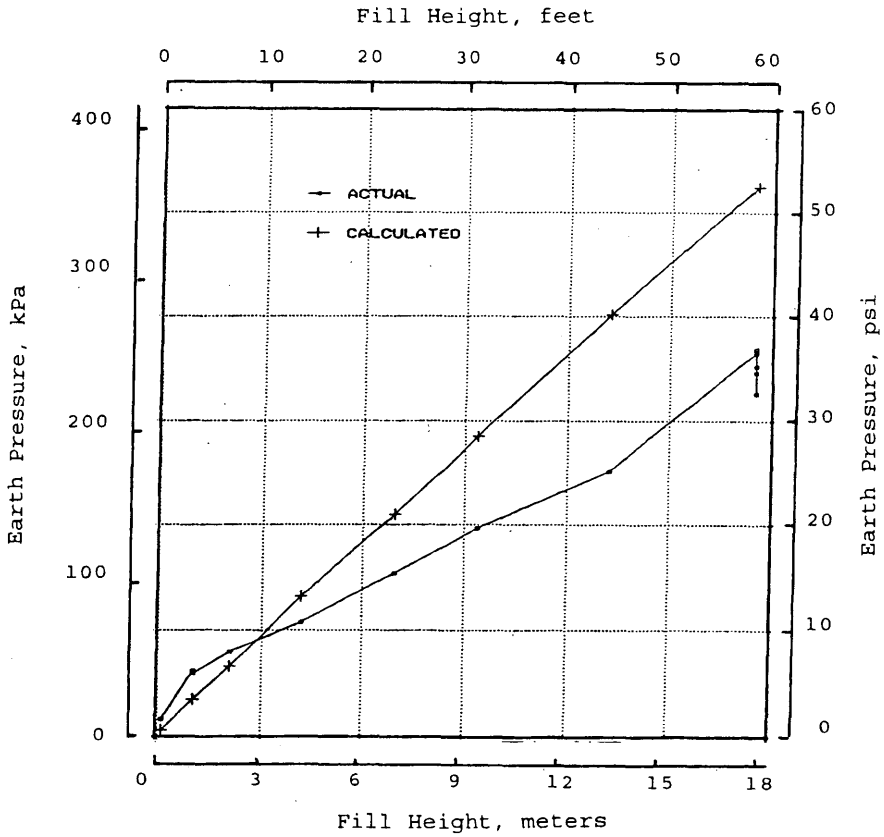

FIGURE 6 Variation of Cell 3 measured and calculated earth pressures with increasing fill height.

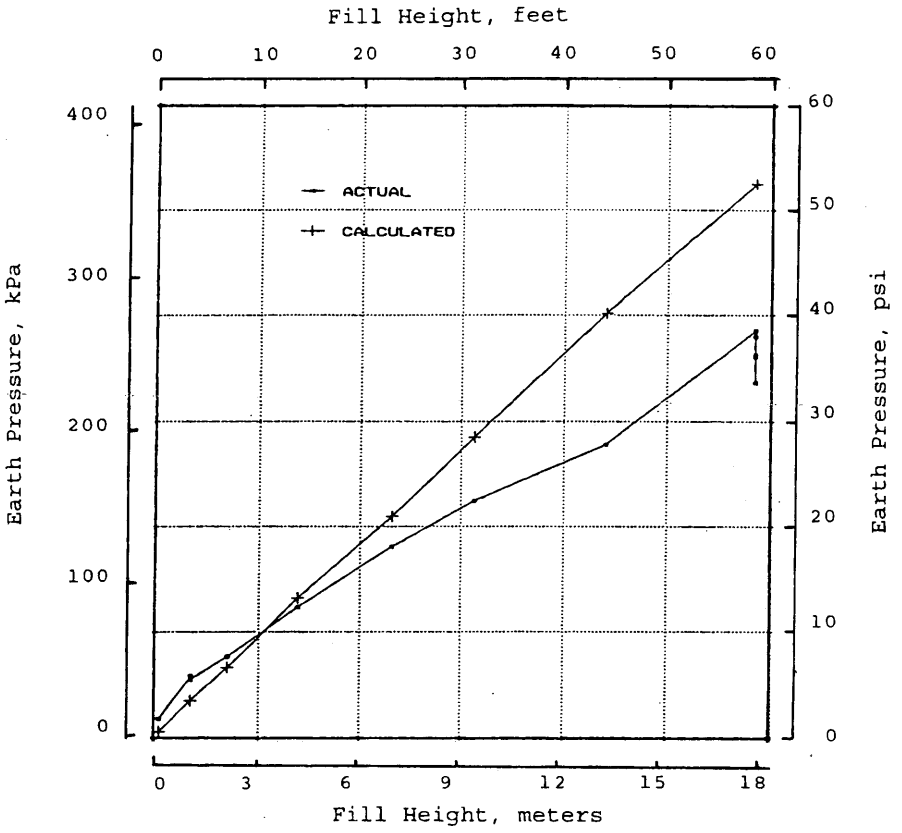

FIGURE 7 Variation of Cell 4 measured and calculated earth pressures with increasing fill height.

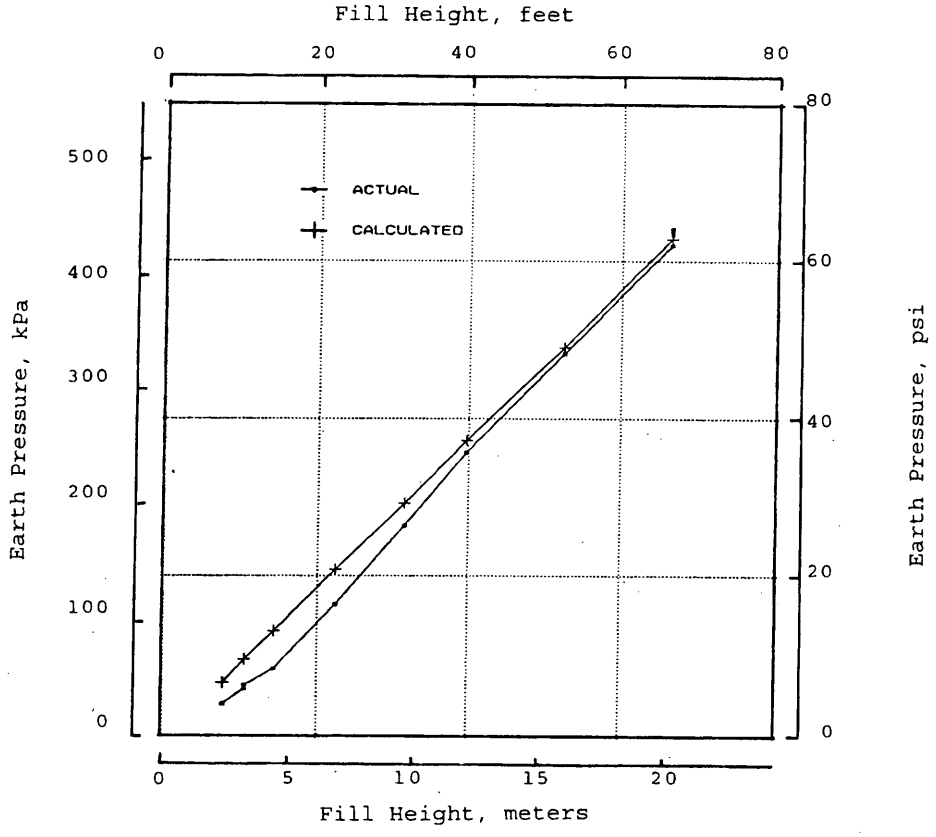

FIGURE 8 Variation of Cell 11 measured and calculated earth pressures with increasing fill height.

ure 11. Vertical flattening increases in a similar pattern as backfill placement increases. Maximum flattening occurs between 125 to 168 m in from the upstream end of the conduit. The maximum vertical flattening at the end of fill placement was 82 mm or approximately 1.9 percent of the as-built diameter.

Deformation measurements were continued for two years after completion of backfill construction. The objective was to observe the behavior of the culvert geometry with the passage of time. Conduit deformations at midlength as a function of time following the completion of the fill are shown in Figure 12. In the first 30 days the vertical flattening increased by 9.9 mm (0.39 in.); in the next 64 days the increase was only 4.1 mm (0.16 in.). Similarly, the horizontal elongation increased by 2.0 mm (0.08 in.) in the first 30 days and then by 1 mm (0.04 in.) in the next 64 days. Quarter point (3-3,4-4) measurements changed but slightly in the first 8 days and since then have been constant.

Keyhole-Slotted Joint Movement

Slippage of the keyhole-slotted joints between plates was monitored at numerous locations. As the fill reached its maximum height, the slippage was closely monitored. Slippage along the springline and the invert on both sides of the conduit was recorded. Stations were established as follows:

- C-20 = 20 bolts upstream of center;
- C-10 = 10 bolts upstream of center;
- C = mid-length (124 m into the conduit);
- C+10 = 10 bolts downstream of center; and
- C+20 = 20 bolts downstream of center.

The movement of the right and left abutment plates at the conduit midlength are noted in Figure 13. The decrease in slot movement following the completion of the fill is evident. To indicate how much slip occurs along the length of the conduit, 16 locations in the central 122 m were monitored. A graphical representation of this data is given in Figure 14.

Replication of Measured Pressures

Replication of earth pressure cells was completed at three locations to check the accuracy of stress cell measurements. Cells 3 and 4 placed at the crown have shown very comparable values. Readings have been within 14 kPa (2 psi) at all times (Figure 15). Cells 6 and 7 located at the springline have also shown excellent agreement (Figure 16).

CONCLUSIONS

The conduit geometry undergoes constant change with changing fill height. During backfilling up to the crown of the structure, the culvert flexes upward at the crown and inward at the springline, and the magnitude of these movements increases as the height of backfill

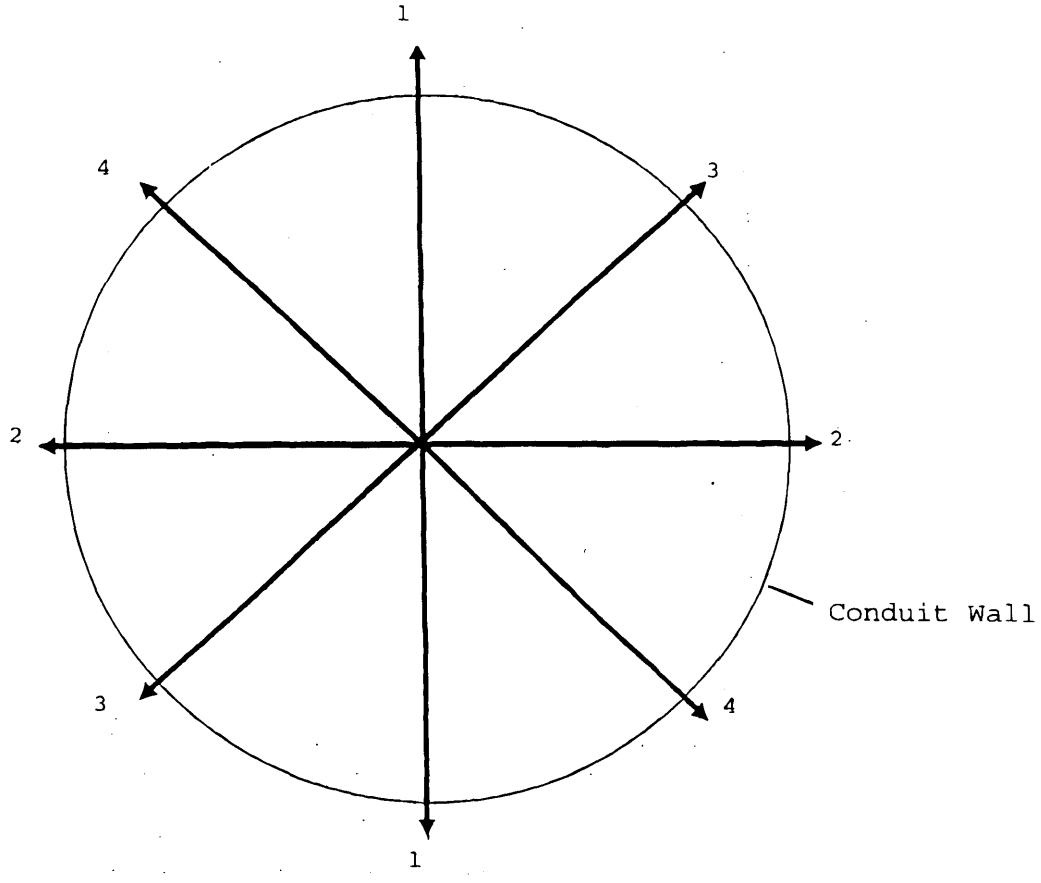

FIGURE 9 Orientation scheme for measurement of deformations in diameter of the conduit (looking downstream).

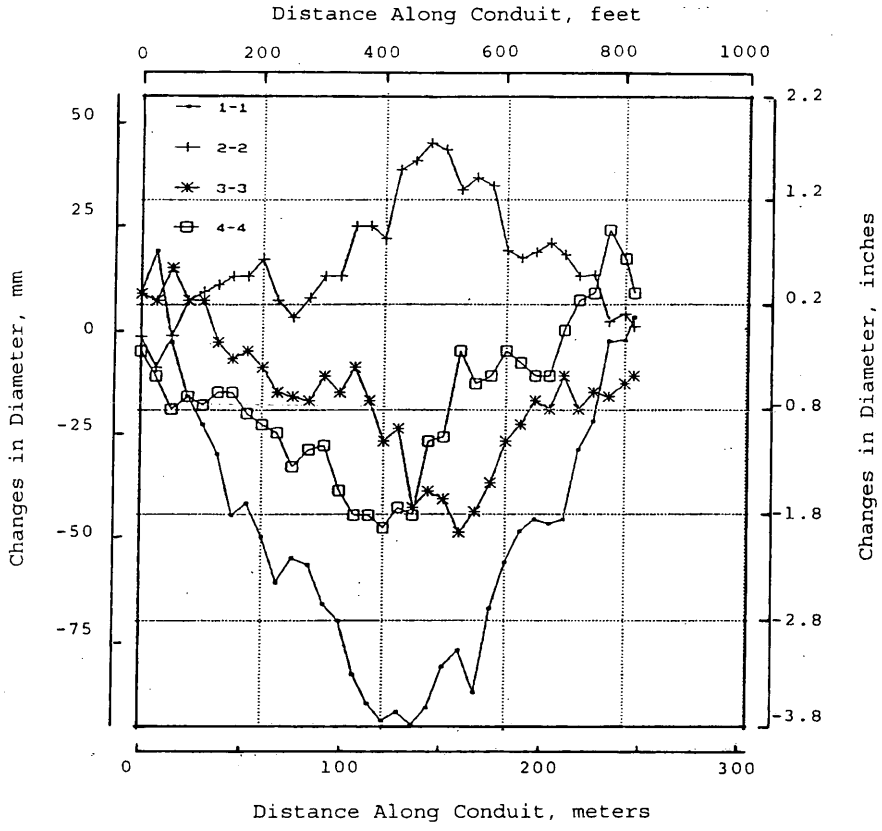

FIGURE 10 Accumulated changes in diameter of conduit 3 months after the fill was completed.

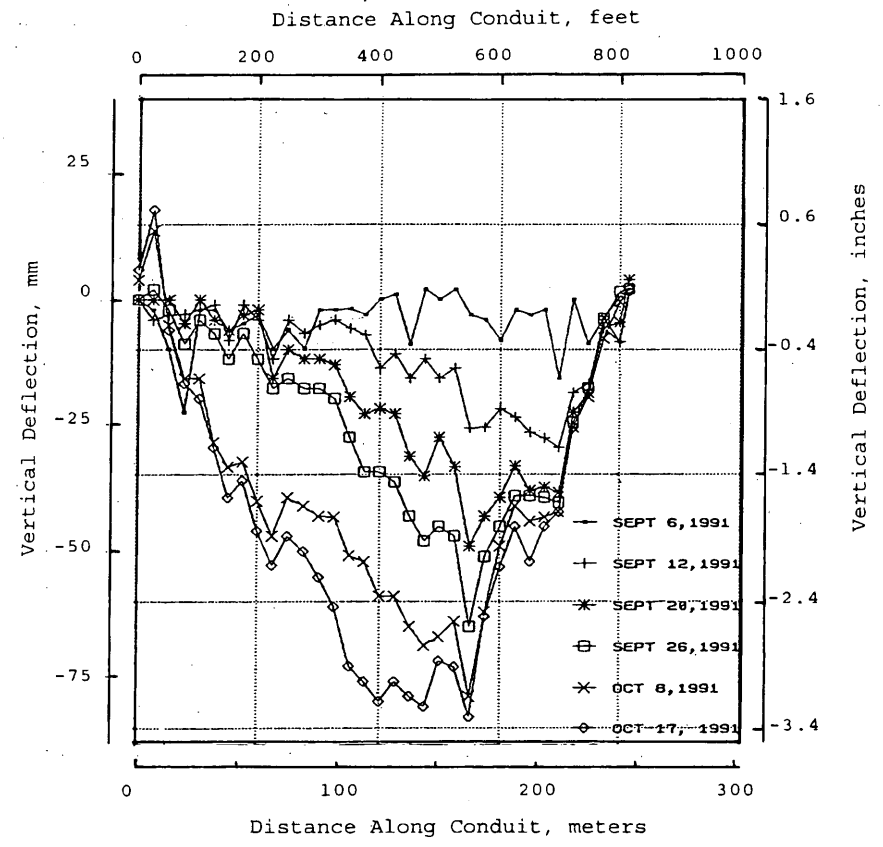

FIGURE 11 Variation in crown movement along entire length of conduit at different stages of fill placement.

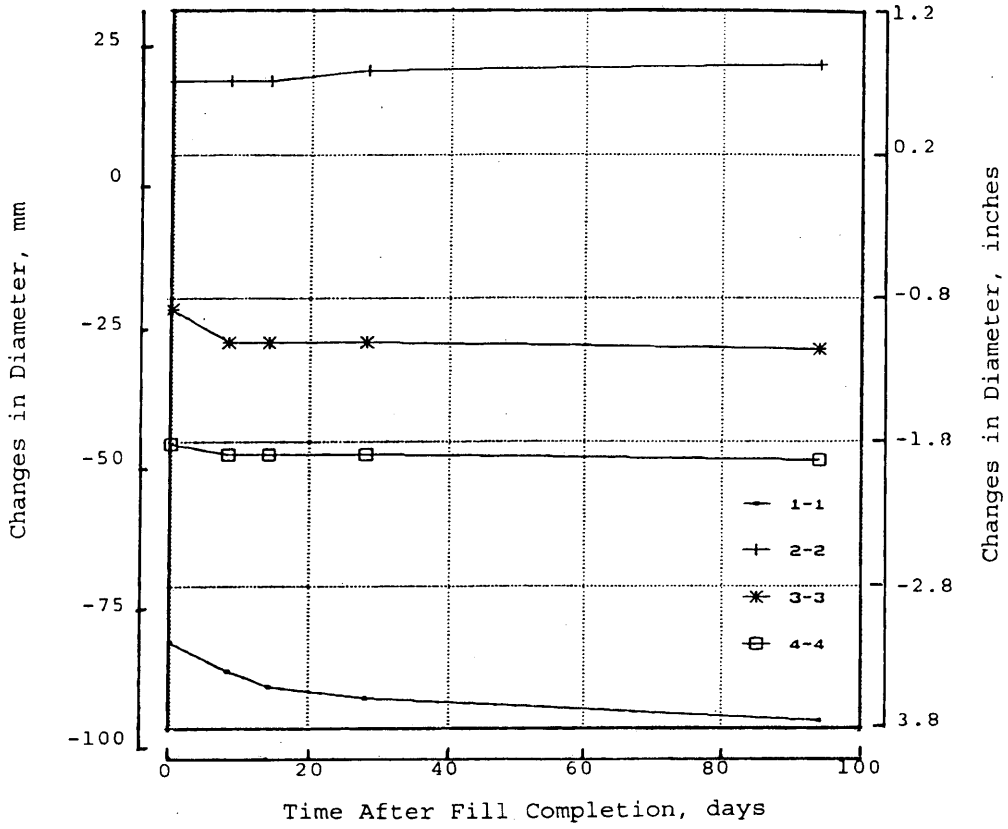

FIGURE 12 Long-term deformation of conduit measured at midlength (124 m into the conduit).

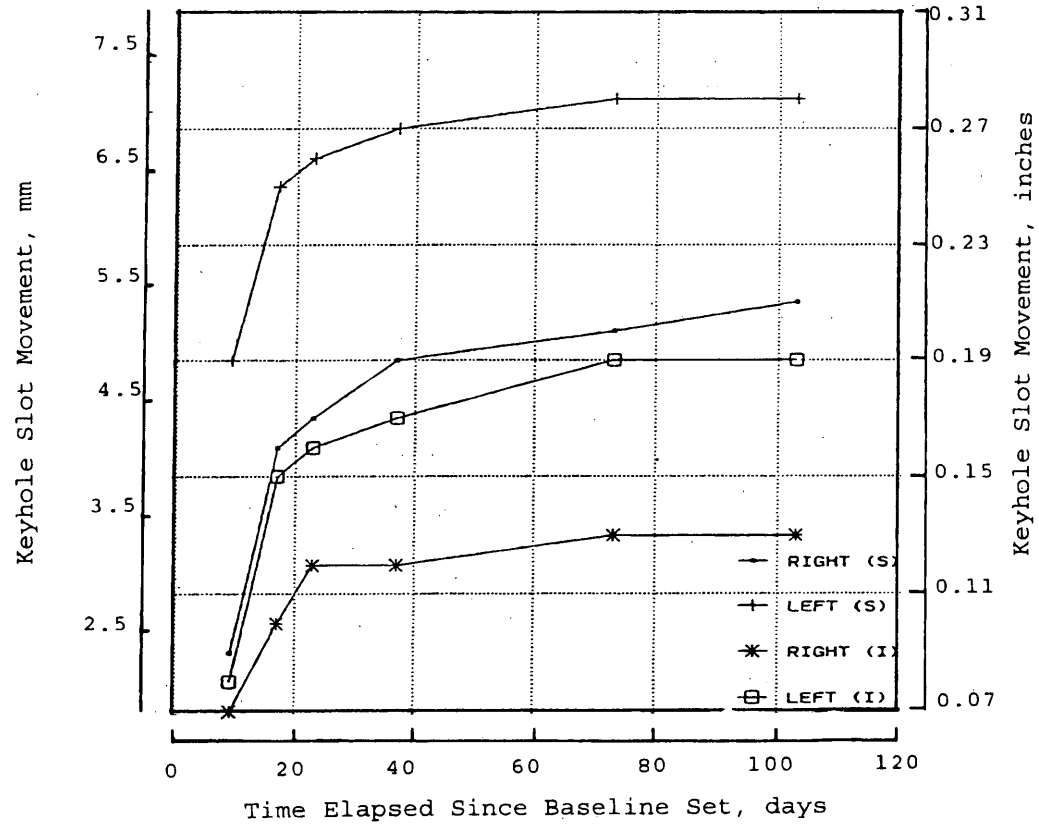

FIGURE 13 Keyhole slot movements at right and left walls of conduit at midlength (both springline (S) and invert (I)).

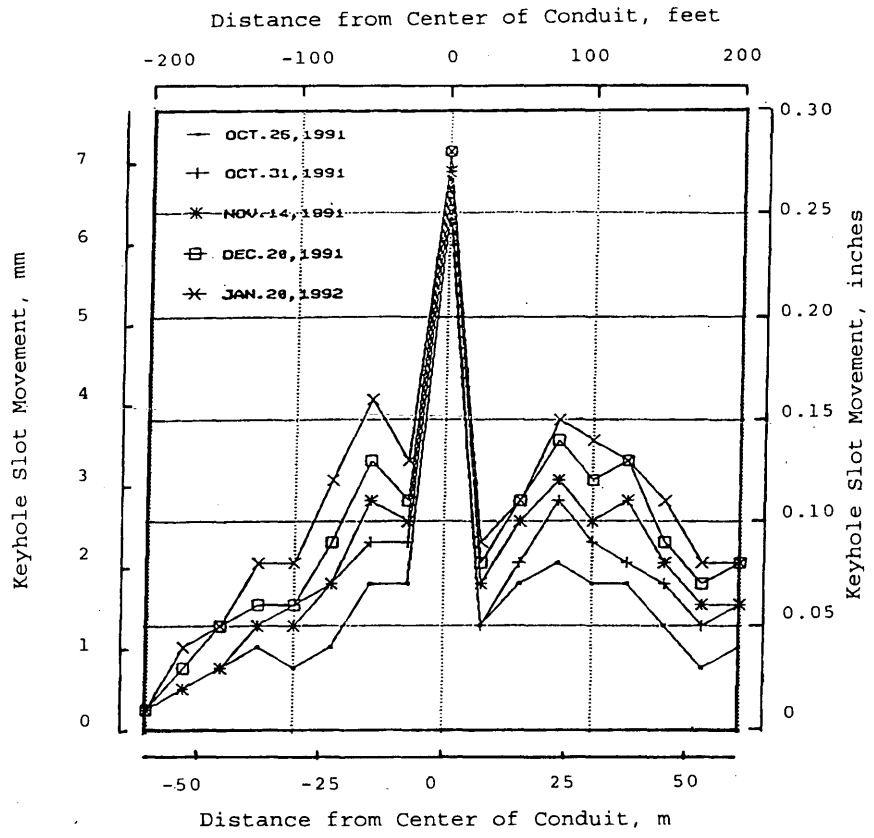

FIGURE 14 Keyhole slot movement of springline along left side of conduit (looking downstream) over time.

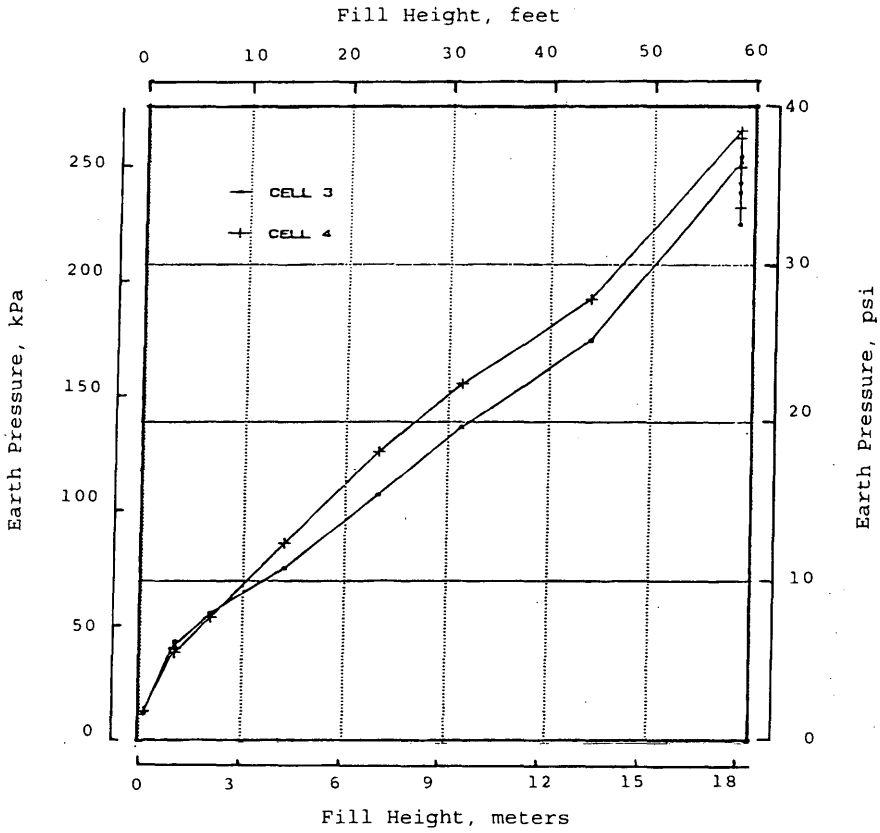

FIGURE 15 Comparison of earth pressure readings for Cells 3 and 4 with increasing fill height.

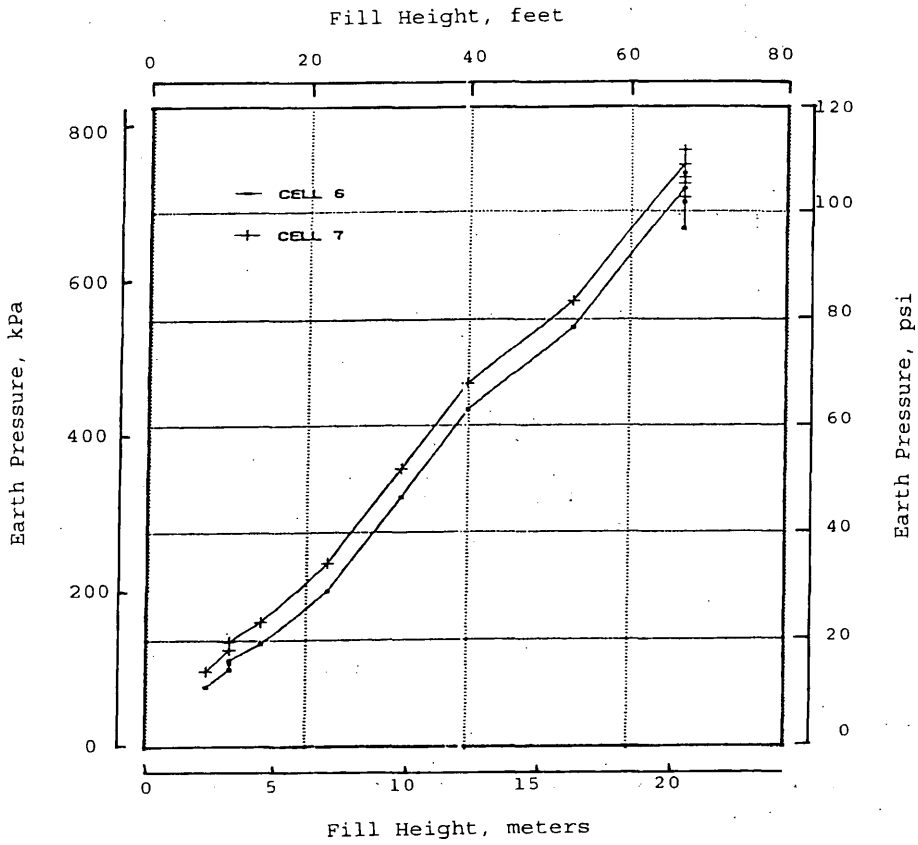

FIGURE 16 Comparison of earth pressure readings for Cells 6 and 7 with increasing fill height.

increases. As the backfill is placed on top of the structure, the magnitude of the movement decreases. Eventually, with a sufficient depth of cover over the structure, the movements reverse so that the crown of the structure flexes downward, and the conduit flexes outward at the springline.

The maximum movement during fill construction on the monitored conduit was at the crown, which moved inward about 96 mm (3.78 in.); this is just about the allowable crown deflection of 2 to 3 percent of the span considered in culvert design. The maximum elongation was 44.5 mm (1.75 in.). Fill placement sequence and compaction pressures had a significant impact on deformation. Both the quarter point measurements reflected inward flexing. As the conduit was founded on rock (with shallow sand bedding), settlement of the conduit from fill placement was considered minimal and not taken into consideration. No significant changes from temperature variations were found.

The measured lateral soil pressure near the conduit wall was within 25 percent of the overburden stress at the end of construction. The lateral stress near-field (within one pipe diameter of the conduit wall) was not too different from the far-field pressure. This could be from lateral compression of the soil near-field as the conduit elongated in the horizontal direction.

The vertical soil pressure in the structural backfill at the springline was in excess of the overburden stress at the end of construction just as found by Selig et al. (2). This increase is believed to be caused by load transfer from the more compressible embankment soil. Although both the vertical and horizontal soil pressures at the springline are greater than the free-field stresses, the ratio of the horizontal to vertical stress at the end of construction was about 0.40.

Positive soil arching at the crown was demonstrated. The measured vertical soil pressure at the crown at midlength was less than 60 percent of the overburden pressure at that elevation, but at free-field distance the vertical soil pressure was very comparable to the overburden pressure.

Long-term observations have indicated a slight decrease in recorded earth pressures. Decrease in cell pressures has not been significant. Conduit deformations have shown little change after 90 days following completion of the fill.

Keyhole slip at the springline of 8.1 mm (0.32 in.) was measured. Slip at the springline was higher than that at the invert. Most of the slip occurred within 15 days of fill completion. Long-term slip measurements have revealed a decrease in movement between the plates. Slippage could be responsible for larger crown flattening and hence increased positive arching over the crown. Load transfer (arching) caused by the slotted joint slip makes deeper burial of the conduit possible.

ACKNOWLEDGMENTS

Partial funding for this study was provided by the Ohio Department of Transportation. The assistance of ODOT engineer John Hurd is appreciated. Additional partial funding was provided by Contech Construction Products of Middletown, Ohio. The helpful suggestions made by Contech's engineer, James Schluter are appreciated. Graduate students Joseph Keiser and Robert Sheets are acknowl-

edged for their assistance during the initial setup of the instrumentation. Graduate student Prasad Rege is noted for his contributions in field measurements and finite element modeling reported in another thesis on this same conduit.

REFERENCES

1. Katona, M. G., and A. Y. Akl. Analysis and Behavior of Buried Culverts with Slotted Joints. In *Transportation Research Record 1008,* TRB, National Research Council, Washington, D.C., 1985, pp. 22–32.
2. Selig, E. T., C. W. Lockhard, and R. W. Lautensleger. Measured Performance of Newton Creek Culvert. *Journal of the Geotechnical Engineering Division,* ASCE, Sept. 1979, pp. 1067–1087.

Publication of this paper sponsored by Committee on Culverts and Hydraulic Structures.

First Precast Concrete Box Culverts in Minnesota

JAMES J. HILL AND FLOYD J. LAUMANN

The first known precast concrete box culverts were installed in Minnesota in 1974 on T.H. 60 with up to 9.75 m (32 ft) of overfill. The twin precast barrel sections were placed at the same elevation, and 1 m (3 ft) apart. The heaviest sections had 280-mm (11-in.) top and bottom slabs and 250-mm (10-in.) thick sidewalls. The 82-m (268-ft)-long box culverts plus precast apron sections were placed in less than 4 days. Actual construction time for this project was 4 weeks. The advantages of precast concrete box culverts over cast-in-place concrete culverts are shorter construction time and better quality control. The time savings is desirable because of the short seasonal construction time in Minnesota and heavy traffic usage. After 20 years these box culvert structures do not show any structural distress.

In 1974, the first precast concrete box culverts were installed in Wanamingo, Minn., on T.H. 60 under 9.75 m (32 ft) of fill. The double line of box culverts was 2.75 m (9 ft) high by 3.05 m (10 ft) wide. The box sections were designed for 9.75 m (32 ft), 7.60 m (25 ft) and 4.9 m (16 ft) of fill above them. They were placed 1 m (3 ft) apart at the same flow line elevation (see Figures 1 and 2).

One of the major concerns of the precast box sections was tongue and groove laps of the 1.2-m (4-ft)- and 1.5-m (5-ft)-long sections. The tongue and groove of the box sections were set at 150 mm (6 in.) long and had an inside slope of 13 mm (0.5 in.) to help slide the sections together (see Figure 3). Some cracking and/or spalling occurred at the haunch tongues on a few sections (see Figure 4).

Tie rods 25 mm (1 in.) in diameter were placed through tie holes at about midheight to prevent culvert settlements and frost action from pulling the sections apart (see Figures 5 and 6). These tie rods were also used on precast culvert end sections.

DESIGN CONSIDERATIONS AND STRESSES

The design of conventional concrete box culverts was based on service load stresses and moment distribution. No allowance was made for corner fixity/restraint. The precast boxes were designed for an embankment load condition using Marston-Spangler loading theory with 1|925 kg/m^3 (120 lb/ft^3) soil weight. This produced an earth load range of 1.13 to 1.4 times the earth column load over the box.

Side pressures were taken at 0.16 and 0.75 of the vertical load to determine maximum steel in top and bottom slabs and sidewalls. A dead load factor of 1.50 and a live load factor of 2.50 were used according to existing AASHTO specifications. Live load based on HS20 loading with impact and distribution through earth fills was based on 1973 AASHTO Standard Specifications for Highway Bridges.

The design yield strength of the wire mesh was held to a maximum of 413|685 MPa (60,000 lb/in.^{2}) even though 448|160 MPa (65,000 lb/in.^{2}) material was used. The design shear reinforcing stress limit was 206|840 Mpa (30,000 lb/in.^{2}) with the allowable concrete compressive stress at 34,470 MPa (5,000 lb/in.^{2}).

The concrete cover on the reinforcement was set at 25 mm (1 in.) which was taken from ASTM specifications. In some cases this yields 13 mm (1/2 in.) of cover when ASTM tolerances are employed (see Figure 6).

Cracks occurred in most sections at the center of the inside side wall, and at the bottom of the top fillet before the sections were placed in the field. This was apparently due to stresses from handling and/or shrinkage. The side walls inside faces did not have any steel.

The wall thicknesses of the box sections were held to a minimum for hauling purposes (see Table 1 for actual thicknesses used).

When dead and liveload shear stresses exceeded allowable concrete shear stress, shear stirrups were added as required (see Table 2). Several different types of shear steel were allowed, but all types were required to lap around primary reinforcement (see Figures 7 and 8). The J bar option shown in Figure 7 was used on 7.6-m (25-ft) and 9.75-m (32-ft) sections.

Mastic rope was placed in the tongue and groove joint to prevent the movement of soil materials through them. The rope was packed into the exposed joint before the adjacent culvert section was placed (see Figure 3).

BACKFILL MATERIAL AND COMPACTION

Granular bedding as per Minnesota/U.S. Department of Transportation (MN/DOT) Specification 2451.3C2 was required beneath the culverts. Granular bedding contains natural or partly crushed natural gravel obtained from a natural gravel deposit. The foundation material was required to be shaped to closely fit the bottom of the box culvert. Bedding material was placed in 150-mm (6-in.) lifts and compacted to 95 percent of maximum density. The immediate 150 mm (6 in.) of bedding beneath the bottom of the culvert sections was only consolidated to sufficiently produce uniform pipe support. A subcut of 300 mm (12 in.) was made.

Selected material as per MN/DOT Specification 2451.3D was used around the sides and on top of the culvert sections. The selected material is acceptable mineral soil which is free of clods, sod, and roots. This material was compacted to 90 percent maximum density in 200-mm (8 in.) lifts. All backfill progressed in simultaneous uniform horizontal layers.

J. J. Hill, MN/DOT Bridge Office, 1500 W. County Road B2, Roseville, Minn. 55113. F. J. Laumann, Hancock Concrete Prod. Co., Inc., 5275 Edina Industrial Boulevard, Minneapolis, Minn. 55439-2919.

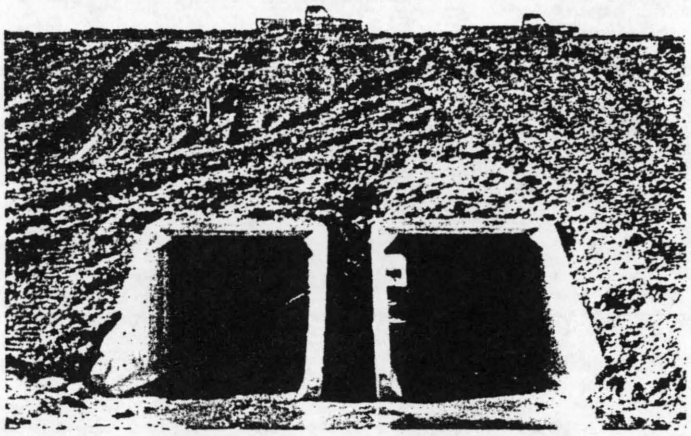

FIGURE 1 Inlet view of box culverts.

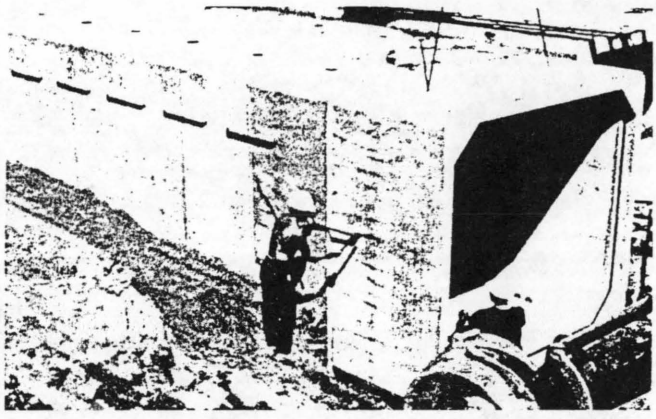

FIGURE 2 Side view of box culverts.

The two lines of boxes were placed 1 m (3 ft) apart to provide sufficient room for adequate compaction. Riprap was placed on the fill slope adjacent to the boxes (see Figures 9 and 10).

OTHER DESIGN CONSIDERATIONS

To prevent piping and undermining of culvert inlets and outlets, riprap or concrete dropwalls were used by MN/DOT on cast-in-place concrete culverts. Riprap was used on this box culvert project with reasonable success.

To improve the flow characteristics at the inlets to the box culverts, 100-mm (4-in.) chamfers were added to the concrete edges (see Figures 11 and 12). Based on FHWA's published data on inlet loss coefficients, the sloped/beveled ends appear to have a 0.5 inlet loss coefficient.

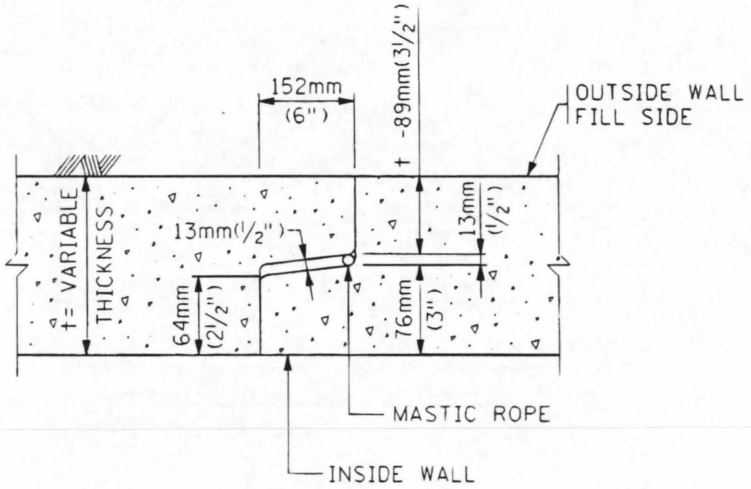

NOTES:

1. TONGUE AND GROOVE TO BE 152mm(6").
2. TONGUE 64mm(2½") MIN. MEASURED FROM INSIDE WALL.
3. 13mm(½") ANNULAR SPACE BETWEEN TONGUE & GROOVE ALLOWS ROOM FOR MASTIC WHEN NECESSARY.

FIGURE 3 Tongue and groove detail for precast box culverts.

FIGURE 4 View of concrete spalling at bottom haunch tongue section.

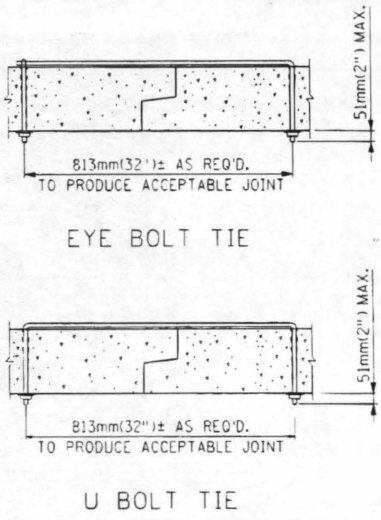

FIGURE 5 Bars at joints.

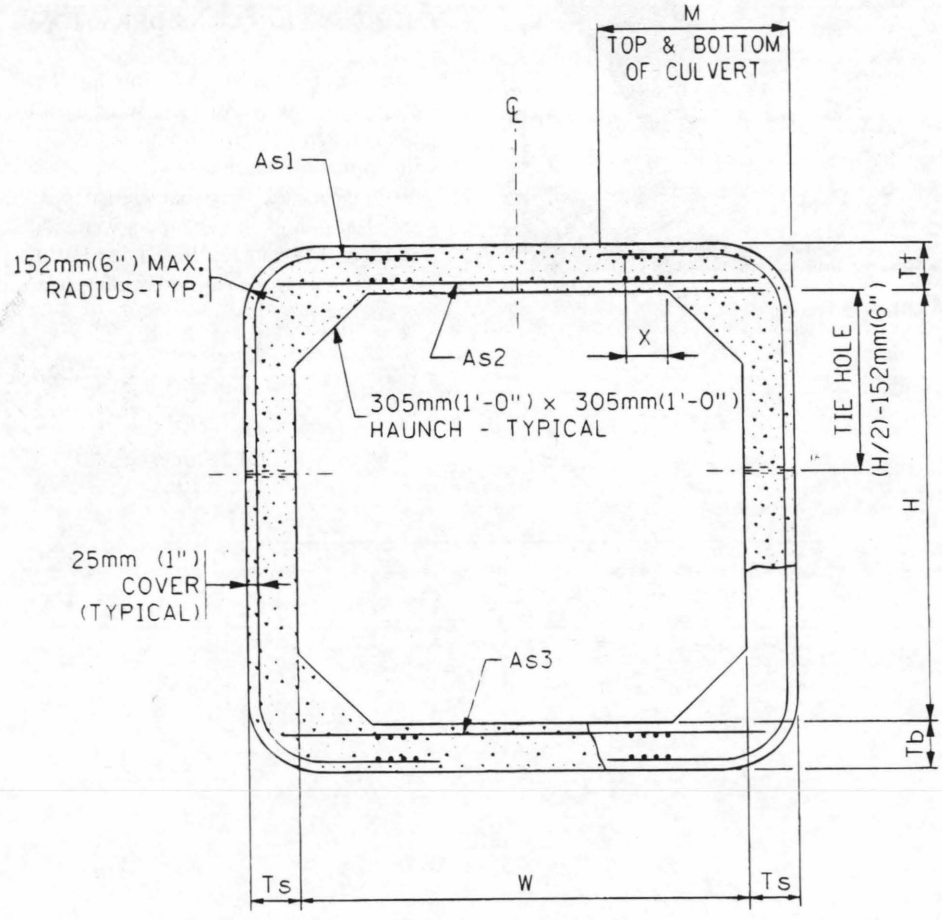

FIGURE 6 Cross section of box culvert.

TABLE 1 Box Culvert Wall Thickness

Design Fill Height	Top Slab	Bottom Slab	Sidewall
9.75 M (32 ft.)	280 mm (11 in.)	280 mm (11 in.)	250 mm (10 in.)
7.60 M (25 ft.)	250 mm (10 in.)	250 mm (10 in.)	200 mm (8 in.)
4.90 M (16 ft.)	250 mm (10 in.)	250 mm (10 in.)	200 mm. (8 in.)

TABLE 2 Steel Reinforcement Requirements

DESIGN STEEL REQUIREMENTS IN SQ. MM/300 MM (SQ. INCHES/FOOT)			
	4.88M (16') Overfill	7.62M (25') Overfill	9.75M (32') Overfill
A_{s1}	226 (.351)	433 (.671)	612 (.948)
A_{s2}	540 (.837)	995 (1.543)	1186 (1.838)
A_{s3}	570 (.884)	1032 (1.600)	1220 (1.891)

NOTE: See Figure 5 for location of reinforcement.

SHEAR STEEL					
	4.88M (16') Overfill	7.62M (25') Overfill		9.75M (32') Overfill	
		x distance	Area Req'd	x distance	Area Req'd
Top Slab	Not Req'd.	650 mm (25.5")	75 mm²/300 mm (.117 in²/ft)	850 mm (33.25")	130 mm²/300 mm (.206 in²/ft)
Bottom Slab	Not Req'd.	SAME AS TOP SLAB		SAME AS TOP SLAB	

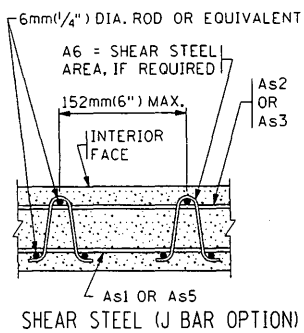

FIGURE 7 Shear steel (J bar option).

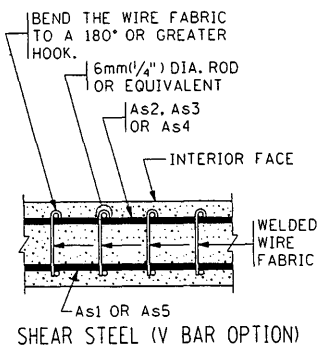

FIGURE 8 Shear steel (V bar option).

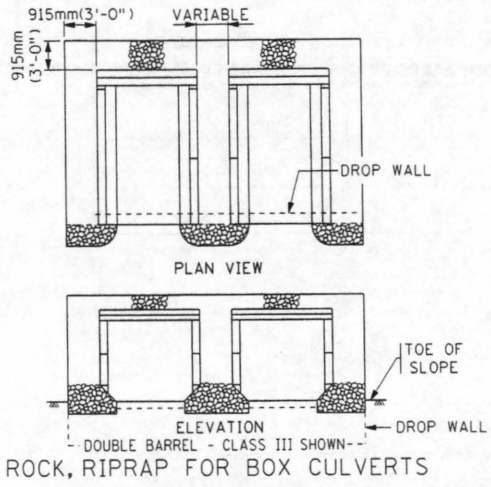

FIGURE 9 Rock riprap for box culverts.

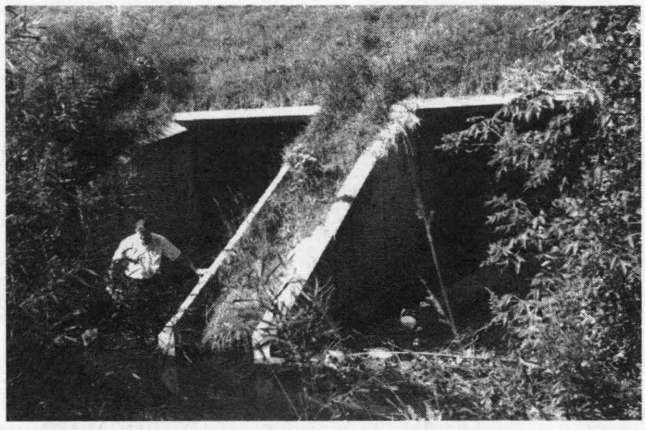

FIGURE 10 View of inlet end of concrete box culvert.

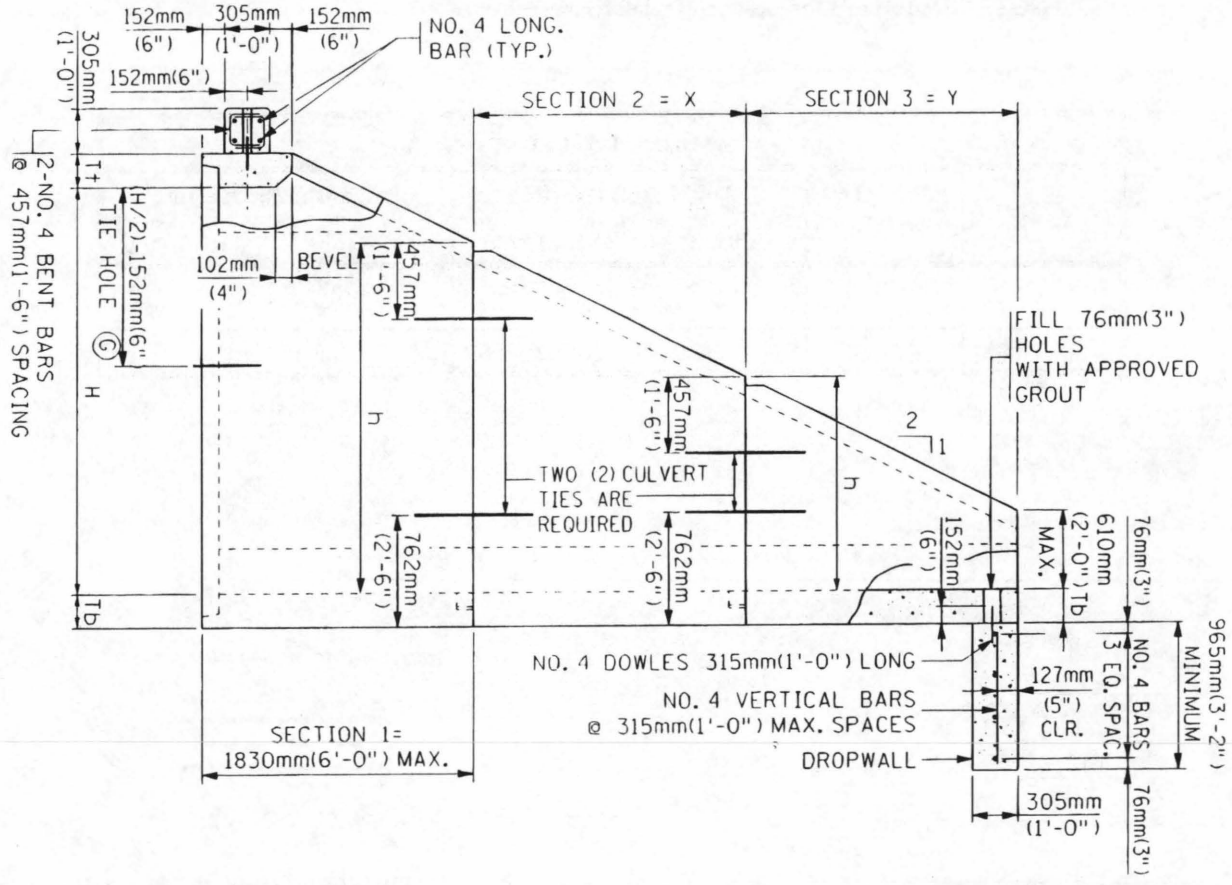

FIGURE 11 Box culvert side elevation.

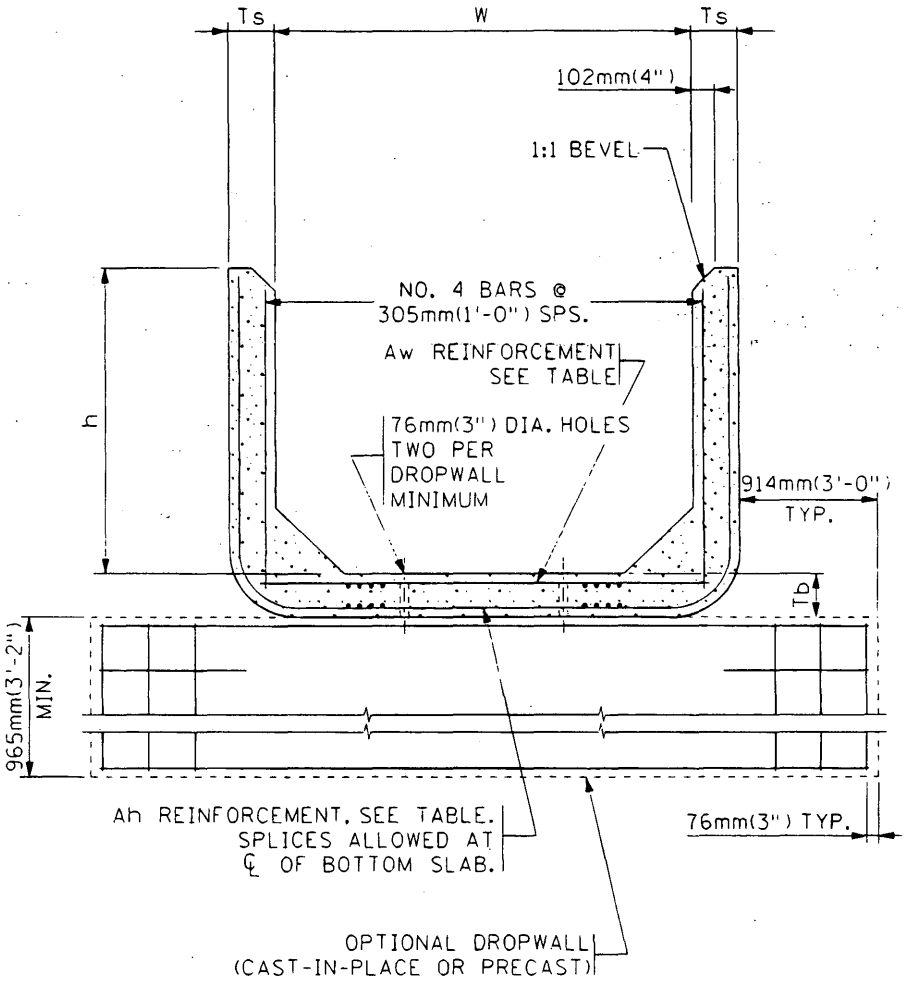

FIGURE 12 End section of box culvert.

CONSTRUCTION AND SUBSEQUENT INSPECTIONS

These concrete box culverts were inspected after construction and at least semiannually for 10 years after construction. During these inspections the following items were observed:

- There was some piping action under the inlet end of one box culvert line. Water at low flow disappeared under the inlet section and resurfaced inside the pipe at about 5 m (16 ft) downstream.
- On about midheight of the inside face of the vertical walls a small horizontal hairline crack occurred. No reinforcement steel had been used on inside face of side wall.
- Also slight hairline cracks appeared at the location where the sidewall met the 300 mm (12 in.) fillets. These cracks would sometimes appear in culvert sections while in the manufacturer's yard and/or at the project site before installation. These appeared to be shrinkage and/or handling stress cracks. They did not increase in size when installed in the field and to date are unchanged. See Figure 13 for a view of the interior of one box culvert which was taken in a September 1994 inspection.

DESIGN MODIFICATIONS

Newer designs added minimum temperature steel in the side walls plus no. 3 bars in the fillets, which eliminated the cracking problem. Reinforcement in the top of the top slab and bottom of the bottom slab was also added in later designs for potential handling stresses.

Standard thicknesses of 230-mm (9-in.) top slab, 250-mm (10-in.) bottom slab and 200-mm (8-in.) sidewalls were adopted for standard box culvert designs.

Later box culvert joint designs allowed a 600-mm (24-in.)-wide filter cloth on the top and sides of the culvert joint with mastic rope placed on the bottom. This method kept sand, and so forth, from going through the joint, but allowed water to effectively move through the joint.

Precast dropwalls have been standardized at locations where required.

Tongue and groove lengths have been reduced from 150 mm (6 in.) to 100 mm (4 in.) to reduce cantilever reinforcement requirements and potential cracking.

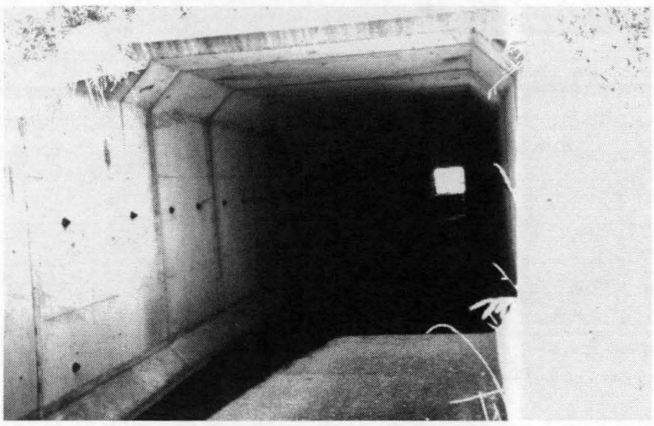

FIGURE 13 View of inlet sections of box culvert.

CONCLUSIONS

Based on this project and other similar box culvert projects, conclusions are as follows:

- To prevent water from piping under the culvert, dropwalls of 1.00 m (3.17 ft) depth are required at inlet and outlet end sections.
- Minimum steel or the amount required by design is now required on inside faces of sidewalls to eliminate cracking from sidefill pressure and handling stresses.
- Reinforcement in the top of the top slab and the bottom of the bottom slab was also added by design to meet temporary handling stresses.
- Reinforcement is now required to have a tolerance between 40 mm (1.5 in.) minimum and 50 mm (2 in.) maximum concrete cover because of severe environment and salt usage in Minnesota.
- To meet AASHTO temperature and minimum reinforcement requirements, 40 mm^2 (0.06 $in.^2$) of reinforcement is placed longitudinally and 125 mm^2 (0.20 $in.^2$) is placed transversely at 305-mm (12-in.) spacings.

After 20 years of service these culvert sections with fills up to 9.75 m (32 ft) are still functioning and in good shape (see Figure 13). However, the items mentioned in the above conclusions have been added to the present design of precast concrete box culverts to assure a good quality structure.

Publication of this paper sponsored by Committee on Subsurface Soil-Structure Interaction.

Response of Profiled High-Density Polyethylene Pipe in Hoop Compression

IAN D. MOORE AND FUPING HU

Profiled polymer pipe is a three-dimensional structural form that behaves in a three-dimensional manner when subjected to soil pressures during burial. The three-dimensional response of profiled high-density polyethylene (HDPE) pipe was recently measured in a soil cell at the University of Massachusetts. The profile tested featured a corrugated section fitted with a smooth internal liner. A finite element analysis for determining the response of buried profiled pipe has been developed by the first author. The soil cell results are examined using the three-dimensional finite element analysis. Distributions of circumferential and axial stress and strain are considered in the profiled pipe and in the soil surrounding it, and different responses of the corrugation and the liner are examined. The analysis is used to examine performance limits for profiled HDPE pipe under large hoop compressions.

To successfully engineer buried profiled high-density polyethylene (HDPE) pipe, several aspects of the soil-structure system should be considered. Some of these issues are common to both HDPE and other pipe products, but others are unique to the HDPE pipes, which are the primary focus of this study. Understanding these issues is necessary to design efficient, reliable products suitable for use in a wide range of applications.

Initially, the structural design of buried HDPE pipe was based on semi-empirical procedures developed for flexible metal pipe products [in particular, the Iowa equation developed by Spangler (*1*)]. Pipe design has generally focused on the change in diameter across the pipe section, although levels of circumferential hoop and bending stress, circumferential strain, and the possibility of circumferential buckling have also been considered.

Culvert and buried pipe technology was significantly advanced in the 1960s and 1970s after the development of closed form solutions [Burns and Richard (*2*)] and finite element analyses [Katona (*3*)] of pipe-soil interaction. These studies have contributed much to the understanding of buried pipe response at working loads. In particular, the behavior of buried profiled polyethylene pipe has been examined using two-dimensional finite element analyses [Chua (*4*) and Katona (*5*)] and three-dimensional finite element analysis [Moore (*6*)]. These computational tools have the potential to ensure that the structural design of buried HDPE pipe is based on rigorous engineering principles, and that it is both safe and efficient.

Concerns remain about several specific issues for HDPE pipes. The three-dimensional nature of the corrugated pipe profile has prompted interest in distribution of circumferential and axial stresses in the profile and the contribution of the liner to the overall structural performance. The time-dependent nature of polyethylene response has led to a series of questions about effective modulus, pipe stiffness, stress relaxation, and creep. Furthermore, the move toward limit state design in North America is prompting demands for more information about stability and serviceability limits for HDPE pipe.

A pipe buried deeply within an earth embankment is subjected to vertical and horizontal field stresses as a result of the overburden and the lateral earth pressures. Those earth pressures lead to the development of hoop compressions in the pipe, which can cause important circumferential strains.

Responding to the demand for direct measurement of pipe performance under hoop compression, a test cell was developed recently by Selig at the University of Massachusetts (UMass) (*7*). This report describes the results of a theoretical investigation of those tests, examining the development over time of circumferential stress and strain and the three-dimensional response of the corrugation and internal lining of the pipe. The analysis is used to consider performance limits for pipe subjected to large hoop compressions.

UMASS COMPRESSION CELL TESTS

Three tests were performed in the compression cell at UMass and involved the application of uniform radial compressions to the external boundary of a thin ring of soil placed around the pipe. Pipe deformations at various stress levels were monitored over time. Details of the test equipment and procedure are described by Selig et al. (*7*) and DiFrancesco (*8*).

Selig et al. (*7*) have clearly stated that the uniform soil support and axisymmetric stress condition the cell induces around the pipe is not wholly representative of the pipe condition in the field. However, the cell provides valuable test data under controlled stress conditions. It induces substantial compressions up to and beyond those that develop in the field [Hashash and Selig (*9*)]. Furthermore, the measurements of pipe response can be used to calibrate a theoretical analysis that can then be used to estimate pipe response under more realistic stress conditions.

One pipe composed of each of three materials was tested. The first material represents a current production compound. The other two are nonproduction compounds.

1. Virgin polyethylene (cell classification 32430C);
2. Recycled material (50 percent virgin material, 50 percent reground industrial material); and
3. Virgin material, together with 7 percent $CaCO_3$.

All three materials were stabilized with 2 percent carbon black (they will be referred to as the "virgin," "recycled," and "filled" materials).

Geotechnical Research Centre, Faculty of Engineering Science, The University of Western Ontario, London, Ontario, N6A 5B9, Canada.

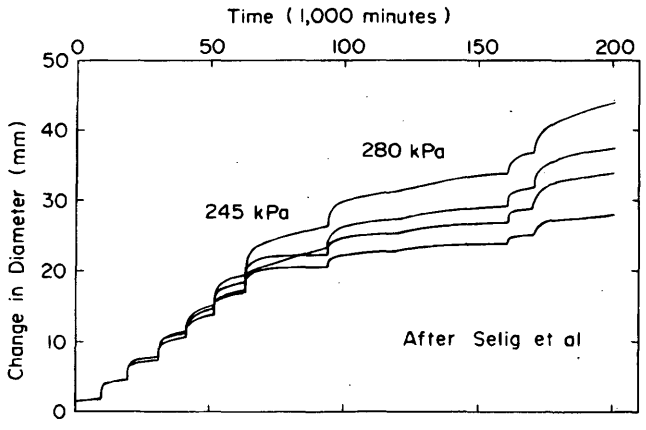

FIGURE 1 Diameter change with time recorded during the compression cell test on a pipe segment composed of the filled material (*7*).

The work at UMass showed that the tensile properties for all three materials were similar, as were the properties measured from samples cut from the pipe in the circumferential and axial directions [Kakulavar (*10*)]. Tests were inconclusive regarding the differences between compressive and tensile properties.

Figure 1 shows one trace of diameter change versus time for the pipe composed of $CaCO_3$-filled resin. This test featured the highest level of applied radial stress. It was loaded in 10 stress increments of 35 kPa (5 psi). The first six radial stress increments were held for about 10,000 min. The seventh to tenth stress increments were held for 30,000, 65,000, 10,000, and 30,000 min, respectively.

Pipe deflection measurements are shown at four different locations. The deflections are reasonably uniform during the first four increments. Beyond that, differences between minimum and maximum measured deflection are 10, 17, and 25 percent, growing steadily up to 45 percent at the end of the test.

Load deflection response for the pipe composed of filled material is shown in Figure 2. Pipe deflection at the end of each deflection increment is shown relative to the applied pressure. The test cell successfully loaded the pipe well beyond current use of the product in the field. Figure 2 shows the points at which the internal liner of the pipe was observed to develop "ripples" and to start cracking. These observed responses have been proposed as potential performance limits for these structures [Selig et al. (*7*)].

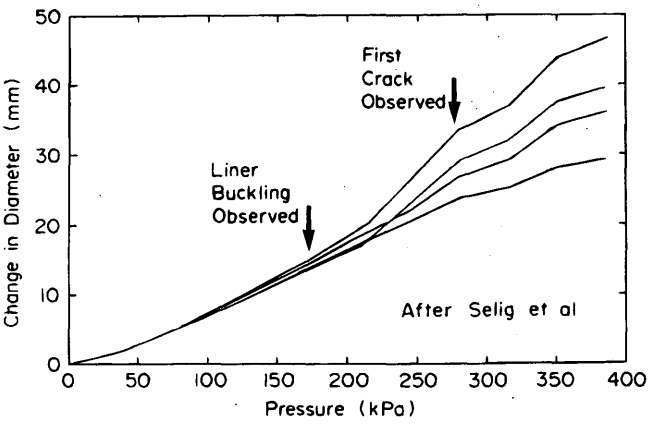

FIGURE 2 Load deflection response recorded during the compression cell test on a pipe segment composed of the filled material (*7*).

FINITE ELEMENT MODELING

Since much of this study focuses on the analysis and interpretation of observed pipe behavior, it is important to briefly describe the computer analysis used. For corrugated pipes with annular (not helical or spiral) design and with linear elastic or viscoelastic material response, the axisymmetric geometry can be used to simplify the analysis [Moore (*6*)]. A two-dimensional finite element mesh is used to model the geometry and strain fields in the r, z plane (Figure 3), and a Fourier series is used to model variations around the pipe circumference. Pipe response to each Fourier harmonic around the pipe is determined independently, and the full pipe response is assembled from each of these separate components using superposition.

To determine the pipe response in the compression cell of Selig et al. (*7*), only one axisymmetric loading harmonic is required (Figure 4).

One specific lined corrugated pipe profile has been examined by Selig et al. (*7*), and a finite element mesh has been developed for analysis of that profile. Figure 5 shows the mesh used to analyze the pipe in the compression cell. The analysis features explicit modeling of the three-dimensional pipe profile, as well as the thin ring of soil that is placed between the pipe and the PVC bladder around the outside. More than 800 six-noded triangular finite elements were used, 184 for one-half corrugation of the annular pipe and 661 for the granular soil surrounding it. Smooth rigid boundaries are used at the edges of the half corrugation, since these are lines of symmetry of the long axially constrained pipe sample. The pipe and soil are modeled as "bonded" together. A uniform radial compression is applied at the external boundary, simulating the pressures imposed by the PVC bladder used in the UMass compression cell.

HDPE exhibits very noticeable time-dependent behavior, and any detailed evaluation of HDPE pipe response will certainly involve a treatment of this constitutive characteristic. Fortunately,

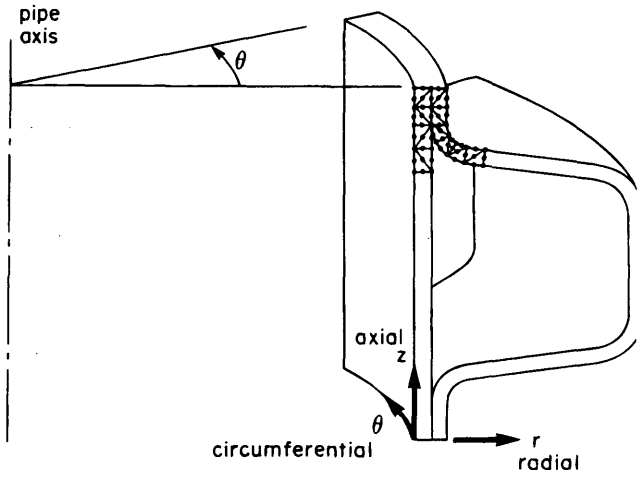

FIGURE 3 Finite element model for three-dimensional profiled pipe analysis.

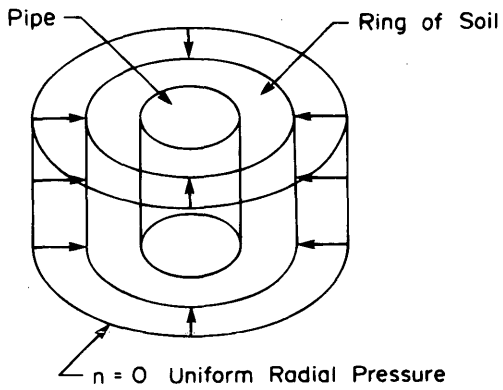

FIGURE 4 Loading and harmonic model used for the hoop compression test.

polyethylene appears to respond in a linear viscoelastic manner at stress levels up to about 30 to 50 percent of tensile yield stress. Well-established techniques in applied mechanics can be used for modeling such behavior. In particular, conventional rheology using sets of "springs" and "dashpots" is used. The multi-Kelvin model has been implemented featuring one independent spring and a series of nine Kelvin elements (each a spring and dashpot in parallel). For linear behavior of both structures, Laplace transforms are used to convert the linear viscoelastic problem into an equivalent elastic problem. Analysis is performed in the "Laplace" domain, and the real displacements, strains, and stresses are found after inversion of the Laplace transforms (*11*). For problems featuring nonlinear soil behavior, an iterative analysis is undertaken directly in the time domain, using the procedure of Zienkiewicz et al. (*12*) for the linear viscoelastic material (the pipe), and an incremental elastic-plastic analysis for the soil [Zienkiewicz (*13*)].

Material parameters for the polyethylene used in pipe manufacture have been developed by Moore and Hu (*14*) based on the data of Janson (*15*), Chua (*4*), and Hashash (*16*). The independent spring has a modulus of 1120 MPa (161.2 ksi), and moduli for the Kelvin springs are 3615.6 MPa (520.2 ksi), 0.845×3615.6 MPa, $0.845^2 \times 3615.6$ MPa, . . . , $0.845^8 \times 3615.6$ MPa, and Kelvin dashpot viscosities are 0.503 MPa.days (72.4 psi.days), 5.03 MPa.days, up to 5.03×10^7 MPa.days.

More difficult is the choice of soil parameters. The soil is characterized as either an isotropic linear elastic or elastic-plastic material. Elastic soil models have been found to be a reasonable first approximation to many buried pipe problems [Burns and Richard (*2*), Katona (*3*), and Moore and Brachman (*17*)]. It requires the selection of elastic modulus and Poisson's ratio. When granular soil is subjected to low confining stresses, soil failure can occur followed by an elastic-plastic response. Both soil models have been used to evaluate the development of plastic deformations in the soil and to examine their significance.

A valuable reference for soil properties is the laboratory study reported by Selig (*18*). A series of different partially saturated soils were examined, with stress strain characteristics measured at a number of different relative densities.

DiFrancesco (*8*) describes the backfill as a moist coarse-to-fine sand, and denotes a poorly graded material under the Unified Classification System. He suggests that at the measured water content of 3.5 percent, unit weight for the compactive effort used to backfill the compression cell is 113 kN/m^3. This is 92 percent of the maximum dry unit weight for the Proctor test, and 96 percent of the Proctor dry unit weight at a water content of 3.5 percent.

Selig (*18*) does not provide data for poorly graded materials, and the actual unit weight or relative density was not measured after the soil was placed around the pipe and pressurised in the compression cell.

To resolve these problems, an iterative approach was used to estimate the soil properties. First, Poisson's ratio was estimated as 0.3, which is reasonable for a granular soil at low levels of strain. Next, a series of calculations were performed to evaluate pipe deflections at 1,000 min, based on soil modulus for well-graded sands at a variety of relative densities. Using the Lagrangian method to interpolate between densities, a match between predicted and measured deflections was obtained for an SW93 material. Elastic modulus is 40 MPa (5.8 ksi) at that stress level.

This relative density appears to be reasonable given the 92 to 96 percent range quoted previously and assuming the SP material performs as Selig's SW material. This good performance for an SP material may be because the soil is not simply a single grain-size material (it has a uniformity coefficient C_U of 3.6 and a coefficient of curvature C_z of 1.3; the former is not that far from the 4 and 6 minimums required for well-graded gravels and sands; the latter value is within the 1 to 3 range characteristic of well-graded soils).

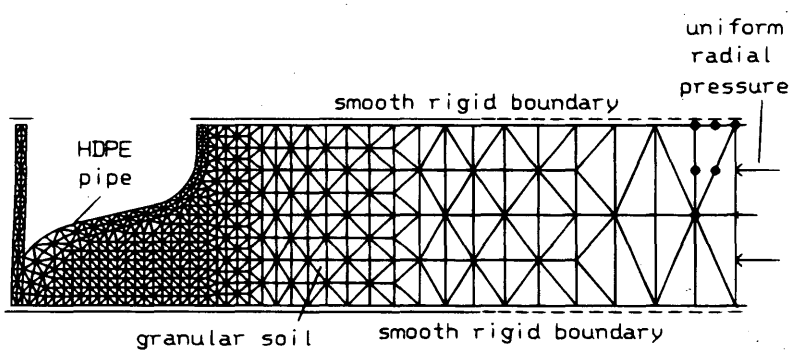

FIGURE 5 Finite element mesh used for analysis of the compression cell tests (*7*).

Several calculations were performed using these soil properties to examine the response of the pipe in the soil cell.

INVESTIGATION OF SOIL RESPONSE

The soil model used treats the soil as a uniform isotropic elastic continuum. Before proceeding with the investigation of the pipe, it is useful to examine the nature of stresses in the soil and review the differences between elastic and elastic-plastic soil models.

The shear stresses in real soil materials are limited by the shear strength. If shear stress estimated using elastic analysis is in excess of the shear strength, then it is likely that the soil would not remain elastic. For a dry granular soil, the soil strength is usually expressed using an angle of internal friction, ϕ. That angle controls the maximum normal stress in the soil (the major principal stress σ_1), which is limited by the magnitude of the minimum normal stress (the minor principal stress σ_3):

$$\sigma_1 \leq \sigma_3 \tan^2(45 + \phi/2) \quad (1)$$

or

$$\frac{\sigma_1}{\sigma_3} \leq \tan^2(45 + \phi/2) \quad (2)$$

Figure 6 shows contours of principal stress ratio σ_1/σ_3. By comparing stress ratio σ_1/σ_3 to values of $\tan^2(45 + \phi/2)$, it is possible to gauge the extent of shear failure in the soil. When stress ratio estimates from the elastic analysis exceed $\tan^2(45 + \phi/2)$, shear failure is expected.

Table 1 gives a number of $\tan^2(45 + \phi/2)$ values for soil materials. An examination of Figure 6 (in addition to Table 1) shows that zones of shear failure are likely to occur near the pipe. For the soil placement used in the UMass compression cell tests, the relative density estimate of 93 percent implies a friction angle ranging from 42° to 48°. According to Figure 6 and Table 1, the zone of soil in the corrugation valley and a small zone at the corrugation crest should experience shear failure (the soil in the corrugation valley is expected to have lower density, strength and stiffness in any case caused by the difficulties of compacting soil in this region).

These calculations imply that the use of an elastic soil model may not be appropriate.

To check that elastic analysis provides a reasonable prediction of the extent of soil failure, a nonlinear analysis has been performed using the elastic-plastic soil model. This analysis provided a yield zone for the SW93 soil, which closely matches the location based on a stress ratio of 5.8 ($\phi = 45°$). Comparisons of deflection, stress, and strain revealed that the yield in the soil and the subsequent nonlinear soil response does little to change the pipe stresses and displacement. For simplicity, therefore, the results quoted in this study are for elastic soil response.

LOCAL STRESS DISTRIBUTIONS

Calculations of stress distribution within the pipe profile have been made for a radial stress of 35 kPa (5 psi) applied by the air bladder at the outside of the soil ring. The circumferential (hoop) stress σ_θ and axial (longitudinal) stress σ_z are examined, as defined in Figure 7. These stresses are distributed in some manner across the profile. The manner in which they generate local bending moments m_θ and m_z locally in the corrugation and liner elements of the profile can also be inferred.

Figure 8 shows contours of circumferential stress. It reveals that three-dimensional effects occur in the profile, particularly in the pipe liner. A fully compressive stress field develops in the profile in the hoop direction. Compressions (shown as negative quantities in Figure 8) develop in the circumferential direction, ranging in magnitude from 0.5 MPa to 0.6 MPa (70 psi to 85 psi) throughout most of the corrugation. In the liner, local bending causes compressions to drop below 0.1 MPa (10 psi) at the outside of the liner (*i.e.*, at the surface not in contact with the fluid carried in the pipe). This occurs midspan (*i.e.*, at the centerline of the liner section that stretches from one corrugation valley to the other). Hoop compressions also drop below 0.4 MPa (60 psi) on the inside of the liner where the liner connects to the corrugation. Hoop compressions increase to a maximum of more than 0.8 MPa (100 psi) at the outside of the liner at the liner-corrugation connection.

An almost uniform compressive hoop stress of the type seen in Figure 8 for the corrugation can be predicted using two-dimensional analysis. Such compressions are generally not of great concern, and although high compressions may cause yield (as defined by an offset yield stress), they should not lead to rupture and are unlikely to cause distress in the polyethylene material. The effect of the three-dimensional profile on the hoop stress distribution can be summarized as local bending in the liner, causing variations in stress above and below the uniform hoop compression.

Figure 9 shows contours of axial stress. It also indicates that three-dimensional effects occur in the pipe liner. Compressive (negative) stresses in the liner are similar in magnitude to those in the hoop direction (the lowest contour interval shown corresponds to −0.6 MPa or −90 psi, the lowest axial compression is less than −0.8 MPa or 110 psi). In the corrugation, the stress field is generally compressive, ranging in magnitude from 0 to −0.2 MPa (30

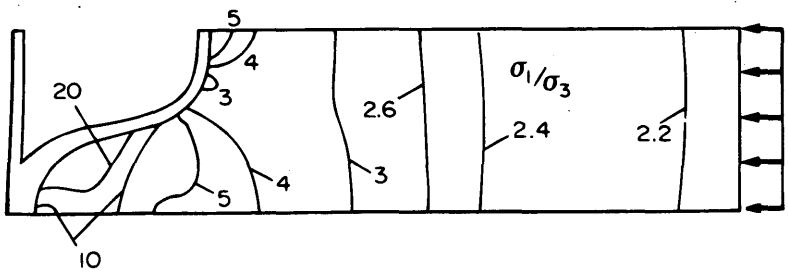

FIGURE 6 Stress ratio calculated for an elastic soil material; pipe response in the compression cell with 35 kPa (5 psi) bladder pressure; stresses at 1,000 min.

TABLE 1 Stress Ratio as Function of Friction Angle and Relative Density

σ_1/σ_3	ϕ	soil
3	30°	SW62
4	37°	SW80
5	42°	SW90
10	55°	SW98

psi). The latter value corresponds to a small region of local bending at the crest of the corrugation.

Tensile (positive) axial stresses occur at certain points in the corrugation and the liner. In the liner, tensions occur on the inside surface, adjacent to the liner corrugation junction. Careful examination of the local stresses shows a peak tension of 0.84 MPa or 120 psi (the maximum contour shown is 0.4 MPa, 60 psi). Tension also develops on the outside of the liner midspan. The value at this location is about 0.4 MPa (60 psi).

To help explain the nature of the local bending, Figure 10 shows the finite element prediction of deformed shape after 1,000 min at 35 kPa (5 psi) radial pressure. Careful examination of the deformed and underformed geometry of the profile reveals that the local bending stresses shown in Figure 9 are associated with a nonuniform radial movement that occurs along the liner. For the corrugation, continuous contact with the soil around the pipe leads to an almost uniform radial contraction (compression of the pipe with movement toward the pipe axis). For the liner, however, only that section bonded to the corrugation moves inwardly to that extent. The remainder of the liner (that section spanning from across one corrugation valley to the other) resists that radial movement, and at midspan less than half the radial movement experienced by the corrugation occurs. The liner, therefore, is acting like an encastered beam, where rotations at midspan and at the liner-corrugation junction are prevented, and the liner corrugation junction moves relative to the liner midpoint. Axial bending stresses, therefore, develop in the liner (in the direction of the beam axis), consisting of the regions of compression and tension shown in Figure 9.

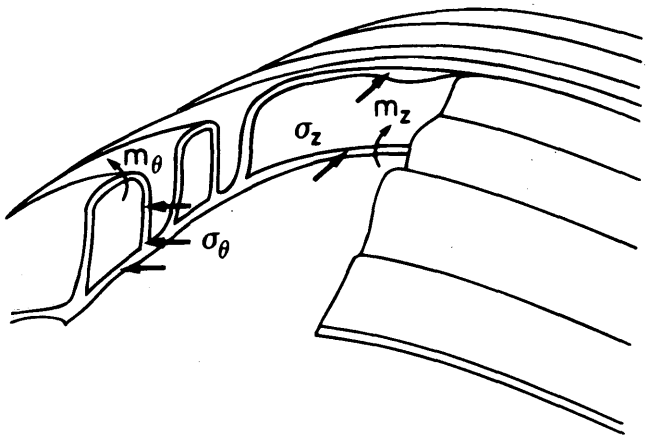

FIGURE 7 Schematic showing circumferential stress σ_θ and axial stress σ_z acting in the HDPE pipe profile.

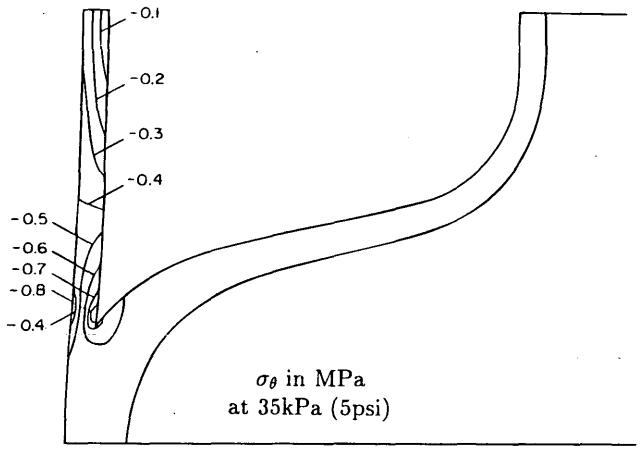

FIGURE 8 Contours of circumferential stress σ_θ acting in the HDPE pipe profile with 35 kPa (5 psi) bladder pressure in the UMass compression cell; stresses at 1,000 min.

LINER RIPPLING

Selig et al. (*7*) report that when each of the pipes tested in the UMass compression cell were loaded sufficiently to cause about 1.9 percent radial contraction, a series of regularly spaced ripples were observed in the liner. Figure 11 is a schematic of the phenomenon. A series of ripples developed around the pipe circumference, as well as along the pipe axis. As effective burial depth was increased, virtually the whole of the liner of the pipe specimens being tested developed these regular, uniformly sized wave-like deformations.

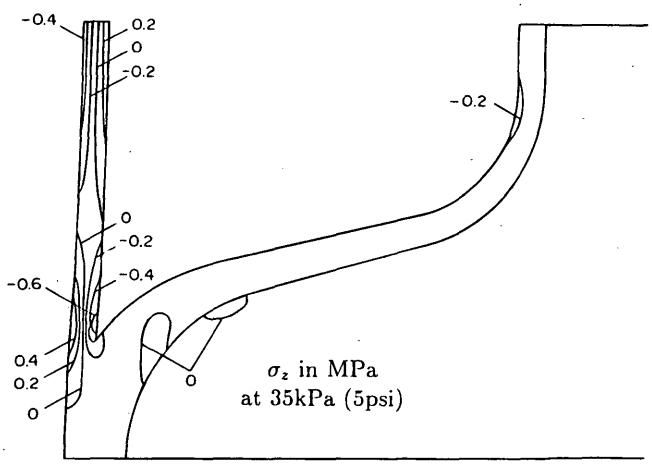

FIGURE 9 Contours of axial stress σ_z acting in the HDPE pipe profile with 35 kPa (5 psi) bladder pressure in the UMass compression cell; stresses at 1,000 min.

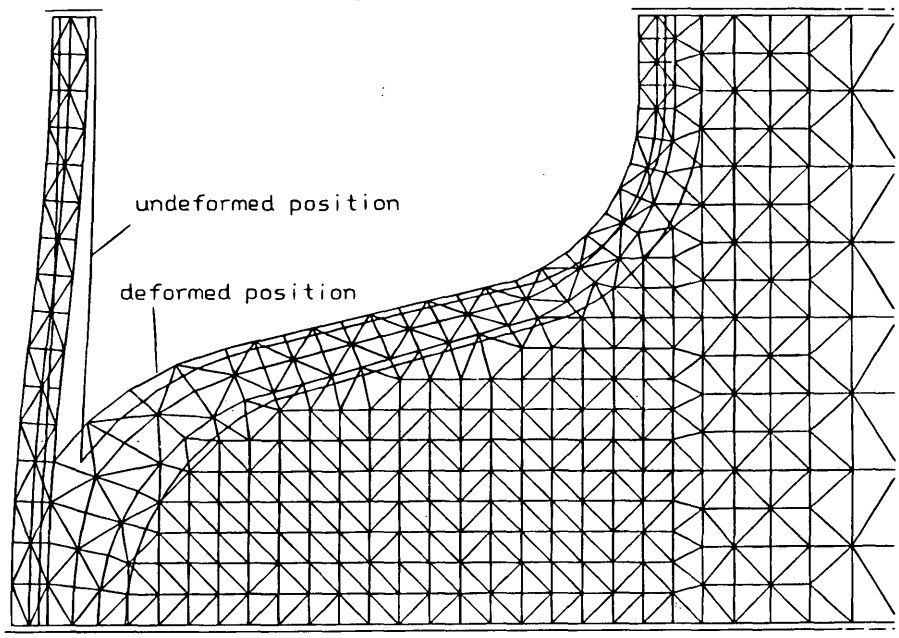

FIGURE 10 Deformations of profile at 35 kPa (5 psi) bladder pressure in the UMass compression cell; prediction for 1,000 min.

One possibility is that these ripples are local buckles that develop from compressive stresses that occur in the hoop direction as the pipe contracts into the cavity. This type of local buckling develops in many stiffened shell or plate structures (such as aircraft wings), and is well known for being a stable phenomenon (the load capacity of the structural element does not decrease after it has buckled). Such stable plate and shell buckling mechanisms are amenable to linear buckling analysis (an analysis developed on the basis of the original undeformed structural geometry).

To investigate whether the ripples were the result of local shell buckling, a linear three-dimensional buckling solution of thin cylindrical shells was used to determine the radial contraction necessary to cause buckling (*19*). The valley of the corrugation was assumed to be sufficiently thick to prevent rotation of the liner at the corrugation-liner junction, so the wavelength of the buckles in the longitudinal direction was assumed equal to the "clear span" of the liner from one corrugation valley to the next. The liner was also assumed to be a flat, uniform thickness cylindrical shell.

For a cylindrical shell of radius 307 mm (12.1 in.), thickness of 2.8 mm (0.11 in.), and "clear span" of 77 mm (3.03 in.), the analysis indicates that elastic buckling occurs at a radial contraction of 1.8 percent, and with 40 buckles developing around the pipe circumference. Selig et al. (*7*) report that rippling was first observed at a radial contraction of 1.9 percent, and observed about 50 ripples around the circumference of the pipe.

It appears, therefore, that the ripples observed in the pipe tests are the result of local buckling in the pipe liner.

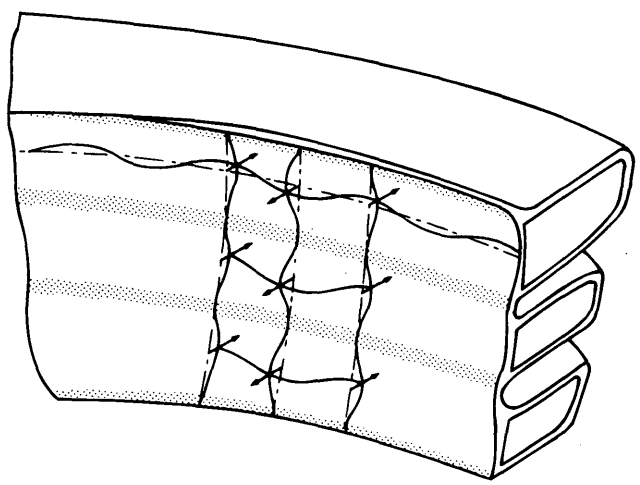

FIGURE 11 Schematic of the rippling deformations observed at 1.9 percent radial contraction (*7*).

LOCAL TEARS IN LINER AT HIGH HOOP COMPRESSION

Selig et al. (*7*) report that one of the pipes tested in the UMass compression cell, which was loaded to very high cell pressure, developed a regular series of short circumferential tears in the liner close to the liner-corrugation junction.

The contours of axial stress shown in Figure 9 indicate that the local tearing is located directly at the point of highest tension. Clearly, these tensions in the axial direction may be wholly or partly responsible for the tears that occur normal to them in the circumferential direction. The possibility exists that the tears are a ductile rupture caused by excessive local bending stress associated with the nonuniform liner contraction.

Selig et al. (*7*) report that the small, regularly spaced tears were observed through the liner at about 270 kPa (39 psi) cell pressure (equivalent to 30 m or more of pipe burial). This is about 7.7 times the pressure acting to generate the axial stresses shown in Figure 8.

Simple scaling of those stress values suggests that local tension of approximately 6 MPa (900 psi) is expected at this load level. This is close to the long-term AASHTO yield stress.

The value of local axial bending stress is approximate. Shear failure in the soil placed in the corrugation valley is expected to increase local bending stress, whereas the stiffening of the soil material expected with increasing applied stress would act to decrease the local stresses in the polyethylene. Some stress relaxation is also expected, which would decrease stresses.

Axial stresses will also be modified by the local buckles that develop in the liner. These local buckles will increase the axial tensions at the inner surface where the buckle moves away from the pipe axis, and will decrease the axial tension where the buckle moves toward the pipe axis. The short, regularly spaced tears observed in the pipe tests match the positions where maximum tension is expected.

To obtain further information concerning the tears observed during the compression tests, an electron micrograph was taken of the polyethylene rupture surface revealing a rupture surface consistent with ductile tearing (Sheasby, J. S., personal communication (1994)).

It appears then that the regular pattern of tears in the liner represent a ductile failure resulting from the local axial tensions (Figure 9) as well as some additional tension associated with the local buckling.

PERFORMANCE LIMITS

The local buckling and local tearing phenomena outlined in the report relate to the three-dimensional effects in lined corrugated HDPE pipe and have implications for pipe design.

Local buckling in the liner does not cause overall instability of the lined corrugated pipe because the corrugation continues to provide structural support. This form of deformation may, however, be treated as a serviceability limit caused by some effect on the hydraulic performance of the sewer pipe.

The axial tensions in a lined corrugated pipe should be examined during the design of highly loaded lined corrugated pipe. The corrugation integrity does not appear to be threatened, and the pipes tested in the compression cell did not experience instability. However, the development of local tears in the pipe lining is obviously undesirable. A parametric study estimating axial stresses for pipes in situ would assist in the design of these pipes for very deep burial. Future research to examine other profiled HDPE pipe products for three-dimensional effects would also be valuable.

CONCLUSIONS

The three-dimensional response of a lined corrugated HDPE pipe was observed during the testing program undertaken at the University of Massachusetts. Analysis of the pipe-soil system in the compression test cell has revealed that local bending occurs in the pipe liner, modifying the stress state in the pipe beyond that predicted using conventional two-dimensional pipe-soil interaction analysis. The local bending is confined to the liner, and it is likely that a corrugated unlined pipe will not be subject to the same phenomenon.

Conventional "ring" theory predictions for profiled pipe response cannot estimate levels of axial stress, but the three-dimensional analysis has clearly shown that axial bending stresses do develop at certain locations in the pipe profile. The junction between the liner and the corrugation is the site of the largest axial tensions. These axial tensions develop on the inside surface of the liner and exceed the circumferential tensions that develop. The magnitude of these local axial stresses suggests that the liner tearing observed by Selig et al. (*17*) is associated with ductile tensile failure at these locations.

Three-dimensional linear buckling analysis reveals that the rippling deformations observed by Selig et al. (*7*) are, in fact, local buckles that are a stable buckling mechanism often found in stiffened plate or shell structures.

ACKNOWLEDGMENTS

This work was sponsored by the Corrugated Plastic Pipe Association and the Natural Sciences and Engineering Research Council of Canada through an industrially oriented research grant. Theoretical models were developed with the assistance of research and equipment grants from the Natural Sciences and Engineering Research Council of Canada. Assistance was also provided by E. T. Selig, who supplied details of the hoop compression tests.

REFERENCES

1. Spangler, M. G. Stresses in Pressure Pipelines and Protective Casting Pipes. *Journal of Structural Engineering,* ASCE, Paper 1054, 1956, pp. 33.
2. Burns, J. Q., and R. M. Richard. Attenuation of Stresses for Buried Cylinders. *Proc., Symposium on Soil-Structure Interaction,* ASTM, University of Arizona, 1964, pp. 379–392.
3. Katona, M. G. CANDE: A Modern Approach for the Structural Design and Analysis of Buried Culverts. Report FHWA-RD-77-5. FHWA, Department of Transportation, October 1976.
4. Chua, K. M. *Time-dependent Interaction of Soil and Flexible Pipe.* Ph.D. thesis. A&M University, Texas, 1986.
5. Katona, M. G. Allowable Fill Heights for Corrugated Polyethylene Pipe. *Transportation Research Record,* 1988, pp. 30–38.
6. Moore, I. D. Three Dimensional Time Dependent Models for Buried HDPE Pipe. In *Proc. of the Eighth International Conference on Computer Methods and Advances in Geomechanics* (H. J. Siriwardane, ed.), Morgantown, W.V., A. A. Balkema, Rotterdam, May 1994, pp. 1515–1520.
7. Selig, E. T., L. C. DiFrancesco, and T. J. McGrath. Laboratory Test of Buried Pipe in Hoop Compression. In *Special Technical Publication 1222, Buried Plastic Pipe Technology* (D. Eckstein, ed.), ASTM, Philadelphia, Pa., 1994, pp. 119–132.
8. DiFrancesco, L. C. *Laboratory Testing of High Density Polyethylene Drainage Pipes.* M.Sc. thesis, Department of Civil Engineering, University of Massachusetts, 1993.
9. Hashash, N. M. A., and E. T. Selig. Analysis of the Performance of a Buried High Density Polyethylene Pipe. In *Structural Performance of Flexible Pipes* (G. Mitchell, S. Sargand, and J. Hurd, eds.), Balkema, Rotterdam, 1990, pp. 95–103.
10. Kakulavar, S. *The Effect of Compound Composition on the Mechanical Properties of HDPE Corrugated Pipes.* Master's thesis. Department of Mechanical Engineering, University of Massachusetts, 1993.
11. Moore, I. D. Local Strain in Corrugated Pipe: Experimental Measurements to Test a Numerical Model. *Journal of Testing and Evaluation,* ASTM, March 1994, pp. 132–138.
12. Zienkiewicz, O. C., M. Watson, and I. P. King. A Numerical Method of Visco-elastic Stress Analysis. *Journal of Mechanical Science,* 1968, pp. 807–827.
13. Zienkiewicz, O. C. *The Finite Element Method in Engineering Science.* McGraw-Hill, New York, 1979.

14. Moore, I. D., and E. Hu. Linear Viscoelastic Models for HDPE. *Canadian Journal of Civil Engineering,* (in press), 1995.
15. Janson, L. E. Investigation of the Long Term Creep Modulus for Buried Polyethylene Pipes Subjected to Constant Deflection. In *Advances in Underground Pipeline Engineering* (J. K. Jeyapalan, ed.), Madison, Wis., August 1985, pp. 253–262.
16. Hashash, N. M. A. *Design and Analysis of Deeply Buried Polyethylene Drainage Pipes.* Ph.D. thesis. Department of Civil Engineering, The University of Massachusetts at Amherst, 1991.
17. Moore, I. D., and R. W. Brachman. Three dimensional Analysis of Flexible Circular Culverts. *Journal of Geotechnical Engineering,* ASCE, 1994, pp. 1829–1844.
18. Selig, E. T. Soil Properties for Plastic Pipe Installations. In *Special Technical Publication 1093, Buried Plastic Pipe Technology,* ASTM, Philadelphia, Pa., 1990, pp. 141–158.
19. Moore, I. D. Influence of Rib Stiffeners on the Buckling Strength of Elastically Supported Tubes. *International Journal of Solids and Structures,* 1990, pp. 539–547.

Publication of this paper sponsored by Committee on Subsurface Soil-Structure Interaction.

Ground Movements Caused by Trenchless Pipe Installation Techniques

C. D. F. ROGERS AND D. N. CHAPMAN

The ground movements caused by trenchless pipe installation techniques can have a significant effect on adjacent services and road structures. A fundamental understanding of how these techniques affect the ground is lacking. This can result in the stipulation of an overly conservative distance between trenchless pipelaying and other services, and a concomitant lack of confidence in the techniques. To rectify this, a series of laboratory simulation tests was conducted at Loughborough University of Technology, U.K. These tests simulated pipejacking or microtunneling (convergent) operations using different shield arrangements and pipebursting (expansive) operations, with the aim of determining the patterns and magnitudes of displacements in the surrounding soil. This in turn permits the prediction of movements in adjacent services and structures, as well as the development of techniques for their minimization. The tests were conducted in a rigid, glass-sided tank using semicircular shields and pipes buried in different dry sands. This arrangement allowed direct observation of the sand displacements on the centerline of the simulated operations. For the pipejacking tests, two face-support methods (open and closed faces) were used. The pipebursting operations used different sizes of existing plaster pipe, which was progressively broken out as the burster advanced, to simulate different bursting ratios. Various combinations of sand density and cover depth were used. Selected results from the three test programs are presented in terms of ground movement contour plots and vector displacement diagrams. The results confirmed that soil density strongly influences the magnitude and extent of the ground displacements. The denser soils produce a greater effect in compression situations, and looser soils have a greater effect when the soil is moving into cavities. Increasing cover depth creates a confining effect and restricts the extent of the soil movements. The open shield behaves differently than the closed shield, which displaces more soil and produces broadly similar results to those of the angled pipebursting unit. The results presented herein are essentially visual, thus permitting a full appreciation of the ground movements under various boundary conditions.

Trenchless technology has become firmly established as an alternative method of pipeline construction to compete with trenching, or open-cut, methods and traditional tunneling. Several techniques are available (*1*), all of which have their own particular applications; these have considerable advantages over open-cut techniques where they can be used. Due to the location of many services beneath road pavements, particularly in urban areas, trenching is necessarily slow, causing considerable traffic congestion and incurring the large social, or indirect, costs associated with such congestion (*2*). In addition, open-cut methods result in damage to road pavement structures and adjacent buried services, with consequent loss of structural life. This is due to displacements that occur within the soil that are caused by changes to the stress field, and hence loss of support to the structure or service, in addition to any direct damage to the structure or service caused by the excavation (*3*).

C. D. F. Rogers, Department of Civil and Building Engineering, Loughborough University of Technology, Loughborough, Leicestershire, LE11 3TU, U.K. D. N. Chapman, Department of Civil Engineering, University of Nottingham, University Park, Nottingham, NG2 7RD, U.K.

Many of the trenchless pipelaying techniques have been developed with the goal of reducing such damage to a minimum. Nevertheless there will be ground displacements associated with these techniques that will necessarily affect road pavement structures and buried services. It is often quoted in the extensive and growing literature on the subject that trenchless techniques are far better than other techniques in this respect, although these quotes are made on the basis of minimal data. The project reported herein is aimed at quantifying the movements that can be expected from the use of such construction operations.

A comprehensive program of research has been carried out at Loughborough University of Technology, U.K., to study the ground displacements caused by pipejacking (excavation) and pipebursting (expansion) operations by simulation in physical model tests. In microtunneling, which is a fully automated development of pipejacking that is used for smaller diameter tunnels and pipelines, sophisticated slurry and earth pressure balance techniques have been adopted to deal with the problems of ground loss and groundwater ingress. In certain cases the perceived need to ensure the avoidance of soil or water ingress has resulted in overcompensation for soil or water pressure (*4*). This overcompensation has resulted in a lack of excavation and in soil being forced away from the shield. Such a situation has also been simulated, in the extreme condition, in the test program by the use of a shield with a closed face.

Extremes of behavior were examined using loose and dense dry sands, which also facilitated development of a simple theoretical model for ground displacement prediction. Data are presented from all three types of test in order to establish patterns of movement. This is achieved by a series of vector displacement diagrams in the plane of longitudinal cross section. A method of interpretation, by interpolation and extrapolation, is presented to allow the results to be extended to practical situations.

PLANE STRAIN TEST FACILITY

The plane strain test facility in which the tests were conducted consists of a 1.5-m long × 1.5-m high × 1.0-m wide steel tank with two perpendicular glass sides. A water bag arrangement in the lid of the tank is able to supply a vertical stress to the surface of the soil placed within the tank, allowing simulation of different cover depths. The steelwork supporting the sides of the tank is designed to maintain plane strain conditions at the viewing faces throughout each test. The tank allows complete observation of the soil movements while simulated trenchless technology operations are carried out within it. Quantification of the ground movements was achieved by analyzing a series of photographs of the sand taken through the glass faces at different stages of the operation.

The ground movements were measured in two different types of dry sand, a uniform Leighton Buzzard sand (C_u = 1.36, C_c = 1.04, D_{10} = 1.18 mm) and a well-graded gravelly sand (C_u = 2.84, C_c = 0.66, D_{10} = 0.67 mm, where C_u = coefficient of uniformity, C_c = coefficient of curvature, and D_{10} = diameter below which 10 percent of soil particles fall). These sands were placed in both loose and dense states in the tank prior to testing, using a sand-raining technique to ensure consistency. The sands were chosen to provide materials that had sufficiently large particles to be readily identified from photographs while having different shearing (frictional and volume change) behavior. Dry sands were used to remove the effects caused by time-dependent equilibration of both positive and negative porewater pressures.

A semicircular pipe arrangement was jacked behind the appropriate head (shield or pipeburster) and adjacent to the glass front of the tank to simulate the jacking operation. Thus the observations of movement made were those taking place along the centerline of the installed pipe. The pipe was kept tight against the glass using a guide rail system. The jacking force was supplied by a single 30-t hydraulic jack that bore onto a steel thrust plate. The pipes were jacked forward, forcing the shield or head into the tank in 10-mm increments over a total distance of 1 m. This procedure enabled the effect of the sides of the tank on the measured displacements to be gauged. It also permitted a comprehensive series of observations to be made, establishing that the results were consistent. Several of the tests were duplicated to ensure repeatability of the results. Further details of the equipment are given elsewhere (*5*).

The external diameter of the installed pipes in all tests was 200 mm. For the pipejacking tests the front of the lead pipe was attached to a 100-mm-long semicircular shield with a diameter of either 220 or 240 mm, depending on the degree of overcut being investigated. It was considered important for the tests to have an overcut dimension (t) that matched the overcut dimension used in practice, rather than to scale down the overcut dimension by the same factor as that used to scale down the size of the pipe and shield. This would allow for a more realistic representation of the movements at the overcut while causing no significant influence at the front of the shield. For the pipebursting test a 12° steel cone was attached to the lead pipe. The existing pipe (i.e., the pipe to be renewed) was simulated by using semicircular plaster pipe sections fixed to the inside of the glass. Two sizes of existing pipe were used to provide two different bursting ratios (external diameter of burster divided by internal diameter of existing pipe). The maximum diameter of the steel cone was designed to be larger than the installed pipe sections, to allow the effect of overbursting to be investigated.

It should be stressed that the pipebursting tests represented full-scale models of these operations, albeit on the lower bound of sizes found in practice. The pipejacking tests, however, are scaled versions of field operations, with the scaling factor typically being 5 to 10.

EXPERIMENTAL PROCEDURE

Pipejacking Tests

Simulation of the pipejacking operation (i.e., forward jacking and insertion of new pipe sections) is relatively straightforward, whereas simulation of face excavation and support characteristics with the necessary repeatability and consistency is very difficult. The complex nature of many of the face support systems in use today, such as slurry pressure balance systems, means that accurate modeling is impossible. In order to overcome this problem in the model tests, the two extremes of face support were considered, a completely open face and a completely closed face, and interpolation between the two was made.

Due to the nature of dry sand, the open-face shield allowed the sand to form a stable natural slope within the shield, and had angled cutting edges designed to maintain this stability. During the jacking stage of the model tests, more sand was forced into the shield, which would rapidly create a plug of sand if the additional sand were not removed. The jacking process was therefore stopped after 10-mm forward movement to allow excavation of the excess sand. The excavation was performed using a carefully controlled suction technique, taking care not to overexcavate the face and cause instability. Further details of this technique are reported elsewhere (*6*). Forward jacking, again in 10-mm increments, of the closed shield caused the sand necessarily to move away from the face and thus to simulate excessive overpressurization of the face support provided by a slurry pressure balance machine. The pipejacking model tests described in this paper concentrated on the jacking part of the pipejacking operation, rather than on the excavation process, which had no influence on the surrounding soil.

Photographs were taken at every stage (before and after every jacking operation), and pairs of photographs were viewed in stereoprojection to obtain the pattern of sand displacements. Measurements of the displacements were then made directly from the photographs to enable the patterns, in the form of horizontal and vertical movement contours, to be quantified and vector diagrams to be produced.

Pipebursting Tests

The steel cone section, attached to the front of the pipe train being installed, was advanced into the tank by a static force (*7*). This closely models the expansion process that occurs during a hydraulic pipebursting operation. The burster ran along the invert of the existing pipe because of the shallow nature of the bursting operations simulated. The existing pipe was progressively broken out as the burster advanced, forcing the pieces of existing pipe into the surrounding sand.

The test proceeded in 20-mm forward jacking stages; photographs were taken before and after each stage. The sand displacements were obtained in a manner similar to the pipejacking tests.

EXPERIMENTAL RESULTS

A comprehensive program of tests was carried out to vary test parameters such as cover depth, type and density of sand, overcut ratio (pipejacking) or overburst ratio (pipebursting), and surface confinement for the three techniques (*8*). In this paper comparisons are made between the results of selected tests (Table 1) that illustrate differences in shield arrangements, soil density, and cover depth. The results of tests using the uniform sand are quoted because the well-graded sand produced broadly comparable results, although they were somewhat more random and less repeatable. More importantly, these results were less extreme in both extent and magnitude. Thus the uniform sand produced the upper-bound displacements for the dense (heave) and loose (settlement) sand tests.

An example of the contour plots produced from the photographs is given in Figure 1, in which the general pattern of forward and

TABLE 1 List of Laboratory Tests Referred to in this Paper

Test[a]	Operation	Sand		Cover Depth (m)	Overcut/ Overburst Ratio[d]	Bursting Ratio[e]
		Type[b]	Density[c]			
OPJ1	Pipejacking	uniform	dense	0.9	0.1	-
OPJ2	Pipejacking	uniform	loose	0.9	0.1	-
OPJ3	Pipejacking	uniform	dense	4.0	0.1	-
CPJ4	Pipejacking	uniform	dense	0.9	0.1	-
CPJ5	Pipejacking	uniform	loose	0.9	0.1	-
CPJ6	Pipejacking	uniform	dense	0.4	0.1	-
CPJ7	Pipejacking	uniform	loose	0.4	0.1	-
PB8	Pipebursting	uniform	dense	0.9	0.05	1.7
PB9	Pipebursting	uniform	loose	0.9	0.05	1.7
PB10	Pipebursting	uniform	loose	0.4	0.05	1.7
PB11	Pipebursting	uniform	dense	0.9	0.05	1.2

[a]OPJ refers to open shield pipejacking, CPJ refers to closed shield pipejacking.
[b] The uniform sand is Leighton Buzzard sand (C_u = 1.36, C_c = 1.04, D_{10} = 1.18mm).
[c]Dense sand = 2.07 Mg/m^3 and loose sand = 1.94 Mg/m^3.
[d]The overcut ratio is the ratio of external diameter of the shield to the external diameter of the following pipe. The overburst ratio is the ratio of the maximum external diameter of the bursting head to the external diameter of the following pipe.
[e]The bursting ratio is the ratio of the external diameter of the burster to the internal diameter of the existing pipe.

upward movements in front of a closed shield in dense, uniform sand can be seen clearly. The downward movements at the overcut, which were limited by dilation within the dense sand, are equally apparent. The dashed contour lines represent areas of movements that were not well defined, due to either the random nature of the movements or their small magnitude.

Comparison Between Open- and Closed-Shield Pipejacking Tests

Figures 2 through 5 show the vector displacement plots for four tests (OPJ1 and CPJ4 in dense sand, and OPJ2 and CPJ5 in loose sand, respectively) to illustrate the effects of volume of excavation, the only difference between the pairs being the (open or closed) shield type. Figures 2 and 4 illustrate the general pattern of sand movements in the longitudinal plane as one of a circular motion around, and particularly over, the shield. There were outward (forward) and upward movements in front of the shield, which above the shield crown altered progressively to backward and upward movements. In addition there were downward movements of the sand lying above the shield into the void created by the overcut of the shield, and forward movements into this void by sand lying behind the shield. It should be noted that, for the reasons given in an earlier section, the movements at the overcut were exaggerated and that this influenced the overall pattern to a degree, although the influence can be easily allowed for from visual interpretation.

The main observation when comparing the open- and closed-shield tests concerned the extents and magnitudes of the resulting movements. For the open-shield test in dense sand (OPJ1) the maximum extent of the sand movements in front of the shield was only approximately three diameters from the shield, whereas the movements for the equivalent closed-shield test (CPJ4) extended to the surface. This difference was expected, because the sand in front of the closed shield cannot move into the shield and consequently must move forward during jacking, causing much more sand to be displaced. The extents for the equivalent loose sand tests (OPJ2 and CPJ5) were similar in many respects, with neither test producing movements in front of the shield that reached the ground surface, because of sand compression. The closed-shield test movements did, however, extend further in front of the shield.

Over the shield and at the overcut, the observed movements for the open- and closed-shield tests were very similar, once allowance was made for the greater upward and resultant spreading (hence soil disturbance) effects in front of the closed-shield tests. This caused the plane separating the horizontal forward movements and the horizontal backward movements at the shield crown to have a much greater angle to the horizontal for the closed-shield tests. Sand behavior at the overcut was largely influenced by the relative density of the sand. The movements in dense sand diminished and extended only a small distance above the pipe. In loose sand, the movements extended much further and in the shallower (0.9-m deep) tests reached the surface, giving rise to a funneling effect caused by sand compresion.

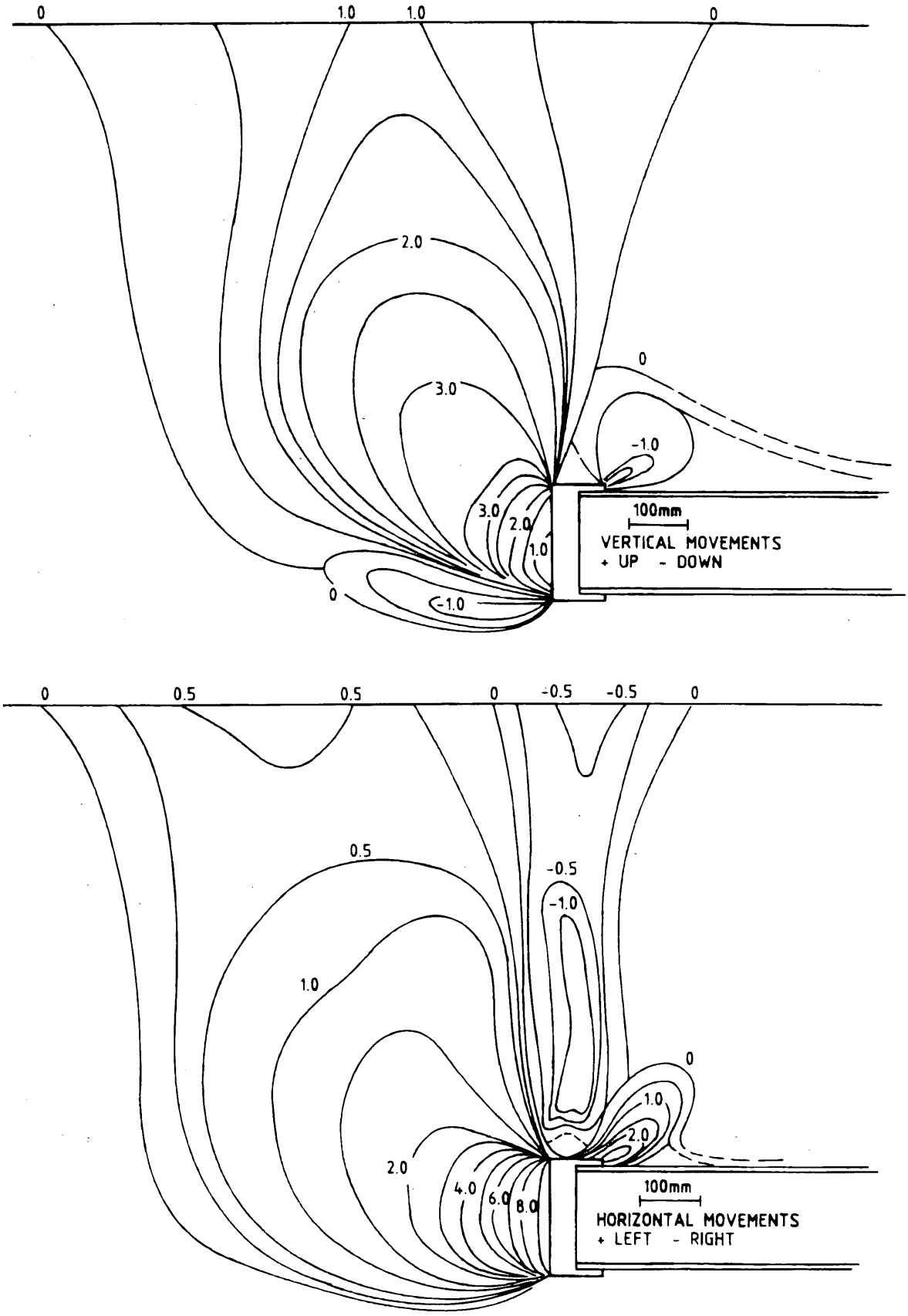

FIGURE 1 Typical example of displacement contour plots (Test CPJ4) from analysis of laboratory test data (10-mm jacking distance, contours in mm).

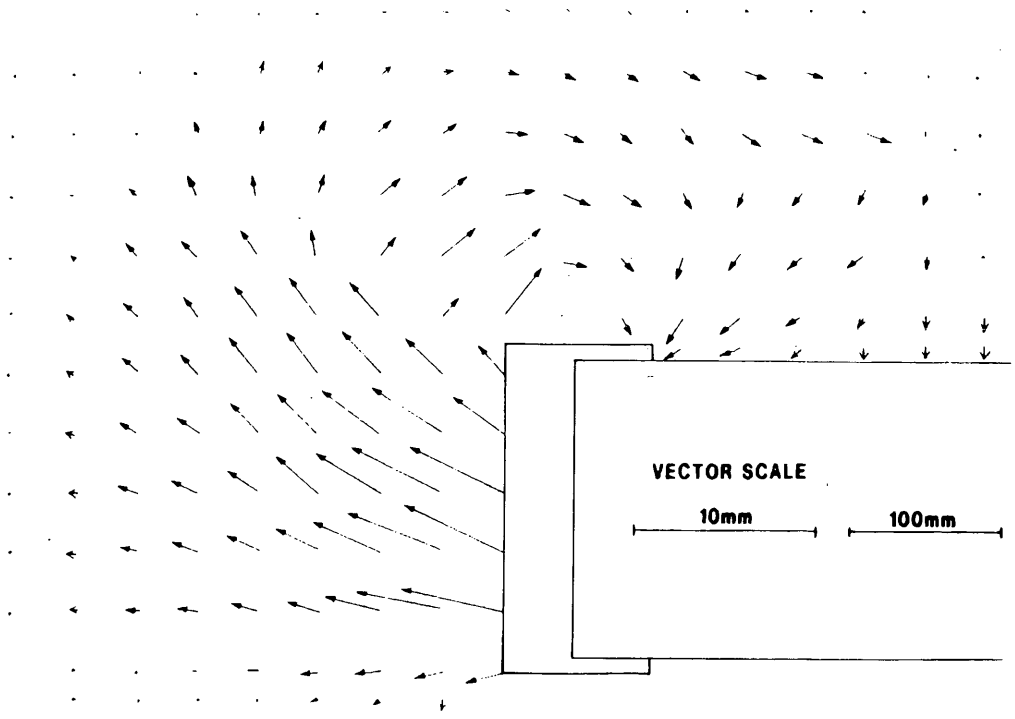

FIGURE 2 Vector displacement plot for Test OPJ1 (0.9 m deep in dense sand, 10-mm jacking distance).

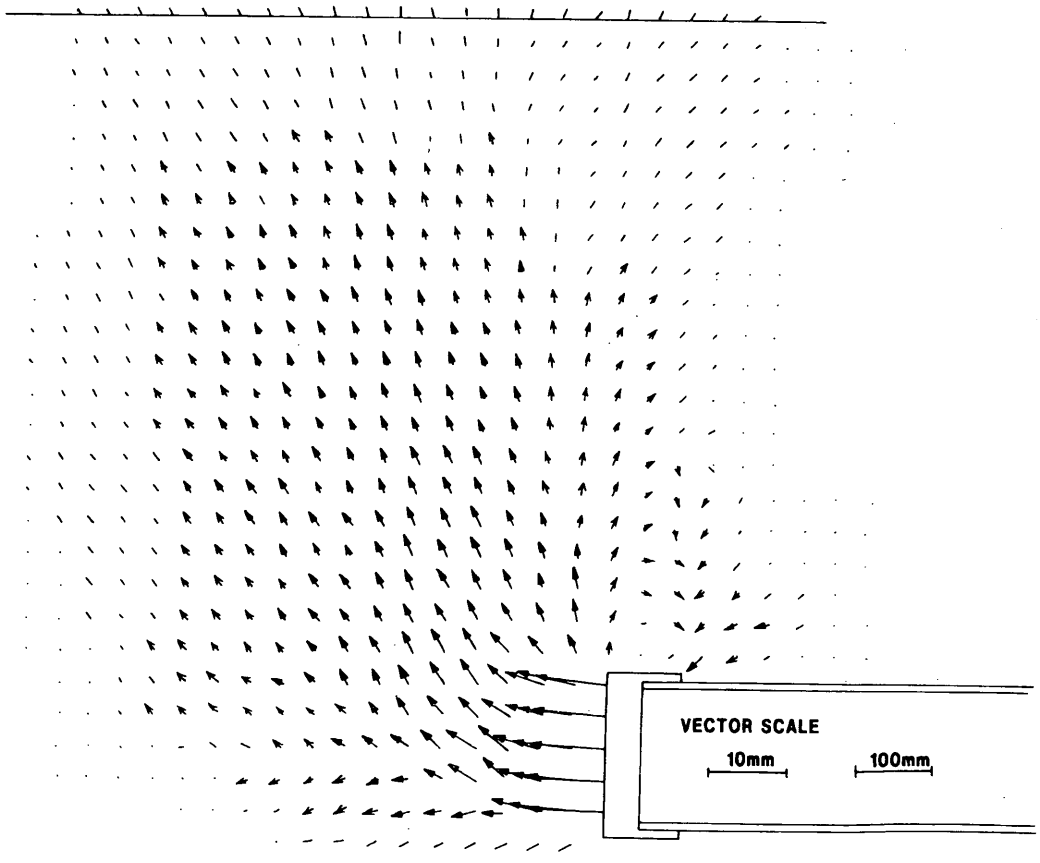

FIGURE 3 Vector displacement plot for Test CPJ4 (0.9 m deep in dense sand, 10-mm jacking distance).

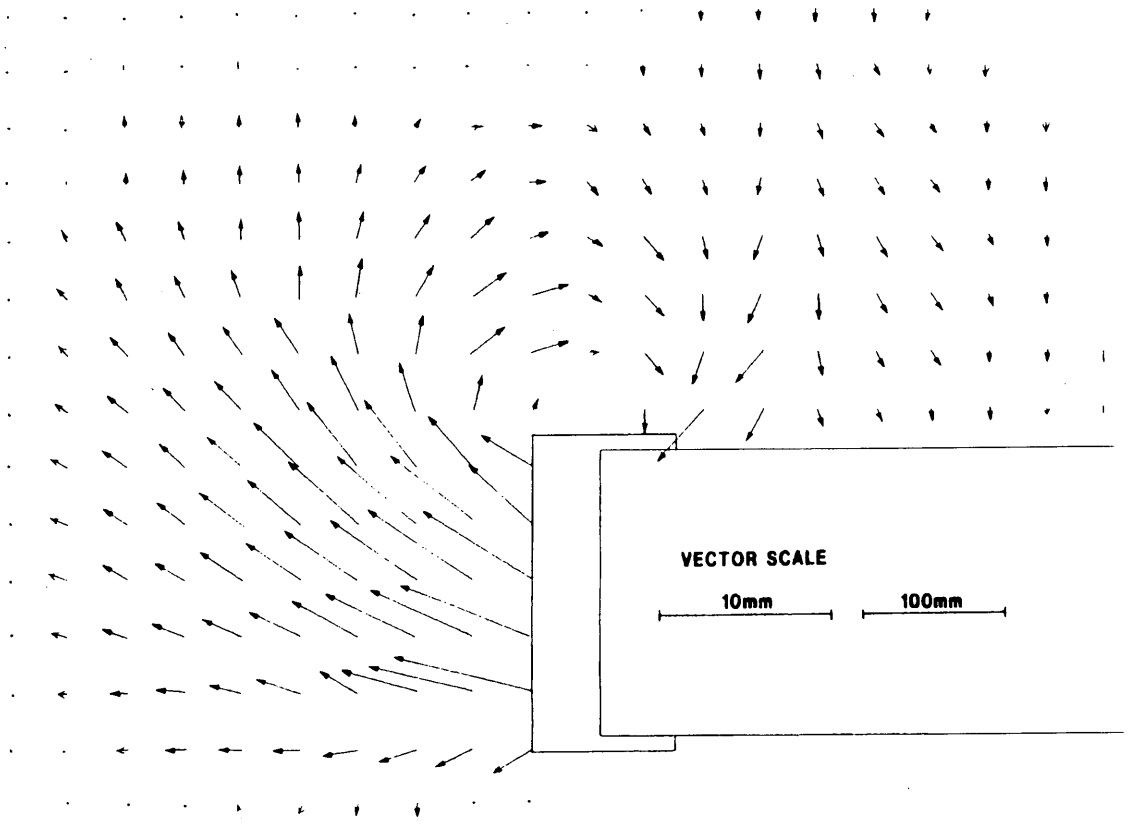

FIGURE 4 Vector displacement plot for Test OPJ2 (0.9 m deep in loose sand, 10-mm jacking distance).

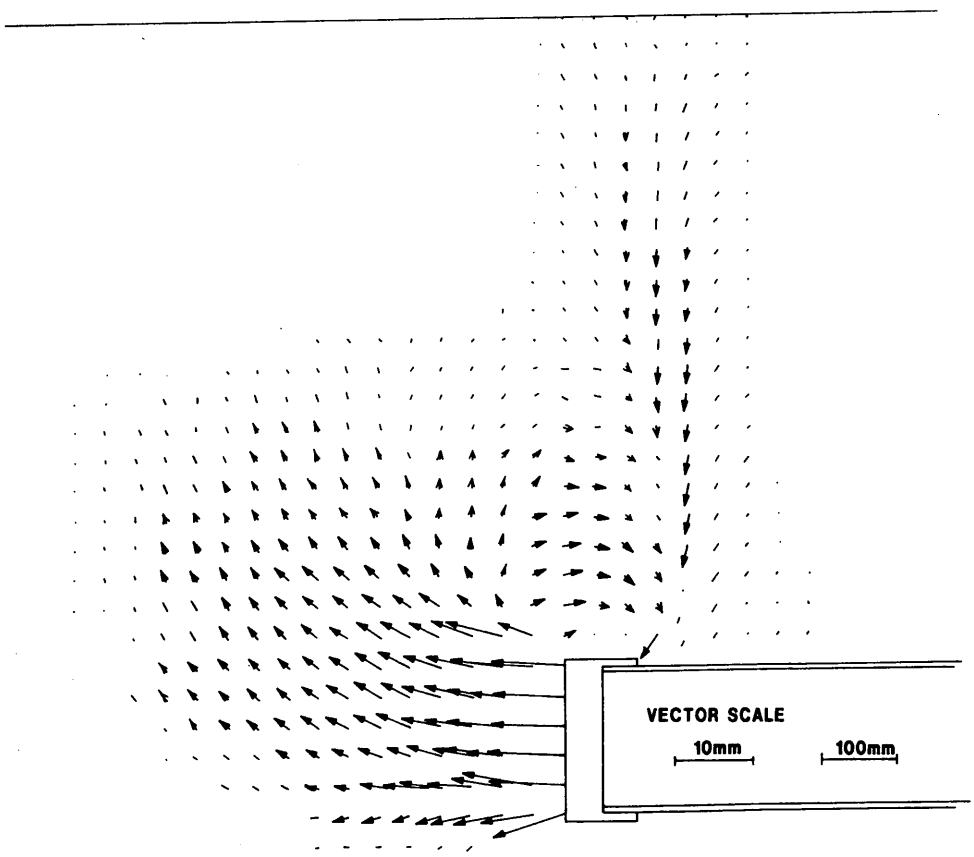

FIGURE 5 Vector displacement plot for Test CPJ5 (0.9 m deep in loose sand, 10-mm jacking distance).

The effect of increasing the cover depth from 0.9 m to 4.0 m in the open-shield pipejacking tests in dense sand can be seen in a comparison of Figures 2 and 6. It is clear that the higher vertical (hence mean normal) effective stress forced more sand into the shield, thus reducing the magnitude of the outward movements and preventing the spread of movements away from the operation. The closed-shield pipejacking tests were conducted only at relatively shallow depths. The results for cover depths of 0.4 m and 0.9 m in dense sand are presented in Figures 7 and 3, respectively. The increase in cover depth caused the movements immediately in front of the shield to become more horizontal before moving upward and, because of the greater mean normal effective stress, to reduce significantly in magnitude. The greater lateral spreading was also seen in a reduction in movements at the overcut.

Comparison Between Closed-Shield Pipejacking and Pipebursting Tests

In this section the results from pipebursting tests PB8 and PB9 (Figures 8 and 9) are compared with those from closed-shield pipejacking tests CPJ4 and CPJ5 (Figures 3 and 5). Although trenchless pipelaying techniques are superficially very different, the measured ground displacements were surprisingly similar. Indeed, if the plaster pipe in the pipebursting tests is ignored, the movements above the bursting head were very similar, in terms of both extent and magnitude, to those obtained in the closed-shield tests for both dense and loose sand. It should be remembered, however, that the pipebursting movements were obtained from a 20-mm forward jacking distance, as opposed to 10 mm for the pipejacking tests.

For the dense-sand tests (Figures 3 and 8), the vector displacement plots show a large area of upward and forward movement in front of (or above) the particular operation, with some backward movement due to spreading effects. A smaller, localized area of rapidly diminishing downward movement was observed at the overcut/overburst due to sand moving into the cavity created by the forward jacking operation. These observations are typical of a dilatant material and result in surface heave effects.

For the loose-sand tests (Figures 5 and 9), the outward and upward movements did not reach the surface, dissipating 0.5 m above the operation, whereas the settlement caused by the overcut/overburst did reach the ground surface and became the dominant feature of these tests. These observations are typical of a soil with a very small dilation angle. At shallower depths (PB10 and CPJ7, Figures 10 and 11, respectively) in loose sand the movements did extend to the surface in front of (or above) the operation, although the high compressibility of the sand was evident and the settlement trough again dominated. The plots generally show a greater proportion of forward movement and more concentrated rotational movements in the pipebursting tests, the latter being due to the length of the shield separating the heave and settlement effects.

These results indicate that a pipeburster with a 12° cone, determined from the comparisons with pipebursters used in practice, that was pushed twice the distance of a vertical closed shield of similar size would cause similar soil movements. This allows interpretation

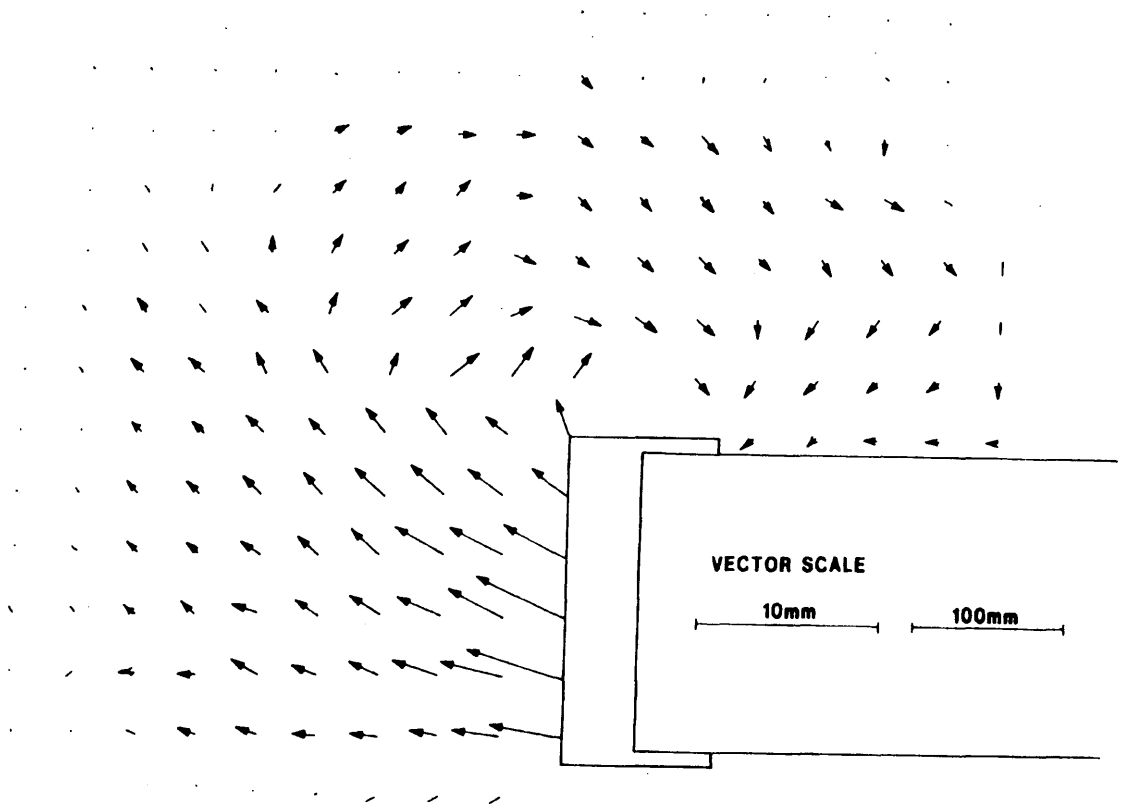

FIGURE 6 Vector displacement plot for Test OPJ3 (4.0 m deep in dense sand, 10-mm jacking distance).

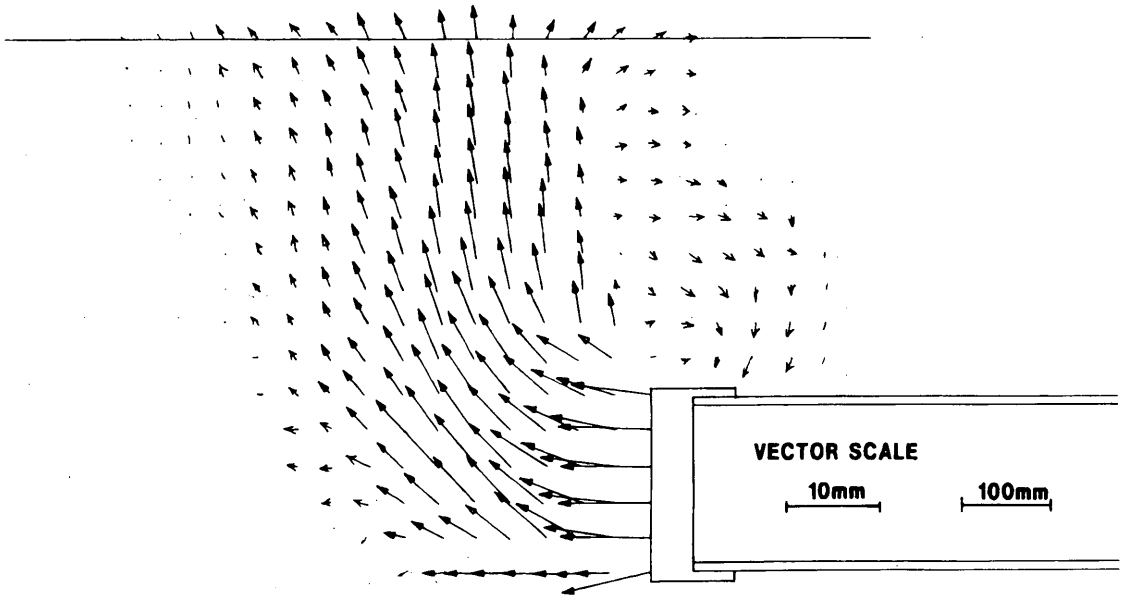

FIGURE 7 Vector displacement plot for Test CPJ6 (0.4 m deep in dense sand, 10-mm jacking distance).

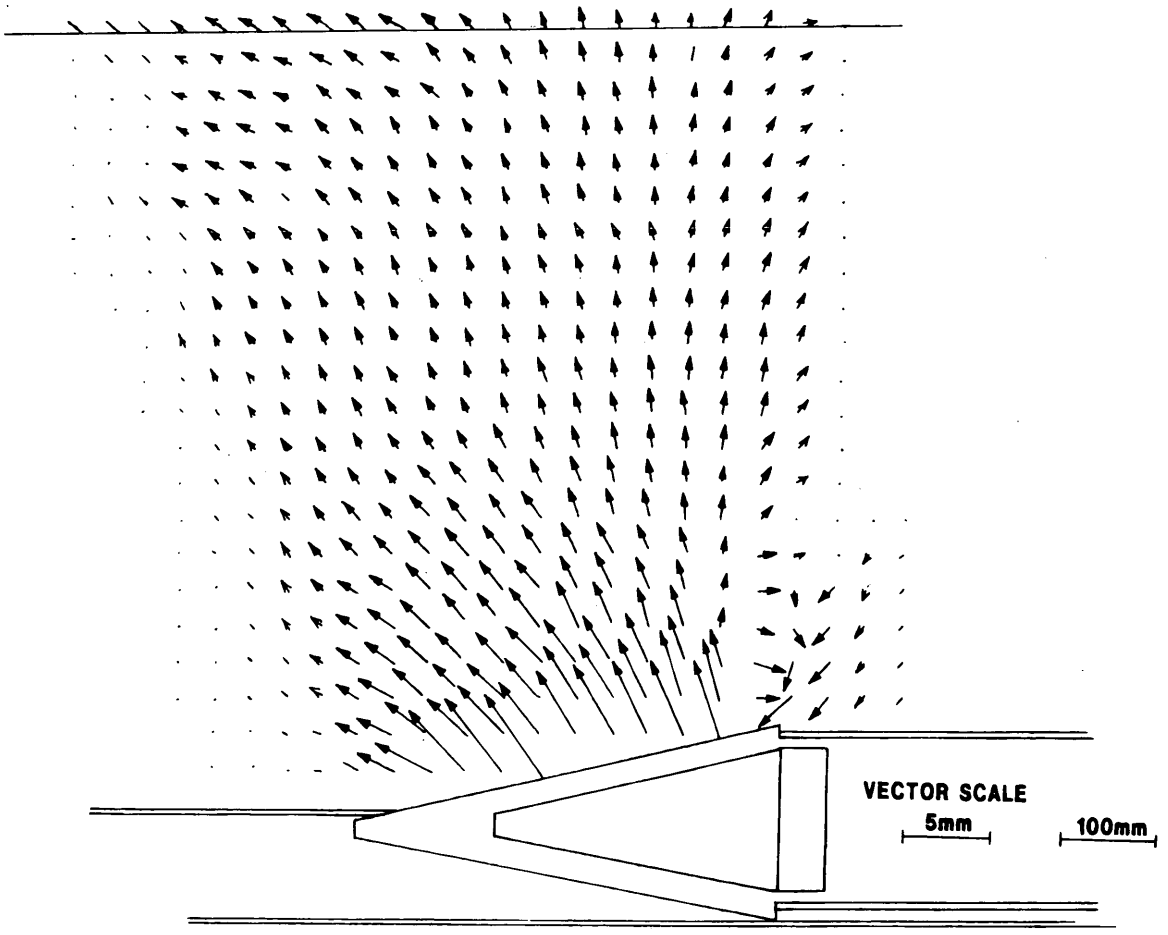

FIGURE 8 Vector displacement plot for Test PB8 (0.9 m deep in dense sand, 20-mm jacking distance).

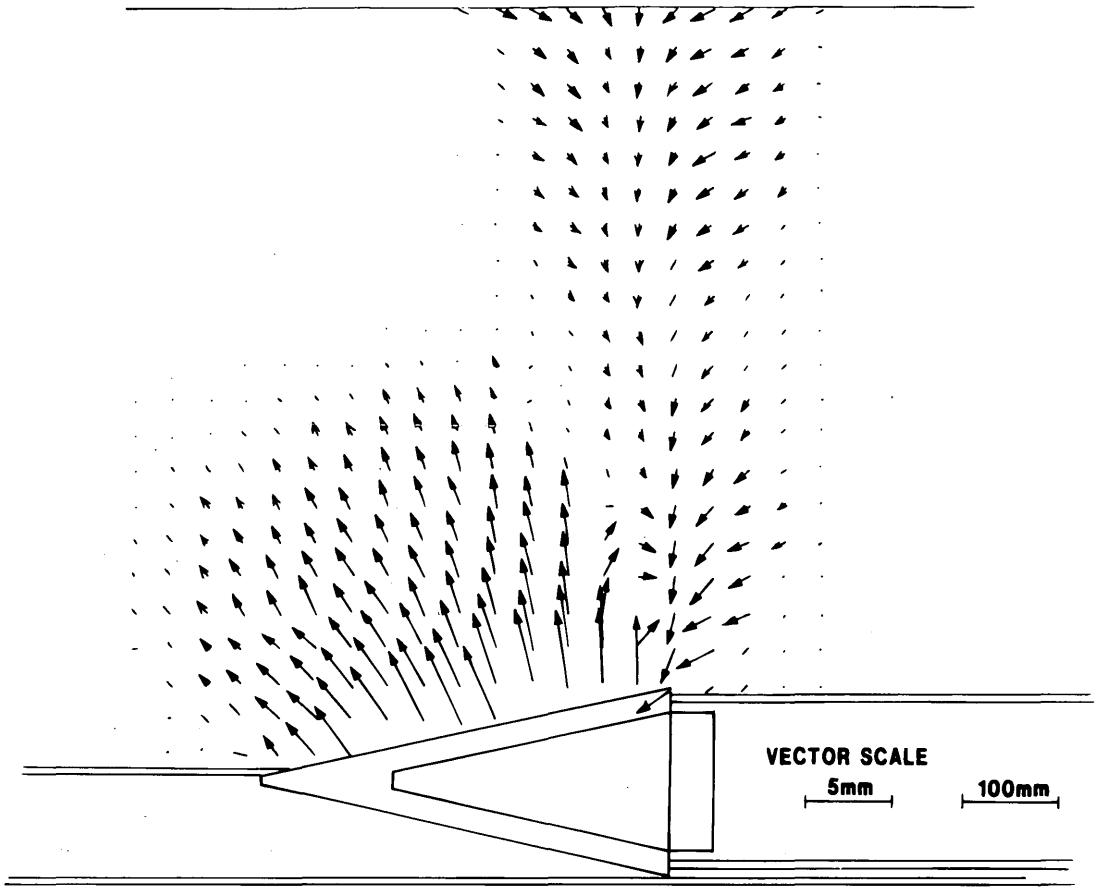

FIGURE 9 Vector displacement plot for Test PB9 (0.9 m deep in loose sand, 20-mm jacking distance).

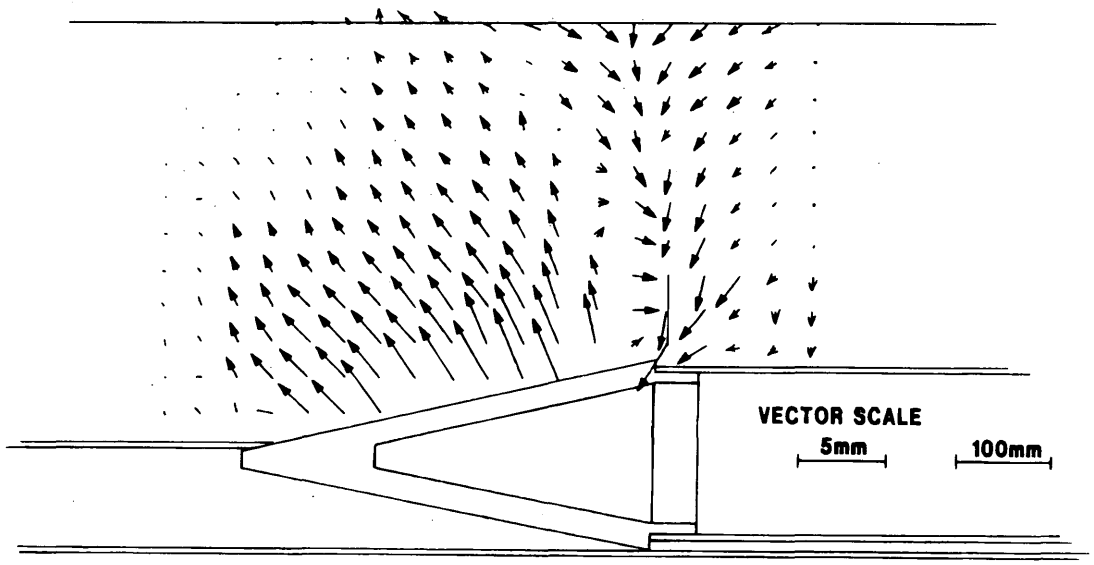

FIGURE 10 Vector displacement plot for Test PB10 (0.4 m deep in loose sand, 20-mm jacking distance).

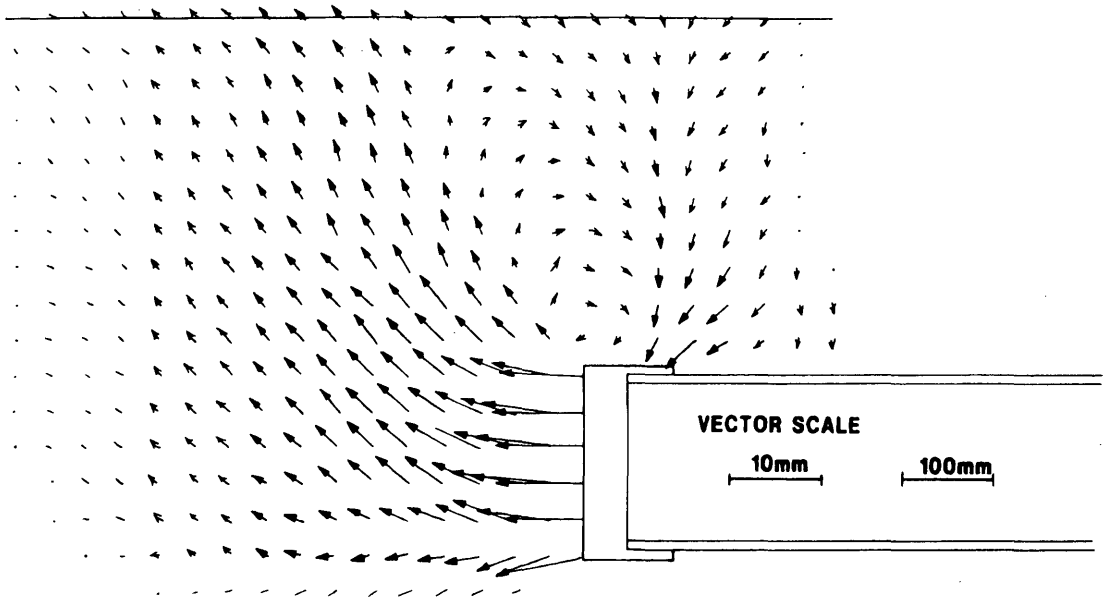

FIGURE 11 Vector displacement plot for Test CPJ7 (0.4 m deep in loose sand, 10-mm jacking distance).

of the likely ground movements caused by variations in the bursting head angle. If the whole passage of these operations is considered, the closed-shield pipejacking tests produced twice the magnitude of movements of the pipebursting tests. It should be noted that the overburst for the pipebursting tests (5 mm) was smaller than the overcut for the pipejacking tests (10 mm). However, the cavity is twice as long due to the 20-mm forward jacking distance, so the volume loss is similar.

For pipebursting operations the bursting ratio is clearly important in ground movement prediction. The smaller this ratio, the smaller the amount of burster exposed outside the old pipe, and hence the reduced extent of the observed movements in front of the operation. This is clearly illustrated by the results from tests PB11 and PB8 (Figures 12 and 8, respectively), which showed bursting ratios of 1.2 and 1.7, respectively. This means that the greater the bursting ratio, the more similar the movements were to the closed pipejacking tests in terms of extent. The bursting ratio has little effect on the *magnitudes* of the resulting movements for a 20-mm forward jacking distance, but because of the great *extent* of the displacements, the total magnitudes of the soil displacements will obviously be greater for greater bursting ratios after summation (the process of which is described later). This would be expected because of the greater volume of soil displaced.

PRACTICAL APPLICATION OF RESULTS

The results for the three types of operation, open-shield and closed-shield pipejacking and (angled-shield) pipebursting, indicate clearly that there are close relationships between the resulting ground movements. For the pipejacking tests it is the degree of face support and amount of overcut that dictate the extent and magnitude of the resulting soil movements, whereas for pipebursting tests it is the angle of the burster, the bursting ratio, and the degree of overburst that are important. The results presented herein thus provide a fundamental understanding of the effects of the operation on the surrounding soil. In addition, because of their consistency, the results can be extrapolated and interpolated, using engineering judgement, to predict the effects of pipejacking operations (using various face support methods) and pipebursting operations in practice.

It will be apparent that this discussion is wholly dependent on the type of soil through which the operation is being carried out. Extreme cases of running sand, cohesionless soils below the water table, and very soft saturated alluvial soils would result in a continuous flow of soil into an open pipejacking shield. This would clearly be unacceptable and some degree of face support would be used, thus restricting the movements to levels that are much closer to those that have been modeled here. Whether they are closer to the closed-shield or open-shield movements would depend on the type and degree of face pressure used. For cases in which porewater pressures (both positive and negative) will be generated, due allowance for the time dependency of movements and subsequent consolidation of clay soils must be made.

The type of soil is similarly very important in predicting the movements that are caused by pipebursting. A stiff, dense soil will produce considerably greater outward displacements within the ground than a loose, compressible material, which will in turn produce greater settlement at the overburst. These movements have direct implications for other pipes, services or other structures within the vicinity of these operations as different movement regimes will be induced into them.

The vector displacement plots shown in this paper all refer to a "snapshot" of the respective operations, 10-mm forward jacking for the pipejacking tests and 20 mm in the case of the pipebursting tests. In order to determine the full effects of the movements on adjacent services and structures it is necessary to obtain the total ground movements for the passage of the whole operation. This is achieved by a summation process of the results obtained from the snapshot plots, whereby the movements at 10 mm (in the case of pipejacking) or 20 mm (for pipebursting) horizontal increments at the height of the service or structure under consideration are added together according to the principle of superposition (*7*). By considering the

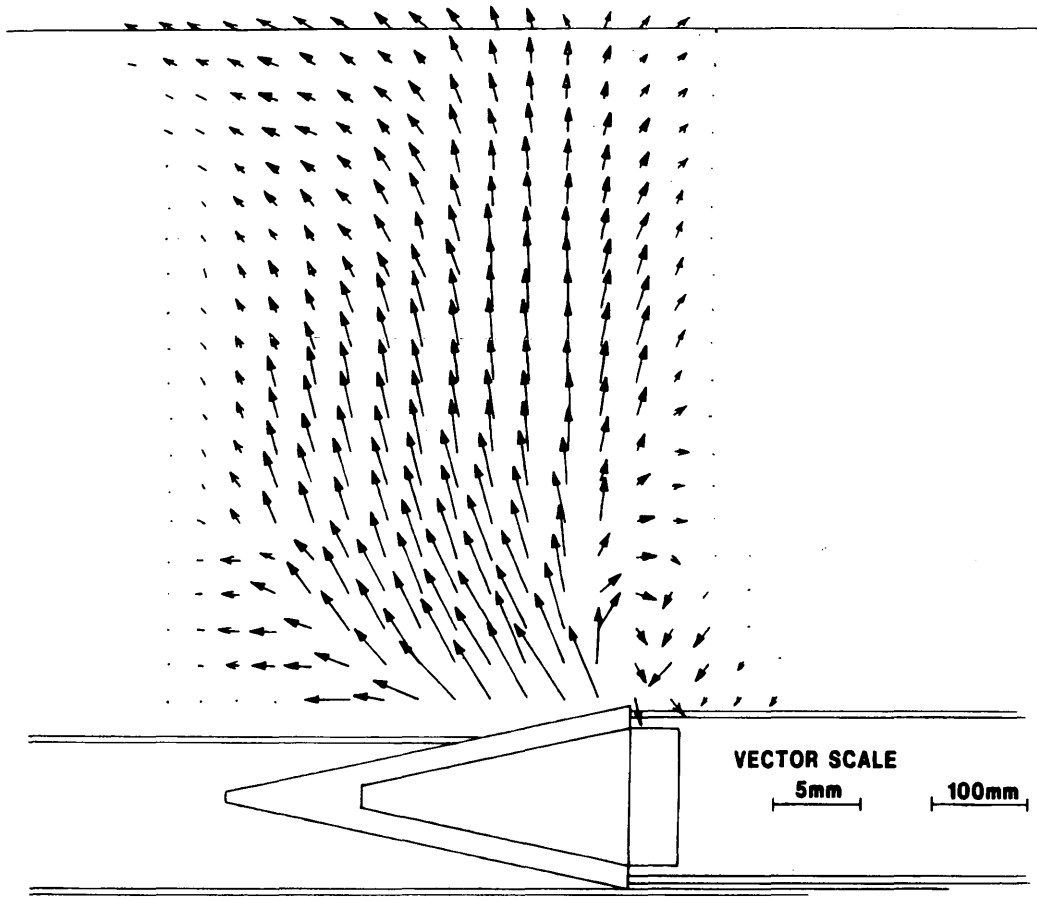

FIGURE 12 Vector displacement plot for Test PB11 (0.9 m deep in dense sand, 20-mm jacking distance).

relative stiffnesses of the soil and the service or structure, an estimation of the movements in the latter can then be made.

CONCLUSIONS

The results presented in this paper allow good visualization of the movements that occur in the ground during the jacking stage of various trenchless pipelaying operations. It is apparent from the results that there are many similarities between the patterns of movements observed, particularly between closed-shield pipejacking and pipebursting. The effects of variation of cover depth and, for pipebursting operations, the bursting ratio have also been demonstrated and conform broadly to expectations.

A knowledge of the ground movements caused by trenchless pipelaying operations and their effects on adjacent services and structures is of considerable importance if these operations are to be more widely accepted. This is particularly important in the congested urban environment, where the density of services is very high. A procedure for calculating the movements inducted in adjacent services or structures using the vector displacement plots has been described. It is intended, therefore, that the paper will provide a basis of understanding and data on which predictions of ground movements in practice can be based. Ideally these can be refined further by field monitoring, resulting in greater confidence in the use of trenchless pipelaying operations.

ACKNOWLEDGMENTS

The research described in this paper was supported by the U.K. Science and Engineering Research Council, whose support is gratefully acknowledged.

REFERENCES

1. Kramer, S. R., W. J. McDonald, and J. C. Thomson. *An Introduction to Trenchless Technology.* Van Nostrand Reinhold, New York, 1992.
2. Read, G. F., and I. Vickridge. The Environmental Impact of Sewerage Replacement and Renovation. *Proceedings of the Fifth International Conference on Trenchless Construction for Utilities.* Rotterdam, The Netherlands, April 1990, Paper A3.
3. Fry, R., and P. B. Rumsey. *Ground Movements Caused by Trench Excavation and Their Effect on Adjacent Buried Services.* Technical Report TR195. Water Research Centre, Swindon, U.K., July 1984.
4. DeMoor, E. K., and R. N. Taylor. Ground Response to a Sewer Constructed in Very Soft Ground. *Proceedings of the Sixth International Symposium on Tunnelling.* London, April 1991, pp. 43–54.

5. Chapman, D. N., and C. D. F. Rogers. Ground Movements Associated with Trenchless Pipelaying Operations. *Proceedings of the Fourth International Conference on Ground Movements and Structures.* Cardiff, Wales, U.K., July 1991, pp. 91–107.
6. Rogers, C. D. F., and D. N. Chapman. Laboratory Modeling of Ground Movements Caused by Pipejacking. *Ground Engineering,* Vol. 27, No. 8, Oct. 1994, pp. 27–36.
7. Rogers, C. D. F., and D. N. Chapman. Laboratory Simulation of Pipebursting Operations in Sand. *Proceedings of the Institution of Civil Engineers, Geotechnical Engineering,* Vol. 108, No. 1, Jan. 1995, pp. 38–50.
8. Chapman, D. N. *Ground Movements Associated with Trenchless Pipelaying Operations.* Ph.D. thesis. Loughborough University of Technology, U.K., 1992.

Publication of this paper sponsored by Committee on Culverts and Hydraulic Structures.

Three-Dimensional Response of Deeply Buried Profiled Polyethylene Pipe

IAN D. MOORE

Three-dimensional finite element stress analysis is used to examine the response of profiled polyethylene (PE) pipe under various burial conditions. Radial, circumferential, and axial normal stresses are examined for three pipes of different diameter buried at various depths in different soil materials. The implications for PE pipe design are examined in relation to arching, time-dependent pipe response, and tensile rupture. The study found that circumferential stresses are predominantly compressive and can be predicted reasonably well using conventional two-dimensional analysis. Tensile axial stresses, which develop in the inner liner of the pipe, cannot be evaluated using three-dimensional analysis. These tensions are greatest at the spring line and may be an important performance limit for lined corrugated PE pipe under deep burial. The pipes considered have a peak tension of not more than half the AASHTO allowable value at 22-m burial in very good quality (SW95) backfill material or 11 m in the same soil at lower density (SW85).

In the design of HDPE pipe for storm water sewer applications, several performance limits must be considered. Besides established limits such as buckling (*1*) and excessive deflection (*2*), the maximum circumferential bending stresses in the pipe are often considered in order to prevent tensile yield or rupture of the pipe (*3*). However, for a complex three-dimensional structure such as a lined corrugated HDPE pipe, there is no guarantee that the maximum tensile or compressive stresses are in the circumferential direction. A three-dimensional analysis is required to examine the distribution of radial and axial stresses in the buried pipe, according to Moore and Hu in another paper in this record.

A theoretical study of the three-dimensional stress state of a buried HDPE pipe is presented. Pipes with diameters of 300, 460, and 760 mm are examined. The pipe profiles consist of an annular corrugated section with an internal liner that provides improved hydraulic properties. Three-dimensional finite element analyses of the pipe-soil system were used to detect stresses in the pipe under various burial depths and for various backfill materials.

After defining the buried pipe problem and describing the three-dimensional finite element analysis, the authors examine the response of a 460-mm pipe buried 11 m within a granular soil embankment. The circumferential stresses that were predicted using the three-dimensional finite element analysis and the conventional two-dimensional analysis are compared, and radial and axial stresses are examined. The nature of the local three-dimensional pipe deformation is considered in order to explain the axial stresses that occur. Pipe stresses are then examined for other burial depths, soil materials, pipe diameters, and HDPE moduli. A discussion of the significance of the three-dimensional pipe response in relation to various performance limits is also presented.

I. D. Moore, Geotechnical Research Centre, The University of Western Ontario, London, Ontario, N6A 5B9, Canada.

PROBLEM DEFINITION

Figure 1(*a*) is a sketch of the the pipe-soil system that was studied. A circular pipe with annular corrugation and smooth internal liner is buried deeply within an earth embankment (this is generally the most conservative case, as the loads that develop on a pipe in an embankment burial condition will be more than those for the trench case where shear stresses develop on the sides of the trench, which provide some support to the column of soil over the pipe). The geometry of the pipe profile illustrates the three-dimensional nature of the problem Figure 1(*b*). The stresses that must be examined act in the circumferential σ_{tt}, radial σ_{rr}, and axial σ_{zz} directions as shown.

The usefulness of two-dimensional linear and nonlinear elastic analyses of buried pipe systems has been well established through the work of Katona (*4*) and others. Undertaking a full, three-dimensional analysis of the buried pipe system, however, is a more formidable task. To understand the three-dimensional stress distribution through the pipe, it is essential to accurately model the corrugated pipe profile. Recognizing that the central axis of the annular pipe is an axis of symmetry [Figure 1(*b*)], the three-dimensional pipe geometry can be efficiently modeled using axisymmetric finite element theory. It is then possible to obtain a reasonable first approximation of the stresses in the pipe provided the correct soil stiffness and stress state are modeled near the pipe.

The annular axisymmetric structure shown in Figure 1 is assumed to be buried in a region of elastic soil subjected to biaxial stress field (uniform vertical stress σ_v and uniform horizontal stress σ_h). Residual stresses are neglected and it is assumed that the pipe has been installed with a uniform backfill envelope around the full circumference (the impact of local bending at the pipe invert associated with variable support under invert and haunches is neglected). The research indicates that the spring line is the critical location for tensile stress in the pipe and that the use of uniform support for invert and haunches should not significantly affect those results.

The finite element analysis so performed (*5*) is really the three-dimensional equivalent of the well-known, two-dimensional elastic solutions [such as those of Burns and Richard (*6*) and Hoeg (*7*)], which are used as design tools in various buried pipe industries [e.g., CANDE (*8*) and the design practice of the German Waste Water Association ATV (*9*)]. These use the plane strain continuum theory to determine the response of a uniform thickness tube buried in a uniform elastic soil.

Table 1 contains details of the three pipe profiles to be considered. The section properties have been calculated by numerical integration of each of the three pipe profiles.

Tables 2 and 3 describe the soil materials selected. For the embankment, three alternatives represent the kind of embankment materials that could be expected in the field. They include (*a*) one

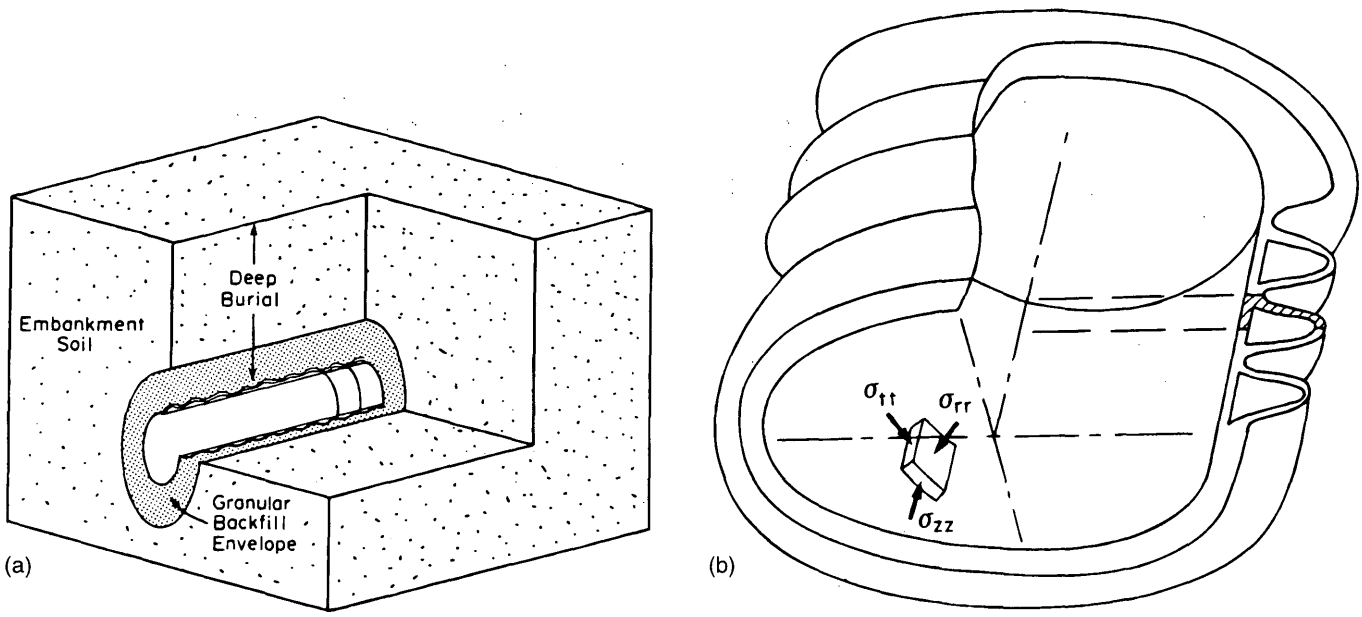

FIGURE 1 Geometry of buried HDPE pipe: (a) exposed view, (b) detail of pipe with annular corrugation and smooth internal liner.

well-graded granular material compacted to 85 percent of the AASHTO T-99 maximum dry density (classified as SW85), (*b*) one silty material compacted to 90 percent of the AASHTO T-99 maximum dry density (classified as ML90), and (*c*) one clayey soil compacted to 90 percent of the AASHTO T-99 maximum dry density (classified as CL90). Two well-graded granular backfill materials were considered: one at 85 percent of the AASHTO T-99 maximum dry density (classified as SW85) and one at 95 percent (classified as SW95). The latter material has a stiffness similar to a crushed rock backfill, which shows that these backfill materials represent the full range of materials that should normally be used in the field. The backfill zone is assumed to extend 300, 300, and 380 mm from the sides of pipes with diameters of 300, 460, and 760 mm, respectively. The density and coefficient of lateral earth pressure are also given for the SW95 material, because this soil is used as an embankment soil for one analysis (see the section, Pipe Response for One Typical Installation).

The hyperbolic soil parameters given in Table 2 were used to estimate the elastic soil modulus. Table 3 shows estimates of stress and secant (not tangent) modulus at three depths within the backfill and embankment materials for embankments constructed from the SW85, ML90, and CL90 soils. These estimates are judged to be "average" values for the soil materials and stress values considered, but are neither unique nor exact. Elastic soil modulus is not E', the empirical model-dependent parameter used in the Spangler deflection equation. Instead, it is a real physical quantity that can be measured in the laboratory and for which data exist based on extensive laboratory testing (*10*).

The selected pipe burial depths (3.6, 11, and 22 m) exceed the typical range for pipes of these diameters. Poisson's ratio for the soil has been estimated as 0.3. The interface between the pipe and the soil is assumed to be a "zero-slip" or "bonded" condition. For two-dimensional analysis, the "zero-slip" assumption leads to the largest bending stresses in the structure (*6*).

Three HDPE modulus values were examined. In accordance with AASHTO design recommendations, a short-term value of 760 MPa and a long-term value of 152 MPa were selected to indicate the possible extremes. An intermediate modulus value of 310 MPa also was examined. The selection of this intermediate modulus and the significance of short-and long-term HDPE moduli will be discussed in more detail in a subsequent section. Most of the analyses were performed using the pipe modulus value of 152 MPa. A value of 0.4 was assumed for Poisson's ratio of the HDPE (trial analyses using both 0.4 and 0.46 revealed that this parameter can affect the results by about 10 percent).

TABLE 1 Circumferential Pipe Properties per Unit Length

diameter mm	area mm²/mm	I_{zz} mm⁴/mm
305	5.4	541
457	7.5	1606
762	9.8	5211

PIPE RESPONSE FOR ONE TYPICAL INSTALLATION

Before undertaking a parametric study to examine the limits of pipe stress for a range of burial conditions, pipe diameters, and effective pipe moduli, it is instructive to examine in detail the pipe response for one particular burial condition; namely, at a depth of 11 m in an embankment constructed from SW95 well-graded granular material with the same SW95 material used as backfill [this use of a uniform soil allows direct comparisons with the two-dimensional analysis of Hoeg (*7*)]. The 460-mm-diameter pipe was used for this first phase of the study.

TABLE 2 Soil Materials Including Density γ Coefficient of Lateral Earth Pressure K_0 and Hyperbolic Modulus Data

material	classfctn	K	n	R_f	c kPa	ϕ_0	$\Delta\phi$	K_0	density kN/m^3
well graded granular	SW95	950	0.6	0.7	0	48°	8°	0.43	21.7
well graded granular	SW85	450	0.35	0.8	0	38°	2°	0.43	21.7
well compacted silt	ML90	200	0.26	0.89	24	32°	0	0.47	18.1
well compacted clay	CL90	75	0.54	0.94	48	17°	7°	0.71	15.7

Figure 2 shows the finite element mesh used for the analysis near the 460-mm diameter pipe. This is a two-dimensional mesh, with variations in stress and displacement around the pipe circumference modeled using harmonic terms. Actually, the mesh stretches five pipe diameters away from the pipe, but the stresses within the pipe and the soil directly adjacent to it are the principal concern. Six noded linear strain triangles (800 for the full mesh) are used to model the pipe and the soil material surrounding it. A mesh refinement study was conducted and revealed that the use of finer meshes would affect the stress predictions by a few percentage points for large stress values, or by as much as 10 kPa for low stress levels (those less than about 30 kPa). For consistency, all solutions reported for the 460-mm-diameter pipe were performed using the mesh shown, and the solutions given later for the pipes of 300-mm and 760-mm diameter are based on very similar meshes.

TABLE 3 Vertical and Horizontal Stress in Different Embankment Soils and Secant Moduli (MPa) in Embankment and Backfill Soils at Various Depths

embkmt soil	depth	σ_v kPa	σ_h kPa	embkmt modulus	SW85 modulus	SW95 modulus
SW85	3.6m	99	43	28	28	53
SW85	11m	238	102	37	37	88
SW85	22m	476	205	47	47	132
ML90	3.6m	83	39	14	28	51
ML90	11m	199	93	16	37	85
ML90	22m	396	186	19	47	127
CL90	3.6m	72	51	5	34	62
CL90	11m	172	123	7	46	105
CL90	22m	345	245	10	58	158

Figures 3 to 5 show contours of circumferential stress σ_{tt}, radial stress σ_{rr}, and axial stress σ_{zz} for the pipe and for the soil near the pipe. All stress values given in the figures and reported in subsequent sections are tension positive.

Circumferential stress has long been a concern of pipe designers trying to limit tensions associated with pipe bending. Figures 3(*a*), 3(*b*), and 3(*c*) show the distributions of circumferential stress at the pipe crown or invert; the spring line; and the quarter points (haunches and shoulders). A conventional two-dimensional analysis of the pipe [e.g., Hoeg (*7*)] can be used to estimate the distributions of hoop thrust and circumferential bending moment, as well as circumferential stresses in the pipe wall. At 11-m depth with soil modulus 88 MPa and HDPE modulus 152 MPa, the resulting two-dimensional predictions of circumferential stress at the pipe centroid (neutral axis) are 30, 1,100, and 570 kPa, respectively. These values are very similar to those calculated using the three-dimensional finite element analysis. The three-dimensional analysis also reveals local variations away from the neutral axis as follows:

- Stress in the section farthest from the pipe axis increases as one would expect at the crown-invert position, but remains close to the neutral axis values at the other two pipe locations. These extreme fiber stresses are less affected by bending than would be expected from calculations based on two-dimensional analysis. The mass of soil adjacent to the pipe at this location appears to be acting with the HDPE material to carry much of the bending stress.
- A stress concentration occurs where the corrugation section and the lining intersect.
- Stresses in the sections of lining spanning the corrugation decrease below the neutral axis values at each point around the pipe circumference. This is associated with the local bending that occurs here. This bending is examined later in this section in relation to the axial stress distributions shown in Figure 5.

Radial stress values are all relatively low. Two-dimensional analysis of the system indicates that the radial stress at the neutral axis is about 14 kPa, which is consistent with what is shown in Figure 4. This is only about 8 percent of the vertical overburden pressure (172 kPa). This high amount of "positive arching" is associated

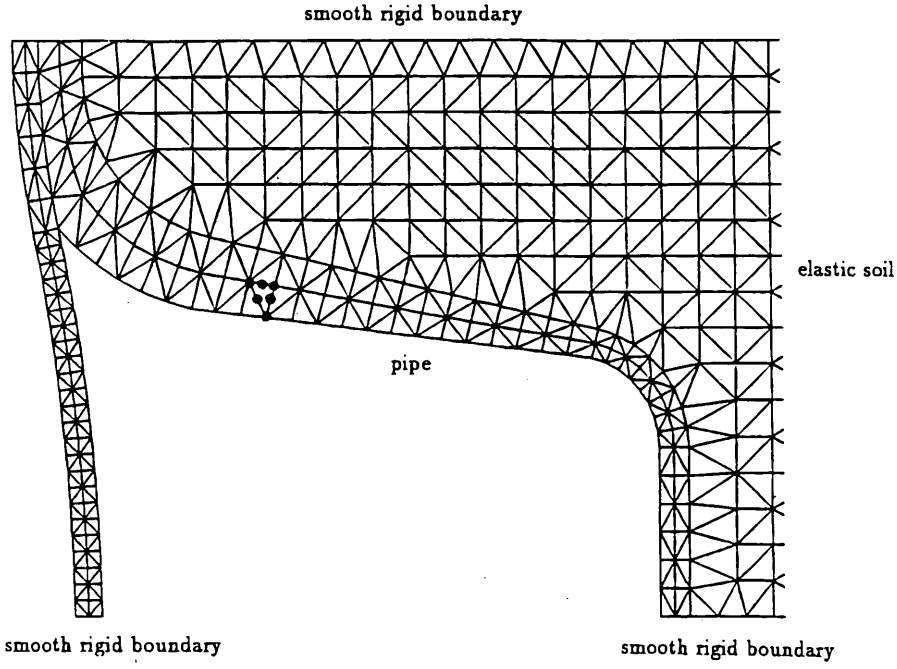

FIGURE 2 Finite element mesh close to the 460-mm-diameter pipe.

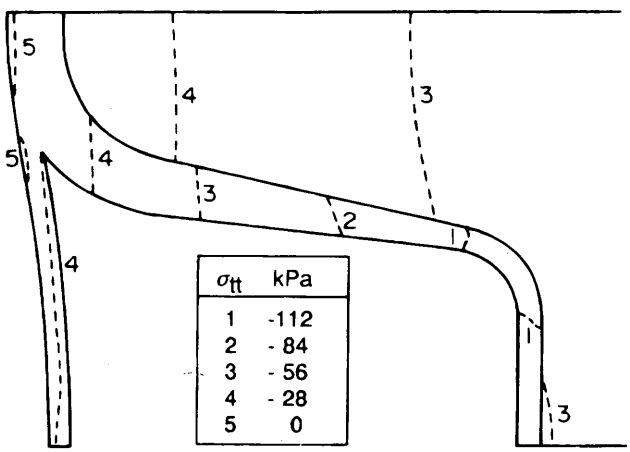

(a)

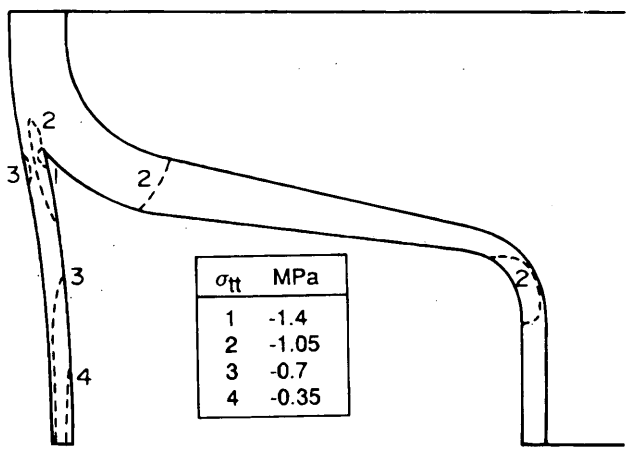

(b)

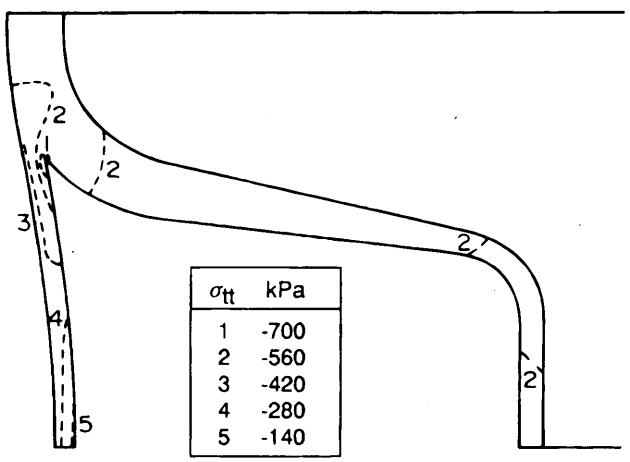

(c)

FIGURE 3 Circumferential pipe stresses at (a) crown-invert, (b) spring lines, and (c) quarter points.

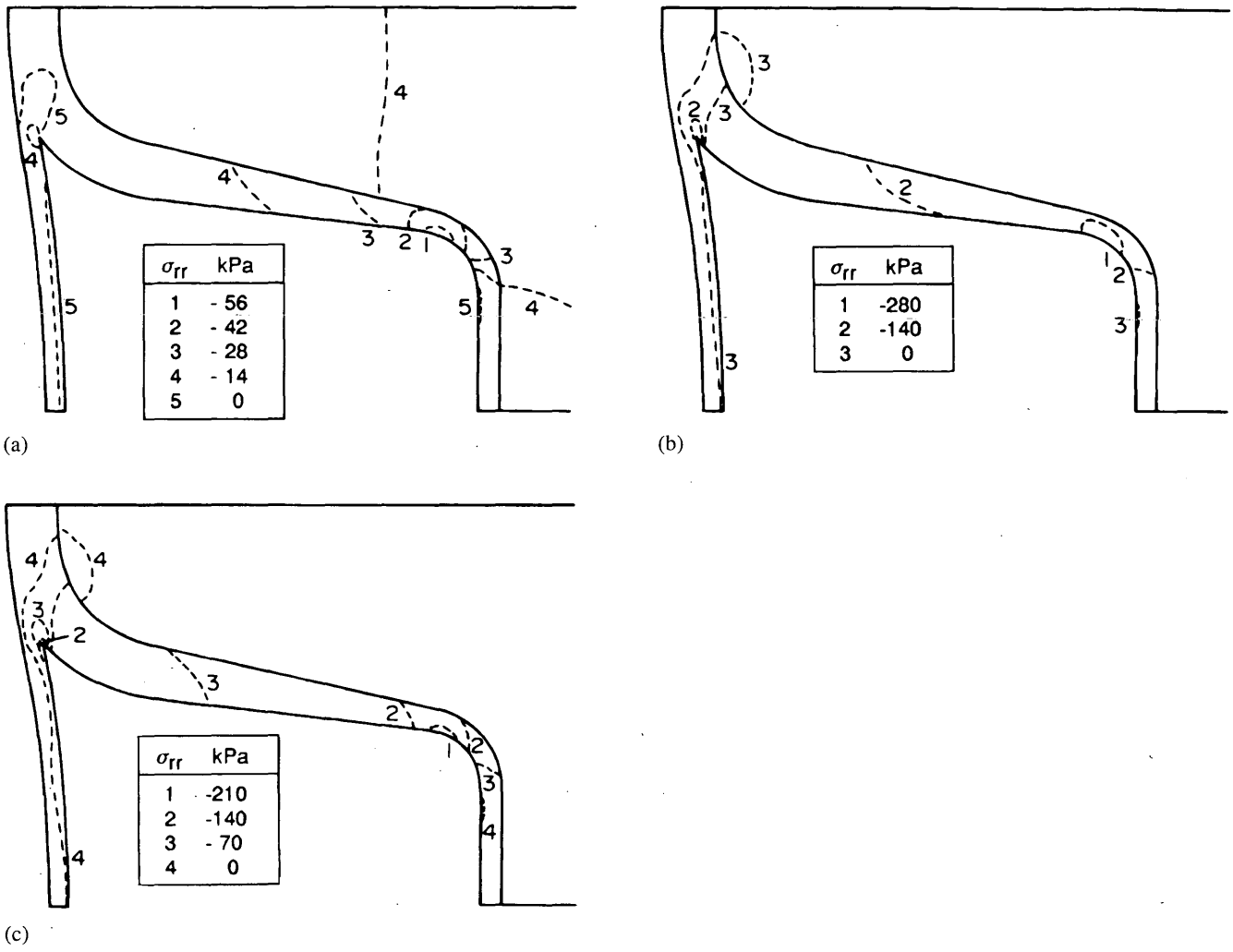

FIGURE 4 Radial pipe stresses at (a) crown-invert, (b) spring lines, and (c) quarter points.

with circumferential shortening of the pipe, which also will be discussed in more detail later.

The radial stresses increase somewhat in the area where the corrugation section and the lining intersect, with the maximum and minimum values in relatively close proximity. Of particular interest are the small regions of radial tension predicted within the pipe.

The axial stress distributions shown in Figure 5 reveal that tensile stresses do develop in the pipe liner. These stresses are the result of local bending and have been explained and investigated by Moore and Hu elsewhere, and by Selig (*11*) in relation to pipe response under hoop compression.

The tensions in the liner that develop close to the liner-corrugation junction represent an important performance limit for lined corrugated pipe under very deep burial.

DIFFERENT DEPTHS AND BACKFILLS

A parametric study was performed to determine how minimum and maximum stresses are affected by burial depths and backfill quality. The results are shown in Table 4 for the 460-mm pipe with HDPE modulus of 152 MPa and with the ML90 embankment soil (closest to the soil used in real embankments). For each burial depth, backfill type, stress direction, and pipe location, the largest tensile (positive) stress is shown above the largest compression (negative). Where the upper value is negative, this represents the lowest compressive stress value (no tension occurs in that case).

Also shown are estimates of the pipe deformation for each of the pipe burial conditions considered. Changes in vertical pipe diameter ΔD_v and horizontal pipe diameter ΔD_h are given, in addition to percent changes in diameter.

The results reveal that:

- Stresses within the pipe decrease as soil stiffness is increased (this is consistent with well-known trends for buried flexible and rigid pipe).
- Pipe deformations decrease as backfill stiffness is increased (this also is consistent with what is expected for the flexible pipe, in which the pipe deformations are controlled predominantly by the soil, not the pipe itself.
- Stresses in the pipe increase with burial depth, but at a rate that is less than linear. As soil depth increases the soil stiffness also

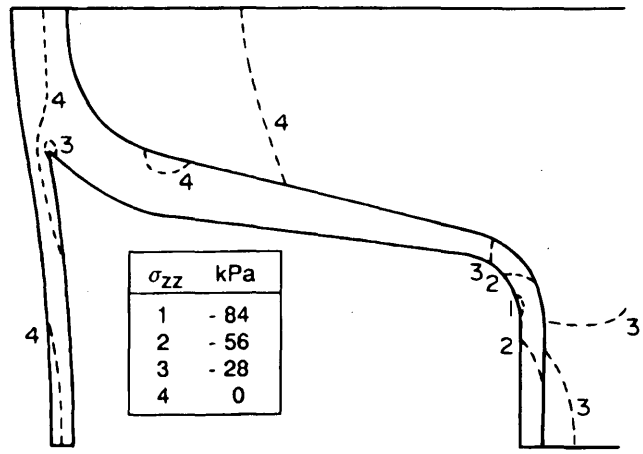

(a)

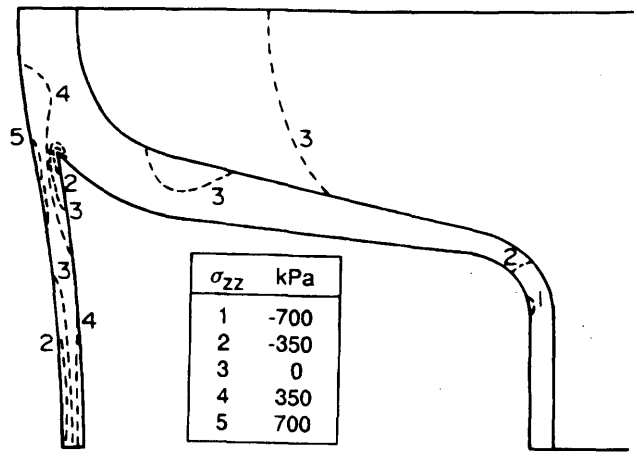

(b)

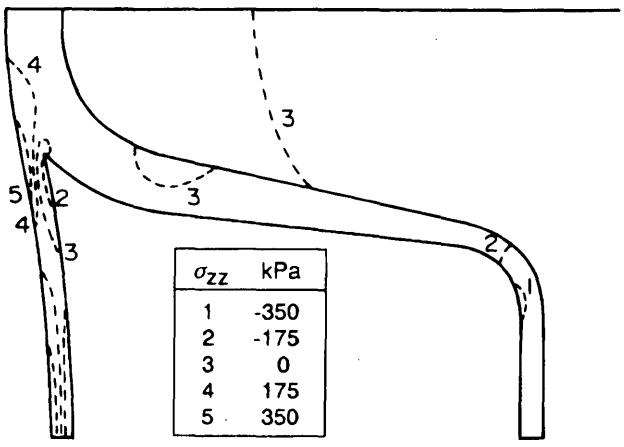

(c)

FIGURE 5 Axial pipe stresses at (a) crown-invert, (b) spring lines, and (c) quarter points.

increases so that additional "positive arching" somewhat reduces the resulting loads.

- The only tensile circumferential stresses that occur develop at the crown of pipes buried deeply in the stiffer backfill; the magnitude of these tensions is quite small (the largest tension is 160 kPa).
- Tensile radial stresses do develop in the pipes, but are of relatively low magnitude (less than 410 kPa) except at the spring line of the pipe deeply buried with lower density backfill.
- Axial tensions σ_{zz} develop in the liner of all of the pipes. They are highest at the spring lines (for the SW95 backfill, maximum tensions range from 1 MPa to 2.7 MPa for 3.6-m and 22-m burial, respectively).

PIPE MODULUS

A parametric study was performed to examine how minimum and maximum stresses and pipe deformations are affected by HDPE modulus. The results are shown in Table 5 for the 460-mm pipe buried 11 m within an ML90 embankment with SW95 backfill. Pipe moduli of 760, 310, and 152 MPa are considered; these are effective (or "secant") moduli over the time period for which the load is applied.

Time-dependent analysis using viscoelastic material models has demonstrated that for a parallel plate test performed on an HDPE pipe over a period of a few minutes, the effective pipe modulus is about 390 MPa (*12*). For a pipe burial with a depth of 3.6 m over 1 hr or less (a rapid case), a modulus value of about 310 MPa applies. Modulus for the pipe as it responds to this earth load over most of its design life ranges from 152 to 310 MPa, generally occurring closer to the lower value. Incremental HDPE pipe modulus for live loads will be much closer to 760 MPa, depending on the rate at which the live load is applied and then removed. The net pipe response at a particular time involves adding the short-term live load response to the long-term response to dead load.

Table 5 indicates that stresses are highest with an HDPE modulus of 760 MPa, decreasing substantially with decreases in the effective HDPE modulus. This is not surprising given that there is circumferential shortening in the pipe and, therefore, "positive arching"; hence, decreases in effective pipe modulus lead to additional "positive arching" (i.e., more of the overburden load is redis-

TABLE 4 460-mm Pipe Response at Crown, Spring Line, and Quarter Points for Burial at Various Depths in Two Different Backfills; Minimum and Maximum Stresses Given, Tension Positive

burial condtn	σ_{rr} crown	σ_{tt} crown	σ_{zz} crown	σ_{rr} sprgl	σ_{tt} sprgl	σ_{zz} sprgl	σ_{rr} qrtr	σ_{tt} qrtr	σ_{zz} qrtr	ΔD_vmm (%D)	ΔD_hmm (%D)
SW85	40	-40	220	220	-70	1400	130	-60	820	-4.1	-0.2
3.6m	-150	-340	-280	-710	-2200	-1700	-410	-1300	-990	(0.9%)	(0.0%)
SW85	60	-70	370	450	-160	2800	250	-140	1600	-8.1	-0.3
11m	-270	-590	-450	-1400	-4400	-3400	-800	-2500	-1900	(1.8%)	(0.1%)
SW85	80	-140	550	750	-300	4700	420	-280	2600	-13.5	-0.5
22m	-430	-920	-680	-2400	-7500	-5700	-1300	-4200	-3200	(3.0%)	(0.1%)
SW95	10	-10	80	170	-50	1000	90	-50	560	-3.0	0.1
3.6m	-90	-170	-100	-520	-1700	-1300	-280	-880	-670	(0.7%)	(0.0%)
SW95	0	40	20	280	-100	1800	140	-120	890	-5.1	0.3
11m	-220	-290	-150	-890	-2800	-2100	-450	-1400	-1100	(1.1%)	(0.1%)
SW95	40	160	80	410	-200	2600	200	-220	1300	-7.4	0.5
22m	-460	-640	-320	-1300	-4100	-3100	-640	-1200	-1500	(1.6%)	(0.1%)

tributed into the surrounding ground). This beneficial effect has been observed in the field for profiled HDPE pipes (*13*).

Two-dimensional analysis can be performed for the soil-pipe system using the same geometrical and material data used to generate the results in Table 5. This indicates that as the modulus decreases, the average radial stress applied to the pipe decreases from about 32 percent to about 9 percent of the vertical overburden pressure, with a value of 16 percent for modulus 310 MPa.

These data have important consequences for HDPE pipe design. Current design practice is based largely on procedures developed for the metal pipe industry. The basis of these procedures is the ring compression theory of White and Layer (*14*), which asserts that the full overburden load acts on the pipe.

Clearly the ring compression theory is not valid for HDPE pipes because there is substantial positive arching and only a fraction of the overburden load reaches the pipe. For the case considered, the ring compression theory leads to overestimates of pipe stress levels by a factor of 100/16 = 6 in the short term and 100/9 = 11 in the long term. As can be seen, this is very conservative.

From the pipe deflection data, it appears that small increases in pipe deflection are associated with the changes in HDPE modulus. From the 310-MPa to 152-MPa modulus reduction, there is a 10 percent increase in pipe deflection. This small increase is a direct result of the action of the granular backfill, which is largely controlling the pipe deflection. Again, this is consistent with field observation (*13*).

These results have implications for the labels used to describe the time-dependent HDPE response. The observed behavior can be labeled as "stress relaxation" (decreases in stress with time for HDPE kept at constant strain) or "creep" (increases in deformation with time for HDPE kept at constant stress). Although the actual behavior lies somewhere between these two simplified conditions,

TABLE 5 460-mm Pipe Response at Crown, Spring Line, and Quarter Points for Different HDPE Moduli; Burial Depth 11 m; ML90 Embankment Soil; SW95 Backfill; Minimum and Maximum Stresses Given, Tension Positive

pipe modulus	σ_{rr} crown	σ_{tt} crown	σ_{zz} crown	σ_{rr} sprgl	σ_{tt} sprgl	σ_{zz} sprgl	σ_{rr} qrtr	σ_{tt} qrtr	σ_{zz} qrtr	ΔD_vmm (%D)	ΔD_hmm (%D)
760	100	-60	660	960	-100	6000	540	-110	3300	-3.6	0.4
MPa	-640	-1400	-820	-3000	-9600	-7300	-1700	-5200	-4000	(0.8%)	(0.1%)
310	30	0	160	500	-110	3200	270	-120	1700	-4.6	0.3
MPa	-230	-470	-290	-1600	-5100	-3800	-850	-2600	-2000	(1.0%)	(0.1%)
152	0	40	20	280	-110	1800	140	-120	890	-5.1	0.3
MPa	-220	-290	-150	-890	-2800	-2100	-450	-1400	-1100	(1.1%)	(0.1%)

it is most similar to the "stress relaxation" condition in that the soil keeps the pipe deformations fairly constant, and the principal effect of the time-dependent HDPE response is a beneficial reduction in internal stresses.

The predictions for pipe deflection that result from the present work are consistent with field data but are very different from what would be predicted using the Spangler equation for pipe deflection. The problem with the Spangler equation is that it ignores the substantial positive arching associated with circumferential shortening and uses an E', or "soil spring" model, which is generally not adjusted to account for the real stiffness of the backfill surrounding the pipe. A better approach would be to use two-dimensional elastic continuum analysis for the pipe-soil system. Improved estimates of pipe stresses and deformations would be the result:

- The elastic continuum solution includes the possibility of circumferential shortening and thus can predict the positive arching that occurs in the field. The assumption that the full overburden stress is active across the pipe (an approach that works well for flexible metal pipes, which experience little circumferential shortening) is not appropriate for the HDPE pipes examined in this report.
- The elastic continuum solution demonstrates that it is quite normal for horizontal diameter change to be different from the vertical diameter change (this difference is not an indication of a perceived problem, such as "squaring."
- The elastic continuum solution leads to the conclusion that decreases in effective HDPE modulus are beneficial. Because of historical circumstances, the design of HDPE pipe is currently based on ring compression theory and the Spangler equation. Unfortunately, this has led to the incorrect conclusion that it is beneficial to use the higher AASHTO modulus in design.

DIFFERENT EMBANKMENT SOILS

A parametric study was performed to examine how minimum and maximum stresses and pipe deformations are affected by the embankment material. The results are shown in Table 6 for the 460-mm pipe buried at various depths within SW85, ML90, and CL90 embankments with SW95 backfill. Pipe modulus of 152 MPa was used.

It appears that the stresses and pipe deformation are not greatly affected by the embankment material (Table 6). The trends are complicated somewhat because although there are higher vertical load levels in the denser granular embankment, there is increased positive arching, which offsets this effect.

TABLE 6 460-mm Pipe Response at Crown, Spring Line, and Quarter Points for Burial at Various Depths in Various Embankment Soil Materials; HDPE Modulus 152 MPa; SW95 Backfill; Minimum and Maximum Stresses Given, Tension Positive

embkmt depth	σ_{rr} crown	σ_{tt} crown	σ_{zz} crown	σ_{rr} sprgl	σ_{tt} sprgl	σ_{zz} sprgl	σ_{rr} qrtr	σ_{tt} qrtr	σ_{zz} qrtr	ΔD_vmm (%D)	ΔD_hmm (%D)
CL90	40	-40	250	130	-40	800	80	-40	520	-2.0	-0.5
3.6m	-130	-380	-310	-410	-1300	-960	-270	-820	-640	(0.5%)	(0.1%)
CL90	60	-90	360	200	-90	1300	130	-100	810	-3.6	-0.8
11m	-220	-560	-440	-640	-2000	-1500	-410	-1300	-1000	(0.8%)	(0.2%)
CL90	70	-120	460	270	-180	1700	180	-200	1100	-4.8	-1.0
22m	-440	-730	-560	-880	-2800	-2100	-560	-1700	-1300	(1.1%)	(0.2%)
ML90	10	-10	80	170	-50	1000	90	-50	560	-3.0	0.1
3.6m	-90	-170	-110	-520	-1700	-1300	-280	-880	-670	(0.7%)	(0.0%)
ML90	0	40	20	280	-110	1800	140	-120	890	-5.1	0.3
11m	-220	-290	-150	-890	-2800	-2100	-450	-1400	-1100	(1.1%)	(0.1%)
ML90	40	160	80	410	-200	2600	200	-220	1300	-7.4	0.5
22m	-460	-640	-320	-1300	-4100	-3100	-640	-2000	-1500	(1.6%)	(0.1%)
SW85	10	-20	80	160	-80	1000	80	-70	540	-2.8	0.0
3.6m	-100	-160	-110	-500	-1600	-1200	-270	-850	-660	(0.6%)	(0.0%)
SW85	10	0	70	260	-190	1700	130	-170	870	-4.6	0.0
11m	-240	-230	-140	-840	-2600	-2000	-440	-1400	-1000	(1.0%)	(0.0%)
SW85	0	50	40	380	-340	2400	200	-240	1200	-6.6	0.1
22m	-490	-510	-280	-1200	-3900	-2900	-620	-2000	-1500	(1.5%)	(0.0%)

TABLE 7 Pipe Response at Crown, Spring Line, and Quarter Points for Various Pipe Diameters at HDPE Modulus of 152 MPa; SW95 Backfill; ML90 Embankment; Minimum and Maximum Stresses Given, Tension Positive

diameter depth	σ_{rr} crown	σ_{tt} crown	σ_{zz} crown	σ_{rr} sprgl	σ_{tt} sprgl	σ_{zz} sprgl	σ_{rr} qrtr	σ_{tt} qrtr	σ_{zz} qrtr	ΔD_vmm (%D)	ΔD_hmm (%D)
300mm	20	-20	120	150	0	1000	80	-40	580	-1.8	-0.1
3.6m	-100	-210	-220	-770	-1800	-1800	-430	-1000	-1000	(0.6%)	(0.0%)
300mm	20	-10	130	250	10	1700	130	-60	900	-2.8	-0.1
11m	-230	-290	-220	-1300	-3100	-3000	-680	-1600	-1600	(0.9%)	(0.0%)
300mm	10	0	120	350	20	2400	190	-90	1300	-3.8	-0.1
22m	-480	-570	-290	-1800	-4400	-4300	-950	-2300	-2300	(1.3%)	(0.0%)
460mm	10	-10	80	170	-50	1000	90	-50	550	-3.0	0.1
3.6m	-90	-170	-100	-520	-1600	-1200	-280	-870	-660	(0.7%)	(0.0%)
460mm	0	40	20	280	-100	1700	140	-120	880	-5.1	0.3
11m	-220	-280	-150	-880	-2800	-2100	-440	-1400	-1100	(1.1%)	(0.1%)
460mm	30	160	80	400	-200	2600	190	-220	1200	-7.4	0.5
22m	-460	-630	-320	-1300	-4100	-3100	-630	-2000	-1500	(1.6%)	(0.1%)
760mm	10	-10	40	130	10	900	70	-60	480	-5.6	0.2
3.6m	-90	-150	-80	-330	-1400	-910	-160	-720	-480	(0.7%)	(0.0%)
760mm	10	80	20	220	10	1500	110	-120	-750	-9.1	0.2
11m	-210	-330	-160	-570	-2300	-1600	-280	-1100	-770	(1.2%)	(0.1%)
760mm	60	250	140	320	20	2300	150	-230	1100	-13.5	0.9
22m	-440	-750	-350	-830	-3500	-2300	-390	-1600	-1100	(1.8%)	(0.2%)

DIFFERENT PIPE DIAMETERS

The final parametric study was performed to examine how minimum and maximum stresses and pipe deformations are affected by the pipe diameter. The results are shown in Table 7 for the 300-, 460-, and 760-mm pipes buried at various depths within an ML90 embankment with SW95 backfill. Pipe modulus of 152 MPa was used.

Again, the data indicate that the pipe diameter is not a particularly significant parameter. This is simply a reflection of the fact that the pipe profiles have been designed to give approximately equal performance under similar burial conditions. The compressive circumferential, axial, and radial stresses are greatest in the 300-mm pipe, whereas the tensile stresses are slightly higher in the 460-mm pipe than in either of the other diameters. The very similar results for each of the pipe diameters supports the use of the 460-mm pipe for most of this three-dimensional buried pipe study.

DISCUSSION AND CONCLUSIONS

It is clear that the three-dimensional bending effects in lined corrugated pipes cannot be predicted using two-dimensional analysis. While the maximum compressive stresses are in the circumferential direction and could be estimated using two-dimensional theory, compressions and tensions develop in the axial and radial directions that cannot be predicted using two-dimensional plane strain theory.

The analysis has shown that at the spring line of a 460-mm storm water pipe buried 11 m within dense granular backfill, a local axial tension of about 1.7 MPa can develop. As burial depth increases or backfill stiffness decreases, the magnitude of this local axial tension rises. The zone of tension is located within the liner, and the corrugated component of the pipe profile is essentially unaffected.

Comparing (*a*) the AASHTO short-term tensile strength of 20.7 MPa (3,000 psi) with short-term stress values (i.e., values calculated using short-term HDPE modulus) and (*b*) the long-term tensile rupture stress of 6.2 MPa (900 psi) with the long-term stress values (i.e., values calculated using long-term HDPE modulus), it appears that the three pipes considered in this report have local stress not more than half the allowable value at 22 m burial in very good quality (SW95) material, or 11 m in the same soil at lower density (SW85).

The analyses suggest that increases in allowable burial depths may be possible for the profiled HDPE pipes in relation to the expected performance for deflection and local bending stress. This is conditional on a careful construction of the soil envelope, sufficient soil quality to maintain stability against buckling, and successful comparisons with field data to confirm the validity of the idealized soil-structure interaction model used in this study.

ACKNOWLEDGMENTS

The research was sponsored by Hancor Incorporated. Support for development of the three-dimensional finite element analysis was provided through a research grant to Ian Moore from the Natural Sciences and Engineering Research Council of Canada as well as IBM Canada through the donation of RS6000 work stations to the Faculty of Engineering Science at the University of Western Ontario.

REFERENCES

1. Moore, I. D., and E. T. Selig. Use of Continuum Buckling Theory for Evaluation of Buried Plastic Pipe Stability. In *Special Technical Publication 1093, Buried Plastic Pipe Technology*, ASTM, Philadelphia, 1990, pp. 344–359.
2. Janson, L. E., and J. Molin. Design and Installation of Underground Plastic Sewer Pipes. *Proc., International Conference on Underground Plastic Pipes*, New Orleans, 1981, pp. 79–88.
3. Chambers, R. E., and T. J. McGrath. Structural Design of Buried Plastic Pipes. *Proc., International Conference on Underground Plastic Pipes*, New Orleans, 1981, pp. 10–25.
4. Katona, M. G. Allowable Fill Heights for Corrugated Polyethylene Pipe. *Transportation Research Record 1191*, 1988, pp. 30–38.
5. Moore, I. D. Local Strain in Corrugated Pipe: Experimental Measurements to Test a Numerical Model. *Journal of Testing and Evaluation*, ASTM, Vol. 22, No. 2, March 1994, pp. 132–138.
6. Burns, J. Q., and R. M. Richard. Attenuation of Stresses for Buried Cylinders. *Proc., Symposium on Soil-Structure Interaction*, ASTM, University of Arizona, 1964, pp. 379–392.
7. Hoeg, K. Stresses Against Underground Structural Cylinders. *Journal of Soil Mechanics and Foundation Engineering*, ASCE, Vol. 94, No. SM4, 1968, pp. 833–858.
8. Katona, M. G. *CANDE: A Modern Approach for the Structural Design and Analysis of Buried Culverts*. Report FHWA-RD-77-5, FHWA, U.S. Department of Transportation, Oct. 1976.
9. ATV: The German Waste Water Association. *Guidelines for Static Calculation of Drainage Conduits and Pipelines*. Regulation DK 628.22/083, (Gesellschaft zur Forderung der Abwassertechnik, E.V.), 1984.
10. Selig, E. T. Soil Properties for Plastic Pipe Installations. In *Special Technical Publication 1093, Buried Plastic Pipe Technology*, ASTM, Philadelphia, 1990, pp. 141–158.
11. Selig, E. T., L. C. DiFrancesco, and T. J. McGrath. Laboratory Test of Buried Pipe in Hoop Compression. Dave Eckstein, ed. *Special Technical Publication 1222, Buried Plastic Pipe Technology*, ASTM, Philadelphia, 1994, pp. 119–132.
12. Moore, I. D., and F. Hu. Linear Viscoelastic Models for HDPE. *Canadian Journal of Civil Engineering*, (under review), 1995.
13. Hashash, N. M. A. *Design and Analysis of Deeply Buried Polyethylene Drainage Pipes*. Ph.D. thesis. Department of Civil Engineering, The University of Massachusetts at Amherst, 1991.
14. White, H. L., and J. P. Layer. The Corrugated Metal Conduit as a Compression Ring. *HRB Proc.*, Vol. 39, 1960, pp. 389–397.

Publication of this paper sponsored by Committee on Subsurface Soil-Surface Interaction.

Structural Performance of Buried Polyvinyl Chloride Pipes Under Large Distributed Load

SHAD M. SARGAND, GLENN A. HAZEN, XUEGANG LIU, TERUHISA MASADA, AND JOHN O. HURD

Two polyvinyl chloride (PVC) pipes of nominal diameters 457 and 914 mm (18 and 36 in.) were fully instrumented and loaded to failure at the Ohio University load frame facility site as part of a major field testing program of plastic pipes. Before load testing, each pipe was backfilled with crushed limestone material meeting the Ohio Department of Transportation no. 310 subbase specifications. Height of backfill soil over crown was 610 mm (24 in.) for the 457-mm (18-in.) diameter pipe and 305 mm (12 in.) for the 914-mm (36-in.) diameter pipe. A specially designed rotational linear variable differential transformer (LVDT) deflection measurement system was inserted into the pipe to monitor the cross-sectional deformation. During the incremental stages of backfilling and load testing, readings from the strain gages and the LVDT system were recorded by computerized data acquisition units. Test data were analyzed to establish load-deflection curves, bending moment and thrust responses, and failure modes of the buried PVC pipes. In addition, analytical results from modified Iowa formula and elastic solutions of J. Q. Burns and R. M. Richard were compared with the experimental results to evaluate general applicability of these analytical methods. The findings of this study indicated that the elastic solutions are valuable for analyzing flexible pipes buried in a homogeneous soil with loaded boundary more than one pipe diameter away.

Increasing use of profile-wall, plastic pipes in the transportation facilities has led to numerous studies on performance of these plastic pipe products. Adams et al. (*1*) studied a 610-mm (24-in.) plastic pipe under high fill conditions and noted that the change in vertical diameter was in the 3 to 5 percent range, whereas variation in the horizontal diameter was only 0.5 percent. The vertical deflection was determined to result from compression instead of bending. Minimal fill conditions were examined by Katona (*2*). He suggests that a conservative allowable deflection criteria of 7.5 percent can be used to determine minimum fill height. Because all pipes depend on the mechanical properties of the soil, a minimum overburden of 305 mm (12 in.) is recommended. Culley (*3*) suggests that pipe stiffness be incorporated in design procedures for diameters over 610 mm (24 in.) and viscoelastic behavior be considered for depths of over 15.24 m (50 ft).

This study presents both experimental and analytical results for two profile-wall polyvinyl chloride (PVC) pipes. The reason that this report is focused on the PVC pipes is that it appears in recent years an increasing number of publications has been made by others on high density polyethylene (HDPE) pipes than on PVC pipes. The research program, initiated by Ohio University, was founded on multiple objectives. The first objective was to examine failure modes of profile-wall design plastic pipes. The second aim was to establish design parameters based on true mechanical properties of backfill material and flexibility of pipe. The third objective was to develop design criteria and analytical procedures to determine soil and pipe performance. And, if necessary, recommendations may be made as to the material and design specifications for the various profile-wall plastic pipe types. The last objective was to develop laboratory test procedures to simulate actual field behavior for quality assurance testing of profile-wall plastic pipes.

S. M. Sargand, G. A. Hazen, X. Liu, and T. Masada, Civil Engineering Department, 145 Stocker Center, Ohio University, Athens, Ohio 45701-2979. J. O. Hurd, Ohio Department of Transportation, 25 South Front Street, Columbus, Ohio 43215.

TEST PIPES AND INSTRUMENTATION METHOD

The first pipe, PVC-1, was a profile-wall PVC pipe with a nominal diameter of 457 mm (18 in.). Structural design of this pipe combines a seamless uniform cross-section wall with perpendicular radial ribs. The second pipe, PVC-2, had a nominal diameter of 914 mm (36 in.). The wall profile was smooth (rib-free), consisting of hollow core I-beam design. Table 1 summarizes some of the basic properties of the pipes, and typical wall profile is graphically shown in Figure 1. Both of these pipes are being used as gravity sewer pipes in the United States.

Figure 1 illustrates a typical strain gage instrumentation plan applied to the pipes. Each pipe was instrumented with strain gages at two circumferential cross-sections along 4.268 m (14 ft) length. A total of 16 biaxial strain gages were placed at the primary section, located at the mid-length at eight equally spaced points (crown, shoulders, springlines, haunches, and invert) on both interior and exterior pipe wall surfaces. The secondary section, located 152 mm (6 in.) away from the primary section, received six biaxial strain gages. The purpose of instrumenting this additional section was to provide a backup strain gage data for the crown and springline regions. The strain gages installed on the exterior surface of PVC-1 and all surfaces of PVC-2 were type EA-50-125TQ-350, manufactured by Micro-Measurement. The resistance and gage factor of this gage were 350 ohms and 2.18, respectively. A different type of strain gages (KFG-5-120-D16-11L3M3S by Kyowa Electronic Instruments) was applied to the interior surface of PVC-1 because the space was limited and this gage came with presoldered 3-m long lead wires. The resistance and gage factor of this gage were 120.4 ohms and 2.13, respectively.

PIPE BACKFILLING PROCEDURE

In this study, the PVC test pipes were installed in the field according to the current Ohio Department of Transportation (DOT) stan-

TABLE 1 Basic Properties of Test Pipes

	PVC-1	PVC-2
Average Inside Diameter	448 mm (17.656 inch)	896 mm (35.275 inch)
Average Outside Diameter	502 mm (19.766 inch)	952 mm (37.475 inch)
Wall Area	7.8 mm^2/mm (0.3066 $in.^2/in.$)	14.4 mm^2/mm (0.5676 $in.^2/in.$)
Moment of Inertia	464 mm^4/mm (0.0283 $in.^4/in.$)	17190 mm^4/mm (0.1049 $in.^4/in.$)
Minimum Pipe Stiffness	413.7 KN/m/m (60 lbf/in/in)	317.17 KN/m/m (46 lbf/in/in)

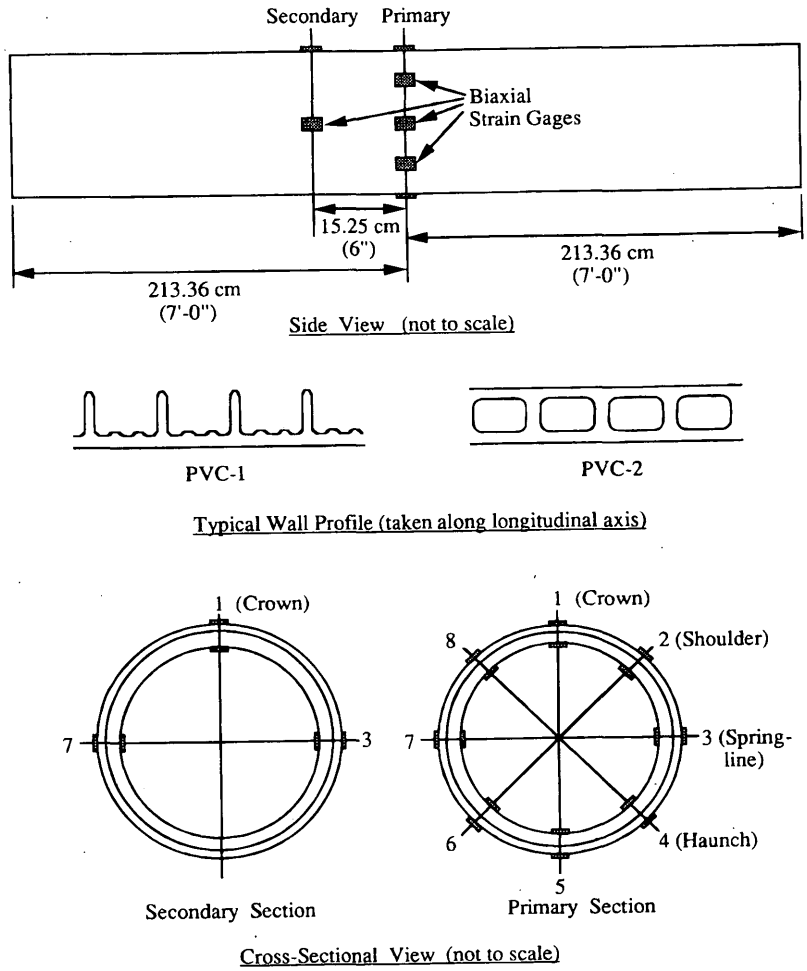

FIGURE 1 Typical wall profile and strain gage instrumentation plan for PVC-1 and PVC-2.

dard practices and subjected to loading incrementally by utilizing an unique load frame facility. This load frame facility, shown in Figure 2, was designed by the Center for Geotechnical and Environmental Research (CGER), Ohio University. It consists of two major components—two high capacity hydraulic cylinders and a structural frame anchored deeply into bedrock. The facility is somewhat similar to the loading system often used when load tests are performed on pile foundations. Instead of selecting a dead weight, a total of eight tension rock anchors were installed to supply large uplifting capacity. Four concrete columns, spaced 7.622 m (25 ft) center-to-center, rest directly on top of a shaley bedrock. They function as a support for the structural I-beam frame. The two hydraulic

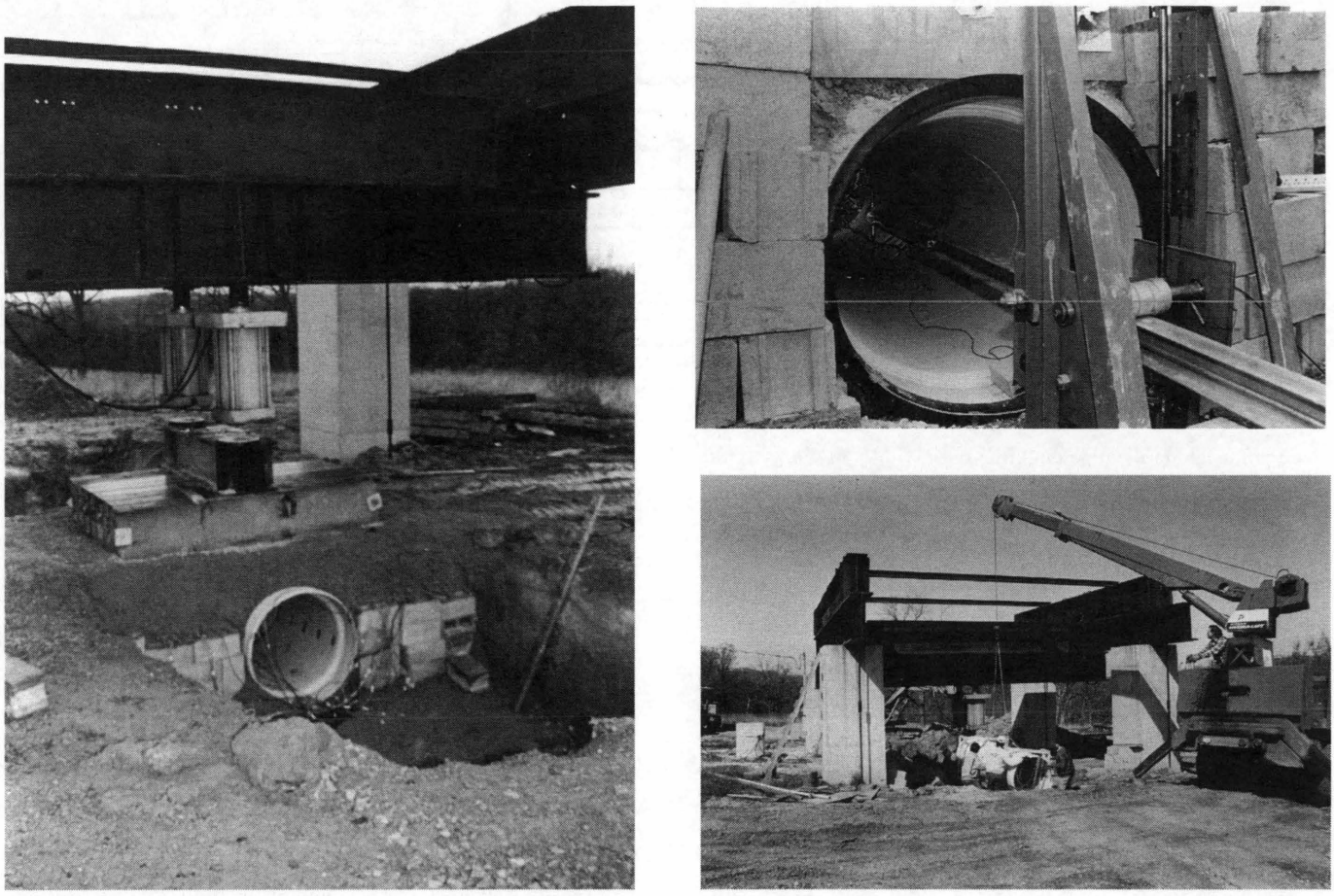

FIGURE 2 Load frame facility and LVDT deflection measurement system.

cylinders were connected to a hydraulic power supply/control unit for synchronized operation.

Installation procedures for the two pipes were basically the same. First, a trench of approximately 7.622 m (25 ft) length and 3.658 m (12 ft) width was excavated by backhoe under the load frame facility. The depth of the trench was extended down to the top of bedrock so that no soft soil layer might support the test pipe. A bedding layer of suitable thickness was formed by spreading and compacting in lifts crushed limestone material meeting the Ohio DOT no. 310 subbase material specifications. Actual bedding layer thickness was 508 mm (20 in.) for PVC-1 and 914.4 mm (36 in.) for PVC-2. Initial laboratory gradation test results (in terms of percent finer in mass) on the backfill soil, Table 2, were 100 percent on a 2.5-in. sieve, 100 percent on a 1.0-in. sieve, 25.5 percent on a no. 4 sieve, 5.5 percent on a no. 40 sieve, and 2.7 percent on a no. 200 sieve. The test pipe was carefully set over the bedding under the hydraulic cylinders. Then, the pipe backfilling work commenced by placing the Ohio DOT no. 310 material with a vibrating plate compactor. Lift thickness was usually 254 mm (10 in.) or less when compacted. It was controlled so that the top of lifts would coincide with the springline and crown elevations. The backfill height was extended 610 mm (24 in.) and 305 mm (12 in.) beyond the pipe crown for PVC-1 and PVC-2, respectively. This difference in the installation conditions was introduced to examine general influence of burial depth on the pipe performance and reliability of some of the existing analytical methods. During backfilling, moisture content and dry density of each lift were recorded. The average moisture content and compaction rate were 5.1 percent and 90.8 percent for PVC-1 and 5.3 percent and 91.9 percent for PVC-2, respectively. Efforts were made manually to place the backfill soil densely in the haunch areas.

Once the backfilling was completed, a welded I-beam loading platform was positioned at the top of the pipe/soil system. This platform covered a contact surface area of 1.83 m (6 ft) width by 2.744 m (9 ft) length. The platform placement applied a surface pressure of about 6.89 kPa (1 lb/in.^{2}).

LOAD TEST PROCEDURES

Typical test set-up included a specially designed LVDT/stepper motor system and the biaxial strain gages all connected to computerized data acquisition units and soil pressure cells and a settlement profile-meter read by a readout box. Each pressure cell was embedded within a thick lens of fine sand to prevent bridging effect problem. Cross-sectional deformation of the pipe at the instrumented section was monitored with a specially designed LVDT driven by a stepper motor. This LVDT/stepper unit was secured on an aluminum I-beam section and suspended in air into the center of the pipe through a holding stand (see Figure 2). The advantage of this LVDT unit was that it provided deformation of the pipe at 72 or

TABLE 2 Gradation Data on Backfill Soil

U.S. Sieve No.	Sieve Size (mm)	Percent Finer in Mass (%)	
		Ohio D.O.T. Requirement	Typical Lab Data
2.5 inch	63	100	100
1.0 inch	25	70-100	100
4	4.75	25-100	25.5
40	0.425	5-50	5.5
200	0.075	0-10	2.7

more points along the pipe circumference within 30 sec. A settlement profile-meter (GEOKON Model 4651) probe was attached onto the loading platform to monitor settlement of the platform during the pipe loading test.

After backfilling and placement of the loading platform, a load test was initiated by pressurizing the two hydraulic cylinders. The hydraulic pressure was increased typically in 1379 kPa (200 lb/in.^{2}) increments. This translates to an increase of 54.47 kPa (7.9 lb/in.^{2}) per increment in the intensity of the surface pressure applied, based on the number of hydraulic cylinders (= 2) used, the bore size inside each cylinder (= 355.6 mm = 14 in. in diameter), and the surface area covered by the loading platform (= 1.83 m by 2.74 m = 6 ft by 9 ft). Duration of each load increment was 15 min, during which three sets of readings were taken simultaneously from all the sensors every 5 min.

TEST DATA ANALYSIS

Output voltage readings from the strain gages were transformed to corresponding level of strains. Then, the bending moment (M) and thrust (P) across the pipe wall were computed through the strain readings obtained from two biaxial gages located distances C_1 (positive) and C_2 (negative) away from the neutral axis of the pipe wall:

$$M = \frac{E}{1-\mu^2}\left(\frac{I}{C_1 + C_2}\right)\left[\left(\varepsilon_{C_2} - \varepsilon_{C_1}\right) + \mu\left(\varepsilon_{L_2} - \varepsilon_{L_1}\right)\right] \quad (1)$$

$$P = \frac{E}{1-\mu^2}\left(\frac{A}{C_1 + C_2}\right)\left[C_2\left(\varepsilon_{C_1} + \mu\varepsilon_{L_1}\right) + C_1\left(\varepsilon_{C_2} - \mu\varepsilon_{L_2}\right)\right] \quad (2)$$

where

E = Young's modulus of pipe material;
μ = Poisson's ratio of pipe material;
I = moment of inertia of pipe wall per unit length;
ε_C = circumferential strain in pipe wall;
ε_L = longitudinal strain in pipe wall;
A = cross-sectional area of pipe wall per unit length.

Here, sign conventions of Timoshenko are used consistently. In other words, bending moment is positive if its action tends to deflect the beam concave upward. Thrust is positive if it is in tension.

ANALYTICAL METHODS APPLIED

Analytical tools applied to analyze the two PVC pipes were modified Iowa formula and elastic solutions of Burns and Richard (*4*). Iowa formula has been used widely by engineers and researchers. The elastic solutions mentioned above have received little attention since publication in 1964. These solutions are available as Level 1 Solution in CANDE (Culvert ANalysis and DEsign)-89 finite element computer code.

The Iowa formula was originally established by Spangler (*5*) on the basis of elastic ring theory and fill-load hypothesis he reached after testing numerous flexible steel culverts. The formula was later modified by Watkins and Spangler (*6*) through a similitude study to the current form of:

$$\frac{\Delta\chi}{d}(\%) = \frac{100 \cdot D_L \cdot K \cdot P}{0.149(PS_o) + 0.061(E')} \quad (3)$$

TABLE 3 Summary of Backfill Data

	PVC-1			PVC-2		
	Thickness (mm)	Moisture Content (%)	Percent Compaction (%)	Thickness (mm)	Moisture Content (%)	Percent Compaction (%)
Bedding	457	5.3	75.0	229	6.0	86.4
Layer 1	229	4.5	100.0	254	5.0	96.1
Layer 2	229	5.0	93.8	254	4.5	94.5
Layer 3	203	5.3	92.2	254	4.2	87.0
Layer 4	203	5.3	92.2	254	4.6	89.0
Layer 5	203	4.9	91.4	305	7.2	98.4

where

Δ/d = horizontal deflection (percent);
D_L = deflection lag factor;
K = bedding constant;
P = pressure on pipe;
PS_o = pipe stiffness;
E' = modulus of soil reaction.

The above equation may be also applied to evaluate the vertical deflection on the assumption (Uni-Bell PVC Pipe Association) (*7*) that the pipe deforms equally in both horizontal and vertical directions.

More rigorous theoretical solutions were formulated by Burns and Richard (*4*) for an elastic circular ring deeply buried in an infinite elastic soil material. They applied extensional shell theories to the pipe and Mitchell's stress function to the elastic soil medium. First, they assumed that radial displacements are continuous at the pipe/soil interface. Under the full-slip condition, zero shear stress exists at the pipe/soil interface, whereas equality exists at the interface between tangential displacement of the pipe and tangential displacement of the soil medium under the no-slip conditions. Solutions for the two conditions are summarized as follows:

Full-Slip Condition

$$W = \frac{P_v R}{2M_S}\left[UF(1-a_0) - \frac{2}{3}VF(1+3a_2-4b_2)\cos 2\theta\right]$$
$$N = P_v R\left[B(1-a_0) + \frac{C}{3}(1+3a_2-4b_2)\cos 2\theta\right] \quad (4)$$
$$M = P_v R^2\left[\frac{CUF}{6VF}(1-a_0) + \frac{C}{3}(1+3a_2-4b_2)\cos 2\theta\right]$$

No-Slip Condition

$$W = \frac{P_v R}{2M_S}\left[UF(1-a_0) - VF(1-a_2-2b_2)\cos 2\theta\right]$$
$$N = P_v R\left[B(1-a_0) + C(1+a_2)\cos 2\theta\right] \quad (5)$$
$$M = P_v R^2\left[\frac{CUF}{6VF}(1-a_0) + \frac{C}{2}(1-a_2-2b_2)\cos 2\theta\right]$$

where

P_v = pressure applied at top and bottom boundaries;
R = radius of pipe;
M_s = confined soil modulus; and
θ = counterclockwise angle taken from right springline.

Definitions of the other terms, such as UF and VF, are listed below.

$$B = 0.5(1+K) = \frac{1}{2(1-\nu)}$$
$$C = 0.5(1-K) = \frac{1-2\nu}{2(1-\nu)}$$
$$UF = \frac{2BM_S R}{EA} = (1+K)\frac{M_S R}{EA} \quad (6)$$
$$VF = \frac{2CM_S R^3}{6EI} = (1-K)\frac{M_S R^3}{6EI}$$
$$a_0 = \frac{UF-1}{UF+(B/C)}$$

for both no-slip and full-slip

$$a_2 = \frac{C(1-UF)VF - (C/B)UF + 2B}{(1+B)VF + C(VF+1/B)UF + 2(1+C)}$$

for no-slip

$$a_2 = \frac{(2VF-1+1/B)}{(2VF-1+3/B)}$$

for full-slip

$$b_2 = \frac{(B+CUF)VF - 2B}{(1+B)VF + C(VF+1/B)UF + 2(1+C)}$$

for no-slip

$$b_2 = \frac{2VF-1}{2VF-1+3/B}$$

for full-slip

Hoeg (*8*) also developed his elastic solution for deflection (W) of a pipe placed in an infinite elastic media, along with performing some experiments in a test bin. He used a similar model, but he did not impose any specific ratio for the horizontal vertical loads. His solutions are useful only for uncorrugated pipes, since the moment of inertia is being computed based on the pipe wall thickness. Galili and Shmulevich (*9*) conducted an extensive experimental study of flexible to semirigid pipes in a laboratory soil-box and compared the results to the elastic solutions of Burns and Richard (*4*) and of Hoeg. Here, flexible pipes are defined with $S < 0.005$. Pipes with midrange stiffness are characterized with $0.005 < S < 0.5$. S is a pipe/soil stiffness ratio expressed in terms of $EI/(M_S r^3)$ where M_S is a confined one-dimensional modulus and r is the pipe radius. Their outcome indicated that the elastic solutions agree relatively well with the experimental for flexible to midrange stiffness pipes.

DISCUSSION OF RESULTS

The backfilling and load test was conducted on June 5 and 6, 1992, for PVC-1 and on April 29 and 30, 1992, for PVC-2. During backfilling the pipe diameter in the vertical direction increased by 0.2 percent for PVC-1 and by 0.11 percent for PVC-2. This indicates that the backfilling operation induced relatively insignificant structural responses in the pipes.

Upon application of increased loading, the pipes did not respond instantaneously; it generally took several minutes for the effects of the loading to be felt within the pipe/soil system. Once the load influence appeared, the pipe response stabilized quickly. This was due to the use of a stiff, granular backfill material. The test results presented in this section represent for each load increment the final stabilized pipe response. Figure 3, *a* and *b*, presents horizontal and vertical deflections measured during the load test for the two test pipes. A vertical deflection of 7.5 percent was reached under surface pressure of 245.46 kPa (35.6 lb/in.^{2}) for PVC-1 and under surface pressure of 382 kPa (55.4 lb/in.^{2}) for PVC-2. These surface pressure intensities correspond to at least 13.1 and 20.4 m (43 and 67 ft) of depth for PVC-1 and PVC-2, respectively, using an average backfill density of 1.92 g/cm^3 (120 lb/ft^3). These plots also indicate deflections computed from the modified Iowa formula and the elastic solutions of Burns and Richard (*4*). Parametric values used for the modified Iowa formula were:

PS_o = 413.7 kPa (60 lb/in.^{2}); E' = 20.68 MPa (3,000 lb/in.^{2}); D_L = 1.0; K = 0.11 for PVC-1
PS_o = 317.17 kPa (46 lb/in.^{2}; E' = 20.68 MPa (3,000 lb/in.^{2}); D_L = 1.0; K = 0.11 for PVC-2.

The E′ value of 20.68 MPa (3,000 lb/in.^{2}) was selected according to the study by Howard (*10*) as a standard value for relatively well compacted crushed rock material. The K value of 0.11 was recommended by Moser (*11*) and Uni-Bell Pipe Association (*7*), which corresponded to a nearly unhaunched condition. For the elastic solutions, the following input values were utilized:

E = 2.758 GPa (400,000 lb/in.^{2}); u = 0.30 for PVC-1 and PVC-2
M_s = 13.79 MPa (2,000 lb/in.^{2}); u_s = 0.25;
K = 0.333 for backfill soil.

Based on the experimental plots of surface pressure vs. horizontal deflection, the initial E' value of the backfill soil may be back calculated to be about 6.205 MPa (900 lb/in.^{2}) for PVC-1 and about 16.62 MPa (2,410 lb/in.^{2}) for PVC-2. This indicates that the backfill soil was somewhat less stiff around PVC-1, contrary to the data presented in Table 3. The backfill soil, which contained aggregates as large as 25 mm in diameter, could not be compacted effectively in the zone immediately next to PVC-1 due to the presence of narrowly spaced ribs. The field density tests for the backfill were typically performed about 0.6 m (2 ft) away from each test pipe. So, the backfill data presented in Table 3 may not be representing the actual conditions that existed immediately next to PVC-1. Magnitude of the vertical deflection remained at 1.2 to 1.3 times the horizontal deflection for PVC-1, whereas this deflection ratio decreased from 2.5 to 1.1 for PVC-2 as the surface pressure was increased. This contrasts with vertical to horizontal deflection ratio assumed to be 1.0 for the modified Iowa formula. The elastic solutions produced ratios of 1.28 for no-slip condition and 1.23 for full-slip condition between the vertical and horizontal deflections. Progressive stages of actual deformed shape of PVC-1 recorded during the load test is shown in Figure 4. The pipe deformed nearly symmetrically.

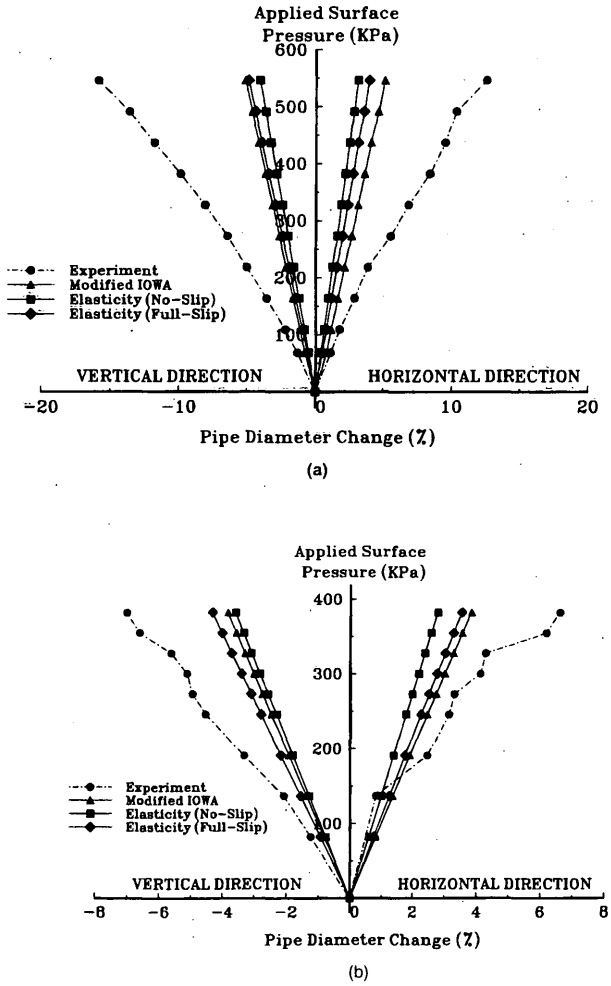

FIGURE 3 Deflection of PVC-1 (*a*) and PVC-2 (*b*) pipe during field load test.

Review of bending moment and thrust around the pipe circumference can indicate the overall response of the pipes to the load for both pipes. The moment responses of the pipes were consistent with the basic principles of engineering mechanics. Positive moment was measured at the crown and the invert, whereas the springline regions experienced negative moment. The magnitudes of moment were more pronounced for PVC-2. Thrust remained entirely compressive in the wall of both pipes, except for the haunch regions where increasing surface pressure induced extensional thrust of small magnitudes. Comparisons between experimental results and elastic solutions for bending moment and thrust at crown and springlines are made in Figures 5 through 12. For PVC-1 the bending moments were relatively close, both at the crown and at the springlines. For PVC-2, agreement between the theory (full-slip) and the experimental was good at the crown. But, at the springlines the theoretical moments were much less than the experimental. General agreement for thrust was somewhat less satisfactory between the experimental and the theoretical. Overall, these plots indicate that for pipe deflections and bending moment level of agreement between the experimental values and elastic solutions was better for PVC-1, the pipe under deeper soil cover. And, between the no-slip and full-slip solutions, the latter predicted values closer to the experimental results. Hoeg stated that the boundary conditions assumed in his elastic analysis are not very severe if the loaded boundaries are at last one pipe diameter away from the pipe wall. The ratio of the soil cover over the nominal pipe diameter was 1.333 for PVC-1 and 0.333 for PVC-2. This may explain the less satisfactory agreement observed for PVC-2 between the experimental and theoretical results. Also, the interface friction angle between the smooth PVC pipe surface and the backfill soil should be relatively small.

During the load test PVC-1 continued to deflect without developing wall crushing or buckling. This pipe reversed its curvature slightly in the crown region during the last load increment (surface pressure 546 kPa = 79.2 lb/in.^{2}, equivalent fill height 29 m = 95 ft or more, vertical deflection 17 percent). Upon removal of the pipe after the test, close examination revealed no physical damage to the pipe wall and ribs. On the contrary, PVC-2 experienced structural failure under the surface pressure of 436.45 kPa (63.3 lb/in.^{2}) through seam failure and longitudinal cracking which was concentrated in the springline regions. This surface pressure is equivalent to more than 23.2 m (76 ft) of cover over the pipe. The pipes are shown in Figure 13.

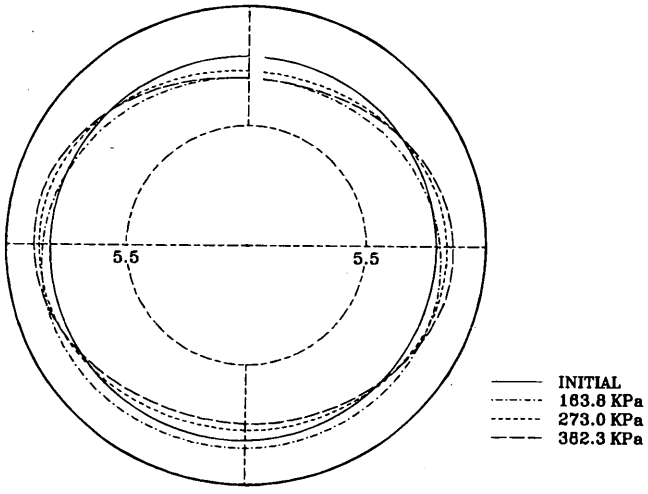

FIGURE 4 Deflected shape of PVC-1 during field load test.

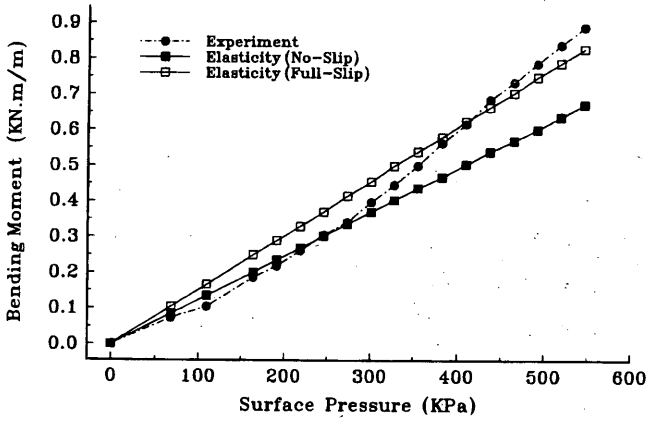

FIGURE 5 Comparison between experimental and theoretical bending moment at crown section for PVC-1 pipe.

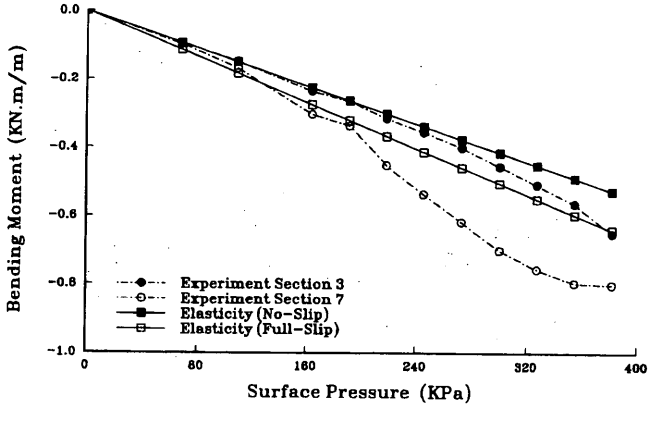

FIGURE 6 Comparison between experimental and theoretical bending moment at springline section for PVC-1 pipe.

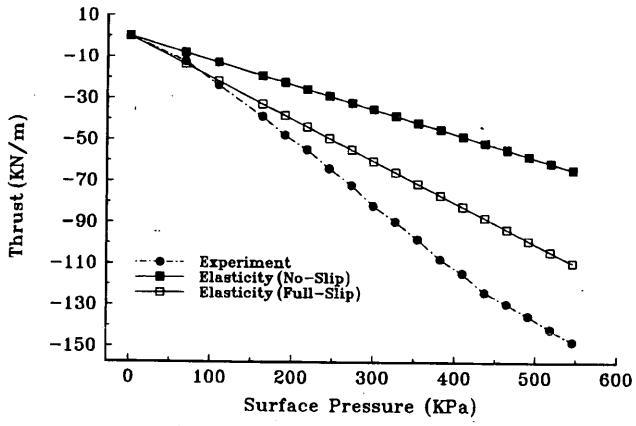

FIGURE 7 Comparison between experimental and theoretical thrust at crown section for PVC-1 pipe.

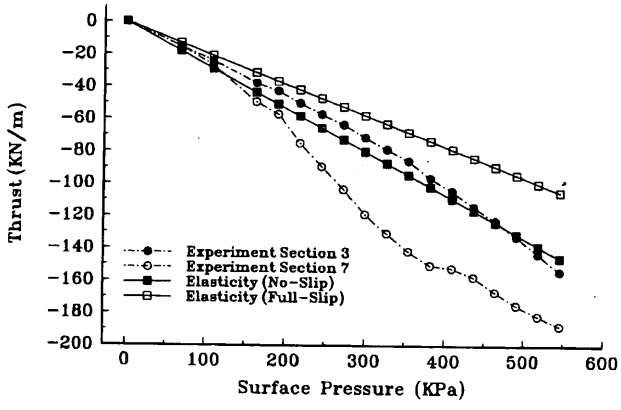

FIGURE 8 Comparison between experimental and theoretical thrust at springline section for PVC-1 pipe.

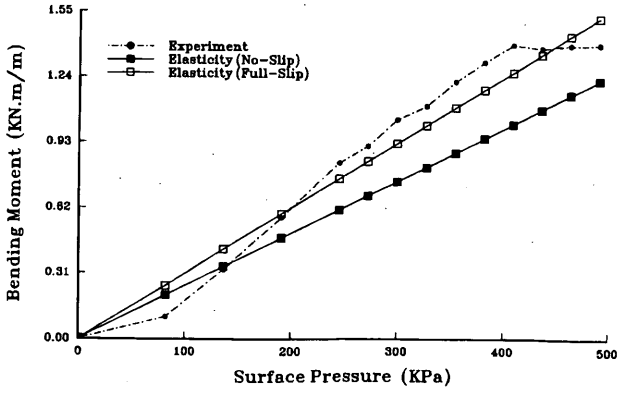

FIGURE 9 Comparison between experimental and theoretical bending moment at crown section for PVC-2 pipe.

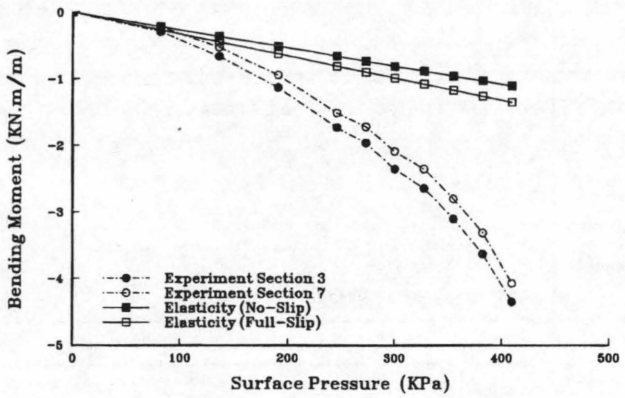

FIGURE 10 Comparison between experimental and theoretical bending moment at springline section for PVC-2 pipe.

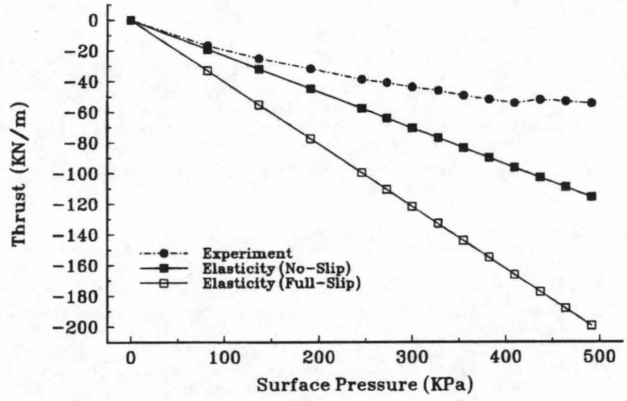

FIGURE 11 Comparison between experimental and theoretical thrust at crown section for PVC-2 pipe.

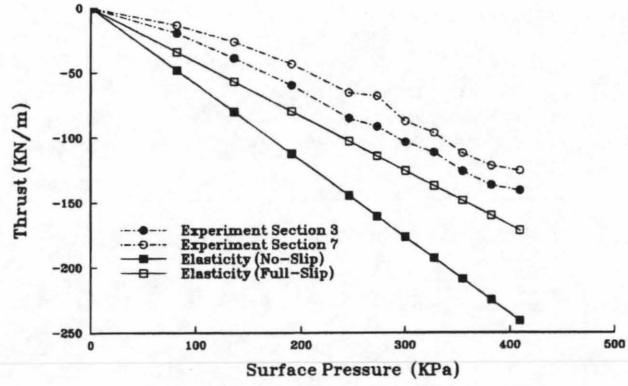

FIGURE 12 Comparison between experimental and theoretical thrust at springline section for PVC-2 pipe.

CONCLUSIONS

Two PVC pipes of diameter 457 mm and 914 mm (18 in. and 36 in.) were instrumented, buried in a stiff backfill soil, and subjected to large loads. An unique, large-scale, load frame facility was utilized to conduct the pipe tests. The loading conditions simulated in this study reflected possibly the worst loading conditions that these pipes can experience during service. These pipes are rarely installed under shallow cover conditions and are seldom subjected to extremely large surface loading. Extremely large surface loading applied only a few feet above the pipe does not allow any development of significant level of soil arching. The profile design differed significantly between the two pipes. The 457-mm (18-in.) diameter pipe (PVC-1) was seamless, solid-walled, and ribbed outside. The 914-mm (36-in.) diameter pipe (PVC-2) had seams running spiral along the length, with its wall section hollowed in the core. The final soil cover was 610 mm (24 in.) for PVC-1 and 305 mm (12 in.) for PVC-2. Both pipes performed satisfactorily during the backfilling, and the field load tests demonstrated that they could both carry substantial loading. Under applied surface pressure, PVC-1 continued to deform without showing any structural distress. Very slight reversal of curvature was observed in the crown region at 17 percent change in vertical diameter. PVC-2 deformed less under the same load. However, its load carrying capacity was limited by seam strength. Deflections predicted by the modified Iowa formula were slightly larger than the deflections obtained from the full-slip elastic solutions of Burns and Richard (*4*). For both pipes, the experimental deflections were larger than those resulted from both analytical methods. The elastic solutions (full-slip) agreed reasonably well

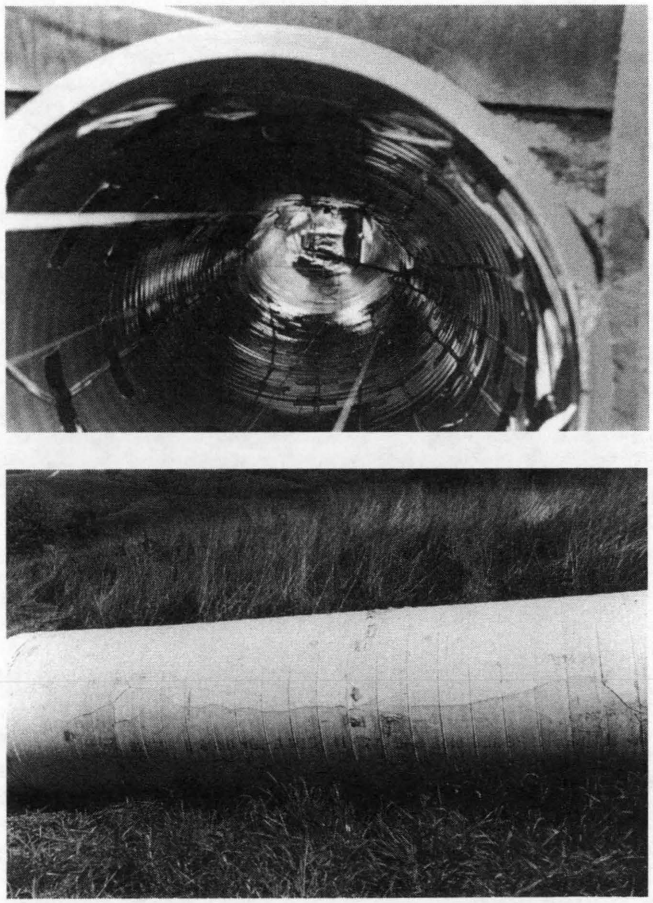

FIGURE 13 Test pipes during and after load test: (*top*) cross-section, PVC-1 (under surface pressure of 546 kPa); (*bottom*) side view, PVC-2 after load test.

with the experimental bending moment results for PVC-1, the pipe under more than one pipe diameter thick soil cover. These findings indicate that the elastic solutions are valuable for analyzing flexible circular pipes buried in a homogeneous soil with loaded boundary more than one diameter away.

REFERENCES

1. Adams, D. N., M. T. Muindi, and E. T. Selig. *Performance of High Density Polyethylene Pipe Under High Fill.* Geotechnical Report No. ADS88-351F, Department of Civil Engineering, University of Massachusetts, Amherst, April 1988.
2. Katona, M. G. *Minimum Cover Heights for HDPE Corrugated Plastic Pipe Under Vehicular Loading.* Report to Corrugated Plastic Tubing Association, November 1988.
3. Culley, R. W. *Structural Tests on Large Diameter Polyethylene Culvert Pipe.* Technical Report 31, Saskatchewan Department of Highways and Transportation, February 1982.
4. Burns, J. Q., and R. M. Richard. Attenuation of Stresses for Buried Cylinders. *Proc., Symposium on Soil-Structure Interaction,* Engineering Research Laboratory, University of Arizona, September 1964, pp. 378–392.
5. Spangler, M. G. *The Structural Design of Flexible Pipe Culverts.* The Iowa State College Bulletin, Vol. XL, No. 30, Iowa Engineering Experiment Station, Ames, Iowa, December 1941, 84 pp.
6. Watkins, R. K., and M. G. Spangler. Some Characteristics of the Modulus of Passive Resistance of Soil—A Study in Similitude. *HRB Proc.*, Vol. 37, 1958, pp. 576–583.
7. *Handbook of PVC Pipe—Design and Construction*, 2nd Ed., Uni-Bell Plastic Pipe Association, 1982, 377 pp.
8. Hoeg, K. Stresses Against Underground Structural Cylinders. *Journal of the Soil Mechanics and Foundations Division, American Society of Civil Engineers*, Vol. 94, No. SM4, July 1968, pp. 833–858.
9. Galili, N., and I. Shmulevich. A Refined Elastic Model for Soil-Pipe Interaction. *Proc., International Conference on Underground Plastic Pipe*, sponsored by the Pipeline Division of the American Society of Civil Engineers, New Orleans, La., 1981, pp. 213–226.
10. Howard, A. K. Modulus of Soil Reaction Values for Buried Flexible Pipe. *Journal of the Geotechnical Engineering Division, the American Society of Civil Engineers*, Vol. 103, No. GT, January 1977, pp. 33–43.
11. Moser, A.P. *Buried Pipe Design.* McGraw-Hill, Inc., New York, 1990, 219 pp.

Publication of this report sponsored by Committee on Culverts and Hydraulic Structures.

Uplift Failures of Corrugated Metal Pipe

R. A. LOHNES, F. W. KLAIBER, AND T. A. AUSTIN

Surveys of county engineers in Iowa revealed that between 1970 and 1975 and between 1983 and 1988 corrugated metal pipe (CMP) uplift failures occurred at a rate of six per year. A similar survey of North American Departments of Transportation (DOTs) revealed only nine failures between 1987 and 1992. All failures involved pipes with diameters greater than 1.83 m. Fifty percent of the agencies responding to the second survey indicated they had standards for end restraint. About 6 percent of the agencies avoid uplift problems by not using corrugated metal pipe and about 12 percent of the agencies limit the diameters of CMP. Eight agencies provided data that allowed calculation of end restraint force as a function of pipe diameter. The forces provided by the end restraints range from about 50 to 300 kN for a pipe 2 m in diameter. A simplistic and very conservative analysis that treats the CMP as a beam was conducted as a basis for comparison. Six standards recommend forces lower than the analysis whereas three agencies actually recommend resisting forces greater than that provided by the analysis. Two CMPs that failed in uplift were analyzed and the apparent force that caused failure was back calculated. For one pipe that had no tie-down, the calculated failure force was below all of the standards; however the presence of a cutoff indicates that cutoffs by themselves are not effective countermeasures to uplift. In the second case history where end restraint was provided, the calculated failure force was greater than that required by six of the nine agency specifications.

Corrugated metal pipe (CMP) culverts are important components of the drainage systems of the country's transportation system. In Iowa, many county engineers have used large diameter flexible pipe culverts to replace small bridges and have realized significant savings; however, in some situations, CMPs have failed as a result of longitudinal uplift. The objectives of this study are to (1) determine the scope of the problem within Iowa and in North America, (2) identify a unique set of pipe configurations that might be more conducive to uplift, and (3) identify types of tie-downs currently being used to resist uplift and synthesize the resisting forces provided by the structures.

PREVIOUS STUDIES

Only one publication was found that documented uplift failures of CMP (*1*). In that report, buoyancy was assumed to be the cause the uplift with no consideration given to the dissipation of pore pressures through seepage. The analysis for a 2.44-m diameter pipe beneath a soil slope of 2.5 to 1 resulted in a moment of 404 kN.m.

The FHWA issued Notice N 5040.3 dated April 26, 1974 (D.C. Coy, personal communication). This notice recommended all pipe culverts with diameters 1.22 m and larger be provided with end protection and was accompanied by design standards for culverts up to 4.57 m in diameter.

The first assessment of CMP uplift problems in Iowa occurred in 1975 when the Iowa Department of Transportation (DOT) surveyed county engineers requesting information on uplift problems within the previous 5-year period (*2*). The questionnaire made no distinction between flotation and folding failures of beveled or step beveled ends. Fifty of Iowa's 99 counties responded and the responses are shown in Table 1. Thirty failures occurred in 8 counties with only 5 percent of pipes with diameters less than 2.43 m diameter having problems; however 16 to 18 percent of pipes with diameters greater than 3.07 m had problems. These data motivated the Iowa DOT in February 1976 to issue a letter to all county engineers urging them to anchor or reinforce inlet ends of unprotected flexible pipe.

Not withstanding these warnings from FHWA and Iowa DOT, CMP uplift failures continued to be reported in Iowa. Concern that current design and/or construction practices are inadequate lead to this study.

SURVEYS TO DETERMINE THE SCOPE OF CMP UPLIFT PROBLEMS

Survey of Iowa Counties 1983 to 1988

A survey of Iowa county engineers in 1988 revealed that 31 CMP had failed by uplift in the previous five years. It was hypothesized that it might be possible to identify a unique set of conditions that resulted in these uplifts. For example, are uplift failures more frequent in skewed and/or projecting conduits where less favorable hydraulic conditions exist at the inlet?

These data indicate that 12 percent of 68 counties who responded to the questionnaire reported CMP failures. This compares to 16 percent of responding counties in the 1975 survey. Table 2 summarizes the range of culvert sizes involved in uplift failures. All uplift failures were associated with pipes 1.83 m in diameter or more. In one instance, the pipe uplift and subsequent washout caused the death of a motorist.

Table 2 shows the range of culvert sizes involved in the failures and lists less than 31 events because some sizes had more than one failure. The majority of respondents indicated that plugging or partial blocking of inlets by vegetative debris contributed to the uplift failures. Tables 1 and 2 suggest that projecting CMPs are not more likely to experience uplift difficulties. No unique geotechnical or hydrologic conditions were identified as contributing to the failures; however, the problems appear more common in regions of the state where significant elevation drops exist across the culverts. This suggests that the flow through the CMP was inlet-controlled and that in part of the pipe the flow will be shallow, high velocity (supercritical). Under these conditions, with the pipe only partially full, blockage of the inlet would not be necessary because buoyant pore water forces outside the pipe could be greater than the resisting weight of the water in the pipe.

Of the counties reporting failures, 75 percent indicated that they used some form of tie-down including: piles and cables, concrete curtain walls, concrete slope collars, and sheet piling cut-off walls.

Civil and Construction Engineering Department, Iowa State University, Ames, Iowa 50011.

TABLE 1 Summary of CMP Uplift Failures in Iowa 1970 to 1975

Pipe diameter (m)	Number of structures		Number of failures	
	Projecting	Beveled	Projecting	Beveled
1.52 to 2.44	226	166	2	11
2.46 to 3.05	19	46	1	5
>3.07	11	53	2	9

TABLE 2 Summary of CMP Uplift Failures in Iowa 1983 to 1988

Diameter (m)	length (m)	Inlet geometry*
1.83	76.8	unknown
1.98	32.9	beveled
2.29	36.6	projecting
2.59	16.5	beveled
2.74	18.9	unknown
2.74	21.3	beveled
3.25 x 2.11**	38.1	beveled
3.35	44.5	projecting
3.51	36.6	beveled
3.66	21.9	projecting
4.54 x 2.92**	46.3	beveled
4.52 x 2.92**	unknown	beveled
4.57	36.5	unknown
5.18	36.5	unknown
9.78 x 5.85**	79.2	unknown

** elliptical arch pipe
*Projecting inlets are CMP with square ends; beveled inlets are CMP with ends parallel to the embankment.

Survey of North America 1987 to 1992

Uplift problems

In order to define the uplift problem on a wider geographic scale and to identify the types of end restraints being used, Iowa DOT with Iowa State University sent questionnaires to the DOTs in each of the 50 states, Washington, D.C., Puerto Rico, and the eight provinces of Canada, requesting information on the use of restraints and any uplift problems encountered between 1987 and 1992.

Fifty-two of 60 agencies queried responded to the questionnaires. Of those responding, 9 (17 percent) agencies reported uplift problems in the previous 5 years, and 26 of the 52 report incorporating some type of an uplift restraint. Eighteen of those 26 agencies developed the restraints in response to earlier problems. Table 3 summarizes data from seven of the reported uplift problems. Two agencies that experienced uplift problems provided no specific data on the nature of their problems. In all cases, except one, the pipes were circular with diameters ranging from 0.91 to 2.90 m. For the agencies who reported soil cover depths, the cover ranged from 1.5 to 3 m with the deepest cover of 3.05 m over the largest diameter pipe (2.90 m) reported by Agency 6. All problematic pipes had projecting inlets except for one step beveled inlet and one beveled inlet. Table 3 suggests that skew is not an essential contributor to uplift. In all cases, the damaged pipes were replaced with new CMP and in most situations end restraint was added.

TABLE 3 Summary of CMP Uplift Failures, United States and Canada 1987 to 1992

Agency	Diameter or span/rise (m)	Length (m)	Skew (deg)	Cover depth (m)
1	4.5/2.7	nd	nd	nd
2	1.82	nd	90	1.52
	2.44	nd	90	2.44
3	1.52	5.8	nd	nd
4	0.91	12.2	10	(very little)
5	1.52	nd	nd	1.52
6	2.90	50	30	3.04
7	2.44	27.4	0	1.83

"nd" indicates that no data are given.

Types of End Restraints

Twenty-two agencies provided copies of their design standards for end restraints. The variety of end restraints can be classified as anchors, head walls, wing walls, and slope collars. Figure 1 shows schematic drawings of each type of end restraint.

Anchors consist of vertical concrete walls with considerable mass of concrete below ground, perpendicular to the axis of the pipe, that extend to midheight of the culvert. Bolts connect the concrete to the pipe. The pipe ends are beveled above the top of the concrete. In some situations, cutoff walls extend below the concrete anchors.

Head walls are vertical concrete walls, perpendicular to the axis of the pipe, that extend above the top of square ended pipe. Wing walls are similar to head walls but incorporate vertical walls on both sides at an angle to the axis of the pipe. The angled wing walls serve to direct flow into the pipe, prevent erosion or piping adjacent to the inlet, and add mass to resist uplift.

Slope collars may be either concrete or metal. The collars surround the culvert inlet, perpendicular to the pipe axis, and are parallel to soil slope of the embankment above the culvert.

Three agencies avoid CMP uplift problems by not using CMP. Six other agencies limit the maximum diameter of CMP, with the maximum diameters ranging from 1.37 to 2.13 m, thereby reducing the probability of uplift failure.

Anchor walls are used by eight agencies, headwalls by six, wing walls by four, concrete slope collars by five, and metal slope collars by three. One agency uses anchor walls for CMP less than 1.22 m in diameter and either slope collars or wing walls for pipe larger than 1.22 m in diameter. A northern agency uses anchor walls on pipes 0.30 to 1.37 m in diameter with the latter as the maximum diameter CMP they will use. An agency from eastern United States recommends wing walls on CMP between 0.91 and 1.83 m diameter and headwalls as an option on pipes less than 1.22 m in diameter. The maximum diameter CMP that this state uses is 1.83 m. One north-central agency uses a system of longitudinal stiffeners. The variety of end restraints used suggests that in many cases the standards are based on experience and not on theoretical analyses or results of load tests.

Analysis of Resistance to Uplift

In order to compare the resisting forces of the various end restraints, an analysis was conducted in which the pipe was treated as a simple beam. The details of the analysis can be found elsewhere (*3*) but

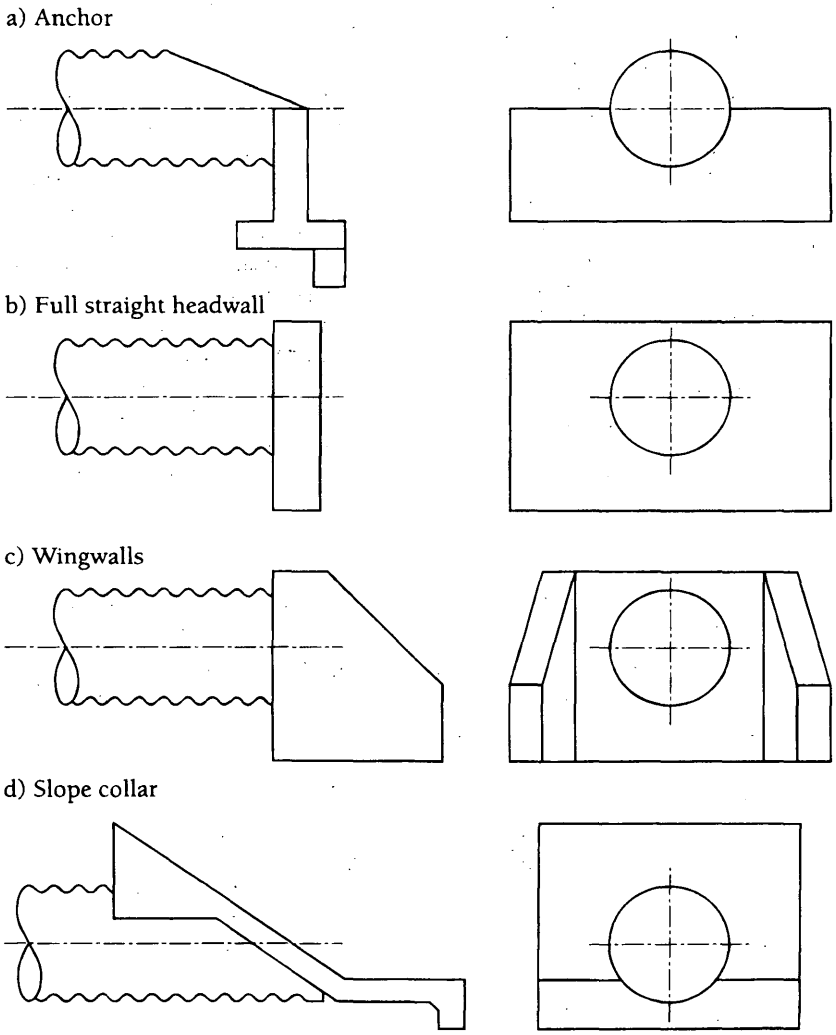

FIGURE 1 Types of headwalls described by agencies responding to survey.

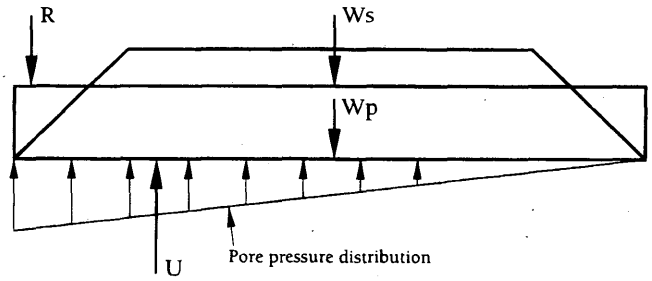

FIGURE 2 Schematic of CMP showing pore water pressure distribution and resultant forces for simplified analysis.

an overview of the results is summarized here. The uplift was assumed to result from a linear distribution of pore pressure with the maximum head equal to the pipe diameter at the inlet and a minimum head of zero at the outlet as shown in Figure 2. The pipe was conservatively considered to be plugged at the upstream end. The stiffness of the pipe and shearing resistance of the adjacent and overlying soil was neglected; thus, the only resistance to uplift was provided by the weight of the pipe and the overlying soil. The soil unit weight was assumed to be 18.85 kN/m^3, roadway width 10 m shoulder to shoulder, and the embankment slope extending from the bottom of the culvert to the edge of the shoulder at a slope of 1 vertical to 2 horizontal. Cover above the pipe was taken as 610 mm; the pipe is not beveled. With these constraints, the pipe length and embankment height increases with increasing pipe diameters.

The forces used in the analyses are shown in Figure 2 where W_s is the weight of the soil cover, W_p is the weight of pipe, U is the resultant of the pore pressure distribution, and R is the resistance of the tie-down. The soil and pipe weight resultants act through the center of the embankment and the pore water force acts through the centroid of the triangular pore water pressure distribution, which is at a distance of one-third the pipe length measured from the inlet. The required resisting force is calculated from:

$$R = U - W_p - W_s$$

Obviously, this is a very simplified analysis that provides resisting forces that are conservatively high, because it ignores the CMP stiffness and the soil-structure interaction.

Force Comparison of Various Restraints

For each agency's standard, the resisting force of the restraint was computed for a range of pipe diameters and with a soil cover depth of 610 mm. These relationships between the resisting forces and pipe diameters can be classified as either linear or exponential shaped curves and are shown in Figures 3 and 4. In all cases but one, the last point on the curve represents the maximum diameter CMP that the standards allow.

Figure 3 shows resisting force versus pipe diameter for the standards in which the relationship between pipe diameter and resisting force is linear. Also shown is the relationship resulting from the simplistic, conservative analysis (*3*). All of the standards with a linear relationship between force and diameter have much lower forces than those calculated by the rational analysis. The agency with the lowest forces in its standards is also the only one which had an uplift failure when restraint was used.

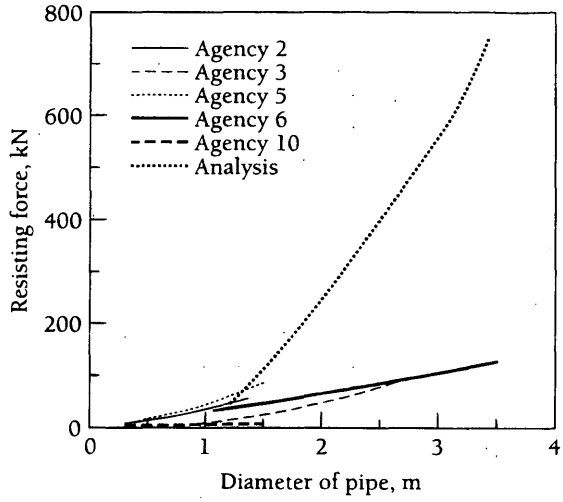

FIGURE 3 Linear relationship between resisting force and pipe diameter from various DOT specifications.

Agency standards that have an exponential relationship between resisting forces and pipe diameters are shown in Figure 4. Although the curve from the simplistic analysis very is conservative, only one standard in this group has lower forces. The other three standards have resisting forces that are equal to or exceed those of the analysis.

This synthesis points out the diversity in resisting forces among these agencies with a 500 percent variation for pipes about 2 m in diameter. It appears some standards may be providing resistance to uplift that is dangerously low whereas others are extremely conservative and may be too restrictive. The force comparison reinforces the interpretation that existing standards are not based on experimental results nor on rigorous theoretical analyses.

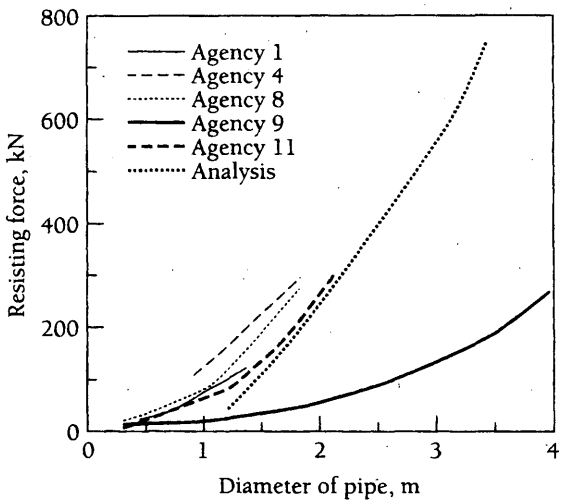

FIGURE 4 Exponential relationship between resisting force and pipe diameter from various DOT specifications for tie-downs.

CASE HISTORIES

As part of the survey of Iowa counties, a few uplift failure sites were identified in which additional data were available for analysis. Two such sites are described here. Unfortunately data on prior rainfall, flooding, and maintenance were not available.

Site 1

This site had a corrugated structural steel plate culvert installed in February 1954 that failed in June 1976. The pipe was circular with a diameter of 3.66 m, a length of 29 m, a beveled inlet 1.5 to 1, and a slope of 3.81 percent. The fill above the pipe was 853 mm deep and the roadway 8.53 m wide with a slope of 8 to 1 at the inlet and 6 to 1 at the outlet. The fill extended to the top of the beveled inlet. No information was found on high water marks or discharge through the pipe during the flow that caused the failure.

The pipe bent at a distance of 7.92 m from the inlet until it was at about the same elevation as the shoulder of the roadway. This type of bending failure is illustrated in the photograph of Figure 5*a*. The pipe bottom collapsed inward beginning at about 6.71 m upstream of the centerline of the road and extended approximately to the centerline. Subsequent to the bending, the road grade washed out, but it was not clear whether water overtopped the road or undermined the pipe to cause the embankment failure. No tie-down structure or cutoff wall was used.

Shear and moment diagrams were constructed from the soil loading. The maximum shear was found to occur at a distance of 8.84 m from the inlet. The bend in the pipe at a distance of 7.92 m occurred close to the point of maximum shear. The moment that must be resisted at 8.84 m is 643 kN.m and could be resisted by a force of 75.2 kN located 305 mm from the inlet. In this case, the calculated resisting force for this 3.66-m diameter pipe falls considerably below the extrapolated resisting forces specified by any of the state or provincial agencies.

Site 2

The CMP at Site 2 was installed in July 1976 and failed in September 1986. The pipe was a structural plate pipe with a diameter of 3.05 m, a length of 36.6 m, a slope of 3.67 percent, and a projecting inlet. The roadway width was 8.53 m with slopes of 2.5 to 1 on both inlet and outlet ends and a depth of soil cover averaging 850 mm. A seepage collar was place 6.1 m downstream from the inlet. A tie-down consisting of two wood piles driven on each side of the pipe with two 76 × 406-mm horizontal wood planks across the top of the CMP and a 13-mm wire rope cable attached to the piles. Figure 5*b* shows a similar tie-down that failed by pulling the piles out of the ground.

At Site 2 no data on high water or discharge were available, but the pipe failed by breaking the planks of the tie-down and stretching the cable. The broken tie-down at Site 2 is shown in Figure 5*c*. The road grade washed out and the culvert was moved 100 m down stream. The bottom of the pipe collapsed inward so there was only about 610 mm of clearance between the top and bottom of the failed pipe.

The force required to break the tie-down was estimated from available data. The flexural strength of the wood plank was assumed to be 49.6 MPa and the moment of inertia calculated to be 57.1 m^4.

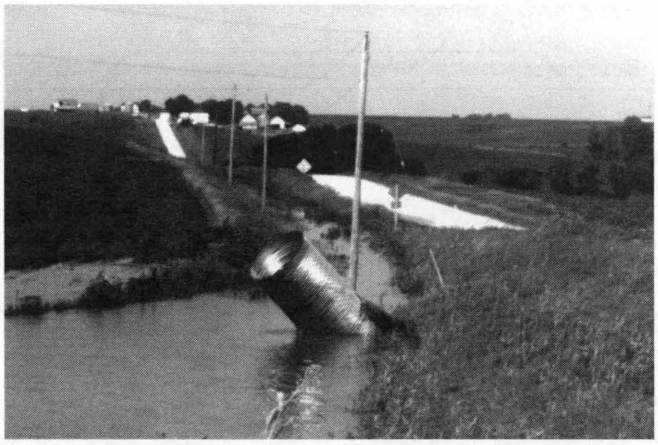

a. FAILED CMP WITHOUT TIE-DOWN SYSTEM.

b. PULL-OUT OF TIE-DOWN SYSTEM.

c. FAILED TIE-DOWN SYSTEM.

FIGURE 5 Examples of CMP uplift failures.

Using the flexural equation, the failure moment is estimated to be 160 kN.m. This moment corresponds to a uniform load of 52.5 kN acting over 1.52 m, the length where the pipe and planks are in contact. The indentation in the pipe made by the planks was obvious, so the total force acting on the planks is estimated to be 262 kN. In addition to the strength of the planks, the stretch of the cable must be included. If the cable is 13-mm wire rope with a yield stress of 1l724 MPa, the ultimate load would be 160 kN; however the cable

was not new so its ultimate strength was reduced by 20 percent to account for corrosion. Thus, the two cables could carry an addition load of 258 kN making the total load to fail the tie-down estimated to be 520 kN. This failure load for the 3.05 m diameter pipe is greater than the specified resisting forces for 6 of the 9 specifications studied and approaches the force calculated in the simplified, conservative analysis.

The history of this pipe also points to the limitations of seepage cutoffs in eliminating uplift on CMP. It is often thought that cutoff walls and graded bedding are sufficient to mitigate CMP uplift problems; however, theoretical flow net analyses indicate that a cutoff needs to extend approximately 80 percent of the distance to an impermeable layer in order to reduce the quantity of seepage by 50 percent (*4,5*) and that incorrect placement of cutoffs can result in a redistribution of pore pressures that might exacerbate the problem (*5,6*). From a practical standpoint differential settlement, cracking, perforation, and burrowing animals can ruin the best designed seepage control system.

CONCLUSIONS

Between 1970 and 1975 and between 1983 and 1988, the secondary road system in Iowa reported approximately six CMP uplift failures per year. Uplift failures of CMP throughout North America are fairly rare with only 17 percent of U.S. states and Canadian provinces reporting nine failures between 1987 and 1992. Failures were limited to pipes with diameters greater than 1.52 m. Three DOTs do not use CMP, and six specify a maximum diameter of CMP of 1.37 to 2.13 m. Although the number of reported failures may appear low, this record is unacceptable when there is potential for loss of life and when it is possible to alleviate the problem with proper end treatment. Of those reporting failures, only one state had used end restraint standards. Twenty-six of 52 agencies have standards for end protection.

Although FHWA and some state DOTs have specifications for flexible pipe tie-downs or headwalls, the bases for their recommendations are not clearly defined. Further, few field data on pore pressure distributions, or uplift loading conditions are available; however, through the analysis of two CMP failures where original designs and post failure measurements were available, the premise that uplift was caused by pore pressures appears reasonable. In one case history, where no end restraint was used, failure occurred at a force less than the least conservative specification. In a second case history, in which end restraint was used, the force to cause failure approached the more conservative specifications.

Of those agencies that provided data to compare end restraint force as a function of CMP diameter, five have lower resisting forces than those computed by a simplistic analysis and three have forces approximately equal or slightly greater. The large range in these standards and the continuation of uplift failures suggest that experimental work including pipe longitudinal stiffness and soil-pipe interaction of pipes greater than 2 m in diameter is needed to develop a rational set of specifications for end restraint. Two studies addressing these issues are reported as part of these proceedings (*7,8*).

ACKNOWLEDGMENTS

This research was conducted through the Engineering Research Institute, Iowa State University, and was sponsored by the Highway Research Advisory Board and the Highway Division, Iowa DOT. The support, cooperation, and counsel of Iowa DOT engineers, especially Darrell D. Coy, and numerous county engineers were greatly appreciated. The opinions, findings, and conclusions expressed herein are those of the authors and are not necessarily those of the Iowa DOT.

REFERENCES

1. Edgerton, R. C. Culvert Inlet Failures—A Case History. *HRB 286, 1960.*
2. *Pipe Culvert Inlet and Outlet Protection.* FHWA Notice N 5040.3, FHWA, U.S Department of Transportation, April 1974.
3. Austin, T. A., R. A. Lohnes, F. W. Klaiber. *Investigation of Uplift Failures in Flexible Pipe Culverts: Final Report.* ERI Project 3024, ISU-ERI-Ames-90227, Ames: Engineering Research Institute, Iowa State University, 1990.
4. Goehring, R. L. *Preliminary Structural and Hydraulic Analysis of Flume Bridges in Western Iowa.* M.S. thesis. Iowa State University, Ames, Iowa, 1981.
5. Cedegren, H. R. *Seepage, Drainage and Flow Nets*, 2nd ed. John Wiley & Sons, Inc., New York, 1977, 535 pp.
6. Lambe, T. W., and R. V. Whitman, *Soil Mechanics, SI Version.* John Wiley & Sons, Inc., New York, 1979, 553 pp.
7. Haven, B. T., F. W. Klaiber, R. A. Lohnes, and L.W. Zachary. *Longitudinal Strength and Stiffness of Corrugated Metal Pipe.* Presented at 73rd Annual Meeting of the Transportation Research Board, Washington, D.C., 1994.
8. Kjartanson, B. K., R. A. Lohnes, F. W. Klaiber, and B. T. McCurnin. *A Full-Scale Field Test of the Uplift Resistance of a Corrugated Metal Pipe Culvert.* Presented at 73rd Annual Meeting of the Transportation Research Board, Washington, D.C., 1994.

Publication of this report sponsored by Committee on Culverts and Hydraulic Structures.

Full-Scale Field Test of Uplift Resistance of Corrugated Metal Pipe Culvert

B. H. KJARTANSON, R. A. LOHNES, F. W. KLAIBER, AND B. T. MCCURNIN

Recent surveys of transportation agencies regarding corrugated metal pipe (CMP) culverts have indicated cases of longitudinal flexural failure due to uplift at the inlet. The surveys indicate that inlet tie-down design standards vary by more than 500 percent in the calculated tie-down force required for similar large diameter CMP. In response to these problems, Iowa State University (ISU) is carrying out a multiphase research project to develop a rational design methodology for CMP inlet tie-downs. As a part of the ISU project, a full-scale field test involving a 16-m long and 3.05-m diameter CMP installed in a simulated highway embankment was conducted to gain insight into the soil-structure interaction processes and to obtain data for use in the development and verification of a CMP tie-down design methodology. Uplift forces were applied at the "inlet" end of the CMP by a system of hydraulic jacks mounted on a reaction frame. CMP deflections, strains, and backfill earth pressures were monitored as the CMP was incrementally loaded to give a maximum inlet uplift of about 76 mm. The test data indicate that the backfilled CMP subjected to inlet uplift forces behaves essentially as a cantilever beam, with the greatest bending occurring near the crest of the embankment slope. Analyses indicate that the backfill soil cover significantly increases the effective longitudinal stiffness of the CMP through soil-structure interaction processes and thus must be taken into account in a CMP inlet tie-down design.

The cost benefits associated with the use of corrugated metal pipe (CMP) culverts in place of small bridges are particularly realized in rural areas where a great number of roadways cross small streams. However, there have been some uplift problems with CMP culverts in recent years. A recent survey of transportation agencies (*1*) indicates cases in which longitudinal flexural failure of CMP have occurred due to bending up (uplift) of the inlet. In some instances, the entire CMP has been dislodged from its existing location (*2*), creating extremely dangerous conditions. The uplift failures occurred with steel culverts so the current study of CMP does not include aluminum culverts. High storm flows and/or partial blockage of the inlet can lead to a significant hydraulic head differential between the CMP inlet and outlet (*3*). Seepage beneath the pipe under these conditions would result in a triangular pore pressure distribution along the underside of the CMP, assuming a uniform loss of total hydraulic head from the inlet end to the outlet. Moreover, under these flow conditions, the water level outside of the CMP inlet can be higher than that inside the CMP, resulting in buoyancy effects in the CMP inlet region. Many CMP are installed with the minimum amount of soil cover and no additional hold down anchorage. In some cases, restraints (tie-downs) are installed at the ends of the CMP to prevent uplift.

B. H. Kjartanson, R. A. Lohnes, and F. W. Klaiber, Construction Engineering Department, Iowa State University, Ames, Iowa 50011. B. T. McCurnin, Black and Veatch, 11401 Lamar, Overland Park, Kans. 66211.

A recent survey of transportation agencies regarding CMP tie-down design standards revealed that a variety of tie-down methodologies are currently being used across the country (*1*). The various tie-down methodologies being used by different agencies result in divergence of the magnitude of required tie-down forces by more than 500 percent for similar large diameter CMP. Thus, a more rational analysis needs to be developed to obtain the best possible combination of safety and cost for CMP tie-down designs.

In response to the problems of CMP uplift failure in the state of Iowa, the Iowa Department of Transportation (DOT) has funded a multiphase study which is being conducted at Iowa State University (ISU) to develop a rational design methodology for CMP tie-downs. Due to the lack of CMP longitudinal strength and stiffness data required in the hold-down force design process, one phase of the CMP research project involved the development of an analytical model to estimate the longitudinal bending stiffness and strength of CMP of any diameter, gage, or corrugation style. The ISU analytical model was verified through the full-scale load testing of two CMP sections without soil backfill (*4*).

In a typical field situation, however, the CMP behavior depends not only on its own strength and stiffness characteristics but also its interaction with the surrounding soil backfill. A full-scale field test of a buried CMP was conducted as a part of the ISU project to gain insight into the soil-structure interaction processes and to obtain data for the development and verification of CMP tie-down design methodologies. This study presents the results of this full-scale field test and a preliminary analysis of the data obtained.

FIELD TEST DESCRIPTION

Design and Installation

The most critical conditions for CMP inlet uplift involve large diameter CMP with minimum soil cover. Therefore, a 3.05-m diameter CMP with 0.61 m of soil cover was tested in a simulated highway embankment with a 2:1 foreslope (Figure 1*a*). To form the embankment, a trench approximately 4.3 m wide at the base with side slopes of 1:1 was excavated in a knob of undisturbed glacial till (see Figure 1*b*). Details for a Class "C" bedding were followed in preparing the base (*5*). Specifications require 10 percent of the CMP height to rest in a saddle cut from compacted soil or natural ground. Accordingly, after 0.31 m of backfill was placed, a template was used to form the concave saddle. Fill around culvert pipes should be compacted to 90 percent of the maximum dry density obtained from a standard Proctor density test (*5*); tests carried out on soil samples obtained from the site indicated a maximum dry unit weight of 18.9 kN/m^3 at an optimum moisture content of 12 percent.

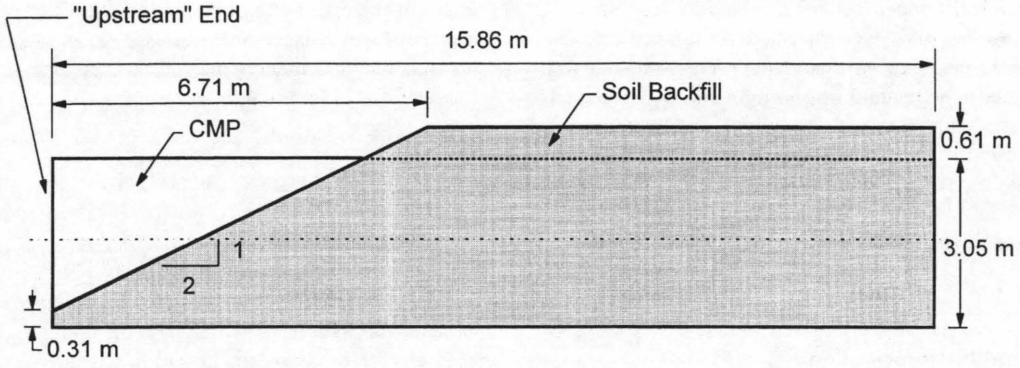

(a)

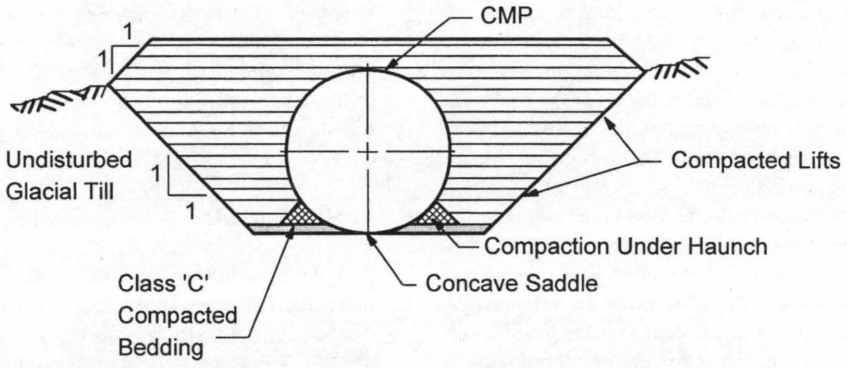

(b)

(c)

FIGURE 1 CMP test installation: (*a*) longitudinal profile; (*b*) transverse section showing excavation and backfill compaction details; (*c*) test setup before backfilling.

Following construction of the concave saddle, two sections of 3.05-m diameter, galvanized steel CMP, 8.24 m and 7.62 m in length respectively, were placed and aligned in the saddle and connected with a 0.25 m wide band (see Figure 1*c*). Both CMP sections supplied for the test were 10 gage, with 3 × 1 helical corrugations and continuously welded seams, with the exception of the last 1.53 m of the 7.62 m "downstream" section which was 8 gage. This 8-gage "downstream" section of the CMP was 9.75 m away from the position where the load was applied to the CMP; therefore, the difference in gage was considered insignificant. To prevent a premature joint failure during the uplift testing of the CMP, the connection between the two sections of CMP was strengthened by welding thirty-four 6.4 mm thick, 63.5 mm wide by 0.46 m long steel plates around the inside circumference of the joint.

The confined haunch areas located near the base of the CMP required compaction with 51 mm /ti 102-mm timber "studs"

and a small mechanical tamper. Above the haunch region, work areas allowed the use of larger mechanical tampers. Loose lifts approximately 0.2 m thick were placed and evenly spread before compaction. The sand cone method was used for compac-tion quality control to confirm compliance with specifications. Data from five levels within the backfill give an average dry unit weight of 17.3 kN/m^3 and average moisture content of 12.3 percent. Backfilling alternated from side to side of the CMP so that the two fills were kept at approximately the same elevation at all times.

Test Apparatus and Instrumentation

The unbalanced triangular pore pressure distribution resulting from seepage beneath the pipe, thought to be the driving force for many inlet uplift failures, was simulated by using two load points located 1.53 and 4.58 m from the "upstream" end of the CMP. As shown in Figure 2, uplift was provided by four hollow core hydraulic cylinders reacting on an overhead load frame. The loads from the hydraulic cylinders were transmitted through a system of high strength rods to 0.38-m wide steel straps that passed under the bottom half of the CMP. A grout mix was pumped between the straps and the CMP corrugations to ensure that the load would be distributed over the full 0.38-m strap width thus deterring any local failures.

Data collected during the test included strains on the inner surface of the CMP, deformations of the CMP cross section, vertical deflection of the top of the CMP, and pressures within the soil surrounding the pipe. The electronic sensors were monitored and the output was recorded using a computer controlled data acquisition system (DAS) whereas the vertical deflection measurements were taken manually during the uplift portion of the test. Details on the individual instruments employed are as follows.

Six longitudinal sections were strain gaged to measure longitudinal and hoop strains at the peaks of corrugations on the inner surface of the pipe (see Figure 3*a*). Two gages (one longitudinal and one circumferential) were placed at each of four locations (the top, bottom, and both ends of the horizontal diameter) at all six sections (see Figure 3*b*). This arrangement of strain gages allowed for calculation of the hoop to longitudinal stress ratio factor required to calculate the longitudinal bending stiffness using the ISU analytical model [see Equations 1 and 10 of Havens et al. (*4*)]. In addition, these gages allowed for tracking of the position of the CMP neutral axis during longitudinal bending. Note, however, that due to local bending effects (see Figure 3*c*), the longitudinal strain gages on the inside surface of the top of the CMP will indicate tensile (positive) strains whereas those on the bottom will indicate compressive (negative) strains.

DCDTs mounted on lightweight rods connected to the inside walls of the CMP near the strain gaged sections were used to measure the changes in vertical (Figure 3*d*) and horizontal diameters of the pipe. The diameter change rods were slightly offset from the strain gages to avoid introducing stress concentrations but are still referenced according to the corresponding strain gaged sections. Vertical deflections of the top surface of the CMP were measured by monitoring the movement of steel rods attached to the top of the CMP and extended vertically above the fill at the seven locations shown in Figure 3*a*. Scales attached to the rods were monitored with a surveying level.

Soil pressure cells were installed in the backfill adjacent to the CMP's horizontal diameter, directly above the CMP, and along the edges of the prism of soil defined by the CMP diameter. The pressure cells were placed at Sections A, B and C as shown in Figure 4*a*. Specific placement of the cells at each of the transverse sections is illustrated in Figure 4, *b*, *c*, and *d*.

TEST PROCEDURES

A series of load increments with a load ratio of 2 between the front lift straps and the back lift straps were applied to the CMP to simulate the unbalanced triangular pore pressure distribution. Load cells beneath the hydraulic cylinders were monitored by the DAS for accurate force measurement and test control. After obtaining the desired magnitude of uplift forces for each load increment, the applied loads, soil pressures, strains, and deformations were recorded. This sequence of events was repeated until a 76-mm upward deflection was achieved at the deflection Rod "a" location (see Figure 3*a*) at the "upstream" end of the CMP; at this point the test was terminated. The loading path is displayed in Figure 5. As indicated in the figure, the desired loading ratio was essentially maintained throughout the entire test.

TEST RESULTS

Figure 6 presents longitudinal profiles of the CMP at different load increments. Minimal movement (<5 mm) was observed at Section d whereas no activity was observed at Sections e, f, and g (see Figure 3*a*). The most significant bending in the CMP occurred in the region 4.58 to 9.15 m from the inlet. The steel load straps provided some support at the "upstream" end of the CMP and limited bending in the first 4.58 m of the CMP. Observed changes in the horizontal and vertical diameters of the CMP during uplift were very small, generally less than 5 mm. Thus, the base of the CMP is essentially tracking the movement of the top of the CMP.

The patterns of longitudinal and hoop strains measured on the inner surface of the CMP were consistent with the deformations of the top of the CMP noted above. As indicated in Figure 7, the longitudinal strains at Section 3 (Figure 7*a*) were significantly larger than those in the hoop direction (Figure 7*b*). Additional longitudinal strain data at Sections 1 and 4 are shown in Figure 7, *c* and *d*, respectively. The longitudinal strains on the sides of the CMP at midheight (indicated by left and right) were very small relative to those at the top and bottom. This indicates that the CMP's neutral axis remained near the midheight of the pipe.

Top and bottom longitudinal strains at Section 1 (see Figure 7*c*) were essentially equal in magnitude throughout the entire test. However, at Section 3 where the entire CMP was covered with soil, the strain on the top was less than the corresponding strain on the bottom (see Figure 7*a*). The base of the CMP at this particular location (Section d in Figure 3*a*) was beginning to separate from the soil as indicated by the deflection data in Figure 6. This separation accompanied by the expansion of the corrugations on the bottom of the CMP may have prevented the adjacent soil from providing any additional resistance to local deformations. In contrast, the top regions of the CMP were being compressed into the soil. The responses of the soil pressure cells located directly above the top of the CMP confirms this behavior. For example, the earth pressure cell located 0.61 m "downstream" from Section 3 began showing an increase in pressure at the same time as longitudinal strains were beginning to develop on top of the CMP at this location. The pres-

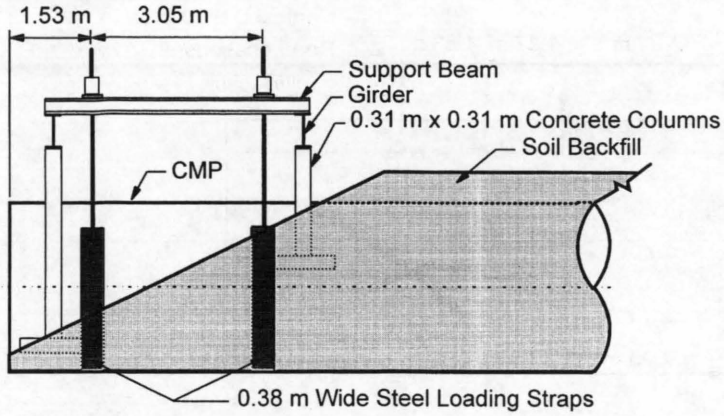

(a)

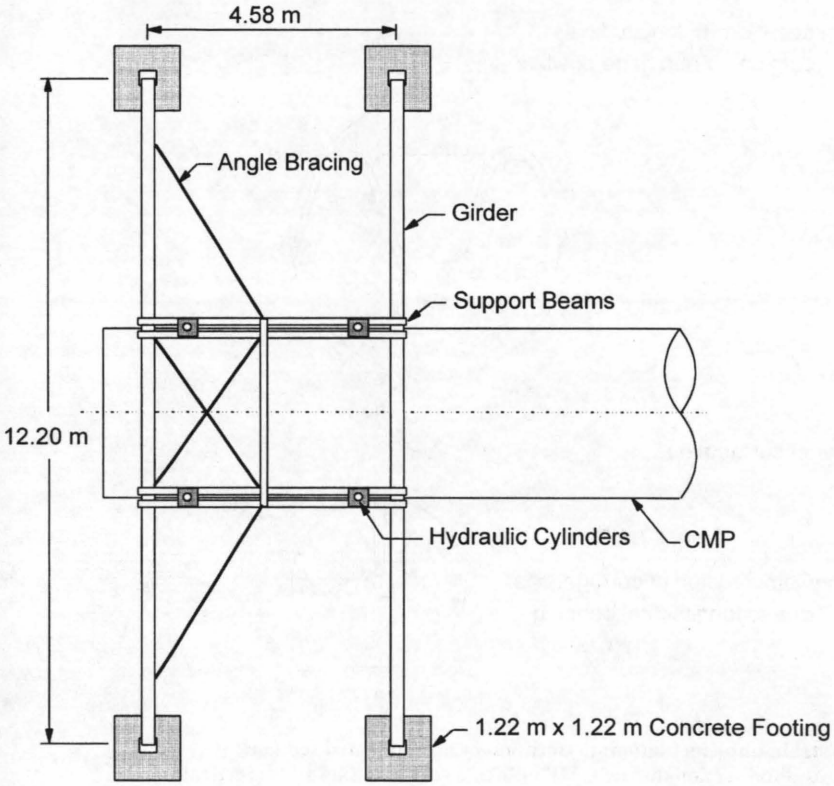

(b)

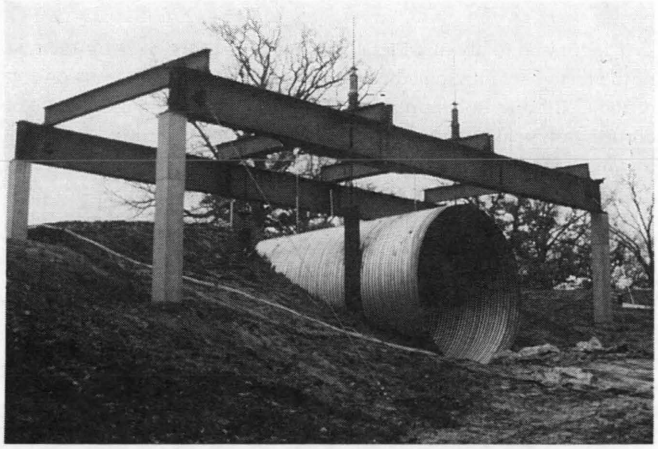

(c)

FIGURE 2 Load frame description: (*a*) profile of load frame; (*b*) plan view of load frame; (*c*) load frame and CMP after backfilling.

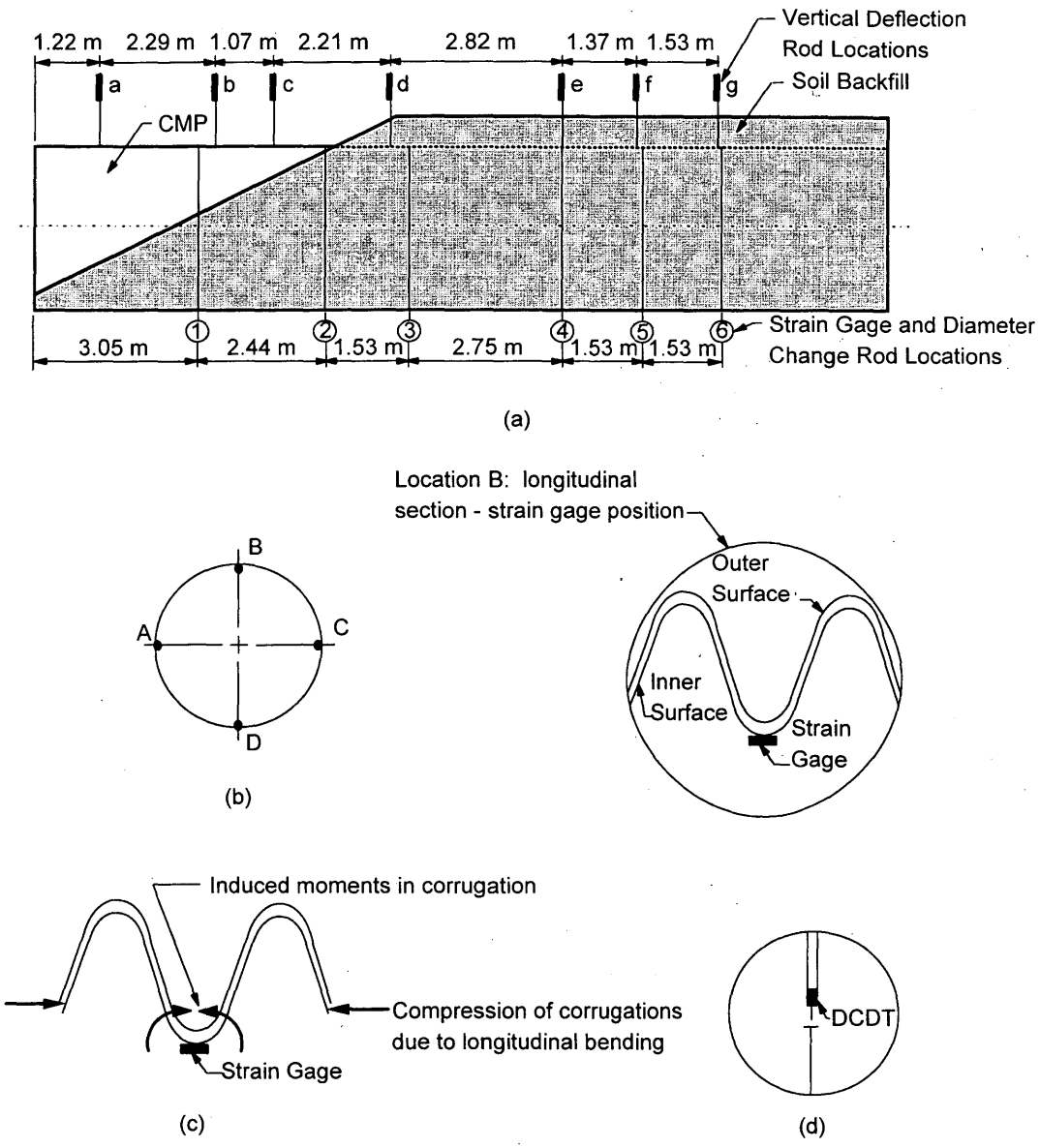

FIGURE 3 Location of deflection and strain implementation: (*a*) location of instrumented sections; (*b*) strain gage locations; (*c*) location B longitudinal section during CMP uplift; (*d*) deformation rods (vertical).

sure increased to about 1 kPa and remained at this level for the rest of the test. The anticipated compression of the corrugations on top of the CMP due to bending (i.e., shortening of the length between corrugation peaks) may have been partially restricted by the interlocking action of soil in the corrugations. This suggests that the top portion of the CMP may have gained additional stiffness from the interacting soil, whereas the bottom portion of the CMP received little benefit from the soil.

ANALYSIS OF CMP UPLIFT

A CMP-soil system subjected to inlet uplift forces and longitudinal bending is a three dimensional, statically indeterminate, soil-structure interaction problem. As such, the problem should be modeled and analyzed utilizing three dimensional numerical techniques with structural, interface, and soil model element capabilities. In geotechnical engineering, however, analytical simplifications are quite often made in the design stage without compromising the performance and reliability of the structure. Thus, several levels of analysis may be considered, each with its own assumptions and potential limitations. The following three levels of analysis could be used in this CMP-soil interaction problem.

1. Given the deformation patterns observed during the test (Figure 6), it is not unreasonable to consider the CMP as a cantilever beam, rigidly restrained at the "downstream" end by the soil cover. In this case, a cantilever beam analytical approach could be used in which the deflected shape of the CMP is analyzed and the longitudinal rigidity of the CMP-soil system is lumped into the CMP beam. The soil, therefore, is modeled simply as a distributed load on the top of the CMP beam. This approach, however, is very site (CMP and soil backfill) specific.

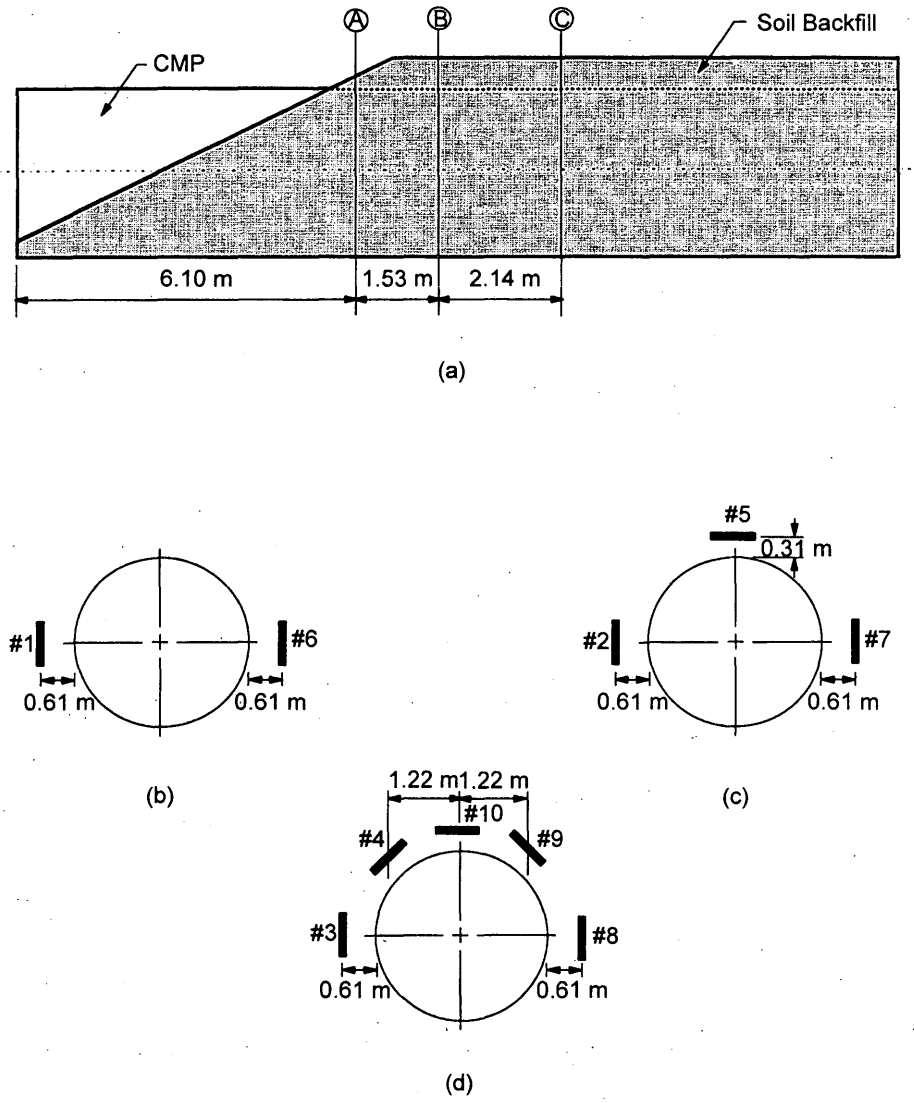

FIGURE 4 Soil pressure cell locations: (*a*) soil pressure cells; (*b*) Section A; (*c*) Section B; (*d*) Section C.

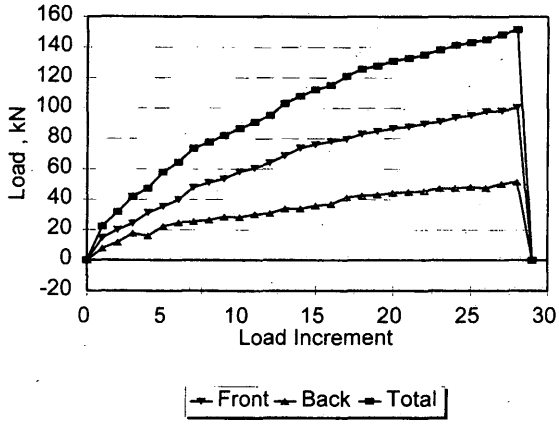

FIGURE 5 CMP uplift loading sequence.

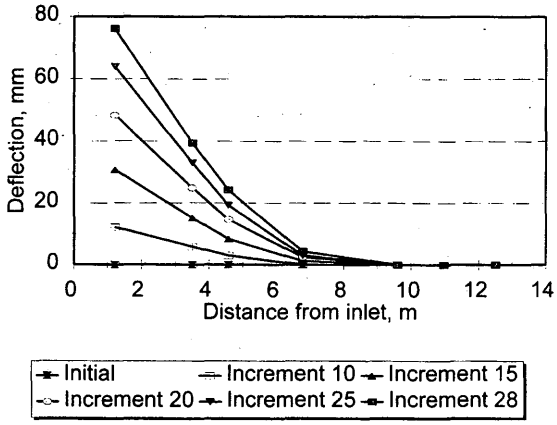

FIGURE 6 Profile of deflected CMP at selected load increments during uplift.

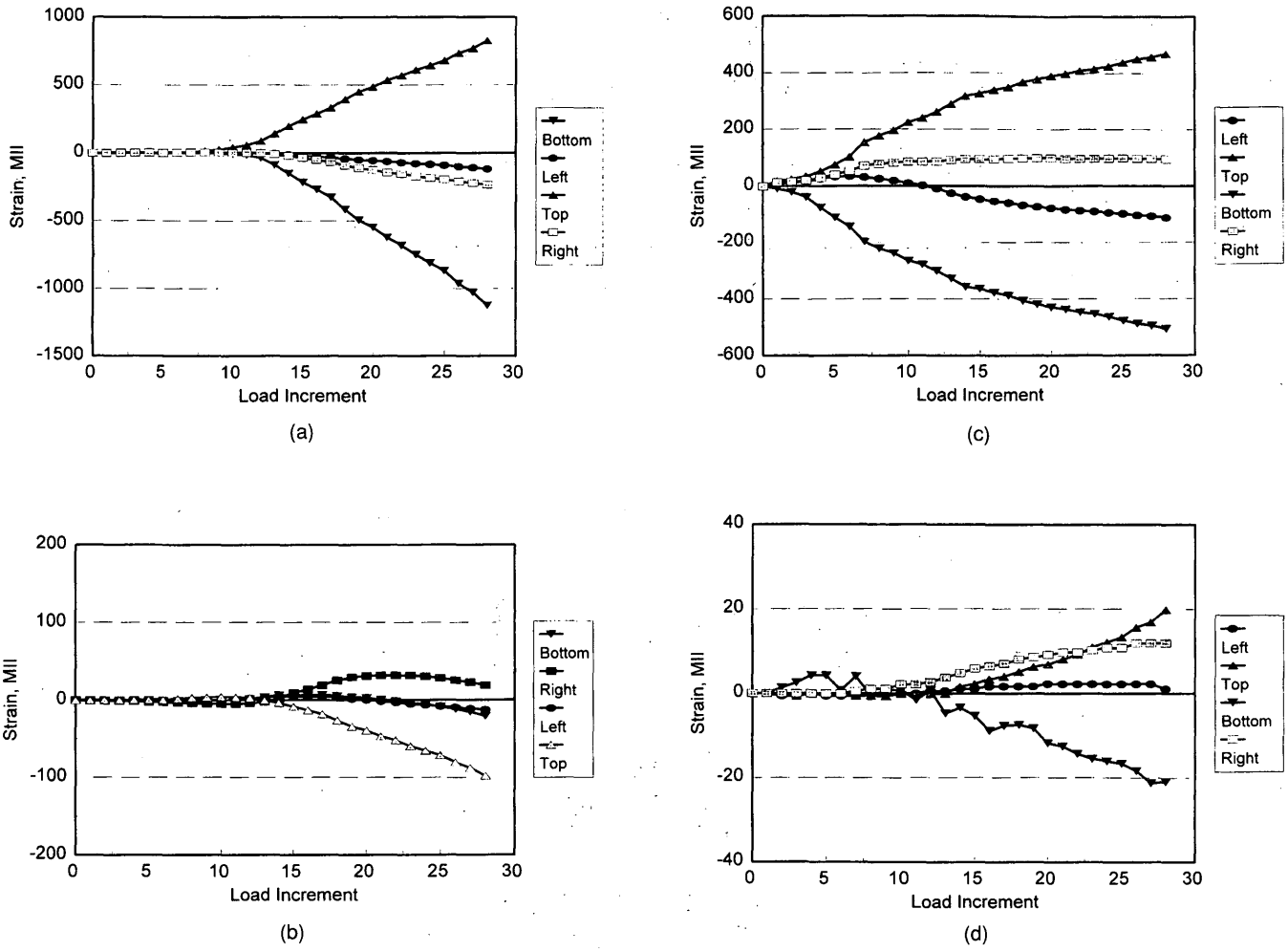

FIGURE 7 CMP uplift strain data: (*a*) longitudinal strains versus load increment (Section 3); (*b*) hoop strains versus load increment (Section 3); (*c*) longitudinal strains versus load increment (Section 1); (*d*) longitudinal strains versus load increment (Section 4).

2. The three dimensional problem could be reduced to two interlinked two dimensional problems; that is, a plane strain analysis of the CMP-soil hoop (transverse) section loosely coupled with a longitudinal bending analysis, as described above. In this case, the transverse section analysis would form the basis for the soil-structure interaction modeling whereas the out-of-plane longitudinal responses would be incorporated through a superposition scheme.

3. Full three dimensional numerical analysis, in which the longitudinal bending of the CMP is fully coupled with the interaction of the surrounding soil would represent the most comprehensive analysis. In this case, CMP's of various sizes, gages and corrugation geometries embedded in backfill with a variety of strength and deformation properties could be analyzed without the need for lumping and superposition of responses.

Considering the experiments and analysis carried out by the ISU researchers on the longitudinal stiffness and strength of large diameter CMP sections without soil (*1*), it is useful and instructive at this point to analyze the CMP-soil system as a soil-stiffened cantilever beam (i.e., Level 1 previously described) so that a direct comparison of results can be made. For the reader's information, the other two levels of analysis (Levels 2 and 3), along with further full-scale field testing, are in progress at ISU.

In the Level 1 analytical approach, the deflected shape of the CMP is defined mathematically by fitting a fifth order polynomial to the deflection data points for a particular load increment; slopes of the deflected shape of the CMP can then be approximated by taking the first derivative of the deflection function. A plot of the CMP's calculated deflected shape versus that actually measured, for the last load increment, is shown in Figure 8. This figure shows that the deflection function precisely fits the deflected shape of the CMP and that the vertical deflection and slope become essentially zero at a distance of 9.15 m from the inlet; this effectively defines the boundaries of the cantilever beam substructure. The CMP-soil substructure can now be analyzed using customary structural analysis techniques. Two unknowns are introduced into the analysis: 1) the soil response along the CMP during uplift, which is assumed to be a distributed load related to the weight of the soil above the midheight of the CMP and 2) the overall flexural stiffness of the CMP, in terms of EI, including the rigidity added by the soil backfill. In this analysis, E represents the CMP material modulus of elasticity which is assumed to be 200,000 MPa whereas I represents the moment of inertia.

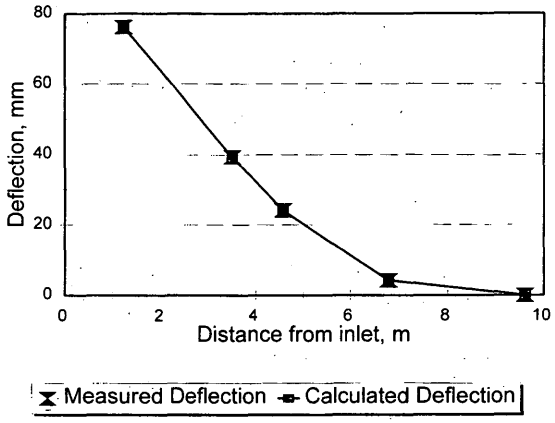

FIGURE 8 Deflected shape of CMP (calculated and measured deflections for load Increment 28).

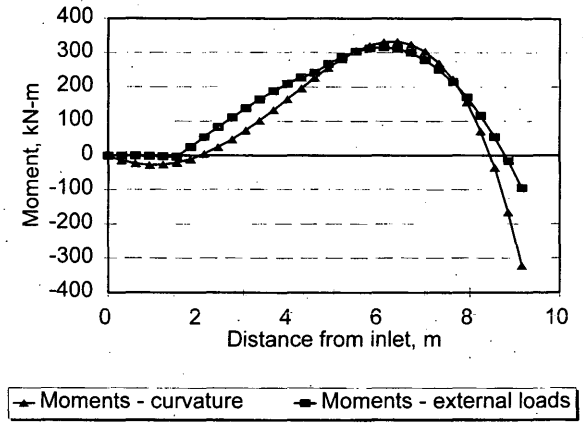

FIGURE 10 Comparison of moment diagrams resulting from the CMP applied loading.

The next step is to formulate a moment diagram using the external loads shown in Figure 9. The CMP weight (W_p), the concentrated uplift forces, and the unknown soil response were the loads used to construct the moment diagram. For this analysis, as described above, the soil response (defined as W_s) is simply considered to be a distributed load related to the shape of the backfill cover overlying the midheight of the CMP.

Relationships between the two unknown parameters, the moment of inertia (I) and the soil response (W_s) were developed using the moment-area theorems for elastically loaded beams undergoing small deflections. The angle change and tangential deviation between the various points were computed using the mathematically determined deflection curve previously described. The unknown moment of inertia (I) and unknown soil response (W_s) were then determined using numerical integration techniques. The analysis yielded $I = 0.0003900$ m^4 and $W_s = 86.48$ kN/m. The weight of the soil above the midheight of the CMP in the region with 0.61 m of cover is 49.29 kN/m. The difference between W_s and the actual soil weight can be attributed to the three dimensional soil strength and stiffness effects which are not accounted for in this analysis.

After determining experimental values for I and W_s, two methods were used to construct moment diagrams resulting from the applied loading. One moment diagram was computed using the external load data shown in Figure 9 assuming cantilever conditions whereas the other was computed using the differential equation of the elastic curvature (i.e., $y'' = M/EI$ where y'' is an approximation of curvature). As illustrated in Figure 10, the two methods give similar moment diagrams. The moments calculated from the external loading are very small in the first 1.43 m of the CMP due to the small self-weight of the CMP.

As previously noted, one of the key reasons for pursuing this simple cantilever beam analytical approach was to compare the longitudinal stiffness of the backfilled CMP with the longitudinal stiffness of the CMP without soil backfill. As noted above, the back analysis of the backfilled CMP uplift test gave an I value of 0.0003900 m^4 whereas an I value of 0.0002668 m^4 was determined for the CMP without soil backfill using the ISU analytical model (*4*) and the assumed material modulus of elasticity E noted previously. Thus, the CMP-soil interaction effects apparently result in a 46 percent increase in the effective I of the CMP. These CMP-soil interaction effects include the restriction of compression of the corrugations on the upper surface of the CMP and the resistance due to the stiffness and shear strength of the surrounding soil.

As an additional assessment of the effects of the soil-structure interaction on the CMP's overall longitudinal stiffness, a CMP effective longitudinal moment of inertia, I, was calculated using the ISU analytical model [Equation 10 of Havens et al. (*4*)]. The model requires calculation of the hoop to longitudinal stress ratio factor [Equation 1 of Havens et al. (*4*)] using hoop and longitudinal strain gage data collected from the CMP wall during bending. The remainder of the terms in Equation 10 are geometric parameters that are fixed for the given CMP. Strain gage data collected from Section 3

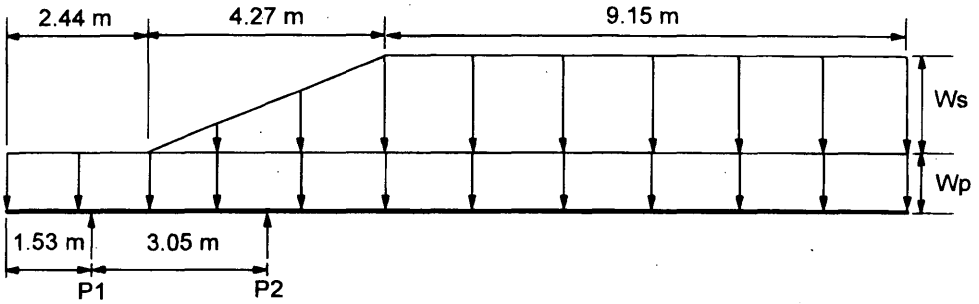

FIGURE 9 CMP cantilever beam analysis (external loads).

of this CMP-soil backfill field test gave a hoop to longitudinal strain ratio of 0.12 which in turn yielded a stress ratio factor of 0.19; substitution of this value of stress ratio factor into the ISU analytical model gives an effective I value of 0.0004549 m^4. This analysis, using the field test strain gage data and the ISU analytical model alone, gives an effective I value which agrees to within 17 percent of the I value back calculated from the deflected shape of the CMP. Thus, two independent methods of calculating I give comparable results and indicate the effects of soil-structure interaction in increasing the effective longitudinal stiffness of the CMP. These analyses indicate that for these field test conditions the buried culvert is essentially behaving as a cantilever beam. Moreover, the ISU CMP longitudinal bending model (*4*), developed assuming no soil backfill, may be used in the analysis of a CMP under inlet uplift conditions.

CONCLUSIONS

The data from this full-scale field test indicate that the backfilled CMP subjected to inlet uplift forces behaves essentially as a cantilever beam, with the greatest bending occurring near the crest of the soil embankment slope. The strain gage data, which shows smaller strains on the top of the CMP than the bottom, indicates that the top region of the CMP is stiffened due to the interacting soil whereas the bottom of the CMP, which separates from the soil, does not receive this stiffening effect. The strain gage data also indicate that the neutral axis of the CMP remains near its midheight. When analyzed as a cantilever beam, the moment of inertia, I, calculated from the deflected shape of the CMP agrees very well with the I independently calculated using the ISU CMP longitudinal bending model in conjuction with the strain data from this test.

These results represent a significant advancement in the understanding of the behavior and in the analysis of the longitudinal bending of buried CMP under inlet uplift conditions, which will be useful for the formulation of rational tie-down methodologies for the inlets of CMP culverts. It must be stressed, however, that the analysis described in this report is very dependent on the particular CMP and condition of the soil backfill (e.g., unit weight, shear strength, and stiffness) used in this field test. The design of field CMP inlet tie-downs will depend on the CMP diameter, corrugation profile, CMP gage, CMP material properties, backfill material properties and placement methodologies. For this reason, two- and three-dimensional soil-structure interaction numerical modeling, along with further full-scale field testing, is in progress at ISU.

ACKNOWLEDGMENTS

The research presented in this paper was conducted by the Engineering Research Institute of Iowa State University, and was funded by the Highway Research Board and the Highway Division, Iowa DOT, Ames, Iowa. The authors wish to thank various engineers from the Iowa DOT, especially D.D. Coy for his support, encouragement, and counseling. Appreciation is also extended to R.L. Meinzer of Contech Construction Products, Inc., Topeka, Kans., for donating the numerous sections of CMP used in the tests. Special thanks are also accorded the numerous undergraduate students who assisted with the various phases of the project. The opinions, findings and conclusions expressed herein are those of the authors and not necessarily those of the Iowa DOT or Highway Research Board.

REFERENCES

1. Klaiber, F. W., R. A. Lohnes, L. W. Zachary, T. A. Austin, B. T. Havens, and B. T. McCurnin. *Design Methodology for Corrugated Metal Pipe Tie-downs: Phase I.* Iowa DOT Project HR-332, ISU-ERI-Ames-93409, Ames: Engineering Research Institute, Iowa State University, February 1993.
2. Pestotnik, C. A letter to County Engineers on "Report on Flexible Culvert Inlet Flotation Failures Survey." Iowa DOT Ref. No. 521.1, February 20, 1976.
3. *Pipe Culvert Inlet and Outlet Protection.* FHWA Notice N 5040.3, FHWA, U.S. Department of Transportation, April 26, 1974.
4. Havens, B. T., F. W. Klaiber, R. A. Lohnes, and L. W. Zachary. Longitudinal Strength and Stiffness of Corrugated Steel Pipe, pp. 1-9 in this Record.
5. *Standard Specifications for Highway and Bridge Construction.* Iowa Department of Transportation, Ames, Iowa, 1990.

Publication of this paper sponsored by Committee on Culverts and Hydraulic Structures.

Structural Performance of Profile-Wall Drainage Pipe—Stiffness Requirements Contrasted with Results of Laboratory and Field Tests

C. D. F. ROGERS, P. R. FLEMING, M. W. J. LOEPPKY, AND E. FARAGHER

This paper describes the development of the current United Kingdom (UK) stiffness requirements for profile-wall flexible pipes and assesses their limitations. Laboratory testing of flexible pipes ranging in diameter from 100 to 375 mm is described. The results indicate that deformations and circumferential strains are small, even under severe loading, and generally fall well within the current limits specified in the appropriate U.K. standards. Creep stiffness specifications and design and installation standards are assessed in light of the collected data, and recommendations for improved criteria are propounded.

United Kingdom requirements for nonpressure drainage pipes cover a range of properties including impact resistance, watertightness, material properties and time-dependent stiffness. This last property is of particular importance to pipe manufacturers in engineering their product and to civil engineers for specification and design purposes.

Profile-wall pipes are a relatively recent innovation and have not yet been considered in British Standards (BS), although they will be included in forthcoming Euro Norms. In the absence of an applicable BS, "fitness for purpose" assessments for construction products are carried out by the British Board of Agrément (BBA), frequently in consultation with the U.K. Department of Transport (DOT). The BBA's mandate also includes conformance testing, using standard, adapted or ad hoc testing methods, to ensure compliance with the established specifications.

DEVELOPMENT OF EXISTING U.K. STANDARDS

Specification criteria for materials used on projects controlled by the DOT are contained in the *Specification for Highway Works* (*1*). This document provides specification requirements for use in public purchasing contracts and is therefore the specification for the majority of applications for the pipes under consideration. A related document, DOT Highway Advice Note HA40/89, *Determination of Pipe and Bedding Combinations for Drainage Works* (*2*) states that the DOT requires profile-wall, non-pressure drainage pipes to meet a minimum 50-year extrapolated stiffness of 1,400 Pa (0.2 lb/in.^{2}) when tested in accordance with Appendix B of BS4962:1989, *Specification for Plastics Pipes and Fittings for use as Subsoil Field Drains* (*3*). Tabulated safe burial depth recommendations in HA40/89 were developed using the Transport Research Laboratory (TRL) method, an analytical approach which treats the pipe-soil structure as the basic structural unit (*4,5*). The calculations are based on conservative assumptions and, predictably, pipes conforming to these requirements have been found to experience long-term diametral strains less than the widely accepted limit of 5 percent. The 5 percent limit is based on a factor of safety of four applied to the historically accepted limit of 20 percent deformation to avoid snap through buckling of large diameter steel corrugated culverts. It should be noted that the term "pipe stiffness" in U.K. standards is analogous to the term "stiffness factor" defined in ASTM D2412-87 (*6*), which refers to a short-term constant rate of deflection test. It is therefore fundamentally different from the long-term constant load creep test specified in the United Kingdom.

The approach of HA40/89 (*2*) is excessively conservative by accepting the traditional 5 percent diametral strain limit in addition to applying a factor of safety of two to the pipe stiffness and assuming worst case installation conditions. This "belt and braces" approach, coupled with the long-term creep test requirements of BS4962 (*3*), has resulted in the substantial overdesign of pipes to meet material and structural criteria. An appraisal of the functional requirements for a pipe in use under load, based on engineering principles, would yield a better engineered, hence more economical design. Flexible pipe design would then follow the route taken by other branches of civil engineering, which have economized on the use of materials by a more sophisticated and rational appraisal of basic structural requirements.

DESCRIPTION OF U.K. TESTS AND REQUIREMENTS FOR FLEXIBLE PIPE

BS4962 (*3*) specifies a parallel-plate loading test, one test of many employed by the BBA in certifying flexible pipe products for use in roads and bridges, in which a constant load is applied to a laterally unrestrained pipe sample for 1000 hr, with deflection readings being taken at set times. A 50-year deformation value is extrapolated from the data, using a computerized nonlinear optimization technique, and the design stiffness calculated.

It is the authors' opinion that the rationale of the test, and of the test method itself, is questionable. The creep performance of the pipe is considered out of context (i.e., with the pipe not buried in a soil surround) and therefore no account is taken of the lateral support provided to the pipe by the sidefill, or of load shedding by the pipe due to arching effects in the soil above the pipe crown as the

Loughborough University of Technology, Loughborough, Leicestershire, England LE11 3TU.

pipe deflects under load. Furthermore, the plate load applied is based not on the pipe diameter, expected static or dynamic loading, or other known parameter, but on the deflection after five minutes, and hence on the short-term stiffness itself. Consequently, two otherwise identical pipes made of different materials may be tested with vastly differing applied loads. Another weakness is the fact that, by using the results of testing over 1000 hr to determine a stiffness fifty years into the future, small experimental inaccuracies will significantly affect the extrapolated result. The test is, however, required for certification and is often justified by its ease of repeatability under controlled laboratory conditions. In addition, there is evidence to indicate that pipes passing the test do perform adequately when installed in accordance with the Specification for Highway Works.

The Specification for Highway Works (*1*) stipulates acceptable products for drainage and ducting applications, in addition to detailing acceptable materials and practices associated with pipe installation. A companion document, *Highway Construction Details* (*7*), provides standard drawings of acceptable trench dimensions and bedding, haunch, and surround criteria. These documents do not make pipe design recommendations, leaving an explanation of flexible pipe design and tabulated safe depth ranges for various installation conditions to HA40/89 (*2*).

The safe depth ranges in HA40/89 (*2*) are calculated using the TRL method (*5*) and assume worst cases of pipe stiffnesses and installation practices, although no precise details of the base data used are given. U.K. pipe manufacturers tend to use the Iowa formula (*8*) which, although regarded as being less theoretically sound, is nevertheless widely accepted as a valid method due to the data accumulated over the years for the modulus of soil reaction (E'), particularly by Howard (*9*), and because it has proved to be a relatively reliable predictor of flexible pipe deflection. The lack of usable back-analyzed soil stiffness data for the more theoretically justifiable TRL method implies uncertainty in the allowable pipe installation conditions tabulated in HA40/89. Indeed, HA40/89 admits explicitly that the charts contained therein are based on conservative design parameters. There is a wide range of factors to consider in predicting the performance of the pipe-soil structure using the TRL method, including installation procedures, site conditions, trench geometry, and withdrawal of trench support. Whichever design method is used, the soil stiffness dominates the design and thus pipe stiffness is not the principal variable. A thorough appraisal of the various design methods is given elsewhere (*10*).

LABORATORY TESTING OF FLEXIBLE PIPE

Testing Equipment

Pipes with an internal diameter of 300 mm or less were tested in a 1.0 × 1.1 × 1.0-m deep box, whereas larger pipes were tested in a 1.5 × 1.8 × 1.5-m deep box. Test boxes should ideally have rigid sides, if zero lateral strain conditions are required. It is appreciated that trench walls in practice will deflect when stressed, and thus a small lateral deflection of the box walls would be acceptable. Measured lateral deflections of the test box walls were very small, typically less than 2 mm under maximum load conditions, and similar to those expected for a natural soil forming the walls of a trench.

The loading arrangement provided an approximately uniform vertical stress, achieved using a natural rubber membrane mounted to the underside of the test box lids. Water was forced between the lid and the rubber membrane until the desired pressure (loading) was achieved. Two magnitudes of loading were applied, 70 and 140 kPa, to simulate burial at two different depths. For cyclic loading, to simulate the passage of a vehicle over the pipe, an automated system applied a pressure varying sinusoidally between 0 and 70 kPa.

Diametral strain measurements were taken using three linear variable differential transformers, mounted on a self-righting sledge. Circumferential strains were measured on the 375-mm pipe using uniaxial, foil-type strain gauges (mounted in epoxy resin) with coefficients of thermal expansion balanced to the pipe material. The gauges were affixed to the internal wall of the pipe at both single- and twin-wall sections to determine any differences in behavior between them. All data were recorded on a dedicated data acquisition system.

Test Procedures

Twin-wall annular corrugated HDPE pipes with inside diameters ranging from 100 to 375 mm were tested. Pipe stiffnesses for 5 percent deflection [as defined by ASTM D2412-87 (*6*)] were 97.8 lb/in.^{2} (674.4 kPa), 66.7 lb/in.^{2} (460.0 kPa), 71.9 lb/in.^{2} (495.5 kPa), 65.4 lb/in.^{2} (450.6 kPa), and 49.1 lb/in.^{2} (338.2 kPa), for 100-, 150-, 225-, 300-, and 375-mm diameters, respectively. The placing and compaction of the surround and backfill to the pipes, carried out in layers in accordance with typical site practice, constitute the installation phase. The bed, surround, and backfill materials used were a well graded river sand ($c_u = 4.37$, $c_c = 0.65$, $D_{10} = 0.19$ mm) and river gravel ($c_u = 1.55$, $c_c = 0.96$, $D_{10} = 5.5$ mm). Bedding layers were 100 mm thick for all tests. The river sand surround and backfill was placed either virtually uncompacted or heavily compacted in layers not exceeding 150 mm in depth. This represents both very poor and very good site practice. The river gravel, being relatively uniform 10 mm sub-rounded (pea) gravel, is essentially self-compacting, and compaction on site would only be justified if required to bed the material into soft trench walls. The river gravel was placed carefully on both sides of the pipe before completion of the backfill in one continuous operation. This represents typical U.K. installation conditions.

There were three loading phases:

1. Application of a static 70-kPa stress, to simulate a stationary heavy vehicle or burial to a depth of approximately 4 m.
2. Application of a cyclic 70-kPa stress, to simulate heavy vehicle loading over a shallow buried pipe. The frequency of the cycle was 0.01 Hz, 1000 cycles being applied.
3. Application of a static 140-kPa stress, to simulate a burial depth of approximately 8 m.

The static stresses were applied for 12 hr and, after unloading, a period of 4 hr was allowed for recovery.

Pipe Deflections

Selected test data are presented in Table 1. The values of vertical and horizontal diametral strain (VDS and HDS) are given after installation (I), just before the load is released at the end of the 70-kPa static load (70 S), 70-kPa cyclic load (70 C), and 140-kPa static load (140 S) sequences, and at the end of the test after final recovery. A set of vertical and horizontal test data is illustrated in Figures

TABLE 1 Experimental Data at Critical Points of Tests

PIPE SIZE	SOIL	SIDEFILL COMPACTION	VDS HDS	I	70S	70C	140S	END
100	RS	Not compacted	VDS	0.07	0.8	2.7	2.8	2.6
			HDS	-0.12	-0.8	-2.4	-2.4	-2.4
100	RS	Heavily compacted	VDS	-0.17	-0.11	0.08	0.10	0.04
			HDS	-0.01	-0.03	-0.19	-0.16	-0.17
100	RG	Not compacted	VDS	0.03	0.4	1.2	1.2	1.2
			HDS	-0.03	-0.3	-0.9	-0.9	-0.9
150	RS	Not compacted	VDS	0.10	1.6	2.6	3.3	3.0
			HDS	-0.10	-1.0	-1.9	-2.1	-2.1
150	RG	Not compacted	VDS	0.15	1.3	1.9	2.3	2.1
			HDS	-0.05	-0.7	-1.1	-1.3	-1.3
225	RS	Heavily compacted	VDS	-0.12	0.1	0.1	0.2	0.1
			HDS	0.06	0.0	-0.1	-0.1	-0.1
225	RS	Not compacted	VDS	0.04	1.2	2.0	2.7	2.1
			HDS	-0.07	-1.0	-1.9	-2.1	-1.8
225	RG	Not compacted	VDS	0.14	1.0	1.5	1.9	1.6
			HDS	-0.11	-0.7	-1.1	-1.3	-1.2
300	RS	Heavily compacted	VDS	-0.31	0.0	0.1	0.4	0.2
			HDS	0.40	0.3	0.2	0.1	0.2
300	RS	Not compacted	VDS	-0.01	2.7	4.2	5.1	4.1
			HDS	-0.05	-2.6	-4.2	-4.7	-4.2
300	RG	Not compacted	VDS	0.18	1.5	2.2	2.8	2.3
			HDS	-0.08	-1.2	-1.9	-2.5	-2.4
375	RS	Not compacted	VDS	0.14	1.3	3.9	4.4	4.0
			HDS	-0.03	-0.6	-2.6	-2.7	-2.6
375	RS	Heavily compacted	VDS	-0.70	-0.6	-0.6	-0.5	-0.7
			HDS	0.80	0.7	0.7	0.7	0.8
375	RG	Not compacted	VDS	-0.30	0.0	0.3	0.6	0.2
			HDS	0.30	0.1	-0.1	-0.2	-0.1

Legend and Sign Convention

Soil Types

RS = Well graded river sand
RG = Relatively uniform, sub-rounded 10 mm gravel

Deflection

VDS = Vertical diametral strain (% of mean external diameter)
HDS = Horizontal diametral strain (% of mean external diameter)
(Positive diametral strain values indicate a decrease in pipe diameter.)

1 and 2 for a pipe with an internal diameter of 375 mm installed in uncompacted, 10-mm pea gravel (typical U.K. site practice).

The test results indicate minimal deformations (less than 1 percent) during the installation phase. Negative values of VDS often occurred, particularly in heavily compacted sand installations, indicating an increase in diameter along the vertical axis [see also Rogers (*11,12*)]. The 70-kPa static load, representing a parked vehicle or a relatively deep burial in the United Kingdom, produced very small deformations, with the maximum VDS for this phase being 2.7 percent (300-mm pipe in a poor surround).

It is appreciated that construction traffic loading subsequent to pipe installation can be significant, particularly on road construction sites, and, depending on the cover depth of the pipe, significant deformations are possible. Minimum burial depths for pipes not protected by special measures are specified (*13*) and implied (2) to ensure that such loading is not critical, the 70-kPa cyclic load being used here to simulate the maximum loading under minimum burial depths. During the 70-kPa cyclic load phase, the rate of increase of VDS and HDS decays exponentially. Associated field trial data, in which cyclic loading was applied to shallow buried pipes using a heavily laden vehicle, demonstrate similar trends and degrees of deformation, thus providing a high degree of confidence in the laboratory simulations. A progressive reduction in the amplitude of the elastic deformation caused by the cyclic load was also observed as the tests progressed.

Tests using heavily compacted well graded river sand demonstrated remarkably good performance. Deflections during all phases of the test were extremely small, typically only just becoming positive at the end of testing (following negative installation deflections). This is because a pseudo-elastic system is in existence in well compacted material, in which little further fill compaction can take place under a subsequently applied load. Tests in which the river sand was placed without any sidefill compaction applied, simulating very poor (and, according to U.K. specifications, unac-

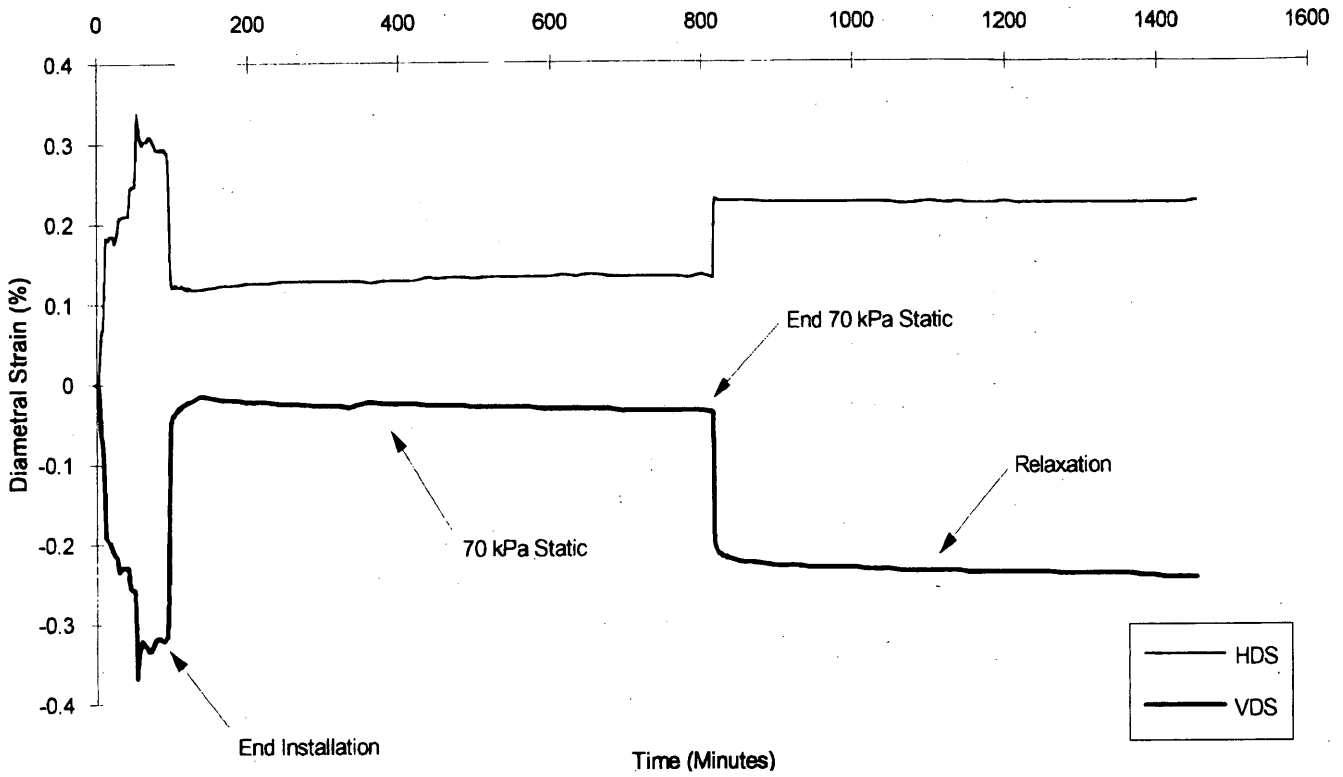

FIGURE 1 Diametral strains due to installation and 70-kPa static stress phases.

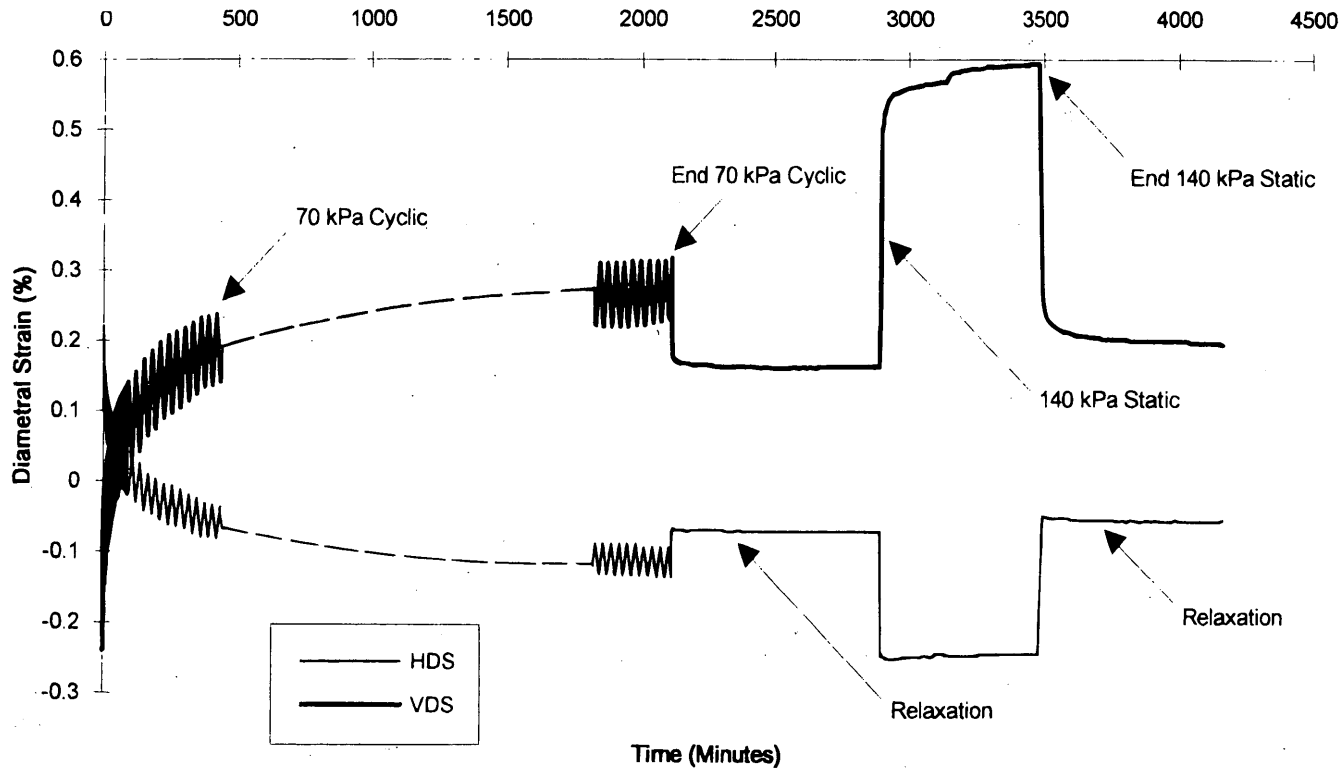

FIGURE 2 Diametral strains due to 70-kPa cyclic and 140-kPa static stress phases.

ceptable) site practice, yielded much greater deformations (because significantly greater pipe deformation is required to generate the supporting equilibrium passive earth pressure). However, in only one case (300-mm pipe in uncompacted sand) does the VDS exceed the benchmark value (5.0 percent), before falling to 4.1 percent at the end of the test. However, this result must be interpreted in the context of the very poor (unacceptable) site practice simulated and the large stresses applied. A similar pattern of results, though with typically far higher VDS for comparable loading, has been indicated by Rogers (*11*) for smooth wall polyvinyl chloride (PVC)-U pipe, which has a standard dimension ratio (SDR, the ratio of external diameter to wall thickness) of 41. Corrugated HDPE pipe, with equivalent SDRs ranging from 12.2 to 20.4 (based on an equivalent single wall pipe with the same moment of inertia as the corrugated profile) is thus structurally superior. In tests simulating typical UK site practice using an uncompacted 10-mm pea gravel surround, the maximum VDS values (2.8 percent under maximum load and 2.3 percent at the end of testing) were recorded for 300-mm pipe.

The best performance was achieved by the 100-mm pipe, indicating that this pipe/soil system is superior because of the existence of a narrower structural span exposed to the applied loading, and a narrower span over which to induce arching in the surrounding soil. The 100-mm pipe is also somewhat stiffer than larger diameter pipes, although still proportionally small compared to the total stiffness of the pipe-soil structure.

Several tests were duplicated under identical conditions and these achieved a very high degree of repeatability, providing confidence in the procedures used. Potential reductions in loads transmitted to the pipes due to frictional effects of the test box walls have also been investigated. The large steel-sided test box was lined with phenolic film-faced plywood, similar to that of the smaller test box, and a polyethylene sheet was placed against the smooth surface to ensure a low friction interface. The results demonstrated that box wall friction effects were insignificant for installations using uncompacted river sand (anticipated to be the critical case), the differences in the comparative tests lying well within normal experimental ranges. It should also be noted that the large test box is four times wider than the largest pipe tested, further minimizing boundary effects.

Pipe Wall Strains

Pipe wall strains were measured beneath the corrugation, or ridge (single wall) and the valley (twin wall) for the tests using the 375-mm pipe only. The data for the two (repeat) tests on the pipe buried in uncompacted river gravel will be presented here to demonstrate the behavior under different applied stress conditions. It should be noted that twin wall strains are plotted to demonstrate behavior since these are in all cases more extreme. Single wall data for full test loading are subsequently presented to illustrate this point. In addition, all strain data are for the pipe with the stress removed and after recovery.

The wall strains caused by installation were expected to be relatively low since no compaction was applied to the gravel. The twin wall strains shown in Figure 3 confirm this. Test 2 exhibits small strains at all points except the invert (180°), where a compression of 1000 με is recorded. In contrast, the pipe used in Test 1, although recording almost identical invert strains, exhibits a compression of 1430 με at 90°. This was caused by the accidental tipping of gravel sidefill at one side of the pipe only when filling the box, subsequent shovelling being required to feed the uncompacted gravel carefully

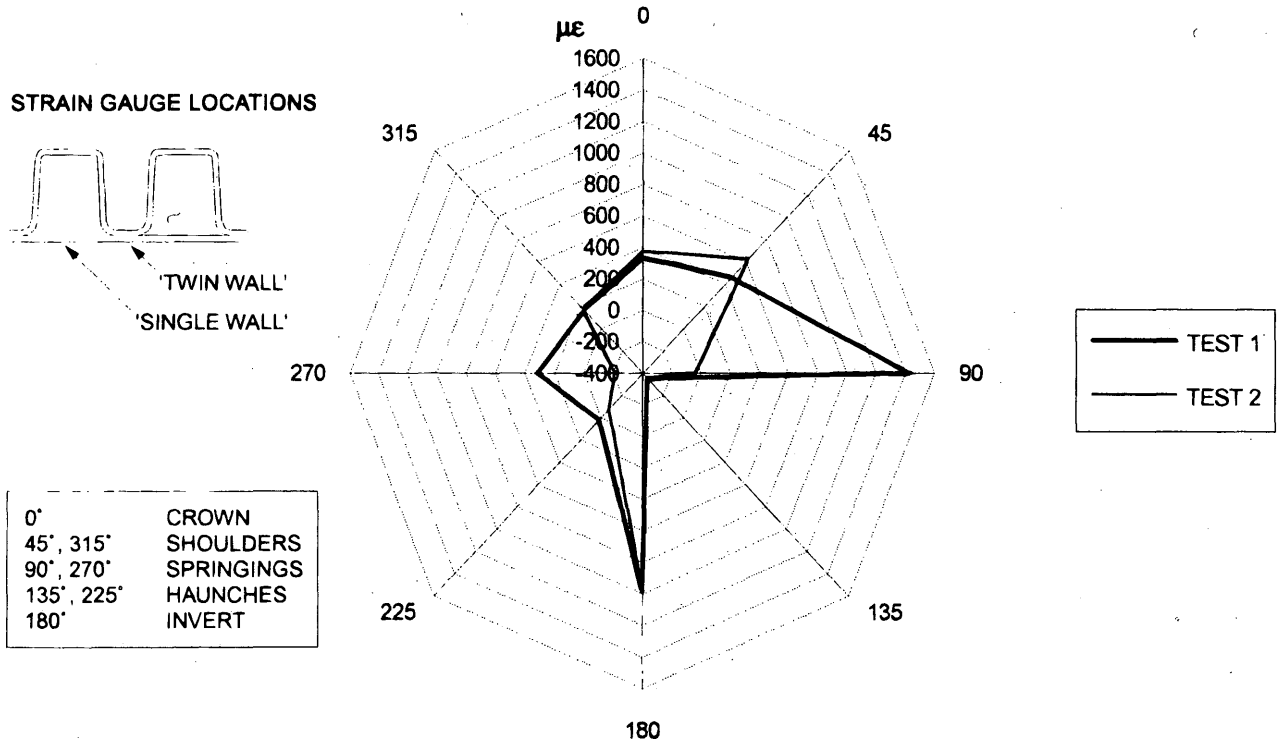

FIGURE 3 Twin wall strains caused by pipe installation.

to the other side. This demonstrates the importance of filling trenches uniformly at both sides of the pipe simultaneously, which practice was used for Test 2. The expected pattern of broadly uniform small compressive strains is otherwise generally demonstrated with the exception that the haunches in both cases exhibit small or markedly tensile strains and the invert relatively large compression. This implies that the careful feeding of gravel beneath the haunches, as specified in good site practice guidance, has caused the haunches to provide the majority of the vertical support from the bedding. Indeed the installation might have caused the pipe invert to have been raised off the underlying bedding layer by a small amount, thus allowing curvature (exhibited by compression on the internal surface) to occur readily at this point.

The wall strain data caused by the loading sequences are presented hereafter as readings averaged about the vertical axis for clarity in description of behavior, although the readings were typically broadly similar about this axis. Readers should note that, for Figures 3 to 8, positive readings indicate compression, and negative readings tension. Strain gauges were placed at the pipe crown (0°), invert (180°), springings (90° and 270°), haunches (135° and 225°), and shoulders (45° and 315°). The dotted lines are lines of equal strain. The overall effect of all three load sequences (i.e., the strain data at the end of the test minus those strains caused by installation) is illustrated in Figure 4, which indicates remarkably similar trends for the two tests. Also shown for comparison are the results of constant rate of deformation parallel-plate tests, in which elliptical deformation was expected. Linearity was demonstrated for all gauges, both during loading and unloading in the plate test, thereby demonstrating that the gauges were working properly. The results indicate tension at the crown and invert (indicating flattening of the pipe wall), compression at the springings (indicating an increase in curvature) and very small compressive strains at the haunches and shoulders. This wall strain distribution indicates elliptical deformation, and thus confirms the link between deformed shape and wall strain (*12*). The expected strain pattern for the entire loading sequence, given in Figure 4, of tensile strains at the crown, high compressive strains at the shoulders and lower compressive strains at the springings (90° and 270°) is a classic demonstration of what was termed "heart-shaped" deformation by Rogers (*12*). This illustrates most action in resisting applied stresses occurring in the upper half of the pipe, with the crown tending to flatten and the shoulders tending to bulge. Although these descriptions sound dramatic, they are not in reality since the deformations are remarkably low (0.5 and 0.65 percent VDS caused by loads) and indeed are indicative of remarkably good pipe performance. The effect of haunch support and invert curvature noticed above is reiterated and causes a pattern of higher strains (although still low in absolute terms) that would otherwise be unexpected if the pipe received uniform support throughout its lower half. Relatively low compressive strains would be expected below the horizontal axis.

The effect of the 70-kPa static load sequence is illustrated in Figure 5. Again the pattern for the two tests is similar, with Test 1 exhibiting a greater degree of hoop compression than Test 2. The heart-shaped deformation pattern modified by haunch support is clearly initiated by this loading. The effect of the cyclic load sequence (Figure 6), in contrast, is much less severe with typically smaller strains being more uniformly distributed. Virtually no change in curvature occurred at the springings (90° and 270°) in Test 1, with flattening at the crown and invert and compression at the shoulders. This pattern lies between that of heart-shaped deformation and elliptical deformation, a tendency to elliptical deformation being expected (*12*). The data for Test 2 are more extreme with a much greater flattening at the crown and much more pronounced heart-shaped deformation. The data for the 140-kPa static load sequence (Figure 7) show relatively small additional strains

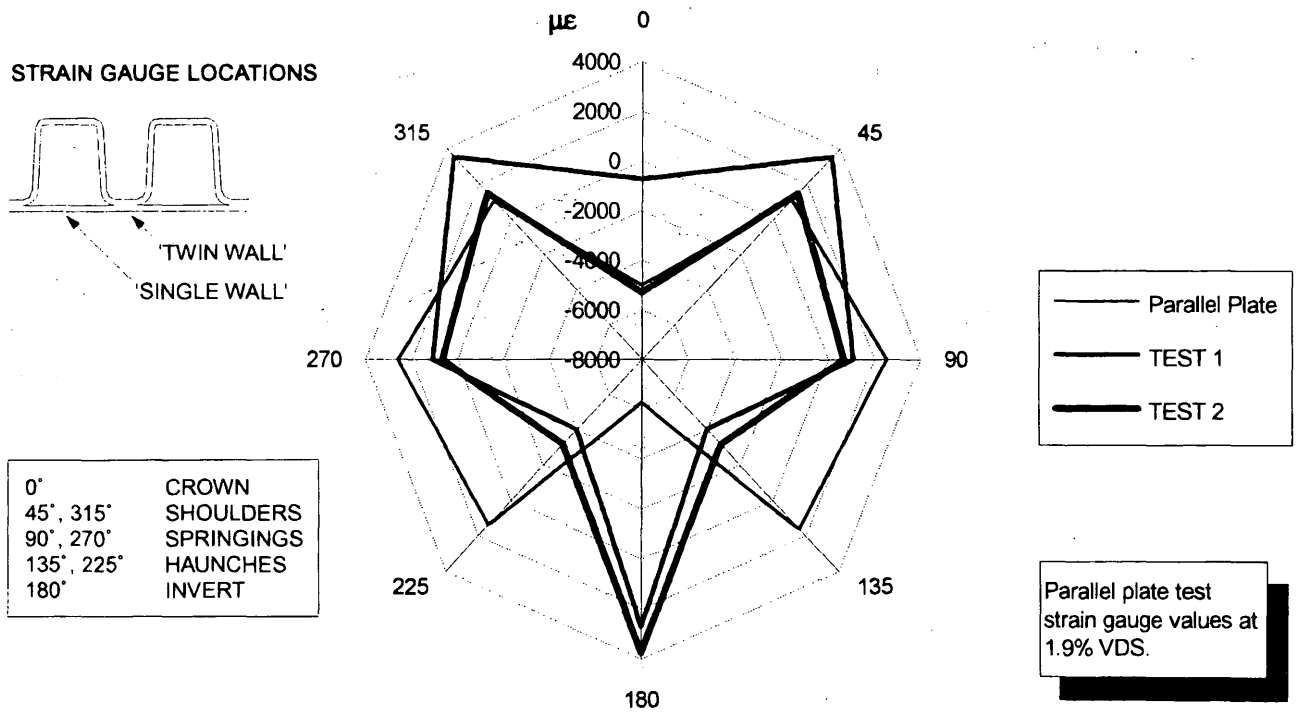

FIGURE 4 Twin wall strains caused by the complete stress sequence (end of test minus installation) and parallel plate testing.

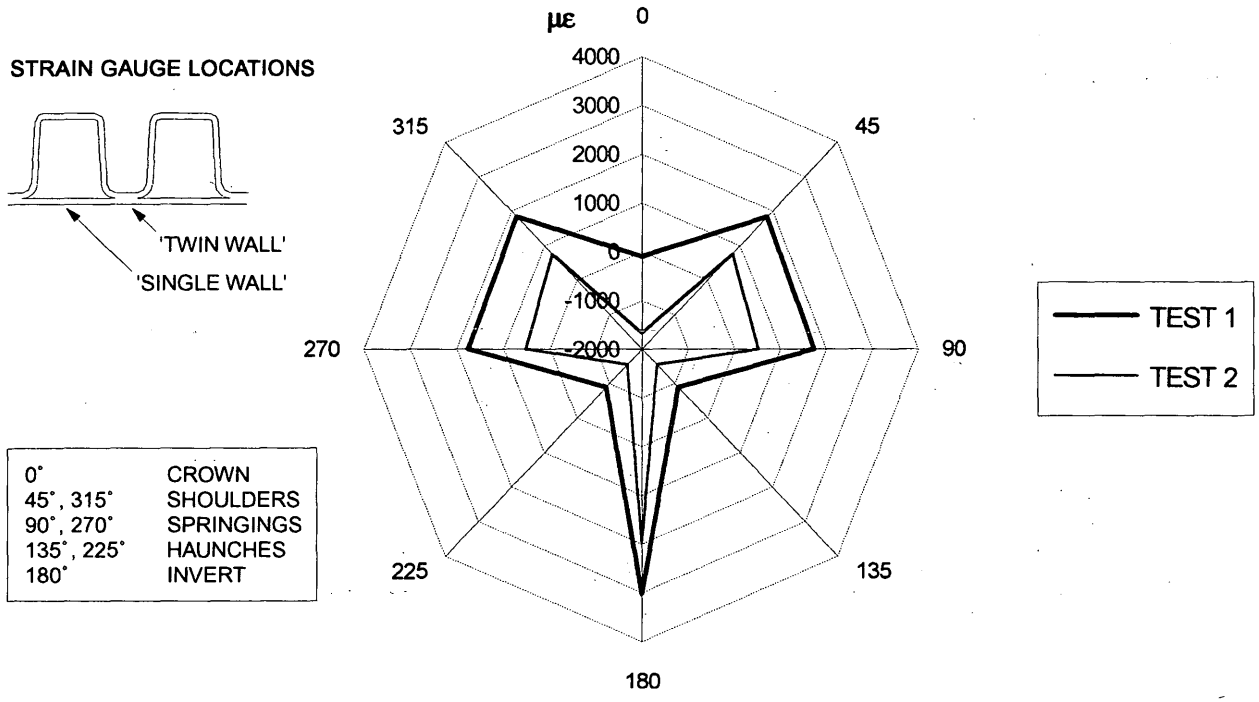

FIGURE 5 Twin wall strains caused by the 70-kPa static stress sequence (end of 70 S minus installation).

that conform broadly to the pattern of the 70-kPa static load sequence, although definitive conclusions are difficult to draw because of their small magnitude in relation to the previous two load sequences.

The wall strain data for the single wall (i.e., beneath the ridge) were in all cases less extreme and exhibited a greater degree of hoop compression than those for the twin wall sections. The effect of the complete load sequence on the single wall is shown in Figure 8, which should be compared with Figure 4. It is apparent that the strain profile here is more uniform for both tests although the fundamental pattern exhibited by the twin wall section is broadly followed. The tendency toward hoop compression is best exhibited at

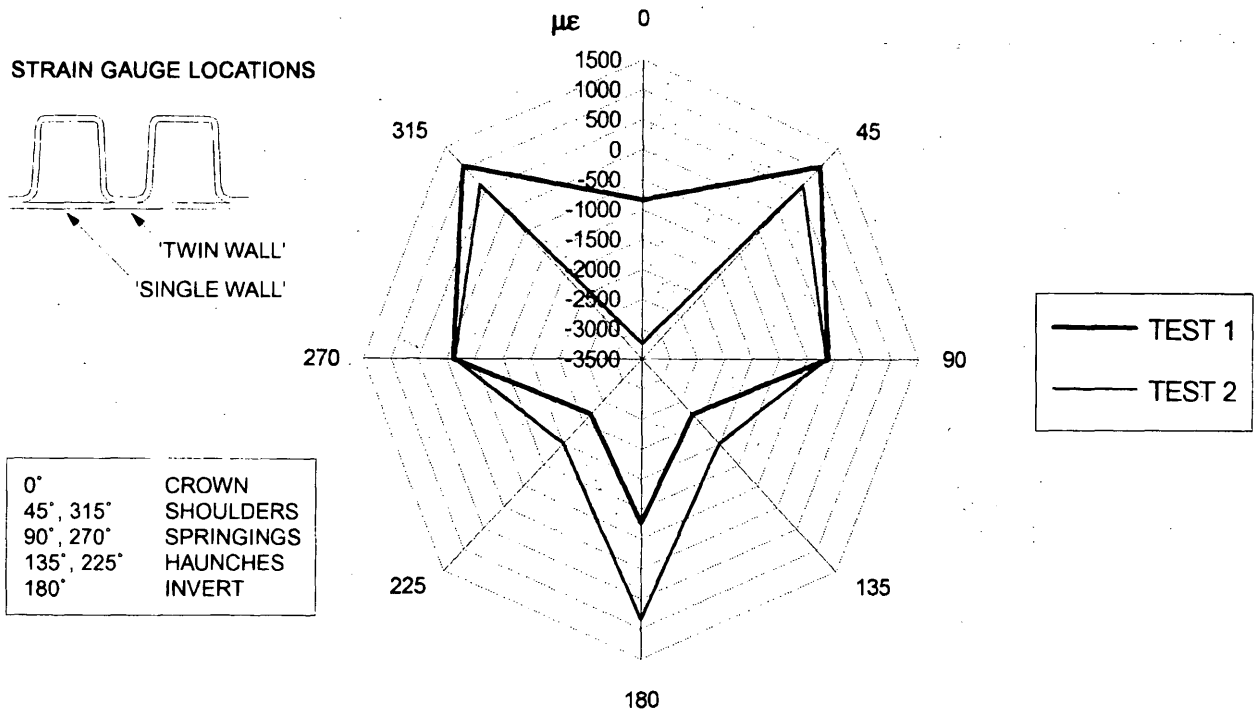

FIGURE 6 Twin wall strains caused by the 70-kPa cyclic stress sequence (end of 70 C minus end of 70 S).

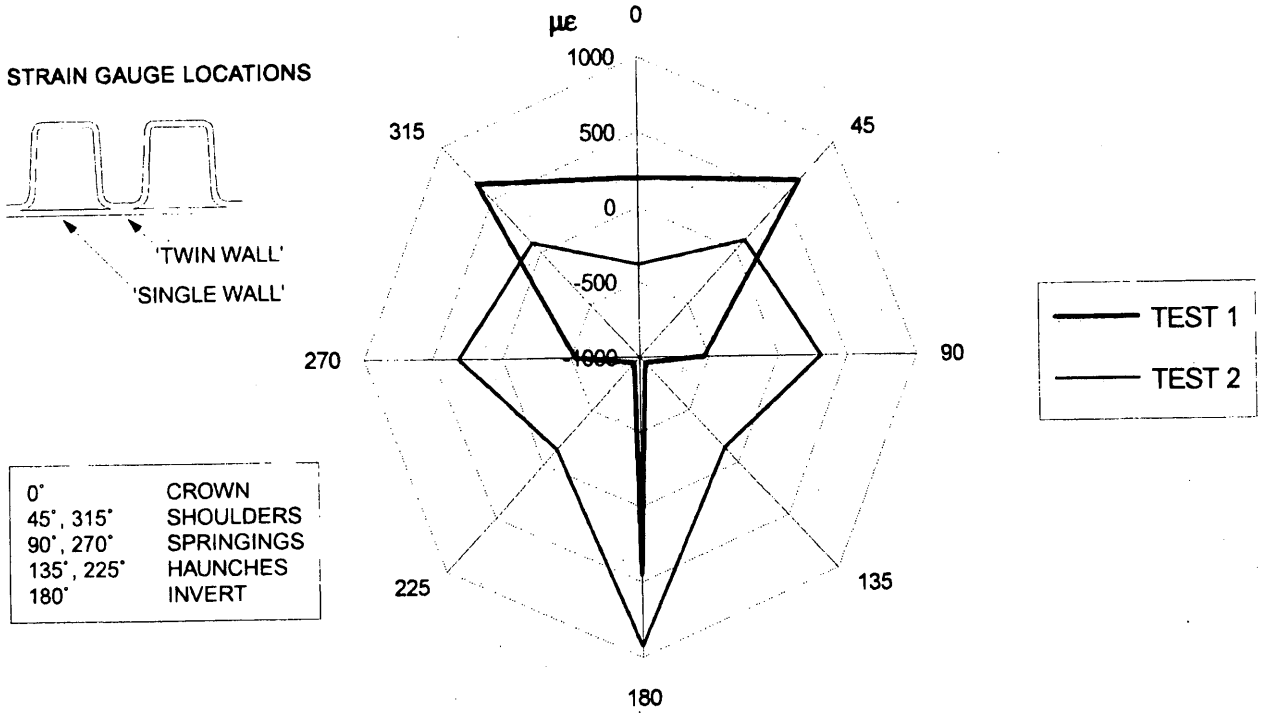

FIGURE 7 Twin wall strains caused by the 140-kPa static stress sequence (end of 140 S minus end of 70 C).

the crown in Test 1. These observations indicate that the ridges and valleys provide a large proportion of the resistance to external loading and that the single wall beneath the ridges is structurally less important.

In well compacted sand, the benefit of good, uniform support has been found to result in a virtually uniform (compressive) strain distribution at all points of the pipe. This implies hydrostatic stress distribution. Even at high loads, the strains were small (typically less than 400 με), indicating the high compressive stiffness of the pipe ring. Circumferential shortening can be approximated from strain gauge data, and for the 375-mm diameter pipe was found not to exceed 0.25 mm under the 140-kPa static stress.

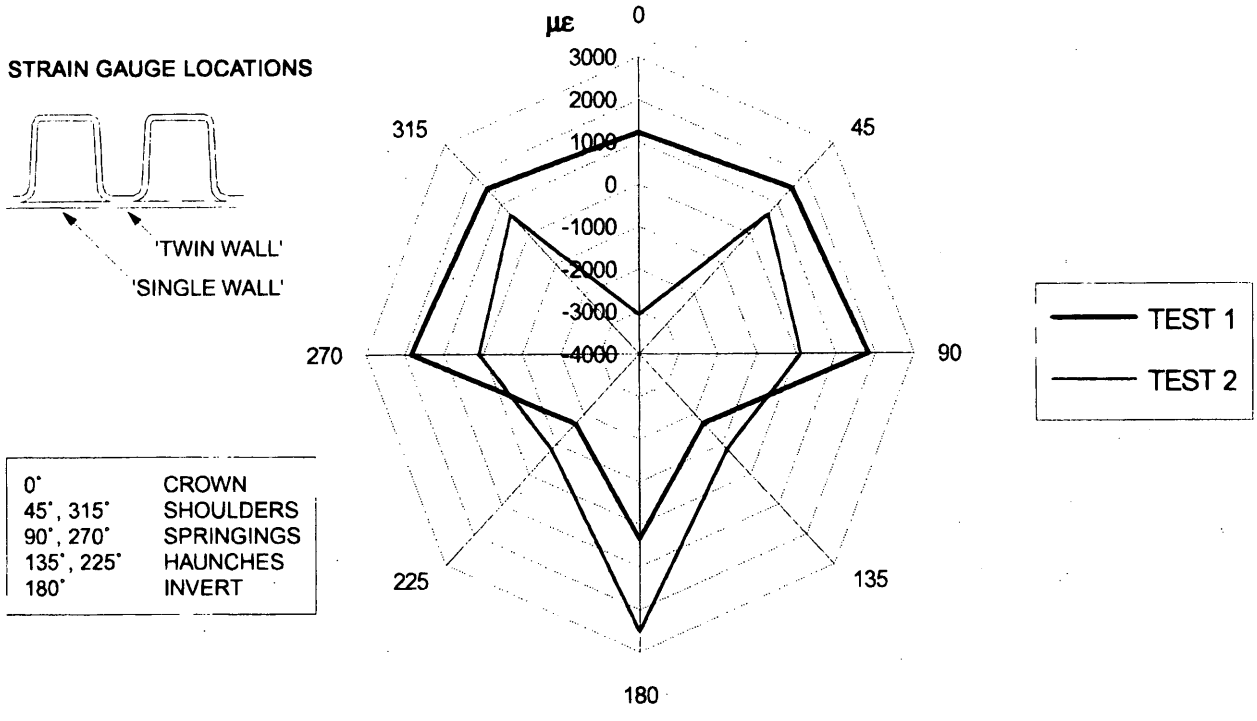

FIGURE 8 Single wall strains caused by the complete stress sequence (end of test minus installation).

Discussion of the Test Results in Relation to Other Work

The results support previous findings in the United Kingdom and elsewhere. Magnitudes of plastic pipe deformation are widely reported in the literature [for example, Rogers (*11*) and Gehrels and Elzink (*14,15*)], and it is now firmly established that remarkably good performance can be achieved with plastic pipes when buried with care, in a wide variety of pipe surround materials. In addition, they confirm the results of the work carried out by Rogers (*10,12*) that the shape of the deformed pipe is a function of the properties of the surround medium. Lightly compacted sand produced the largest deflections, as would be expected due to the inability of arching mechanisms to form in loose material and greater pipe deflection being required to mobilize equilibrium passive earth pressures. Pipes in gravel exhibit far less vertical diametral reduction and deform to a "heart" shape, because of the high degree of lateral support provided to all parts of the pipe circumference by this medium. The analyses of the strain profiles for all of the tests indicate that the greatest tensile strains always occurred at the pipe crown, whereas the distribution of strain around the circumference depended on the type of surround and the type of loading. Good support to the pipe typically resulted in deformation that deviated from an ellipse, most notably under static load. Cyclic loading appears to permit reorientation of the soil particles and cause deformations of a more elliptical nature to be superimposed on the deformed shape. The results of this work thus help in understanding how a flexible pipe resists applied loading in the field.

Implications of the Test Results

Trott and Stevens (*16*) concluded from their series of loading tests that the creep behavior of PVC-U pipes under sustained load is controlled by the properties of the pipe surround instead of those of the pipe. Gehrels and Elzink (*14*) state that the pipe class (i.e., pipe stiffness) is of minor importance in relation to the influence of bedding and backfill on the rate of deformation. These conclusions raise serious questions as to the validity of using 50-year pipe creep stiffness moduli for certification, specification and design purposes, and indicate that a soil creep stiffness is more relevant. Joekes and Elzink (*17*) propose the use of a 2-year stiffness value, based on a single logarithmic model that specifies a minimum value of correlation coefficient. They also reiterate earlier conclusions, stating that pipe stiffness has a minimal contribution to increasing deflection of the pipe after installation caused by settlement of the fill. Trafficking is said to result in the earlier establishment of equilibrium of the pipe-soil structure, adding that the equilibrium condition is reached within 2 years in virtually all cases studied and, under certain conditions, within a month. These observations are further supported by the various pipe design methods, which indicate that the pipe stiffness has only a very small influence on predicted deformation.

The recently published ISO 9967 (*18*) adopts the 2-year stiffness value and other minor improvements, yet, despite acknowledging a virtual cessation of deflection after a short period (and certainly within 2 years), persists in specifying pipe testing in isolation from the soil and applied loads based on the initial stiffness of the pipe. Although the authors acknowledge the need for a repeatable and relatively simple performance test for pipes, the use of a test that does not reflect performance in situ would appear to be poor engineering practice. It is worth noting in this context that pipes certified for use in sewer applications are subjected to a 10,000-hr (nearly 14 month) creep test. In this case simplicity does not equate to facility since the test clearly represents a major constraint on the pipe industry, in terms of development programming and costs, as modifications to the design of the pipe must await the results.

The deformations recorded at the end of all tests were less than 5 percent. Therefore it would appear that the long-term performance of the twin wall corrugated HDPE pipes tested will be excellent under most installation conditions, especially when considered in the context of the large magnitude of the stresses applied. These results are even more impressive when viewed in the context of Gehrels and Elzink's conclusion that diametral deflections of 10 percent to 20 percent have never been shown to cause problems for the proper function of pipelines (*15*). They add that the failure due to deflection is unknown with SDR 41 PVC-U pipes, pipes that are structurally inferior to twin wall HDPE pipes because of their higher SDRs.

CONCLUSIONS

It is concluded that current specification and design criteria used in the United Kingdom are conservative in light of laboratory and field data. The historically accepted limiting deflections of 5 percent of original diameter over the longer-term are still widely held in the United Kingdom, in spite of a large body of evidence indicating that this, too, is excessively conservative. More recent moves to relax this specification to 5 percent of the original diameter at the end of the construction period (*13*) indicate a better appreciation of the structural performance of such pipes. The U.K. Water Research Centre recommends a deformation limit of 6 percent 12 months after construction and accepts that the greatest degree of increase in deformation after installation will occur in the first 2 years (*19*). This demonstrates the incorporation by the water industry of research in their specifications, although drainage pipe specifications have remained unchanged. The test results additionally indicate that a wider range of soil surrounds could be used in practice, which would in turn reduce the costs of pipeline construction.

A major concern with current pipe testing methods has been found to be the fact that the creep stiffness test methods currently available do not address the fundamentals of pipe-soil interaction. Creep stiffness should not be considered in isolation as the installed behavior is more complex, and dependent to a major extent on the properties of the soil surround. Greater consideration must therefore be given to the formulation of representative, and repeatable, tests that take account of the behavior of the pipe-soil structure. Finite element methods would also lend themselves to this problem, and work in this field is being undertaken at many establishments.

It is thus apparent that advances in engineering of pipes and pipeline installation have the potential to reduce the cost of pipeline construction although maintaining the required levels of performance over the full design life of the pipeline. For this to happen, the current standards and specifications must be revised in the light of extensive research data to permit properly engineered solutions based on structural performance.

REFERENCES

1. *Specification for Highway Works*. Department of Transport, HMSO, London, 1991.
2. *Highway Advice Note HA40/89 Determination of Pipe and Bedding Combinations for Drainage Works*. Department of Transport (Highways and Traffic), HMSO, London, UK, 1990.
3. *Specification for Plastics Pipes and Fittings for Use as Subsoil Field Drains*. British Standards Institution, BS4962:1989.
4. Smith, G. N. *Buried Flexible Pipes 2: The Analytical Method Developed by Gumbel for the TRRL*. Contractor Report 229, TRRL, Crowthorne, Berkshire, UK, 1991.
5. Smith, G. N. *Buried Flexible Pipes 3: Applications of a New Design Method*. Contractor Report 230, TRRL, Crowthorne, Berkshire, UK, 1991.
6. *Standard Test Method for Determination of External Loading Characteristics of Plastic Pipe by Parallel-Plate Loading*. ASTM D2412-87, American Society for Testing and Materials, Philadelphia, 1987.
7. *Highway Construction Details*. Department of Transport, HMSO, London, UK, 1991.
8. Spangler, M. G. The Structural Design of Flexible Pipe Culverts. *Bulletin 153*, Engineering Experiment Station, Iowa State College, Iowa, 1941.
9. Howard, A. K. Modulus of Soil Reaction (E′) Values for Buried Flexible Pipes. *Journal of the Geotechnical Division, ASCE*, Vol. 103, 1977.
10. Rogers, C. D. F. *The Response of Buried uPVC Pipes to Surface Loading*. Ph.D. thesis, University of Nottingham, U.K., 1985.
11. Rogers, C. D. F., The Influence of Surrounding Soil on Flexible Pipe Performance. In *Transportation Research Record 1129*, TRB, National Research Council, Washington, D.C., 1987.
12. Rogers, C. D. F. Deformed Shape of Flexible Pipe Related to Surround Soil Stiffness. *Transportation Research Record 1191*, TRB, National Research Council, Washington, D.C., 1988.
13. *Plastics Pipework (Thermoplastics Materials) Part 6. Code of Practice for the Installation of Unplasticized PVC Pipework for Gravity Drains and Sewers*. British Standards Institution, BS5955,1980.
14. Gehrels, J. F., and W. J. Elzink. More Than 15 Years of Distortion Measurement Results with uPVC Pipes. *Proc., Europipe '82 Conference*, Basel, Switzerland, 1982.
15. Gehrels, J. F., and W. J. Elzink. Experience of Long-Term Behaviour of uPVC Gravity Sewers. *Proc., 4th International Plastics Pipes Conference*, University of Sussex, Brighton, U.K., 1979.
16. Trott, J. J., and J. B. Stevens. Loading Tests on uPVC pipes Installed in Cohesive and Non-Cohesive Bedding Materials. *Proc., 4th International Plastics Pipes Conference*, University of Sussex, Brighton, U.K., 1979.
17. Joekes, D., and W. J. Elzink. Deflection of PVC Sewer Pipes and a New Method for Measuring and Specifying Stiffness of Plastics Pipes. *Proc., 6th International Plastics Pipes Conference*, University of York, U.K., 1985.
18. *Thermoplastics Pipes—Determination of Creep Ratio*. ISO 9967, International Standards Organisation, 1994.
19. *ER201E Guide to the Water Industry for the Structural Design of Underground Non-Pressure UPVC Pipelines*. Water Research Centre Engineering, Swindon, Wilts, U.K., 1986.

Publication of this paper sponsored by Committee on Culverts and Hydraulic Structures.